An Experimental Study on Clear Water Temporal Scour around Eccentric Circular Piers

A thesis submitted towards partial fulfilment of the requirements for the degree of

Master of Engineering

in

Water Resources and Hydraulic Engineering

Submitted by

SHUBHASHREE LAHA

Examination Roll No: M4WRE24005

Registration No: 163859 of 2022-23

Under the guidance of

Dr. SUBHASISH DAS

Associate Professor and Joint Director

School of Water Resources Engineering, Jadavpur University

&

Dr. RAJIB DAS

Assistant Professor

School of Water Resources Engineering, Jadavpur University

School of Water Resources Engineering

M.E. (Water Resources & Hydraulic Engineering)

Course affiliated to ***Faculty Council of Engineering & Technology***

Jadavpur University

Kolkata-700032, West Bengal, India

2024

Declaration of Originality and Compliance of Academic Ethics

I hereby declare that this thesis contains literature survey and original research work by the undersigned candidate, as part of my **Master of Engineering** in **Water Resources and Hydraulic Engineering** in the Faculty Council of Interdisciplinary Studies, Law & Management, Jadavpur University during academic session 2023-24.

All information in this document have been obtained and presented in accordance with academic rules and ethical conduct.

I also declare that, as required by these rules and conduct, I have fully cited and referenced all material and results that are not original to this work.

Name	:	**SHUBHASHREE LAHA**
Exam Roll Number	:	**M4WRE24005**
Thesis Title	:	**An Experimental Study on Clear Water Temporal Scour around Eccentric Circular Piers**
Signature with Date	:	

M.E. (Water Resources & Hydraulic Engg.) course affiliated to
Faculty Council of Engineering & Technology
Jadavpur University
Kolkata, India

Certificate of Recommendation

This is to certify that the thesis entitled "**An Experimental Study on Clear Water Temporal Scour around Eccentric Circular Piers**" is a bonafide work carried out by **Ms. Shubhashree Laha** under our supervision and guidance for partial fulfilment of the requirement for the Post Graduate Degree of Master of Engineering in Water Resources and Hydraulic Engineering during the academic session 2023-24.

THESIS ADVISOR
Dr. Subhasish Das
Associate Professor and Joint Director
School of Water Resources Engineering
Jadavpur University

THESIS ADVISOR
Dr. Rajib Das
Assistant Professor
School of Water Resources Engineering
Jadavpur University

DIRECTOR
Prof. (Dr.) Asis Mazumdar
School of Water Resources Engineering
Jadavpur University

DEAN
Prof. (Dr.) Joydeep Mukherjee
Faculty Council of Interdisciplinary Studies, Law & Management
Jadavpur University

M.E. (Water Resources & Hydraulic Engg.) course affiliated to
Faculty Council of Engineering & Technology
Jadavpur University
Kolkata, India

CERTIFICATE OF APPROVAL **

This foregoing thesis is hereby approved as a credible study of an engineering subject carried out and presented in a manner satisfactorily to warranty its acceptance as a prerequisite to the degree for which it has been submitted. It is understood that by this approval the undersigned do not endorse or approve any statement made or opinion expressed or conclusion drawn therein but approve the thesis only for purpose for which it has been submitted.

Committee of

Final Examination

for the evaluation

of the thesis

** Only in case the thesis is approved.

ACKNOWLEDGEMENTS

This thesis could not be completed without the assistance, understanding and counselling of several people throughout the research work. First and foremost, I would like to express my sincere gratitude to my supervisors, ***Dr. Subhasish Das****, Associate Professor and Joint Director, and* ***Dr. Rajib Das****, Assistant Professor of the School of Water Resources Engineering, Jadavpur University, under whose supervision and guidance this work has been carried out. It would have been impossible to carry out this thesis work with confidence without their wholehearted involvement, advice, support and constant encouragement throughout. They have not only helped me in carrying out my thesis but also have given valuable advice to proceed further in my life.*

I also express my sincere gratitude to, ***Prof. (Dr.) Asis Mazumdar****, Director of the School of Water Resources Engineering, Jadavpur University,* ***Prof. (Dr.) Arunabha Majumder****, Emeritus Professor;* ***Prof. (Dr.) Pankaj Kr. Roy****, Professor,* ***Dr. Gourab Banerjee****, Assistant Professor, of the School of Water Resources Engineering, Jadavpur University for their valuable suggestions.*

I am profoundly grateful to ***Mr., Buddhadev Nandi****, Research Scholar, for his unconditional support and unwavering encouragement during my work. I would also express my special thanks to* ***Mr., Saikat Mandal****, Research Scholar;* ***Ms., Priyanka Roy*** *Research Scholar of the School of Water Resources Engineering, Jadavpur University for their unconditional moral support and affection during my work. Also, thanks to my classmates* ***Ms. Tryasa Roy*** *and* ***Mr. Binoy Banik*** *for their helping hand throughout my whole journey in the M.E. course. I would also express my love and affection to* ***my younger brother, Bishal Laha,*** *without his consistence cheerful support I would be unable to continue my degree.*

Thanks, are also due to all staff of the School of Water Resources Engineering and the Regional -cum-Facilitation Centre (RCFC), NMPB, Jadavpur University for their help and support. At last, but not the least, I am very appreciative of our ***"Fluvial Hydraulics Laboratory"*** *for providing a pleasant and friendly environment that consistently fosters a positive atmosphere. This thesis stands as a testament to the collective support and belief of everyone who has been a part of this journey.*

Date : 28 August, 2024

Place : Jadavpur University

Ms. Shubhashree Laha

(Exam Roll No: M4WRE24005)

ABSTRACT

One possible reason for bridge failure has been identified as scour near the piers. Increasing traffic load in an urban area leads to the construction of a new bridge beside the existing one. This type of parallel bridges create situations like tandem and eccentric pier combinations. The literature study confirms that there was much attention given to the work that delves into creating techniques to forecast the depth of scour as well as to understand the dynamics underlying scour only around the single pier. There was limited research found on the eccentric arrangement of piers in clear water conditions. Therefore, in the present study, an attempt has been made to understand how scour depth changes with time, and the effect on maximum scour depth with respect to different flow parameters such as flow intensity, flow shallowness and Froude number. In the present study, a total of 24 experiments were conducted with fixed discharge of 20 lps and longitudinal spacing of 5.19b where b is the pier diameter, and with six different eccentrics spacings (2b-3.5b) as well as with four different flow intensities (0.67-0.97), Froude number (0.20-0.32) and flow shallowness (1.2-1.65). To compare the maximum scour depth around eccentric pier arrangements, four additional single-pier experiments were carried out. The dimensional analysis has been performed to ensure the influential parameters which influence the temporal scour depth. The geometry of scour profiles has been analysed, whether the eccentric-piers arrangement causes a symmetric or non-symmetric scour. If it is not symmetrical, the greater scour is determined on which side of the pier it is shifting. The scour width and the total scour length have been analysed how they affect the sediment shifting process at the downstream of the eccentric pier. The temporal evaluation of the scour depth has been analysed to check the quasi-equilibrium state of the scour. The separate effects of flow intensity, Froude number, time, and flow shallowness on scour depth have been analyzed. Dimensionless analysis reveals that flow shallowness, flow intensity, Froude number, dimensionless time, and dimensionless lateral spacing are the key parameters influencing the scour depth around both front piers and eccentric piers in the current experimental data set. The maximum and minimum scour depth for front and eccentric piers are found to correspond to the maximum value of flow intensity, Froude number, dimensionless time and minimum value of flow shallowness and vice versa. When all of the eccentric pier arrangements are analyzed, it becomes clear that the left portion of the front pier has the maximum and minimum scour length, while the right and left sections have the maximum and minimum scour width. Additionally, it was identified that the left section has the least planar surface area and scour volume, while the right section has the maximum. From an overall perspective, it can be stated that when eccentricity increases, sediment deposition spreads in the right section of the eccentric pier with respect to the flow direction, and when eccentricity decreases, the same things occur on the left side of the front pier. This study may help to select criteria that minimize scour is essential for constructing bridge piers safely and cost-effectively. Maximize scour, which is also necessary for these arrangements, by shifting sediment to one side of the riverbank, which can aid in navigation and be beneficial for protecting the riverbank. For the self-dredging phenomenon, shifting sediment on one side of the bank is also beneficial.

CONTENT

Sl. No.	Chapter No.	Topic	Page No.
		DECLARATION	**iii**
		CERTIFICATE OF RECOMMENDATION	**v**
		CERTIFICATE OF APPROVAL	**vii**
		ACKNOWLEDGMENTS	**ix**
		ABSTRACT	**xi**
		CONTENT	**xii**
		LIST OF FIGURES	**xvi**
		LIST OF TABLES	**xix**
		NOMENCLATURES	**xx**
		GLOSSARY	**xxii**
1	**CHAPTER-1**	**SCOURING**	**1**
		1.1 Introduction	1
		1.2 Scour	3
		1.3 Why be concerned about scour?	3
		1.4 Classification of scours	4
		1.4.1 General scour	5
		1.4.2 Localized scour	5
		1.4.3 Clear water scour	6
		1.4.4 Live bed scour	7
		1.5 Local scour mechanism	7
		1.5.1 Horseshoe vortex and downflow	8
		1.5.2 Wake vortex	8
		1.5.3 Bow wave	9
		1.6 Sediment transport	9
		1.7 Parameters influencing local scour	11
		1.8 Parameter influences	12
		1.9 Influence of dimensional parameters	13
		1.9.1 Pier diameter	13
		1.9.2 Approaching flow velocity	13
		1.9.3 Sediment size	14
		1.9.4 Flow depth	14
		1.9.5 Pier shape	15
		1.9.6 Effect of pier alignment	16
		1.9.7 Angle of repose	17
		1.9.8 Effect of time	17

		1.9.9 Densimetric Froude number	18
		1.10 Influence of non-dimensional parameters	18
		1.10.1 Effect of sediment non-uniformity	18
		1.10.2 Effect of flow intensity	19
		1.10.3 Effect of flow shallowness	20
		1.10.4 Effect of Froude number and Reynolds number	21
		1.10.5 Effect of sediment coarseness	21
		1.10.6 Effect of blockage ratio/contraction ratio	23
		1.11 Equilibrium scour depth	23
		1.12 Temporal variation of scour depth	23
		1.13 Scour at pier groups	24
		1.13.1 Reinforcing	24
		1.13.2 Sheltering	25
		1.13.3 Shed vortices	26
		1.13.4 Compressed horseshoe vortex	26
		1.14 Two pier group	27
		1.14.1 In line (angle of attack = 0°)	27
		1.14.2 Transverse (angle of attack = 90°)	28
		1.14.3 Non-aligned (angle of attack = 45°)	28
		1.14.4 Effect of angle of attack for two pier groups	29
2	**CHAPTER-2**	**LITERATURE STUDY**	**31**
		2.1 Literature review	31
		2.1.1 Single pier	31
		2.1.2 Eccentric piers	34
		2.2 Literature equations for eccentric-pier arrangement	45
		2.3 Research gaps identified	47
		2.4 Need of the work	48
		2.5 Aim of the present study	49
3	**CHAPTER-3**	**OBJECTIVES AND METHODOLOGY**	**50**
		3.1 Objectives	50
		3.2 Experimental conditions adopted by previous researchers	51
		3.3 Pier dimension	52
		3.4 Flow conditions	52
		3.5 Setting the gap between the piers	53
		3.6 Other hydraulic parameters	55
		3.7 Experimental conditions	55
		3.8 Methodology	57
4	**CHAPTER-4**	**EXPERIMENTAL SETUP**	**60**
		4.1 Experimental setup	60
		4.1.1 Experimental flume and equipment	60
		4.1.2 Pump	61
		4.1.3 Laser distance sensor	61
		4.1.4 Flowmeter	62
		4.1.5 Sediment bed	62

		4.2 Experimental procedure	66
5	**CHAPTER-5**	**PARAMETER FRAMEWORK**	**67**
		5.1 Dimensional analysis	67
		5.1.1 Analysis of scouring parameters	67
		5.1.2 Dimensionless analysis	68
6	**CHAPTER-6**	**RESULTS AND DISCUSSION**	**74**
		6.1 Result and Discussion	74
		6.2 Experimental outcomes based on non-dimensional flow parameters	75
		6.2.1 Effect of flow intensity, flow shallowness and Froude number on the scour depth at single pier	76
		6.2.2 Temporal evaluation of scour depth	77
		6.2.3 Effect of pier non- dimensional lateral spacing	79
		6.2.4 Effect of flow intensity	80
		6.2.5 Effect of flow shallowness	82
		6.2.6 Effect of Froude number	83
		6.2.7 Scour profiles of single pier and different eccentric pier arrangements	84
		6.3 Analysis of bed morphology	99
		6.3.1 Effect of lateral spacing on scour area and volume	102
		6.3.2 Effect of lateral spacing on maximum scour length	103
		6.3.3 Effect of lateral spacing on maximum scour width	104
		6.3.4 Effect of lateral spacing on scour planar area	105
		6.3.5 Effect of lateral spacing on scour volume in the entire section	107
		6.3.6 Effect of lateral spacing on deposition area and volume	109
		6.3.7 Effect of lateral spacing on deposition planar area in the entire section	110
		6.3.8 Effect of lateral spacing on deposition volume in the entire section	111
		6.4 Comparisons of scour depth between single pier and around eccentric pier arrangements	113
		6.5 Experimental limitations	116
7	**CHAPTER-7**	**CONCLUSIONS**	**117**
		7.1 Conclusions	117
		7.2 Future scopes	119
		REFERENCES	**120**

LIST OF FIGURES

Sl No.	Figure No.	Topic	Page No.
1	Fig. 1.1	Photograph of a (a) single circular bridge pier structure compared to the (b) eccentric circular bridge pier structure.	2
2	Fig. 1.2	Photograph of Schoharie Creek in New York State bridge collapsed in 1987 due to scouring during a flood.	4
3	Fig. 1.3	Photograph of Jahu bridge (Himachal Pradesh in India) collapsed in 2007 due to scouring during heavy rain (Rajendran, 2019).	4
4	Fig. 1.4	Classification of scour (Melville and Coleman, 2000).	5
5	Fig. 1.5	Photograph of local scour.	5
6	Fig. 1.6	Schematic diagram showing the boundary/key points selected around the pier to determine scour contours.	6
7	Fig. 1.7	Time evolution of scour depth in clear water and live bed conditions.	7
8	Fig. 1.8	Schematic diagrams of flow structures around circular pier showing (a) side view and (b) top view.	9
9	Fig. 1.9	Frequency distribution of boundary shear stress and critical shear stress illustrating the concept of armouring.	10
10	Fig. 1.10	Scour depth in terms of shear velocity or approach velocity.	13
11	Fig. 1.11	Schematic illustrations of some common pier shapes.	15
12	Fig. 1.12	Variation of local scour depth with pier alignment (Melville and Coleman, 2000).	16
13	Fig. 1.13	Diagrammatic scour shapes at a pier aligned with the flow and another angled to the flow direction.	16
14	Fig. 1.14	Angle of repose.	17
15	Fig. 1.15	Local scour depth variation with flow intensity and sediment non-uniformity.	19
16	Fig. 1.16	Variation of local scour depth with flow velocity and time.	20
17	Fig. 1.17	Local scour depth variation with flow shallowness.	20
18	Fig. 1.18	Local scour depth variation with large-scale turbulence.	21
19	Fig. 1.19	Effect of sediment coarseness on local scour.	22
20	Fig. 1.20	Schematic diagram of flow pattern and local scour around two eccentric piers.	24
21	Fig. 1.21	(a) Regions affected by overlapping scour and (b) Schematic diagram showing overlapping of scour between eccentric piers in the present study (Exp. 11).	25
22	Fig. 1.22	(a) Regions affected by individual scour and (b) Schematic diagram showing individual scour around eccentric piers in the present study (Exp. 5).	26
23	Fig. 1.23	Scour depths for two piers in line as a function of pier spacing (Breusers and Raudkivi, 2006).	27
24	Fig. 1.24	Scour depths around two transverse piers represented as a function of pier spacing (Breusers and Raudkivi, 2006).	28
25	Fig. 1.25	Scour depths around two piers positioned with an angle of attack of 45° represented as a function of pier spacing (Breusers and Raudkivi, 2006).	29

26	Fig. 1.26	The effect of angle of attack on scour depths at two piers spaced five pier diameters apart (Breusers and Raudkivi, 2006).	30
27	Fig. 3.1	Circular piers of each 7 cm diameter.	52
28	Fig. 3.2	Schematic diagram showing eccentric-pier arrangement with flow direction.	53
29	Fig. 3.3	Shields diagram showing no sediment motion for the present study.	58
30	Fig. 3.4	Flowchart showing the methodology set for the present study.	59
31	Fig. 4.1	Tilting flume to carry out all the laboratory experiments.	60
32	Fig. 4.2	Schematic diagram showing the tilting flume on which two piers are positioned eccentrically.	61
33	Fig. 4.3	Pump used to recirculate the flow.	61
34	Fig. 4.4	Laser distance sensor.	62
35	Fig. 4.5	Flowmeter.	62
36	Fig. 4.6	Grain size distribution curve.	64
37	Fig. 4.7	Dry flume bed without water before performing the eccentric pier experiment.	65
38	Fig. 4.8	Dry flume bed without water before performing the single pier experiment.	65
39	Fig. 6.1	Experimental photograph of eccentric piers captured during Exp. 14.	74
40	Fig. 6.2	Experimental photograph of a single pier captured during Exp. 4.	75
41	Fig. 6.3	Parameters (a) flow intensity, (b) flow shallowness, (c) Froude number, and (d) temporal variation influencing scour depth at a single pier.	77
42	Fig. 6.4	Variation of temporal scour depth in eccentric pier arrangements for various flow conditions, (a-b) (V/V_c = 0.67, h/b = 1.65, Fr = 0.20) (c-d) (V/V_c = 0.75, h/b = 1.5, Fr = 0.23) (e-f) (V/V_c = 0.85, h/b = 1.35, Fr = 0.27) (g-h) (V/V_c = 0.97, h/b = 1.2, Fr = 0.32) for front and eccentric piers.	79
43	Fig. 6.5	Variation of maximum scour depth with pier lateral spacing for (a) V/V_c = 0.67, h/b = 1.65, Fr = 0.20; (b) V/V_c = 0.75, h/b = 1.5, Fr = 0.23; (c) V/V_c = 0.85, h/b = 1.35, Fr = 0.27; (d) V/V_c = 0.97, h/b = 1.2, Fr = 0.32.	80
44	Fig. 6.6	Variation of maximum scour depth with flow intensity for (a) e = 3.5b, (b) e = 3b, (c) e = 2.75b, (d) e = 2.5b, (e) e = 2.25b, (f) e = 2b.	81
45	Fig. 6.7	Variation of maximum scour depth with flow shallowness for (a) e = 3.5b, (b) e = 3b, (c) e = 2.75b, (d) e = 2.5b, (e) e = 2.25b, (f) e = 2b.	83
46	Fig. 6.8	Variation of maximum scour depth with Froude number for (a) e = 3.5b, (b) e = 3b, (c) e = 2.75b, (d) e = 2.5b, (e) e = 2.25b, (f) e = 2b.	84
47	Fig. 6.9	Photographs of the scour-affected zones around a single pier after the experimental run for flow depths (a) h = 11.6 cm, (b) h = 10.5 cm, (c) h = 9.5 cm, and (d) h = 8.4 cm.	85
48	Fig. 6.10	Contours of scour holes and depositions at equilibrium for the single pier with flow depths (a) h = 11.6 cm, (b) h = 10.5 cm, (c) h = 9.5 cm, and (d) h = 8.4 cm.	87
49	Fig. 6.11	Photographs of the scour-affected and sediment-deposited zones around the eccentric piers after the experimental runs for eccentricity e = 3.5b with flow depths (a) h = 11.6 cm, (b) h = 10.5 cm, (c) h = 9.5 cm, and (d) h = 8.4 cm.	88
50	Fig. 6.12	Contours of scour holes at equilibrium for eccentricity e = 3.5b with flow depth (a) h = 11.6 cm; (b) h = 10.5 cm; (c) h = 9.5 cm; (d) h = 8.4 cm.	89

51	Fig. 6.13	Scour affected zones around piers after the experimental run for eccentricity $e = 3b$ for flow depth (a) $h = 11.6$ cm; (b) $h = 10.5$ cm; (c) $h = 9.5$ cm; (d) $h = 8.4$ cm.	90
52	Fig. 6.14	Contours of scour holes at equilibrium for eccentricity $e = 3b$ for flow depth (a) $h = 11.6$ cm; (b) $h = 10.5$ cm; (c) $h = 9.5$ cm; (d) $h = 8.4$ cm.	91
53	Fig. 6.15	Scour affected zones around piers after the experimental run for eccentricity $e = 2.75b$ with flow varying depths at (a) $h = 11.6$ cm; (b) $h = 10.5$ cm; (c) $h = 9.5$ cm; (d) $h = 8.4$ cm.	92
54	Fig. 6.16	Contours of scour holes at equilibrium for eccentricity $e = 2.75b$ at flow depths (a) $h = 11.6$ cm; (b) $h = 10.5$ cm; (c) $h = 9.5$ cm; (d) $h = 8.4$ cm.	93
55	Fig. 6.17	Scour affected zones around piers after the experimental run for eccentricity $e = 2.5b$ with flow depths (a) $h = 11.6$ cm; (b) $h = 10.5$ cm; (c) $h = 9.5$ cm; (d) $h = 8.4$ cm.	94
56	Fig. 6.18	Contours of scour holes for equilibrium at eccentricity $e = 2.5b$ at flow depths (a) $h = 11.6$ cm; (b) $h = 10.5$ cm; (c) $h = 9.5$ cm; (d) $h = 8.4$ cm.	95
57	Fig. 6.19	Scour affected zones around piers after experimental run at eccentricity $e = 2.25b$ with flow depths (a) $h = 11.6$ cm; (b) $h = 10.5$ cm; (c) $h = 9.5$ cm; (d) $h = 8.4$ cm.	96
58	Fig. 6.20	Contours of scour holes for equilibrium at eccentricity $e = 2.25b$ at flow depths (a) $h = 11.6$ cm; (b) $h = 10.5$ cm; (c) $h = 9.5$ cm; (d) $h = 8.4$ cm.	97
59	Fig. 6.21	Scour affected zones around piers after the experimental run for eccentricity $e = 2b$ with flow depths (a) $h = 11.6$ cm; (b) $h = 10.5$ cm; (c) $h = 9.5$ cm; (d) $h = 8.4$ cm.	98
60	Fig. 6.22	Contours of scour holes for equilibrium at eccentricity $e = 2b$ at flow depths (a) $h = 11.6$ cm; (b) $h = 10.5$ cm; (c) $h = 9.5$ cm; (d) $h = 8.4$ cm.	99
61	Fig. 6.23	Schematic diagram showing the entire section around the eccentric piers.	100
62	Fig. 6.24	Effect of lateral spacing on scour (a) planar area (b) surface area and (c) volume.	103
63	Fig. 6.25	Influence of lateral spacing on maximum scour length for (a) $V/V_c = 0.67$, $h/b = 1.65$, Fr = 0.20; (b) $V/V_c = 0.75$, $h/b = 1.5$, Fr = 0.23; (c) $V/V_c = 0.85$, $h/b = 1.35$, Fr = 0.27; (d) $V/V_c = 0.97$, $h/b = 1.2$, Fr = 0.32.	104
64	Fig. 6.26	Effect of lateral spacing on maximum scour width for (a) $V/V_c = 0.67$, $h/b = 1.65$, Fr = 0.20; (b) $V/V_c = 0.75$, $h/b = 1.5$, Fr = 0.23; (c) $V/V_c = 0.85$, $h/b = 1.35$, Fr = 0.27; (d) $V/V_c = 0.97$, $h/b = 1.2$, Fr = 0.32.	105
65	Fig. 6.27	Effect of lateral spacing on scour planar area in the entire section for (a) $V/V_c = 0.67$, $h/b = 1.65$, Fr = 0.20; (b) $V/V_c = 0.75$, $h/b = 1.5$, Fr = 0.23; (c) $V/V_c = 0.85$, $h/b = 1.35$, Fr = 0.27; (d) $V/V_c = 0.97$, $h/b = 1.2$, Fr = 0.32.	107
66	Fig. 6.28	Effect of lateral spacing on scour volume in the entire section for (a) $V/V_c = 0.67$, $h/b = 1.65$, Fr = 0.20; (b) $V/V_c = 0.75$, $h/b = 1.5$, Fr = 0.23; (c) $V/V_c = 0.85$, $h/b = 1.35$, Fr = 0.27; (d) $V/V_c = 0.97$, $h/b = 1.2$, Fr = 0.32.	108
67	Fig. 6.29	Effect of lateral spacing on deposition (a) planar area (b) surface area and (c) volume.	110
68	Fig. 6.30	Effect of lateral spacing on scour planar area in the entire section for (a) $V/V_c = 0.67$, $h/b = 1.65$, Fr = 0.20; (b) $V/V_c = 0.75$, $h/b = 1.5$, Fr =	111

		0.23; (c) $V/V_c = 0.85$, $h/b = 1.35$, Fr = 0.27; (d) $V/V_c = 0.97$, $h/b = 1.2$, Fr = 0.32.	
69	Fig. 6.31	Effect of lateral spacing on deposition volume in the entire section for (a) $V/V_c = 0.67$, $h/b = 1.65$, Fr = 0.20; (b) $V/V_c = 0.75$, $h/b = 1.5$, Fr = 0.23; (c) $V/V_c = 0.85$, $h/b = 1.35$, Fr = 0.27; (d) $V/V_c = 0.97$, $h/b = 1.2$, Fr = 0.32.	112
70	Fig. 6.32	Comparisons of scour depths between single pier and eccentric pier arrangements for (a) $V/V_c = 0.67$, $h/b = 1.65$, Fr = 0.20; (b) $V/V_c = 0.75$, $h/b = 1.5$, Fr = 0.23; (c) $V/V_c = 0.85$, $h/b = 1.35$, Fr = 0.27; (d) $V/V_c = 0.97$, $h/b = 1.2$, Fr = 0.32.	115
71	Fig. 7.1	Schematic diagram of the significance of scour parameters.	118

LIST OF TABLES

Sl No.	Table No.	Topic	Page No.
1	Table 1.1	Pier shape factor (Shukur and Obeid, 2016).	15
2	Table 1.2	Classification of local scour processes at bridge piers (Ettema et al., 2011).	21
3	Table 2.1	Comparative review of literatures on eccentric piers.	38
4	Table 2.2	Pier arrangement, experimental conditions in different flume sizes used in previous literatures and present study.	44
5	Table 2.3	Functional parameters used in literatures to develop equations to estimate maximum scour depth around the eccentric pier arrangement.	47
6	Table 3.1	Experimental conditions adopted based on literatures review.	51
7	Table 3.2	Flow parameters set to carry out experiments.	52
8	Table 3.3	Setting the gap between piers for the present study adopted based on literatures.	53
9	Table 3.4	Parameters kept constant during the present study.	55
10	Table 3.5	Parameters varied during the present study.	55
11	Table 3.6	List of parameters set for each experiment.	56
12	Table 3.7	List of parameters set for single pier experiments.	56
13	Table 4.1	Sieve analysis data obtained from laboratory experimentation.	63
14	Table 5.1	The classification of parameters that affect the local scour mechanism in MLT system.	67
15	Table 6.1	Experimental outcomes based on all the experiments of single pier and eccentric pier arrangements.	75
16	Table 6.2	Experimental outcomes based on grid data of scour shown in contour graphs.	101
17	Table 6.3	Experimental outcomes based on grid data of deposition shown in contour graphs.	108
18	Table 6.4	Percentage change of scour depths with respect to the single pier.	113
19	Table 6.5	Scour geometry after overall experimental analysis.	115

NOMENCLATURES

The following notations have been used in the present study:

A	–	wetted area, Bh [L^2];
A_p	–	planar surface area of equilibrium scour hole [L^2];
A_s	–	scour surface area [L^2];
Al	–	parameter describing the alignment of the pier [-];
b	–	pier diameter [L];
B	–	width of flume [L];
H	–	height of flume [L];
d_{st}	–	scour depth measured at any instant from initial bed level [L];
d_{sf}	–	temporal scour depth at front/inline pier [L];
d_{sr1}	–	temporal scour depth at rear/eccentric pier [L];
d_{sr2}	–	temporal scour depth at eccentric in lined pier [L];
d_{se}	–	equilibrium scour depth at an isolated single pier [L];
d_{50}	–	median diameter of sand [L];
D_*	–	dimensionless particle parameter [-];
E	–	Percentage change of scour depth w.r.t single pier [-];
e	–	lateral distance between the front and eccentric-pier [L];
f	–	function symbol [-];
Fr	–	Froude number of flow, $V/(gh)^{0.5}$ [-];
$Fr_{d_{50}}$	–	densimetric Froude number, $V/(\Delta g d_{50})^{0.5}$ [-];
Fr_t	–	threshold/critical Froude number [-];
g	–	gravitational acceleration [LT^{-2}];
h	–	approaching flow depth [L];
K	–	parameter [0.95-1.78] [-];
L	–	maximum length of sediment transportation of a single pier [L];
l	–	longitudinal spacing between eccentric piers [L];
l_d	–	diagonal distance between the eccentric piers [L];
l_x	–	maximum length of overlapping area after each experimental run [L];
M	–	length of the flume [L];
Q	–	discharge [L^3T^{-1}];
Q_c	–	critical discharge [L^3T^{-1}];
R	–	hydraulic radius, $bh/(b+2h)$ [L];
Re	–	flow Reynolds number, Vh/v [-];
Re_p	–	pier Reynolds number, Vb/v [-];
Re_{*c}	–	critical shear flow Reynolds number, $u_{*c}Re/v$ [-];
Sh	–	parameter describing the shape of pier [-];
S	–	centre-to-centre spacing between the staggered piers [L];

S_o	–	bed slope of flume [-];
s	–	relative density of sand, ρ_s/ρ_f [-];
T	–	pier position factor [-];
t	–	Run duration of each experiment [T];
t_e	–	time to reach equilibrium scour [T];
t^*	–	equilibrium time scale, Vt_e/b [-];
V	–	depth-averaged approaching velocity, Q/A [LT^{-1}];
V_c	–	critical velocity of water [LT^{-1}];
V_a	–	armour velocity [LT^{-1}];
u_*	–	shear velocity [LT^{-1}];
u_{*c}	–	critical shear velocity [LT^{-1}];
u	–	time-averaged velocity in the y-direction [LT^{-1}];
U	–	time-averaged velocity vector, $\sqrt{(u^2 + w^2)}$ [LT^{-1}];
v	–	time-averaged velocity in the z-direction [LT^{-1}];
w	–	maximum scour width of overlapping area [L];
x, y, z	–	cartesian coordinates [L].

Greek symbols

ρ_f	–	mass density of fluid [ML^{-3}];
ρ_s	–	mass density of sand [ML^{-3}];
τ_o	–	average bed shear stress [$ML^{-1}T^{-2}$];
τ_{oc}	–	critical bed shear stress on the horizontal bed [$ML^{-1}T^{-2}$];
σ_g	–	geometric standard deviation, $(d_{84}/d_{16})^{0.5}$ [-];
ν	–	kinematic viscosity [L^2T^{-1}];
Θ_c	–	critical Shields parameter [deg.];
φ_r	–	angle of repose [deg.];
α	–	pier alignment angle [deg.];
β	–	correction factor for alignment of the pier [-];
$\forall$	–	volume of equilibrium scour hole after each experimental run [L^3];
Δ	–	sediment density ratio, s - 1 [-].

GLOSSARY

Armour (armouring): Surfacing of the channel bed, banks, or embankment slope to resist erosion and scour. (a) natural process whereby an erosion- resistant layer of relatively large particles is formed on a streambed due to the removal of finer particles by streamflow; (b) placement of a covering to resist erosion.

Bed material: Material found in and on the bed of a stream (May be transported as bed load or in suspension).

Median diameter: The particle diameter of the 50th percentile point on a size distribution curve such that half of the particles (by weight, number, or volume) are larger and half are smaller (d_{50}.).

Sediment or fluvial sediment: Fragmental material transported, suspended, or deposited by water.

Subcritical and supercritical flow: Open channel flow conditions with Froude number less than and greater than unity, respectively.

Vortex: Turbulent eddy in the flow generally caused by an obstruction such as a bridge pier or abutment (e.g., horseshoe vortex).

CHAPTER-1

SCOURING

1.1 Introduction

An alluvial river bed is subject to continuous change. Flowing water erodes, transports and deposits sediment in the river, altering its bed elevation and adjusting its boundaries. Changes in bed elevation may be due to natural causes or by the activities of man which lead to changes in the river bed or river geometry, scour around bridge piers is just one example of the many different effects resulting from human interference with the river. Scour holes created by the flow of water past bridge piers are a major cause of the failure of bridge pier foundations. There are several separate processes which can lead to a change of bed elevation at a bridge site.

Local scour around piers is the main cause of the destruction of many bridges inside rivers. An estimate of the maximum possible scour around a bridge pier is necessary for its safe design. It has been observed that in the free surface flow around a bridge pier, horseshoe vortices are formed and the turbulence is intensified in front of, around and behind the piers. In addition, a uniquely shaped scour hole on the loose bed around a pier is observed. Experimental studies have found that both the flow and the sediment transport processes during the scour hole development are highly complex. Another aspect of this pier scour is that the sediments are transported downstream. Much effort has gone into trying to understand the mechanisms of scour and developing methods of predicting the depth of scour. Yet even today new bridges still fail as a result of excessive scour.

While knowledge of scour should now be sufficient among hydraulic and bridge engineers and methods of estimating scour in sands and gravels subject to a given flow are reasonably well developed, it is still the case that estimation of the likelihood of occurrence of scour in a real river situation is difficult. Where scour is likely to occur to an extent, that could endanger the foundations of a bridge, adequate prevention and protection must be considered.

Due to geotechnical and economic reasons, bridge designs often lead to complex piers or pier groups, in which case the direct application of the results derived from single piers may be problematic. Besides, rapid urbanization and increased traffic volume cause a need for the construction of new bridges next to the existing ones, thereby creating problems of pier interference. Sometimes a pier of the new bridge is positioned downstream eccentrically concerning the pier of the existing old bridge. It is like a two-pier arrangement with the rear pier placed eccentrically concerning the front pier. One such example is at Kolkata City of

West Bengal State in India, where a new bridge, namely Nivedita Setu, was constructed in 2007 just downstream of an old existing bridge named Vivekananda Setu (constructed in 1931). There must be the influence of the pier of one bridge onto another if the bridges are constructed closely to each other. The developed horseshoe vortex of the eccentric rear pier comes in contact with the developed wake vortex of the front pier. The combined strength of both vortices increases the scour hole around the rear pier, thereby increasing the rate of sediment transport. The suitability and efficiency of this kind of natural phenomenon with a particular reference to the enhancement of scour may also be explored to use it as an alternative to self-dredging. Figure 1.1 shows photographs of a single circular bridge pier structure compared to the eccentric circular bridge pier structure.



Fig 1.1. Photographs of a **(a)** single circular bridge pier structure compared to the **(b)** eccentric circular bridge pier structure.

In many small channels, it is observed that due to the deposition of sediments, the depth of the channel reduces significantly. This in turn makes it non-navigable. Hence if the sediments could be shifted to one side of the bank of the small channel, it may help in navigation. Bank erosion generally occurs in curves of the meandering parts of river channels, where the interaction between the vertical gradient of the velocity and the curvature of the flow generates a so-called secondary or spiralling flow.

In this study an attempt has been made to check whether the sediments could also be transported on one side of the pier i.e. the aim is to make the scour more importantly the dune downstream, to be nonsymmetrical.

1.2 Scour

Scouring is a natural phenomenon caused by the flow of water in rivers and streams. It is the consequence of the erosive action of flowing water, which removes and erodes material from the bed and banks of streams and also from the vicinity of bridge piers and abutments. Scouring occurs naturally as part of the morphologic changes of rivers and as the result of man-made structures.

Scour can either be caused by the normal flow or flood flow. Normal flow cannot make a big scour, but during a peak flow in which the flow velocity is higher the normal flow and make a big scour hole.

Scour can occur under certain flow conditions. Due to scour, bed materials are washed away from the surrounding area of the pier or abutment from the natural level of the bed.

1.3 Why be concerned about scour?

If sediment or rock on which the bridge supports rest is scoured by a river, the bridge could become unsafe for travel. In 1987, the Interstate Highway Bridge over Schoharie Creek in New York State collapsed during a flood (Fig. 1.2). After this accident, the Federal Highway Administration required every State to identify highway bridges over water which is likely to have scour problems and to identify bridges where scour is severe. The collapse of the Jahu bridge is also one of the examples of Indian bridge failure (Fig. 1.3). This is an important link road which serves and connects three districts Mandi, Bilaspur and Hamirpur. This Point is considered as the centre of Himachal Pradesh. On August 11, 2007 and August 12, 2007, due to heavy rain, the concrete bridge collapsed. Then within two years, the government constructed a new bridge over the site. But again on August 14, 2014, the steel bridge also collapsed due to soil erosion/ scouring from the foundation. Local scour around the bridge abutment is one of the most critical causes of bridge failure. Knowledge of bridge sites where scour is a potential problem will enable the States to monitor and improve conditions at these bridges ahead of time before they become dangerous.



Fig. 1.2. Photograph of Schoharie Creek in New York State bridge collapsed in 1987 due to scouring during a flood.



Fig. 1.3. Photograph of Jahu bridge (Himachal Pradesh in India) that collapsed in 2007 due to scouring during heavy rain (Rajendran, 2019).

1.4 Classification of scours

Scouring occurs naturally as a part of the morphologic changes of rivers and as the result of manmade structures. Generally, any hazard may cause the scour in the river bed. Scour criteria are involved with physical conditions pertaining to the threshold of motion for the material. This threshold point of incipient motion can be determined by the universally famous Shields diagram. Scouring is a natural phenomenon, but the types of scouring can be classified depending on the location and sediment transport capacity of the rivers and streams. Scour can be classified into two major types namely general scour and localized scour. Some subdivisions of scour are shown in Fig. 1.4.

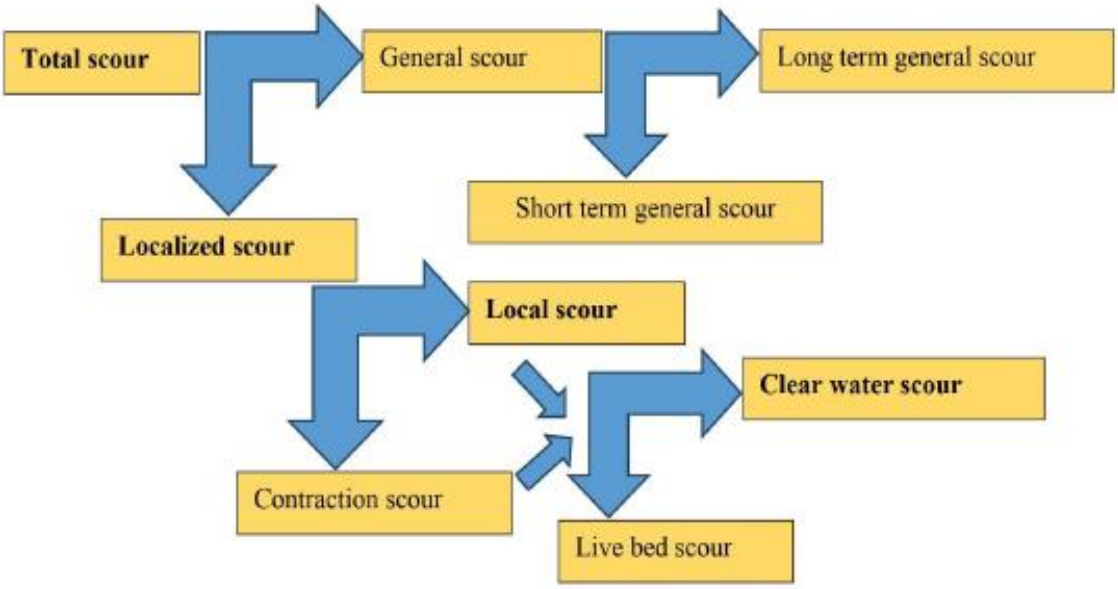


Fig. 1.4. Classification of scour (Melville and Coleman, 2000).

1.4.1 General scour

According to Melville and Coleman (2000), general scour deals with the changes in river beds due to natural or human induced causes. Because of the general scour, the overall longitudinal profile of the river channel is lowered. It occurs through a change in the flow regime in the river system resulting in general degradation of the bed level. General scour occurs irrespective of the existence of the bridge, and it can occur as either long-term scour or short-term scour. Short-term scour is because of a single flood or several closely spaced floods. On the other hand, long-term scour has a considerably extensive time scale (i.e. several years longer), and it includes progressive degradation and lateral bank erosion.

1.4.2 Localized scour

As suggested by Melville and Coleman (2000), localized scour is a collective term of contraction scour and local scour, and they are directly attributable to the existence of the bridge. When the river flow approaches the bridge, it usually converges causing a constriction of flow. Because of this contraction, the flow accelerates to the narrowest section (vena contracta). The flow then decelerates and the live river expands beyond the vena contracta to defuse gradually into the full downstream width of the channel. The accelerated flow induces scour across the contracted section. This scour is referred to as



Fig. 1.5. Photograph of local scour.

contraction scour. On the other hand, when the flow approaches hydraulic structures such as bridge piers, abutments, spurs and embankments, there is a formation of interference between structures and the flow. This also causes acceleration of the flow around the structures resulting in the removal of bed material from around piers, abutments, spurs and embankments. This scour is termed local scour (Fig. 1.5). Local scour and its control are the subject of interest in the present study. Therefore, it is necessary to understand the mechanism of local scour and the influencing factors.

Chiew and Melville (1987) identified two main classifications of local scour at piers based on the mode of sediment transport by the approaching stream, namely clear-water scour and live bed scour. These classifications depend on the ability of the flow approaching the bridge to transport bed material.

According to Brandimarte et al. (2012), by comparing the mean velocity upstream of the bridge, V, with the critical velocity, V_c, of the d_{50} bed material, scour conditions will be:

- Clear water = $V/V_c \leq 1$;
- Live-bed = $V/V_c > 1$.

1.4.3 Clear water scour

Clear water scour occurs when the bed material upstream of the scour hole is not in motion. Therefore, no replenishment of the scour hole takes place. The bed shear stress away from the scour hole will be equal to or less than the critical or threshold shear stress (the shear stress above which bed particles will begin to be set into motion by the flow) of the bed material. With clear water scour, the depth of the scour hole continues to increase until equilibrium is reached, i.e., when the combination of the temporal mean bed shear stress and the turbulent agitation near the bed is no longer able to remove bed material from the scour hole. Figure 1.6 refers schematic diagram showing the boundary/key points selected around the pier to determine scour contours.

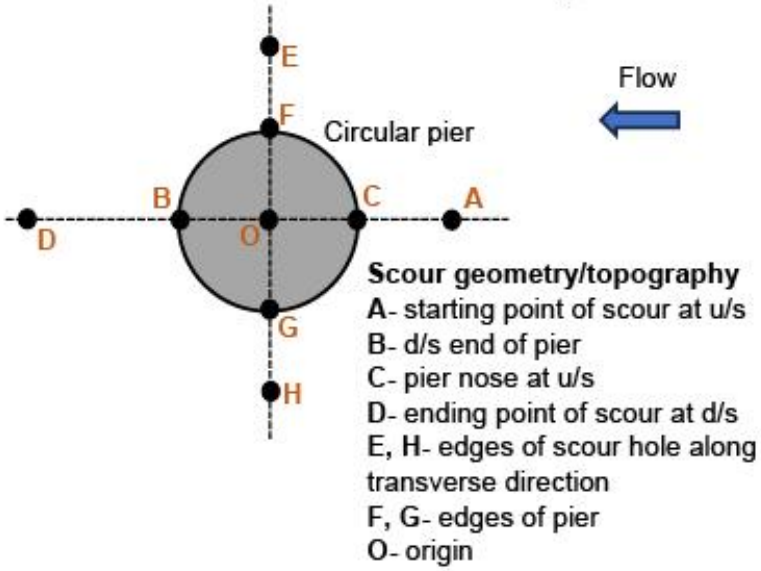


Fig. 1.6. Schematic diagram showing the boundary/key points selected around the pier to determine scour contours.

1.4.4 Live bed scour

Live bed scour occurs when sediment moves from both upstream and downstream of the scour hole. In the case of live bed scour, the bed shear stress is larger than the critical shear stress of the bed material. Bed forms develop with live bed scour on the channel bed. Equilibrium scour depth in live bed scour is reached when the time average amount of sediment entering the scour hole is equal to the time average amount of sediment leaving the hole.

Figure 1.7 shows the two types of scours and the equilibrium scour depth, in which the depth of the scour is presented as a function of time. It is clear from the figure that the equilibrium scour depth for clear water scour is approached asymptotically while for the live bed scour, there are non-periodic oscillations about equilibrium scour depth. According to Shen et al. (1969), the equilibrium scour depth in live-bed condition is less than in clear-water condition by 10%.

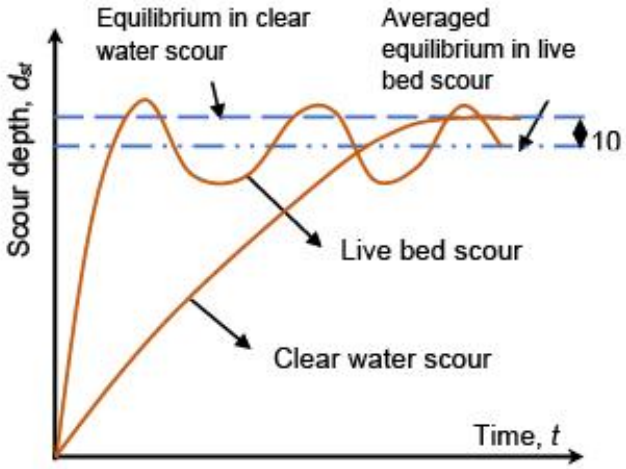


Fig. 1.7. Time evolution of scour depth in clear water and live bed conditions.

1.5 Local scour mechanism

The boundary layer flow past a circular pier undergoes a three-dimensional separation. This separated shear layer rolls up along the obstruction to form a vortex system in front of the element which is swept downstream by the river flow. Viewed from the top, this vortex system has the characteristic shape of a horseshoe and is thus called a horseshoe vortex (Fig. 1.7). The formation of the horseshoe vortex and the associated downflow around the cylindrical pier results in increased shear stress and hence a local increase in sediment transport capacity of the flow. This leads to the development of a deep hole (scour hole) around the circular pier, which in turn, changes the flow pattern causing a reduction in shear stress by the flow thus reducing its sediment transport capacity. The temporal variation of scour and the maximum depth of scour at bridge elements therefore mainly depend on the characteristics of flow, pier and river-bed material. The formation of the horseshoe vortex and the associated downflow cause scour at the circular pier, abutment and spur dike. The basic mechanism creating the loca1 scour around a bridge pier has been identified as the system of vortices which develops around the pier. The strength and size of the vortex system depend on the 'bluffness' of the pier. In order to understand the scour mechanism around a bridge pier, it is necessary to understand the flow field around piers. According to Ettema (1980), a flow field is a class of junction flow, which is characterized by the interaction of three-

dimensional turbulence structures. As reported by Melville and Coleman (2000), the principal features of the flow field at a bridge pier are down-flow at the upstream side of the pier, the horseshoe vortex at the base of the pier, the surface roller at the upstream side of the pier and wake vortices downstream of the pier. The vortices have been separated into components identified as:

1.5.1 Horseshoe vortex and downflow

- Horseshoe vortex is a common flow pattern observed in the vicinity of bridge piers during scour.
- The flow separates at the upstream face of the pier as it travels by the side of the pier, creating a vortex trail, termed the horseshoe vortex (Fig. 1.8).
- The approaching velocity profile along the vertical depth decreases downward and has a maximum at the free surface and zero at the bed. It causes a decrease in the stagnation pressure in the downward direction at the upstream face of the pier and consequently, the downflow is developed (Khaple et al., 2017).
- The downward flow of water near a bridge pier is due to the presence of the pier itself. This downward flow can intensify scour by increasing the velocity of water and the erosion of sediment around the pier. Understanding the dynamics of downflow is essential in predicting and mitigating bridge pier scour.
- The process of digging by the downflow along with the slant bed erosion continues until a quasi-equilibrium state is reached. In this state, the dynamic angle of repose is 10-20% greater than the angle of repose of sediment in still water.
- The primary horseshoe vortex, formed upstream of a circular pier, is the prime agent responsible for scouring over the entire process of scouring (Das et al., 2013*a*).
- This vortex can significantly increase the rate of sediment erosion around the pier, leading to scour, which can compromise the stability of the bridge.

1.5.2 Wake vortex

- Wake vortices form at the downstream side of piers and are the result of flow separation at the sides of the pier (Fig. 1.8) called cast-off vortices by Raudkivi (1986), these have vertical axes. One vortex develops on one side, sheds away, and is moved to the downstream. Immediately, other forms on the other side, finally shedding also.
- The wake vortices dissipate as they move downstream.
- The wake vortex takes place a major role along with the horseshoe vortex for multiple pier configurations (Das et al., 2013*b*).
- Wake vortex scour will be enhanced greatly when two wake streams intersect. The wake vortices get weaker when they come closer to the centerline of flow. Because the shedding of wake vortices develops alternately from the two sides of the cylindrical pier, an alternating lateral force is produced which decreases gradually when comes closer to the centerline (Das et al., 2013*b*).

- The scour can be caused by two streams of wake vortices from adjacent piers intersecting downstream. The vortices that result from the two conflicting velocity fields create local scour. At one bridge, the scour is enhanced by the vortices that occur at the confluence of the main and side channels. This is known as confluence scour.

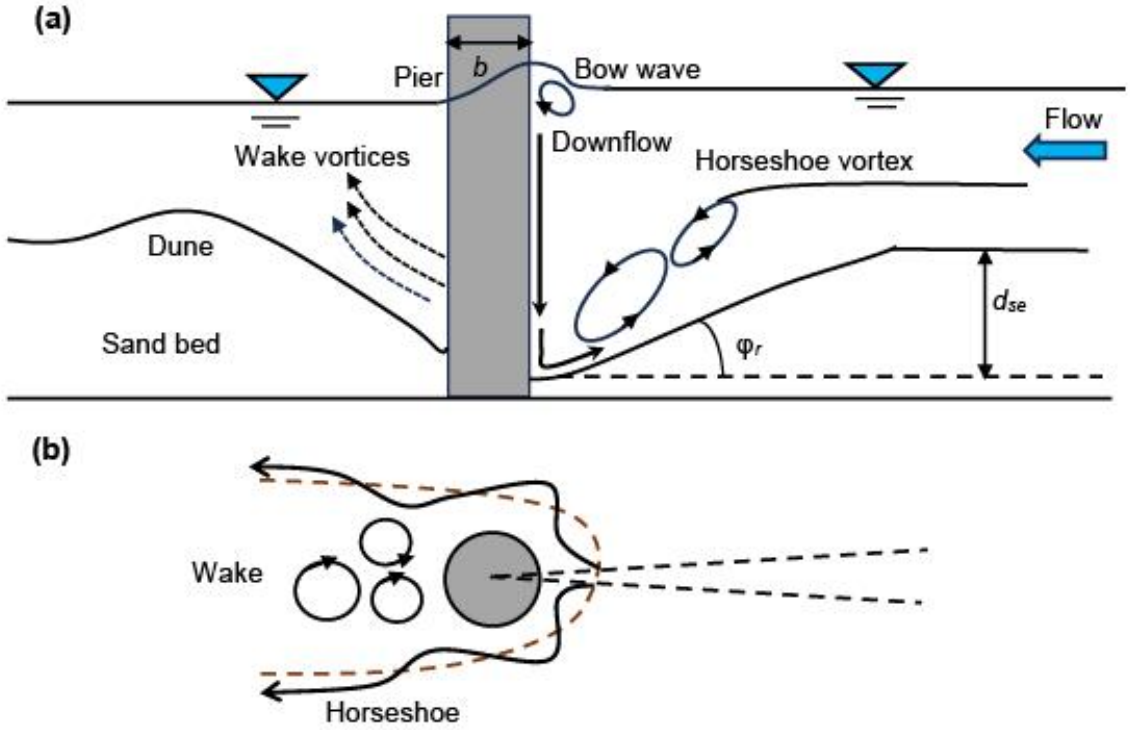


Fig. 1.8. Schematic diagrams of flow structures around circular pier showing **(a)** side view and **(b)** top view.

1.5.3 Bow wave

- Bow wave, formed at the free surface adjacent to the pier face rotating in a direction opposite to that of the horseshoe vortex, becomes pertinent in relatively shallow flow and reduces the downflow velocity.
- A bow wave is formed due to obstruction to the flowing stream at the upstream free surface adjacent to the pier and it rotates in the opposite direction of the horseshoe vortex. The bow wave is rather innocent, not participating as a scouring agent (Khaple et al., 2017).

1.6 Sediment transport

When the average shear stress on the bed of an alluvial channel exceeds the critical tractive stress for the bed material, the particles on the bed begin to move. The total amount of sediment in motion (or the total sediment load) can generally be divided into two parts: the

bed load where the particles move essentially in contact with the stationary bed, and the suspended load where the particles are carried in suspension by the turbulent fluctuations of the flow. There are two conditions which determine the amount of sediment transported at a particular cross section of a stream. These are:

- The geology of the country upstream of the particular cross section under consideration, i.e. the supply of sediment.
- The ability of the water (the stream power) to transport the sediment.

The rate of sediment transport is dependent on the shape, size and density of the bed particles, and their placement among the surrounding particles. Transport as bed-load is the mode of transport of sediments where the sediment particles glide, roll or briefly jump, but stay very close to the bed, which they may leave very temporarily. The displacement of the particle is intermittent; as the random concept of the turbulence plays an important role.

The particles on the bed are called *bed load*. On the other hand, when the particles stay occasionally in contact with the bed and displace them by making more or less large jumps to remain often surrounded by fluid, the mode of transport is termed *suspended load*. This type of transport concerns relatively finer particles. However, the mode of transport of very fine particles is as *wash load*, where the particles are rarely in contact with the bed being washed through the zone of flow. The particles which are in the air beyond the water are called *saltation load*. A review on bed-load transport is available in Raudkivi (1998) and Chien and Wan (1999).

It is important to realize that the rate of sediment transport can be a function of time. In a natural alluvial stream, the sediment is rarely uniform. When the mixture of fine and coarse material is subjection to a relatively low flow velocity, the finer material will be transported downstream while the coarse material will remain intact. This phenomenon, if allowed to continue, will eventually lead to an accumulation of coarse particles on the surface of the bed. This layer of particles acts as a protective layer for the material underneath and is referred to as the "armour layer". Armouring can be viewed in terms of the distribution of the turbulent shear stress on the bed and that of resisting forces to movement. If the distribution of stresses acting on a particular area does not completely overlap the distribution of the critical resisting stresses of the sands on the surface of the same area (Fig. 1.9), armouring occurs. The armour layer will also affect the flow because the roughness of the surface increases.

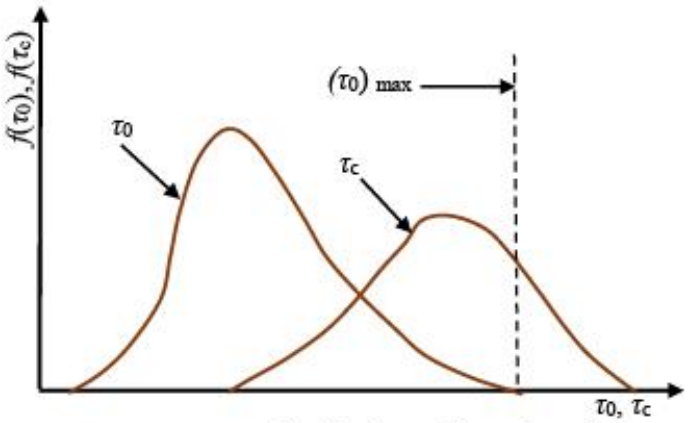


Fig. 1.9. Frequency distribution of boundary shear stress and critical shear stress illustrating the concept of armouring.

There are other processes which occur in sediment transport that will affect the structure of a stream bed, namely overpassing and embedment. Overpassing is described as the

transport of exposed particles over the immobile, often flatbed. The overpassing particles can be larger or smaller than the bed material. When overpassing a bed composed of smaller material, the larger particles move with a rolling or sliding action whereas the smaller overpassing particles saltate on the bed. Embedment is described as the burial of an overlying exposed sand in the bed material. The larger exposed sand causes the formation of a hole in front of itself and rolls forward into the hole to be buried in the sediment surrounding. To summarize the various forms of sediment transport, it is best to define them in the following manner:

If τ_o = the time average of the applied shear stress, τ_c = the critical shear stress of the bed material, τ_i = the minimum shear stress required to move a particular exposed sand on the surface of the bed then there are four possible conditions:

(a) $\tau_i > \tau_c > \tau_o$ and $\tau_c > \tau_i > \tau_o$ indicate no sand movement, the immobile bed;
(b) $\tau_o > \tau_c > \tau_i$ and $\tau_o > \tau_i > \tau_c$ indicate all sands are in motion;
(c) $\tau_i > \tau_o > \tau_c$ indicates embedment condition;
(d) $\tau_c > \tau_o > \tau_i$ indicates overpassing condition.

1.7 Parameters influencing local scour

Fluid parameters, flow conditions, stream bed materials and pier characteristics are the main variables affecting the pier scour phenomenon. Time of scour is also an important parameter for the given conditions of these variables. Parameters influencing the scouring phenomenon are listed as follows:

1.	***Parameters characterising the approach flow*:**	undisturbed mean velocity, depth of approach flow, flow intensity, shear velocity, velocity distribution, roughness and stream-bed slope
2.	***Parameters characterising the channel geometry:***	width and slope, cross-sectional shape
3.	***Parameters characterising the bridge pier:***	pier shape, size, number, orientation of the pier with respect to the main flow direction (i.e., angle of attack), surface condition and protection system
4.	***Parameters characterizing the fluid (water):***	temperature, gravitational acceleration, kinematic viscosity and density of fluid (water)
5.	***Parameters characterising the bed material:***	grain size distribution, mass density, median size and sediment fall velocity, particle shape, angle of repose and cohesiveness of the soil

6. ***Parameters characterising the time:*** time of scouring for an evolving scour hole

7. ***Parameters related to the unsteadiness of the flow:*** passage of a flood wave in rivers and waves in marine environment

According to Ettema et al. (2011), the framework of sets of parameters can be classified as primary and secondary parameters.

The *primary parameters* were directly related to the structure and geometric scales of the pier flow field, which determine the major part of the maximum scour depth. For example, h/b defines the geometric scale of the pier flow field in a vertical plane parallel and perpendicular to the streamwise and the transverse direction, respectively; b/d_{50} is related to the length scale of pier diameter and median particle diameter of the sediments; K_{sh} and K_{α} indicate the pier shape and angle of flow attack parameters.

The *secondary parameters* characterize scour-depth sensitivities within the geometric scale limit and normally lead to scour depths less than the potential maximum scour depth. The values of the secondary parameters are subject to considerable uncertainty at pier sites. The magnitudes of secondary parameters are prescribed by the primary parameters described above. V/V_c, $V/(gb)^{0.5}$, Vb/ν and Vt/b are the secondary parameters in which, V_c is prescribed by d_{50}, and Euler number $V/(gb)^{0.5}$ is related to the inertial force due to vortices. The term Vb/ν is the pier Reynolds number, which accounts for the vortex shedding behind the pier. The parameter Vt/b characterizes the temporal development of scour associated with the flow field and the foundation material. Detailed description of these parameters and their effects on the scour around bridge piers are presented in Section 1.8.

The relationship showing the influence of various parameters on temporal scour depth (d_{st}) increases over time t and can be a function of d_{st} (Eq. 1.1).

$$d_{st} = f\left(\rho_f, \nu, g, h, V, d_{50}, \rho_s, V_c, S_0, b, \alpha, e, \sigma_g, B, t, l, K_S, \beta\right) \tag{1.1}$$

1.8 Parameter influences

This section evaluates the known influences that individual parameters in Eq. (1.1) exert on scour, and points out knowledge gaps. Despite numerous studies aimed at describing the parameter influences of parameters, there remain significant gaps in the overall understanding of scour. The gaps are attributable to difficulties in conducting laboratory flume experiments at large geometric scales, isolating some of the parameter influences, and the large number of parameters influencing to be examined. Also, there is a paucity of reliable field data in certain parameter ranges.

Local scour around bridge piers is dependent on many parameters, most of which are interrelated. This means that the influence of one particular parameter on the depth of the scour hole may be eclipsed by that of the others. The large range of predicted and measured values of local scour depths at bridge piers, for what appear to be identical conditions, can

be explained by the effects of a variety of specific parameters. These include characteristics of the sediment, the flow and the geometry of the pier and the channel. Extensive investigations have been carried out to study the factors affecting the local scour depth around bridge piers by many researchers (Laursen and Toch, 1953; Ettema, 1980; Raudkivi and Ettema, 1983; Chiew, 1984; Melville and Sutherland, 1988; Melville and Coleman, 2000; Ettema et al., 2011). According to Ettema et al. (2011), most of the studies have aimed to describe the influences of different parameters on the scour around bridge piers, although still there are significant gaps in the overall understanding of the scour mechanism and the scour depth prediction.

1.9 Influence of dimensional parameters

Local scour around bridge piers is dependent on many parameters, most of which are inter-related. This means that the influence of one particular parameter on the depth of the scour hole may be eclipsed by that of the others. The large range of predicted and measured values of local scour depths at bridge piers, for what appear to be identical conditions, can be explained by the effects of a variety of specific parameters.

1.9.1 Pier diameter, *b*

One of the most influential variables on scour depth is the pier diameter, which is used extensively to normalize the scour depth enabling data from different piers to be collapsed onto one curve. This is because the scour depth increases almost linearly with the pier diameter according to Raudkivi and Ettema (1983). They found that the time to equilibrium scour depth increases with pier diameter because the scour hole volume is proportional to the cube of the pier diameter and hence larger piers have larger scour holes which take longer to erode. According to Franzetti et al. (2022), in the present study, we refer to circular piers because this is a reference condition for a number of possible variabilities to be taken into account by appropriate correction factors.

1.9.2 Approaching flow velocity, *V*

When discussing the relationship between ambient depth averaged velocity (V) and scour depth, it is important to differentiate between the clear water and live bed regimes. The use of a non-dimensional velocity parameter, V/V_c is known as flow intensity which describes the velocity condition with respect to the critical velocity (V_c) for the sediment and

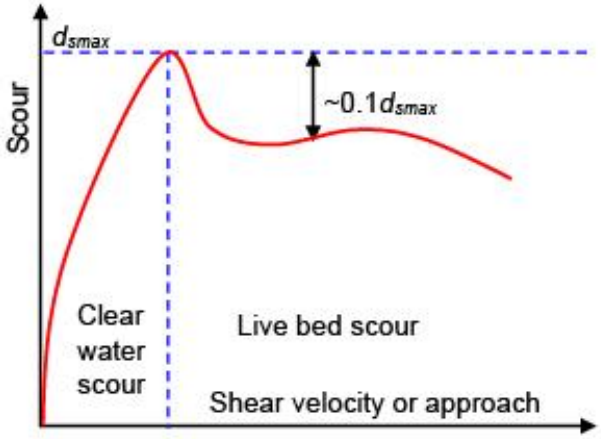


Fig. 1.10. Scour depth in terms of shear velocity or approach velocity.

distinguishes between the live bed and clear water regimes depending on whether the flow intensity is above or below 1. The use of flow intensity rather than flow velocity not only takes into account regime change but also enables data from different sediment sizes which have different critical flow velocities to be collapsed onto one curve. Some researchers prefer to normalize shear stress or shear velocity parameters with the corresponding critical value as these are the true drivers for scour, but the trends are essentially equivalent, and the velocity intensity parameter is more commonly used due to ease of measurement. Melville (2008), Chiew (1984), Raudkivi and Ettema (1983) and Raudkivi (1986) reported that the equilibrium scour depth increases almost linearly with flow velocity through the clear water regime (Fig. 1.10).

1.9.3 Sediment size, d_{50}

The size of sediment plays a significant role in bridge pier scour. Larger sediment particles are more likely to settle and accumulate around bridge piers, increasing the risk of scour. Smaller sediment particles, on the other hand, can be easily carried away by the flowing water, potentially reducing scour depth. However, small sediment can also fill in the gaps between larger particles, leading to a denser accumulation that may exacerbate scour. The specific effect depends on various factors, including flow velocity, sediment supply, and pier geometry. In non-cohesive sediment, erosion depends on factors such as grain size distribution, median size (d_{50}), sediment fall velocity and mass density. Laursen (1960) found that under clear-water scour conditions, maximum scour depth is affected by bed sediment size; however, live-bed scour is independent of sediment size.

1.9.4 Flow depth, h

The influence of flow depth on the scour depth has been discussed by many researchers (Melville and Chiew, 1999; Chabert and Engeldinger, 1956; Laursen and Toch, 1956; Breusers et al., 1977; Ettema, 1980). The presence of the pier in the channel causes a surface roller around the pier and a horseshoe vortex at the base of the pier. Flow depth affects local scour depth when the horseshoe vortex is affected by the formation of the surface roller (or bow wave) that forms at the leading edge of the pier. The two rollers, (i.e., the bow wave and the horseshoe vortex) rotate in opposite directions. In principle, as long as there is no interference between the two rollers, the local scour depth does not depend on the flow depth but depends only on the pier diameter. In such an instance, often called deep flow, the local scour is said to occur at narrow piers. As the flow depth decreases, the surface roller becomes relatively more dominant and causes the horseshoe vortex to be less capable of entraining sediment. Therefore, for shallower flows, the local scour depth is reduced. Subsequently, in a very shallow flow, the local scour is dependent on the flow depth and the local scour is said to occur at a wide pier.

1.9.5 Pier shape

Piers are constructed of various shapes. The most common shapes used are circular, rectangular, square, rectangular with chamfered ends, oblong, lenticular and Joukowski. Figure 1.11 shows a schematic illustration of some pier shapes and Table 1.1 shows the pier shape factor. The effect of pier shape has been reported by many researchers (Breusers, 1977; Breusers and Raudkivi, 1991; Melville and Coleman, 2000).

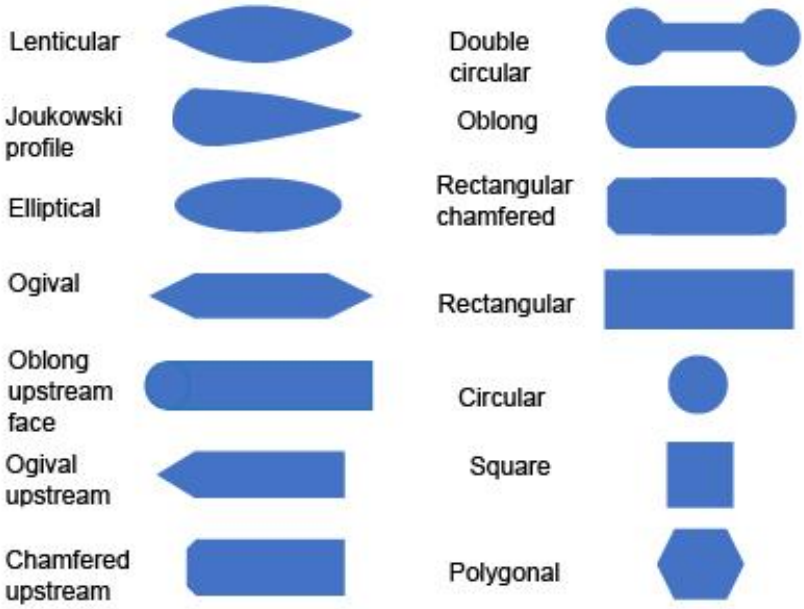


Fig. 1.11. Schematic illustrations of some common pier shapes.

The blunter the pier, the deeper the local scour has been the general conclusion. The shape of the downstream end of the pier is concluded to be of little significance on the maximum scour depth. The pier shape is often accounted for by using a shape factor. Melville and Chiew (1999) discussed shape factors for uniform piers that is piers having constant sections throughout their depth, was proposed. The local scour depths for a variety of different pier shapes all have the same projected width (140 mm). From the results, a circular pier produced the least scour while a rectangular pier having blunt ends produced the maximum scour.

Table 1.1. Pier shape factor (Shukur and Obeid, 2016).

Pier shape	Shape factor
Circular	1.00
Lenticular	0.80
Joukowski profile	0.88
Oblong	0.85
Rectangular	1.11
Streamlined	0.48
Elliptical	0.80
Chamfered	1.01

1.9.6 Effect of pier alignment, α

The pier alignment is also referred to as the angle of flow attack, representing the angle between the longitudinal axis of the bridge pier and the flow direction. According to Melville and Coleman (2000), the depth of local scour for all shapes of the pier, except circular, is strongly affected by the angle of flow attack, α. This effect is shown in Fig. 1.9 in which it is clear that an increase in the angle results in an increase in the scour depth. The multiplying factor, K_α, as shown in Fig. 1.12 is recommended to be used in most of the existing pier scour equations. The projected width of the pier is increased with the increment of the angle of flow attack; hence, the scour depth is also increased. Melville and Coleman (2000) further reported that if the angle of flow attack is zero, there is no effect of the length of the pier on the scour depth, whereas if the angle of flow attack deviates from zero i.e. the pier is skewed to the flow, the pier will experience a substantial effect. It was supported by an example that for a rectangular pier of aspect ratio eight, the scour depth is nearly tripled at an angle of flow attack of 30° when compared to the same pier with $\alpha = 0°$.

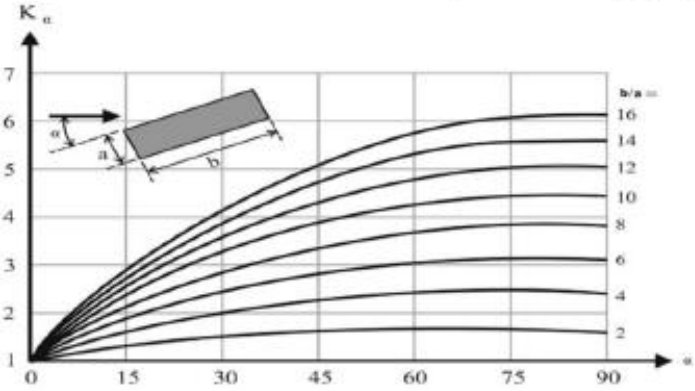


Fig. 1.12. Variation of local scour depth with pier alignment (Melville and Coleman, 2000).

According to Breusers and Raudkivi (1991), the scour depth is a function of the projected width of the pier, where the projected width is the width of the pier normal to the flow. They further suggested that the effect of the angle of flow attack could practically be ignored for its value up to 5° to 10°. Ettema et al. (2011) reported that due to the influence of some parameters such as h/b and b/d_{50}, as discussed in the previous sections, the scour depth may not increase with an increase in the projected width. The effect of h/b and b/d_{50} on scour depth may vary with the angle of flow attack, affecting the projected width of the pier obstructing the flow. Although the effects of the angle of flow attack, flow depth and mean grain size of the sediment are connected, recent studies on the prediction of

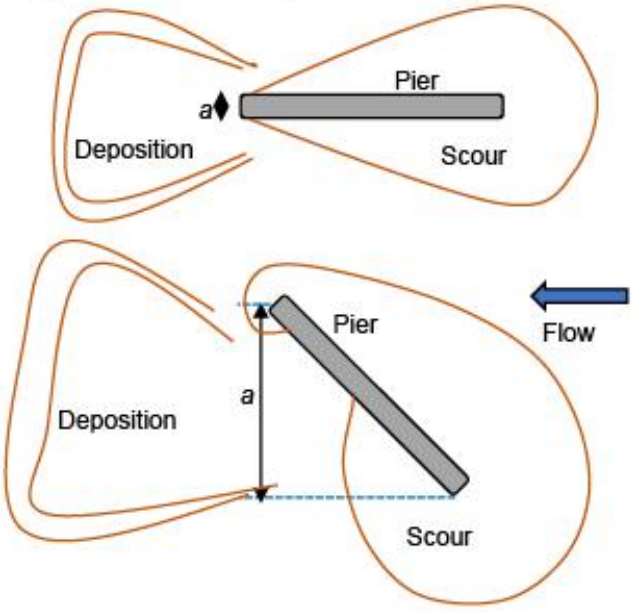


Fig. 1.13. Diagrammatic scour shapes at a pier aligned with the flow and another angled to the flow direction.

scour depth have accepted them as mutually independent parameters. Figure 1.13 shows diagrammatic scour shapes at a pier aligned with the flow and another angled to the flow direction.

1.9.7 Angle of repose, φ_r

The angle of repose, also referred to as the angle of friction, is an engineering property of granular materials. The angle of repose is the maximum angle of a stable slope determined by friction, cohesion and the shapes of the particles (Fig. 1.14). When bulk granular materials are poured onto a horizontal surface, a conical pier will form. The internal angle between the surface of the pier and the horizontal surface is known as the angle of repose and is related to the density, surface area, and coefficient of friction of the material. Material with a low angle of repose forms flatter piers than material with a high angle of repose. In other words, the angle of repose is the angle a pier forms with the ground.

The angle of repose is the steepest angle at which the surface of a mass of loose particulate matter is made with the ground. The angle of repose is affected by the size, mass, angularity, and dampness of the particles, and by the force of downward acceleration, but it is consistent for a given material. Knowing the angle of repose of a material in various circumstances is vital for engineers and landscapers. It is the maximum angle of slope at which sand, loose rock, etc. will remain in place without sliding, as on a hillside.

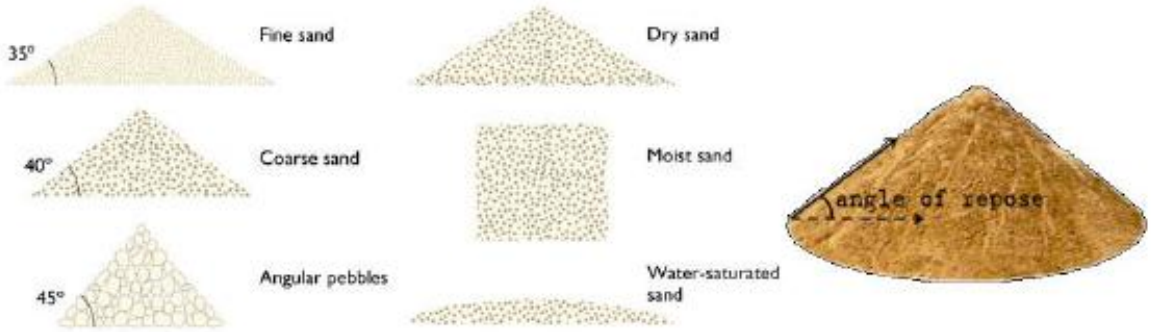


Fig. 1.14. Angle of repose.

1.9.8 Effect of time, t

Temporal variation of local scour depth has been extensively studied in the past by a number of investigators (Ettema, 1980; Melville and Chiew, 1999; Oliveto and Hager, 2002; Oliveto and Hager, 2005; Kothyari et al., 2007). The most common conclusion from the previous studies is that the process of scouring is asymptotic. Ettema et al. (2011) reported that the local scour rate and equilibrium scour depth under clear water and live bed conditions are different. The conceptual illustration of the time development trend of scour depth is presented in Fig. 1.7 which shows that for clear water scour conditions, asymptotic development of scour depth occurs towards the equilibrium condition. While, under live bed conditions, the equilibrium scour depth is reached more quickly and thereafter the scour depth oscillates due

to the passage of bed materials past the piers. Hence, in most of the cases for the scour under live bed conditions, the time development of scour depth is not of major significance.

Chabert and Engeldinger (1956) assumed that equilibrium occurs when the scour depth does not change "appreciably" in time. Ettema (1980) reported that there are three distinct phases of the scour process. He named them as the initial phase, principal phase and equilibrium phase. These phases are as follows:

1. The initial phase is characterized by rapid scouring due to the downflow at the pier's upstream face; the horseshoe vortex does not play an important role and the sediment transport starts at the sides of the pier;
2. The principal phase is dominated by the horseshoe vortex action; during this phase, scour occurs in a narrow strip around the pier. As the scour hole develops, the strength of the horseshoe vortex and the downflow gradually become unable to remove sediment from the entrainment zone;
3. The equilibrium phase is reached when no further "significant" development in the scour hole exists.

1.9.9 Densimetric Froude Number, Fr_{d50}

A particle densimetric Froude number is an alternative criterion to predict hydraulic conditions for the initiation of bed sediment motion. The densimetric Froude number is defined as $Fr_{d_{50}} = V/(g'd_{50})^{0.5} = V/(\Delta g d_{50})^{0.5}$ where g is the acceleration due to gravity and the reduced gravity $g' = g\,(\rho_s - \rho_f)/\,\rho_f = g(s\text{-}1) = g\Delta$.

The theoretical critical value is unity, therefore, if $Fr_{d_{50}} > 1$, no saline wedge will form. In practice, values of $Fr_{d_{50}}$ as well as 0.6 to 0.7 prevent the formation of a saline wedge. Therefore, for the condition $Fr_{d_{50}} < 0.6$, a salt wedge will form (Nandi, 2019).

1.10 Influence of non-dimensional parameters

This may be due to the difficulties in conducting laboratory flume experiments on large geometric scales or the insufficiency of reliable field data. Melville and Coleman (2000) provided comprehensive publications explaining the factors affecting the scour at bridge piers.

1.10.1 Effect of sediment non-uniformity, σ_g

The sediment non-uniformity is characterized using the geometric standard deviation, σ_g, of the sediment particles. Geometric standard deviation as $\sigma_g = (d_{84}/d_{16})^{0.5}$. Melville and Coleman (2000) reported that a number of experimental studies were also carried out for the non-uniform sediment under live bed conditions by Ettema (1976) and Chiew (1984). The experiment was conducted at the threshold motion condition for the sediment used. From these studies, it can be concluded that the rate of scouring and the equilibrium scour depth decreases as the value of σ_g increases. Furthermore, it was reported that for a non-uniform sediment material, around the threshold condition, $V/V_c \approx 1$, armouring occurs at the base of

the scour hole, leading to a considerable reduction of local scour depth. The effect of non-uniformity is minor for the higher values of V/V_c when the flow is capable of entraining most of the sediment particles. At intermediate values of V/V_c, the effect of sediment non-uniformity reduces with increasing flow velocity between these two limits because of which the grains are transported by the flow. This trend is clearly shown in Fig. 1.15, which summarizes the data schematically in a broader context for the effect of flow intensity, V/V_c, on the local scour depth.

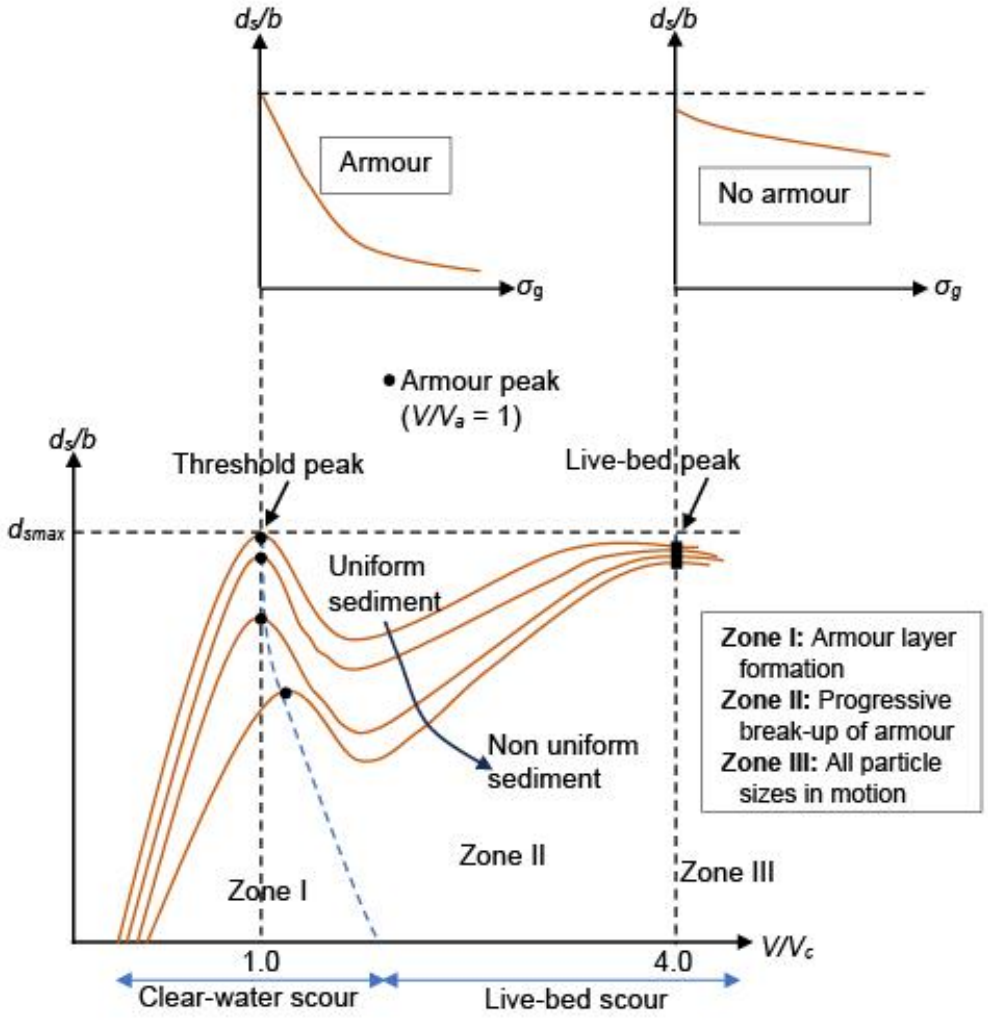


Fig. 1.15. Local scour depth variation with flow intensity and sediment non-uniformity.

1.10.2 Effect of flow intensity, V/V_c

Melville and Coleman (2000) defined the flow intensity as the ratio of the free stream flow velocity, V, to the critical flow velocity of the sediment, V_c. Based on the flow intensity, the local scour at piers can be classified as local scour under the clear water condition and local scour under the live bed condition. Clear water scour occurs for the velocities up to the threshold condition, i.e. $V/V_c \approx 1$. In this condition, there is no supply of sediment to the scour hole; movement of the sediment materials occurs only around the obstruction like bridge

piers. However, in the live bed scour condition, sediment is continuously supplied to the scour hole from the upstream side. In live bed scour condition, the ratio V/V_c is greater than 1.

Under clear-water conditions, the local scour depth in uniform sediment increases almost linearly with velocity to a maximum at the threshold velocity. The maximum scour depth is called the threshold peak. As the velocity exceeds the threshold velocity V_c, the local scour depth in uniform sediment first decreases and then increases again to a second peak, these changes being relatively small, but the threshold peak is not exceeded providing the sediment is uniform. The second peak occurs at about the transition flatbed stage of sediment transport on the channel bed and is termed the live-bed peak. The variation of scour depth at piers with flow intensity is schematically presented in Fig. 1.16.

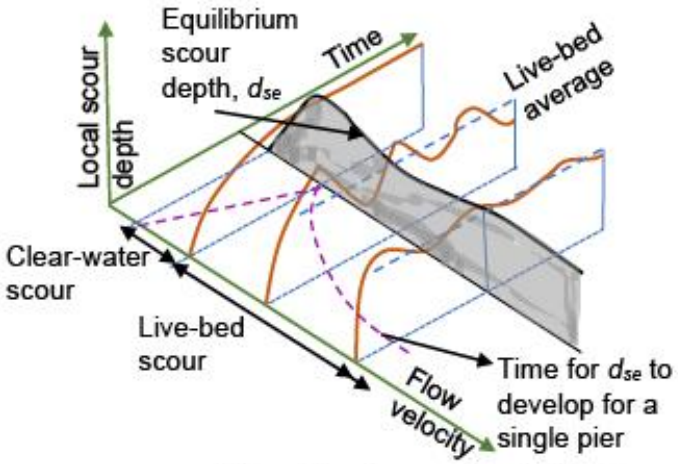


Fig. 1.16. Variation of local scour depth with flow velocity and time.

1.10.3 Effect of flow shallowness, *h*/*b*

According to Raudkivi (1998), the scour depth is independent of the depth of flow when it is greater than three times the pier diameter. He further reported that a decrease in flow depth results in an increase in the surface roller (bow wave) which interacts with the downflow and reduces its strength. The parameter flow shallowness, h/b represents the effect of depth of flow in relation to the width of the pier. Based on the h/b ratio. Ettema et al. (2011) classified scour processes in three different categories as shown in Table 1.2. The laboratory data were used to define the functional relationship, $d_s = f(b,h)$, describing the effect of flow shallowness on the local scour depth. For a narrow pier or deep flow i.e. the large flow depth compared to the width of the pier, the scour depth is directly proportional to the width of the pier and is independent of the flow depth. Conversely, for the shallow flow or wide pier case, the depth

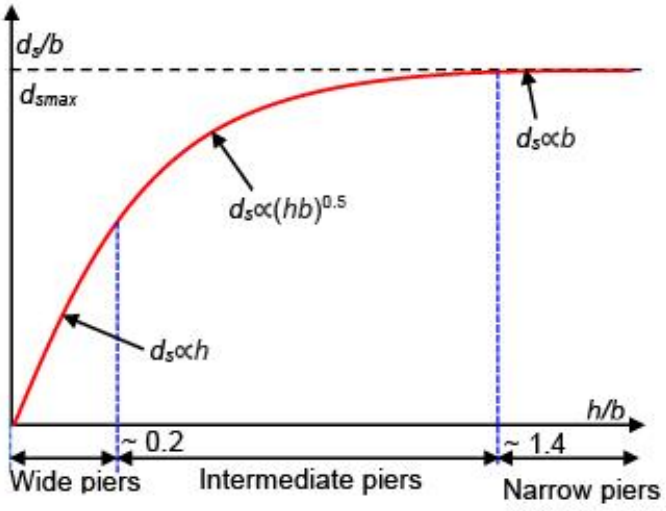


Fig. 1.17. Local scour depth variation with flow shallowness.

of scour is directly proportional to the depth of flow and independent of the pier width. For the intermediate depth of flow, the scour depth depends on both the depth of flow and the diameter of the pier (Fig. 1.17).

Table 1.2. Classification of local scour processes at bridge piers (Ettema et al., 2011).

Pier class	Flow shallowness	Local scour dependence
Narrow	$h/b > 1.4$	$d_s \propto b$
Intermediate/transitional	$0.2 < h/b < 1.4$	$d_s \propto (bh)^{0.5}$
Wide	$h/b < 0.2$	$d_s \propto h$

1.10.4 Effect of Froude number, Fr and Reynolds number, Re

According to Ettema et al. (2006), Froude number [Fr = $V/(gb)^{0.5}$] and pier Reynolds number (Re = Vb/v) are the turbulence structure parameters based on which the energy associated with turbulence structure and frequency of vortex shedding were characterized. Ettema et al. (2006) suggested that the scour depth at the pier does not increase linearly with pier width unless there is complete similitude of pier, flow and sediment particles. This non-linearity results in a deeper scour hole relative to a pier scour depth in a laboratory flume. They suggested that the Reynolds number in terms of viscosity is insignificant on scour depth. However, Reynolds number influences the frequency of shedding. They further showed that the Froude number could describe the energy gradient for flow around piers. The narrower the pier size, the larger the Froude number, and hence the lesser the scour depth. Another study by Ettema et al. (2006) defined the correction factor that could be used to account for the Froude number effect in laboratory scale experiments. Figure 1.18 shows the variation of scour depth with the Froude number.

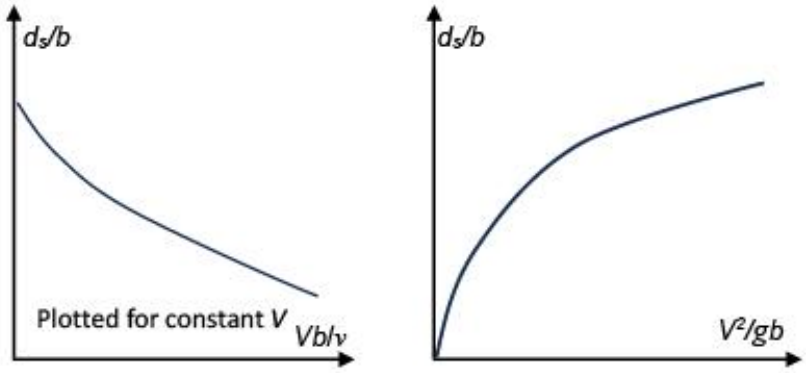


Fig. 1.18. Local scour depth variation with large-scale turbulence.

1.10.5 Effect of sediment coarseness, b/d_{50}

The parameter b/d_{50} represents the relative coarseness of the flow boundary. According to Melville and Coleman (2000), for uniform sediments, local scour depths are unaffected by coarseness. However, the larger sediment size affects the local scour depth. If the value of sediment coarseness ratio, b/d_{50} is less than 50, local scour depth is influenced by sediment

size. The relation between the sediment coarseness ratio and the local scour depth is clearly shown in Fig. 1.19.

Raudkivi and Ettema (1983) subdivided sediment coarseness into four groups:

1. $b/d_{50} \geq 130$**:** The sediment is fine relative to the pier diameter. The sediment is entrained from the groove by the downflow and from the slope by the horseshoe vortex until equilibrium is reached.

2. $130 > b/d_{50} \geq 30$**:** The sediment is of an intermediate size. The sediment is entrained mainly from the groove with only limited entrainment under the horseshoe vortex. The supply of sediment to the groove is accomplished by sliding down the slope.

3. $30 > b/d_{50} \geq 8$**:** The sediment is coarse relative to the pier diameter and relative to the downflow. A significant proportion of the energy of the downflow is dissipated in the coarse bed material at the base of the scour hole.

4. $b/d_{50} < 8$**:** The stones are so large that the erosion phase does not develop. The scour is mainly due to the entrainment at the flanks of the pier.

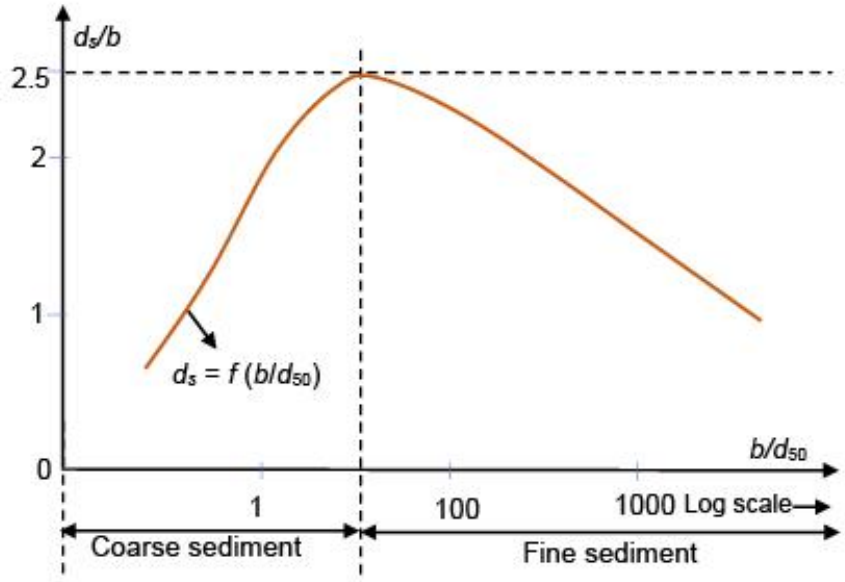


Fig. 1.19. Effect of sediment coarseness on local scour.

Breusers and Raudkivi (1991) reported that when the mean grain size of sediment, $d_{50} < 0.7$ mm, there was the formation of ripples on the bed and for the sediment size of $d_{50} > 0.7$ mm ripples did not develop. A flatbed cannot be maintained for $d_{50} < 0.7$ mm under the clear water flow condition due to the development of ripples with a small amount of sediment transport taking place. This will replenish some of the sand scoured at the piers. Hence, local scour under the clear water flow condition cannot be maintained for ripple-forming sediment.

Ettema et al. (2011) reported that for uniform sediment, local scour depths are affected by sediment coarseness when the sediment is either relatively large or small (Fig. 1.18). The smaller the value of the sediment coarseness ratio, the larger the particle size. Hence, the scouring is reduced as the rough and porous bed dissipates some of the energy of the down-flow. It is suggested that when the value of the sediment coarseness ratio, b/d_{50}, is less than 8, sediment particles are very large relative to the size of the pier. In this case, the scouring is mainly due to erosion at the sides of the pier. Hence, there is a reduction in the scour depth.

1.10.6 Effect of blockage ratio/contraction ratio, *B/b*

The equilibrium depth of local scour at a pier is affected by the contraction ratio. For experimental investigations, the width of an experimental fume should be at least eight times the pier size for clear water scour conditions so that blockage effects are minimized. For live-bed scour, the fume width should be at least 10 times the pier size for scour depths not to be reduced due to bed features being modified as they propagate through the constriction (Raudkivi and Ettema, 1983; Chiew and Melville, 1987; Ballio et al., 2009; Ashtiani, 2012).

1.11 Equilibrium scour depth, d_{se}

Since the early stages of research on scouring, it has become clear that the equilibrium scour depth is the condition at which there is no further movement of bed material from the scour hole. Chabert and Engeldinger (1956) suggested that equilibrium scour occurs when the scour depth does not change appreciably with time. According to Ettema (1980), there are three phases of the scour process the last phase is an equilibrium phase, where the scour depth does not increase anymore. However, Coleman et al. (2003) suggested that an equilibrium scour hole may continue to deepen at a relatively slow rate. Researchers have different opinions regarding the time to reach the equilibrium scour depth. For example, researchers such as Melville and Chiew (1999) and Coleman et al. (2003) defined time to equilibrium as the time at which the rate of scour reduces to 5% of the pier diameter or abutment length in 24 hours. Ettema (1980) defined the time to equilibrium scour as the time at which no more than 1 mm of incremental scour can be realized within a timeframe of four hours. Furthermore, Melville and Coleman (2000) suggested that for small-scale laboratory experiments of clear water scour depth development at bridge foundations, the time to achieve the equilibrium conditions should be several days. It is reported that the data obtained after less time, say 10 to 12 hours, can exhibit scour depths less than 50% of the equilibrium scour depth.

1.12 Temporal variation of scour depth, d_{st}

As suggested by Breusers et al. (1977) and Melville and Chiew (1999), the local scour depth under the clear water condition reaches to equilibrium state asymptotically with time and hence time to develop an equilibrium scour depth may be infinite. However, in the live bed scour condition, the scour depth reaches the equilibrium condition much more quickly and it oscillates in response to the translation of bed features. Due to the complexity of the scour process, the prediction of the maximum scour depth within a given time frame is very difficult. To overcome this inherent difficulty, a new definition for time to equilibrium is used here. Thus, t_e is defined as the time at which the scour hole reaches its equilibrium depth, d_{se}. Here, the rate of increase of scour does not exceed 5% of the pier diameter in the succeeding 24 h period.

1.13 Scour at pier groups

Due to the interaction and interference of flow and sediment transport processes, scour patterns, depths, and extents at pier groups might differ from single pier formations. Therefore, distances and alignments of the piers are additional key factors influencing the scour process. In addition to the local scours at single piers, global scour formation around the entire structure may occur due to local obstruction, flow constrictions, and further turbulence generation, leading to larger scour depths with deepest local scours typically formed at the edge corners of a pier group. Figure 1.20 shows a schematic diagram of the flow pattern and local scour around eccentric pier arrangements.

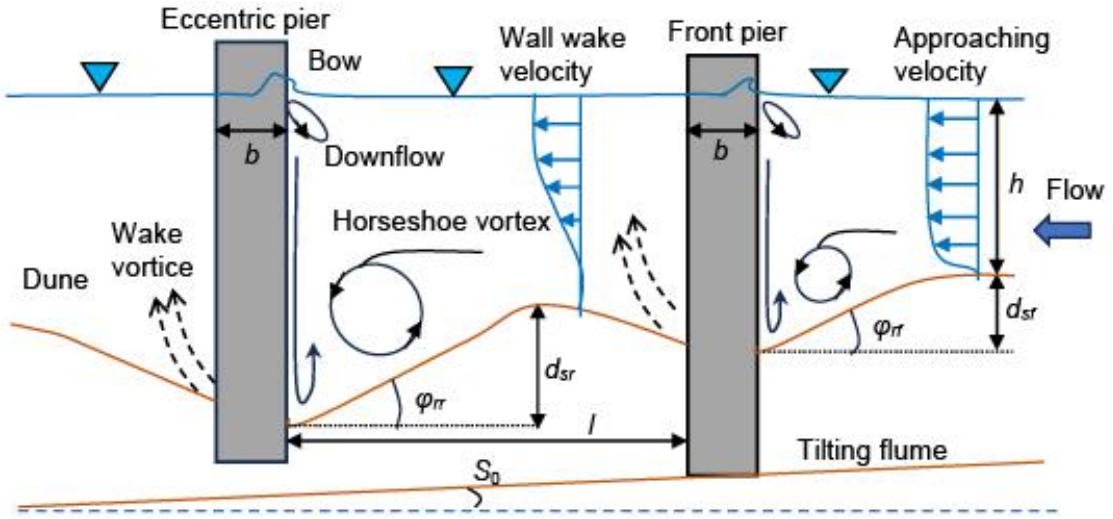


Fig. 1.20. Schematic diagram of flow pattern and local scour around two eccentric piers.

Four of the mechanisms that affect scour at pier groups are not present in scouring at a single pier. These mechanisms are described below:

1.13.1 Reinforcing

- It causes increased scour depths at the front pier and is a consequence of the dynamic equilibrium which exists in the base of a scour hole when stable conditions have been reached.
- A downstream pier be so placed that the scour holes overlap, and then the bed level is lowered at the rear of the upstream scour hole. It is thus easier for the flow to remove bed material from this hole and it deepens.
- Overlapping scour holes reduce the exit slope and the level of the bed in the scour hole around the upstream pier. Thus, the required energy to move the bed materials is decreased.
- As pier separation increases, the reinforcing effect decreases and disappears when the maximum bed level between the piers returns to the undisturbed bed level.

- The strength of reinforcing depends on the distance between the upstream and downstream piers and the eccentric angle. The intensity of reinforcing decreases by increasing the distance between piers and changing the eccentric angle from 0° to 90°.

1.13.2 Sheltering

- The presence of an upstream pier can cause a reduction of the effective approach velocity for downstream piers. This reduction decreases the effect of the horseshoe vortex and thereby reduces scour at downstream piers.
- A second form of sheltering occurs if material scoured from the upstream pier is deposited on the bed in front of the downstream pier. Flow is then deflected upward from the bed and around the downstream pier. The strength and thus the effectiveness of the horseshoe vortex at this pier is thereby reduced.
- As the pier separation increases, the velocity deficit in the wake of the upstream pier disappears and the sheltering effects become negligible.
- Similar to reinforcing, the occurrence of sheltering and its effect on the level of the scour depth depends on the distance between the upstream and downstream piers.

Figure 1.21 shows (a) regions affected by overlapping scour and (b) a schematic diagram showing the overlapping of scour between eccentric piers in the present study (Exp. 11). Figure 1.22 shows the (a) regions affected by individual scour and (b) schematic diagram of individual scour around eccentric piers for the Exp. 5 of the present study.

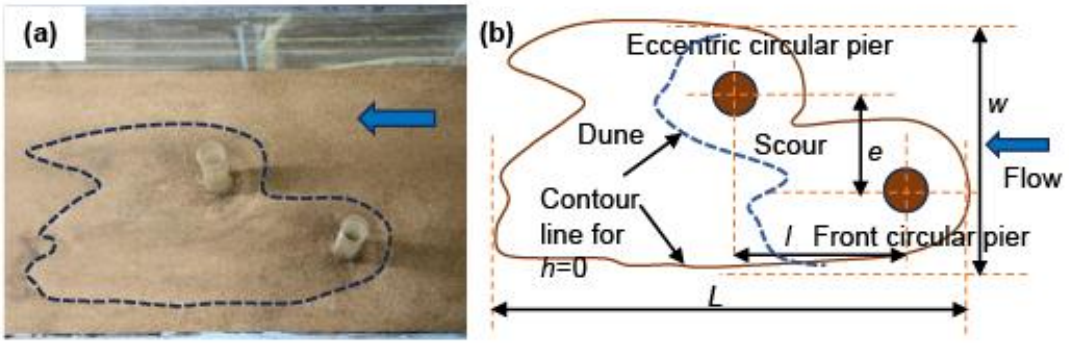


Fig. 1.21. (a) Regions affected by overlapping scour and **(b)** Schematic diagram showing overlapping of scour between eccentric piers in the present study (Exp. 11).

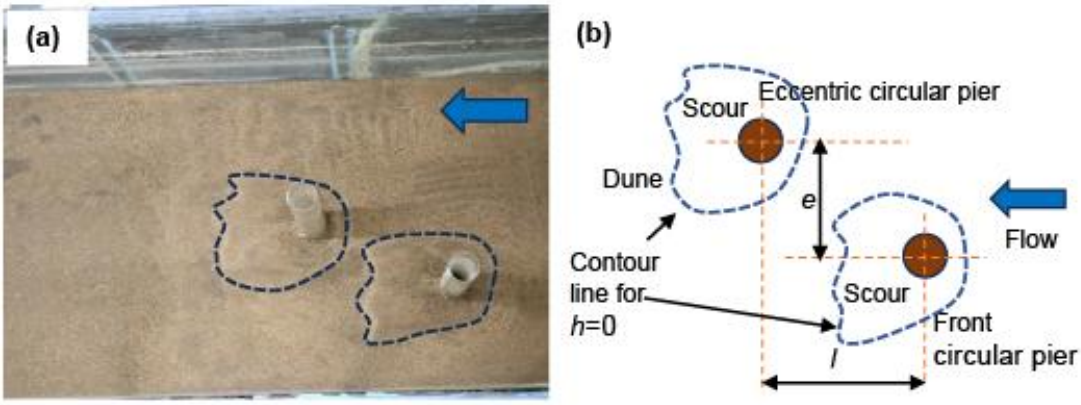


Fig. 1.22. (a) Regions affected by individual scour and **(b)** Schematic diagram showing individual scour around eccentric piers in the present study (Exp. 5).

1.13.3 Shed vortices

- Vortices shed from an upstream pier are convected downstream following paths as followed by a single pier. A second pier should be placed close to one of these paths, the vortices, by virtue of their velocity and pressure distributions, assist in lifting material from the scour hole.
- The scouring potential of the shed vortex is a function of the intensity of its convection speed and of the distance between the path and the elected pier. These effects, therefore, decrease more rapidly for piers in line with the flow than for those at angles of attack for downstream piers on the paths traced by vortices shed by upstream piers.
- The scour depth at a pier may increase if the pier is placed in the path of vortices shed from an upstream pier. The scouring potential of these vortices depends on the flow velocity and position of the downstream pier.
- The volume of removed bed materials by shed vortices depends on the strength of velocity and pressure distribution.

1.13.4 Compressed horseshoe vortex

- An increase in scour depth will occur when two or more piers are placed transverse to the flow and in close proximity to each other.
- When piers are placed transverse to the flow, each will have, except at very close spacing, its own horseshoe vortex.
- As the pier spacing is decreased, the inner arms of the horseshoe vortices are compressed. This causes velocities within the arms to increase with a consequent increase in scour depths.
- This effect will also occur for other (non-zero) angles of attack with its importance for any particular angle being strongly dependent on the pier spacing.
- In the tandem arrangement, the downstream pier is not on the path traced by the shed vortices. Thus, the power of the shed vortices in moving material is less than in staggered arrangements.

- By decreasing the distance between two piers, the horseshoe vortex is compressed and thereby the flow velocity will increase. Increased flow velocity prompts a growth in moving more bed materials around piers and therefore it increases the depth of the scour hole.

1.14 Two pier group

1.14.1 In line ($\alpha = 0°$)

- Figure 1.23 shows how the scour depths at each of the piers and the bed level between the piers depend upon the relative spacing l/b, where l is the distance between the centre lines of the piers and b is the pier diameter.
- For two piers ($l/b = 1$), the scour depth at the front pier is the same as for a single pier (d_{se}) but with increasing separation, the front pier experiences the reinforcing effect which reaches a maximum at $l/b = 2.5$ and is evident until $l/b = 11$. For larger spacings, the scour depth is the same as for a single pier. With three piers in line at equal spacings up to $l/b = 6$, the scour at the middle pier was deeper and at the third pier the scour was shallower than at the downstream pier of the two-pier group (Breusers and Raudkivi, 2006).

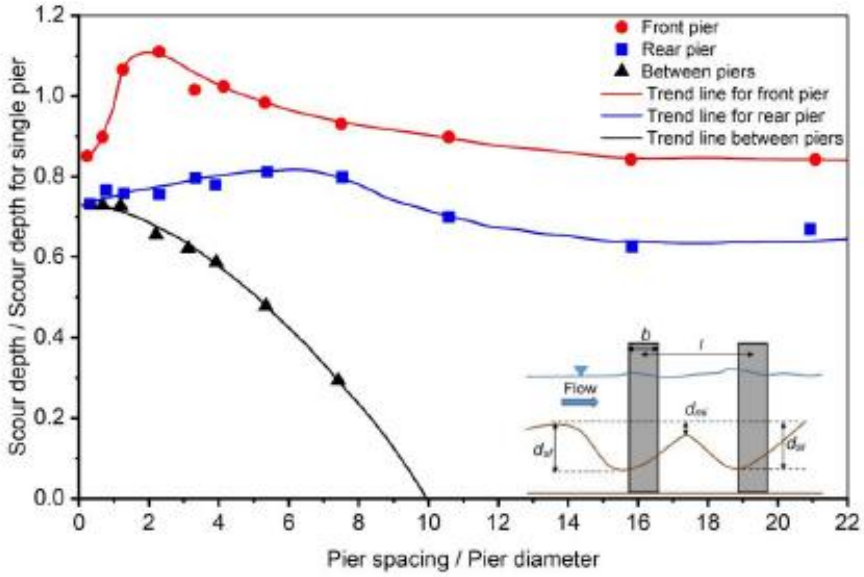


Fig. 1.23 Scour depths for two piers in line as a function of pier spacing (Breusers and Raudkivi, 2006)

1.14.2 Transverse ($\alpha = 90°$)

- Figure 1.24 shows the results of experiments in which two piers were set at right angles to the flow. Both piers caused scour to the same depth (±2 mm) and the results were averaged to define a single curve. The mid-distance scour is also shown in Fig. 1.24.
- For the twin pier, $e/b = 1$, the scour depth is $1.93d_{se}$. This result is in accordance with the concept of scour depth being proportional to the frontal width of the pier. The scour depth decreases rapidly with separation to $1.3d_{se}$, at $e/b = 1.5$, and with e/b greater than 8, the scour depth is essentially that of a single pier. The scour holes become separate entities at $e/b = 11$, and the bed midway between them regains its original level.
- At close spacing, ($e/b < 2$), the increased scouring results from the increase in elective pier diameter. At $e/b > 2$, separate horseshoe vortices form. Between the piers, these are compressed thus creating higher velocities and greater scouring potential. This effect reduces as e/b increases and reaches zero as $e/b = 8$ (Breusers and Raudkivi, 2006).

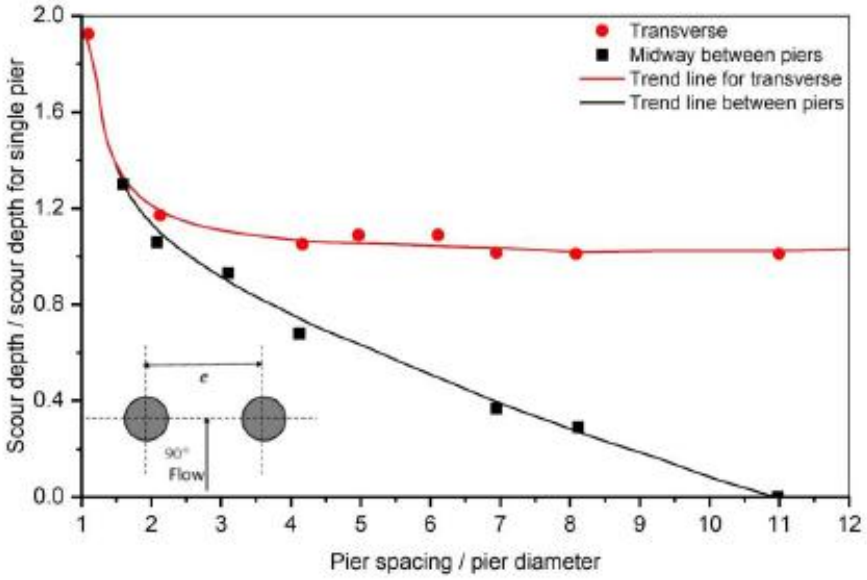


Fig. 1.24. Scour depths around two transverse piers represented as a function of pier spacing (Breusers and Raudkivi, 2006).

1.14.3 Non-aligned ($\alpha = 45°$)

- Figure 1.25 shows the results of experiments with two piers having their line of centres at 45° to the approach flow. The twin pier scour depth was $1.77d_{se}$. This was slightly more than would be suggested by a linear dependence of scour depth on frontal width, namely 1.71 times (Breusers and Raudkivi, 2006).
- Scour depth at the rear pier exceeded that at the front pier for all values at l_d/b between 1 and 11. At larger separations, the piers acted independently having scour depths

equal to that of a single pier and the bed level midway between the piers was unaffected. Increased depths at the rear pier were caused by a combination of the action of the shed vortices from the front pier and the compression of the horseshoe vortices between the two piers. These two processes overcame the sheltering effects (if any) and had their maximum influence at $l_d/b = 4$ where the difference between front and rear scour depths was a maximum.

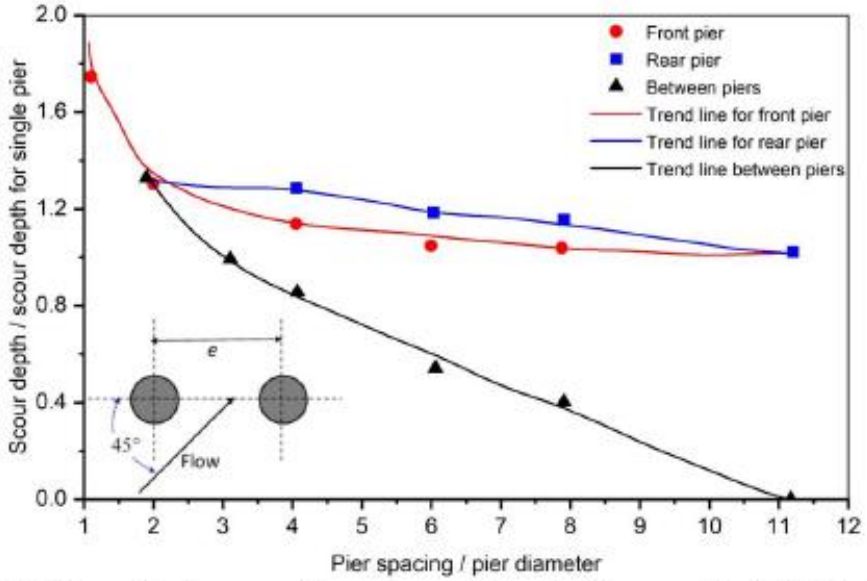


Fig. 1.25. Scour depths around two piers positioned with an angle of attack of 45° represented as a function of pier spacing (Breusers and Raudkivi, 2006).

1.14.4 Effect of angle of attack, α for two pier groups

- Experiments with $l_d/b = 5$ were done for $0° < \alpha < 90°$ at 15° intervals with the results shown in Fig. 1.26. Scour at the front pier was not very sensitive to the angle of attack varying by less than 5% of its value at $\alpha = 0°$. Scour depths at the rear pier are much more sensitive to changes in the angle of attack as the various scouring mechanisms, described above, come into effect.
- At small angles, ($\alpha < 15°$), the dominant effect at the rear pier is sheltering by the front pier. As the angle increases, sheltering is reduced and the pier is affected by shed vortices. Consequently, scour depths increase reaching a maximum (for $l_d/b = 5$) at approximately 45°. Scour depths reduce when the pier moves clear of the shed vortices and approaches that of a single pier as the angle of attack approaches 90° (Breusers and Raudkivi, 2006).

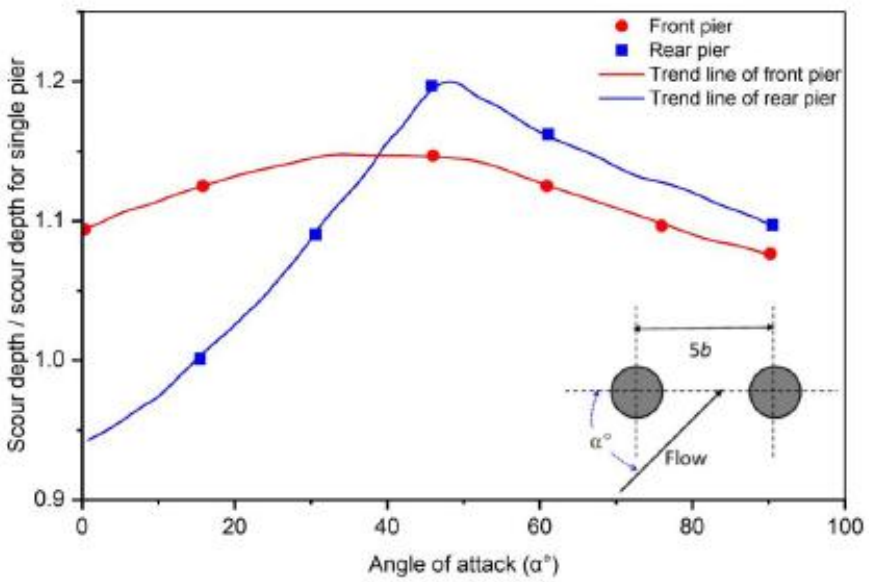


Fig. 1.26. The effect of angle of attack on scour depths at two piers spaced five pier diameters apart (Breusers and Raudkivi, 2006).

CHAPTER-2

LITERATURE STUDY

2.1 Literature review

A comprehensive literature review of bridge pier scour would involve examining a wide range of studies and publications related to the erosion of sediment around bridge piers. This review aims to summarize the current state of knowledge on bridge pier scour, including its causes, mechanisms, and effects on bridge stability. Key aspects to cover might include different types of scours (e.g., local scour, contraction scour, abutment scour), factors influencing scour depth (e.g., flow velocity, sediment characteristics, pier geometry), scour prediction methods, and scour countermeasures. The review would also identify areas where further research is needed to improve our understanding of bridge pier scour and enhance scour mitigation strategies.

2.1.1 Single pier

Scour is a natural phenomenon caused by the erosive action of flowing water on the bed and banks of alluvial channels. In coastal regions scour can also occur as a result of the passage of waves. At a bridge site scour of channel boundaries introduces the possibilities of a reduction in the support given to the bridge foundations or an abutment being undermined. Melville and Chiew (1999) investigated the temporal development of clear-water local scour depth at cylindrical bridge piers in uniform sand beds and presented that the scour depth after 10% of the time to equilibrium was between about 50% and 80% of the equilibrium scour depth, depending on the approach flow velocity. The relation between the depth of local scour at a bridge pier and its dependent parameters [flow intensity (V/V_c), flow shallowness (h/b), Euler number (V^2/gb) and Reynolds number (Vb/v), sediment coarseness (b/d_{50}), sediment non-uniformity (σ_g), time (t), pier shape (Sh), floating debris, pier alignment (Al), superstructure submergence] was discussed by Melville (2008). Scour has been a major concern for the safety of marine and hydraulic structures. Khwairakpam and Mazumdar (2009) reviewed a few previous studies related to scour with emphasis on the mechanism, prediction and reduction techniques of local scour around vertical piers. Das et al. (2012) performed clear water scour experiments to investigate the circulation characteristics of horseshoe vortex in the scour region around circular piers on a single circular pier with varying inflow depths, pier Reynolds numbers and densiometric Froude numbers. Das et al. (2013*a*) provided a study of turbulent flow characteristics of a wake vortex flow at a

cylindrical pier measured by ADV (Acoustic Doppler Velocimeter). The study of local scour around bridge piers is very important for the safe design of piers and other hydraulic structures. Das et al. (2013*b*) investigated clear water scour geometry around circular piers. Shukur and Obeid (2016) conducted an experimental study of bridge pier shapes with different velocities to minimize local scour depth around piers when other parameters remained the same. In the case of successive pier arrangements, the wake vortex of the upstream pier may influence the horseshoe vortex of the pier placed downstream. The formula for temporal scour depth prediction based on 57 years of literature laboratory data on isolated circular pier was developed by Nandi and Das (2023*b*). The comparison using four temporal scour depth formulas was analyzed by Nandi et al. (2024*a*). Nowadays machine learning models are also used for the prediction of maximum scour depth (Nandi et al., 2024*b*).

Raudkivi and Ettema (1983) conducted experiments on the clear-water local scour of cohesionless bed sediment at cylindrical piers. It was concluded that the equilibrium depth of local scour was related to the particle size distribution of the bed sediment, the mean particle size of the bed sediment, relative to the pier diameter, and flow depth relative to both the pier diameter and the mean particle size of the bed sediment. A formula for estimating the maximum depth of local scour was also proposed.

Melville and Chiew (1999) considered the temporal development of clear-water local scour depth at cylindrical bridge piers in uniform sand beds. An equilibrium time scale ($t^*= Vt_e/b$) and the equilibrium scour depth (d_{se}) were subjected to similar influences of flow and sediment parameters because they were inherently interdependent. Here, t^* is a function of flow intensity, flow shallowness, and sediment coarseness. The data were restricted to clear-water scour conditions, uniform sediments, and cylindrical piers. 80% of the equilibrium scour depth is developed in a time varying from only 5% to almost 40% of the time to equilibrium. The equilibrium depth of scour at a bridge pier under clear water conditions was approached asymptotically. Scour depths after 10% of the time to equilibrium varied between about 50% and 80% of the equilibrium depth.

Melville (2008) emphasised the relation between the depth of local scour at a bridge pier and its dependent parameters (flow intensity, flow shallowness, Euler number and Reynolds number, sediment coarseness, sediment non-uniformity, time, pier shape, floating debris, pier alignment, superstructure submergence). The parameters (V^2/gb) and (Vb/ν) were interpreted as expressing similitude in the energy and frequency of eddies shed from the pier. When $b/d_{50} < 8$ individual grains were so large relative to the pier that scour was mainly formed due to erosion at the sides of the pier and scour was further reduced. For the threshold condition, $V/V_c \approx 1$, armouring occurred on the approach flow bed and at the base of the scour hole. Under live-bed conditions, the equilibrium depth was reached more quickly than clear water scour conditions. Thereafter the scour depth oscillated due to the passage of bed features past the pier or abutment. The apparent limit to the influence of flow shallowness on t^* occurred at $h/b \sim 6$. The maximum value of t^* was about 2.5×10^6. For piers founded on a slab footing, caisson or pile cap, the footing, cap or caisson with the top below the general bed level could be effective in reducing the local scour depth through interception of the downflow. If the top of the wider foundation element came to the bed level, or even above, the scour depth was increased. The depth of local scour for all shapes of the pier, except circular, was found to be strongly dependent on the pier alignment to the flow. As the angle

increased, the scour depth increased because the effective frontal width of the pier was increased. Submergence of the superstructure led to an increase in the scour at the bridge foundations compared to that at an unsubmerged bridge.

Khwairakpam and Mazumdar (2009) analysed some literatures on scour with a focus on the mechanism, prediction and reduction techniques of local scour around vertical piers. Armour and flow alteration techniques could be categorised as controlling measures for scour at piers or piles. The average scour depth was found to be decreased by 51.1% in the case of threaded piles and by 61.6% in the case of splitter plates by disrupting the vortex shedding. The effectiveness of collars through studied and discovered that a combination of continuous collars found scour reduction of approximately 50% and 60% took place for the front and rear piers. By adopting different techniques, scour could be reduced up to approximately 60% as reported in the available literature.

Das et al. (2013*a*) carried out an experimental investigation of scour depth and velocity around a circular pier of different sizes with an ADV. Clear water scour experiments were performed on a single circular pier with varying inflow depths, pier Reynolds numbers, and densimetric Froude numbers. The flow was observed almost horizontal above the scour hole ($z > 0$), but it was downward close to the pier. The velocity was reversed within the scour hole in the vertical direction, forming a horseshoe vortex. The circulation decreased with the increase of flow shallowness and increased with the densimetric Froude number. It also increased with the pier Reynolds number at a constant densimetric Froude number, or at a constant flow shallowness. The relative vortex strength (dimensionless circulation) decreased with the increase of the pier Reynolds number.

Das et al. (2013*b*) analysed a study of wake vortex in the scour region around a circular pier. If piers were arranged eccentrically then the sediment movement may take place towards the flume wall along the downstream. The wake vortex played a major role along with the horseshoe vortex for multiple pier configurations. It was proposed that the suitability and efficiency of this kind of technique with particular reference to the enhancement of scour will be explored to use it as an alternative to the dredging mechanism. In this experimental study, the turbulent wake vortex flow within an equilibrium scour hole at a circular pier was measured by an ADV, and was presented with different pier diameters of 0.10 m, 0.075 m and 0.05 m. Results showed that the non-dimensional wake vortex circulation increased at $y = 0$ and ± 3 until the pier Reynolds number (Re_p) reached around 2.40×10^4 but then it decreased with a further increase in Re_p as the wake vortices were washed away due to a further increase of inertia force. A similar trend was observed when the circulation was non-dimensionalised at different pier diameters as well as at different nondimensional inflow depths. Wake vortex scour had little potential as it was downstream from the pier. The non-dimensional circulation increased with increasing pier diameter from 0.05 m to 0.075 m, but the same non-dimensional circulation decreased when the pier diameter further increased from 0.075 m to 0.10 m.

Das et al. (2014) presented an experimental investigation on a series of clear water local scour experiments of cohesionless bed sediment conducted in a tilting flume with a circular pier under different pier widths, densimetric Froude number, inflow depth and pier Reynolds number on a sand bed with a mean particle size 0.825 mm. It was observed that the entire scour geometry, that was, scour depth, length, width, area and volume were found to increase

with densimetric Froude number and relative inflow depth. When the pier diameter increased, approaching flow depth was constant, flow shallowness was found to be decreased while the densimetric Froude number increased.

Shukur and Obeid (2016) showed that the shape of the pier was the main factor for measuring the least scour depth. By reducing the scour depth and remaining the same with the other factors like flow depth, bed material etc. they conducted a series of experiments using three different discharges 10.9, 15.42 and 18 l/s under clear water condition and the maximum depth of scour was recorded for each experiment. Ten different shapes, circular, rectangular, octagonal, chamfered, hexagonal, elliptical, sharp, Joukowsky, oblong, and streamline, were used to conduct the experiments. A pier width of 4.5 cm by changing the shape of the pier was used in all experiments at a constant flow depth of 0.12 m. The formation of the horseshoe and wake vortices, equilibrium depth of scour and initial scour rate depended on the shape of the pier. Rectangular pier had a maximum exposed area which was why the scour depth was found much higher (7.6 cm). While for streamline geometry it was 3 cm because it had a minimum exposed area without side corners. The streamline shape was considered the best shape of piers which reduced the maximum scour depth by 60% as compared with the rectangular shape. The scour depth was found to be increased as the flow intensity increased and vice versa.

2.1.2 Eccentric piers

Some of the significant works on scour around eccentric piers and staggered arrangements are narrated below:

Das et al. (2014*a*) experimented with the kinematics of the horseshoe vortex in a scour hole around a set of two equilateral triangular piers (sides facing the approaching flow) placed in a longitudinal direction to the flow with an eccentricity. Flow depth (h = 0.125 m), bed slope (= 1: 2400), discharge (= 25 lps), eccentricity (=3b) and longitudinal spacing (=0.5L) between the two piers were kept constant, where L is the maximum length of sediment transportation during a single pier experiment. From the previous study, for the two piers with eccentricity 3b, the maximum scour depth was found to be increased by 20%. Instantaneous three-dimensional velocities were determined by using an ADV. The vortex strength of the eccentric rear pier was observed always higher in the inline front pier. The horseshoe vortex was identified as a forced vortex type of flow since the whirl velocity increased in the outward direction from the vortex centre. The magnitude of circulation of the horseshoe vortex for the eccentric rear pier was found always higher than the magnitude of circulation for the inline front pier. It might be due to the presence of strong mixing of turbulent flow between the piers. The magnitude of radial, tangential, and vertical turbulence intensities and kinetic energy above the scour hole were found much higher than their magnitude below the bed level. In the turbulent outer layer and turbulent-logarithmic layer, the turbulence mixing played an important role as the pressure drag was much higher than the skin friction drag.

Das et al. (2014*b*) conducted research with experimental studies of the formation and characteristics of clear water local scour around eccentric multiple piers to shift the line of sediment deposition. Two piers were arranged in line with the flow and one was an eccentric

pier. The objective was to determine the spacing between two piers in line which causes maximum scour under flows with different Froude numbers, inflow depths and the occurrence of maximum scour volume. It was found that the scour volume was higher for $3b$ eccentricity than for $2b$ eccentricity. The sediments removed from around the pier group were deposited downstream so the diversion angle of the scour and also the dune was more on the side of the eccentric pier. The maximum scour occurred around the eccentric pier and the minimum scour occurred around the in-line rear pier.

Das et al. (2014*c*) analysed the local scour around two eccentric piers that had been extensively studied experimentally in clear water equilibrium scour regime under different longitudinal pier spacing 0.25, 0.375, 0.5, 0.625, and 0.75 times the maximum equilibrium length of sediment transportation (L) for a single pier with a constant eccentricity (= $3b$). For a pier in a group, group effects were also an important parameter which affected scouring around a single pier. The scour depth of the eccentric rear pier was always higher than the scour depth of the front pier. For closer spacing of piers, the scour holes overlapped with each other and the sediment removed from around the pier group was deposited downstream, more on the side of the eccentric pier. It was concluded that with $3b$ eccentricity and $0.625L$ longitudinal spacing, the shifting of sediment towards the flume wall will be maximum and the transported sediment load in a river or open channel may be shifted towards the bank by self-dredging with the help of suitable two pier combination, eccentricity and longitudinal spacing.

Das et al. (2016) further conducted research, concerned with experimental studies of the formation and characteristics of local equilibrium scour around a set of two identical circular, square, and triangular shaped piers placed in the longitudinal direction to the flow with a constant eccentricity. The objective was to see the nature of scour evolved due to the effect of mutual interference of one pier on another with the longitudinal spacing between them varying 0.25, 0.375, 0.5, 0.625, and 0.75 times the scour-affected lengths for a single-pier experiment. Analysis of the results showed the variations of individual non-dimensional equilibrium scour parameters with the effective pier width (diameter of the smallest circumscribing circle of the pier) and increasing longitudinal spacing between the piers. From the results, it could be seen that with $3b$ eccentricity and longitudinal spacing within a fraction of L, the scour at the rear pier was enhanced. At $l = 0.75L$, the maximum scour depth at the eccentric rear pier was found about 45–60% greater than that in the single-pier case. In addition, at $l = 0.75L$, the maximum depth of the scour hole at the upstream of in-line front pier was found about 35% more than in the single-pier case.

Khaple et al. (2017) emphasised the interference of an upstream pier on local scour at downstream piers by experimenting three kinds of pier arrangements. These combinations were (i) two piers in a staggered arrangement, and (ii) three piers in symmetrically staggered arrangements. In the arrangement of two staggered piers, the scour depth at the downstream pier for $e/b = 4$, was the same as that of the upstream pier at $S = 8b$, where S is the streamwise distance between the upstream and downstream piers. For three piers in a staggered arrangement, as the lateral spacing (e) between the downstream pier increased, the equilibrium scour depth at the downstream pier was found to decrease. The scour depths at the downstream piers for the streamwise spacing less than $8b$ and for narrow lateral spacing $2b$ were greater than that at the isolated single pier owing to the effect of wake vortices. As

the centre-to-centre streamwise spacing between upstream and downstream piers was increased, the scour depths at the downstream piers were decreased and attained approximately the same scour depths occurring at the upstream pier at a streamwise distance $S = 10b$ and lateral spacing $e = 2b$. Also, as the radial distance between the upstream and downstream piers was increased, the scour depths at downstream piers were decreased. Apart from measuring the equilibrium scour depths, temporal variation of scour depths was measured at downstream piers for the above mentioned conditions. For all the pier arrangements, the estimated scour depths were found within the ±20% error band for the downstream piers. Hence, a safety factor of 1.2 was proposed to be adopted in design calculations.

Jaman et al. (2017*a*) experimented with the hydrodynamics of flow obstructed by inline and eccentrically arranged circular piers on a horizontal bed under clear water condition to study and analyse the hydrodynamic effects of turbulent flow including its pattern and characteristics around three identically circular shaped piers. Two piers were positioned inline along the flow direction and the third pier was placed eccentrically in the middle of two inline piers having a transverse distance equal to three times of pier width. Contour profiles and variations of time-averaged velocity components, kinetic energy and turbulence intensities were measured and analyzed. The longitudinal spacing between the inline front and rear piers had been considered $0.5l_s$ to achieve maximum scour depth in their experiments. The dune formation was found more on the side of the eccentric pier (away from the line of symmetry). The diversion angle for sediment shifting was found to be more on the side of the eccentric pier. The strongest vortices and circulation occurred at the eccentric middle pier.

Jaman et al. (2017*b*) thereafter conducted another experimental study to measure flow formations and characteristics in local scour holes around three identical circular piers arranged inline and eccentrically in a staggered manner. The three-pier combination and the interferences caused by them played a key function in the enhancement of greater scour depth near the eccentric middle pier and more shifting of sand towards the side. Vortices strengths for eccentric-middle and inline-rear piers were found greatest and lowest, respectively, compared with the strength of the inline-front pier. The maximum equilibrium depth of all scour holes gauged for inline-front, eccentric-middle and inline-rear piers was about 40, 61 and 15% larger than the depth for one single-pier experiment. Also, these depths at inline-front, eccentric-middle and inline-rear piers were more than two-pier cases with inline-front eccentric-rear arrangement. As the dune formation was identified more on the eccentric-middle pier side, the diversion angle was also more on the eccentric-middle pier side.

Das et al. (2017) experimented to study the hydrodynamic behaviour of flow in terms of three-dimensional turbulent flow patterns and characteristics around three identical circular piers at two horizontal planes. Three pier groups were placed with inline and eccentric arrangements in a staggered manner on a flume. The scour depth of the eccentric circular pier was observed to be higher than the inline front and inline rear circular piers. The longitudinal velocity increased between the inline and eccentric pier and the velocity in the downstream of the piers near the bed. The transverse velocity changed direction on either side of the contour lines. There was high turbulence intensity near the bed compared to those at the upper middle level. The magnitude of longitudinal turbulence intensity was found to be higher than the transverse and vertical turbulence intensities. The behaviour of turbulence kinetic energy

was similar to the turbulent intensities. The strongest vortices and circulation had taken place at the eccentric middle pier.

Das and Mazumdar (2018) conducted experiments to get outcomes of hydrodynamic flow formations around two square piers of the same width positioned in inline front and eccentric rear arrangement with constant longitudinal spacing and eccentricity. Such outcomes were compared with previous researches where circular and triangular shaped piers were used at the same experimental conditions. The arrangement of square piers and the interference among wake and horseshoe vortices for inline-front and eccentric-rear piers respectively took part in a major role in making and forming a bigger depth of scour near the eccentrically positioned rear pier. Due to bluff body existence, friction drag became less effective than pressure drag. The sheltering effect partially occurred in the longitudinal spacing zone between two piers. The horseshoe vortex strength for the eccentric-rear pier was observed greater than the strength for the inline-front pier. It indicated the occurrence of a coshedding regime developed between two piers. At five azimuthal angles (0°, ±45° and ±90°), the radial velocity for the square pier was found dominating than the other shaped piers. The size of the horseshoe vortex core was observed maximum for the square piers. The size of this core was larger for the triangular pier than the circular one. The downflow at the upstream of the pier was found much higher for the square pier than the triangular and circular piers.

Das et al. (2019) emphasised the impact of the upstream bridge pier on the scouring around the adjacent downstream bridge pier to investigate a relative scour condition around the three-pier group. They identified the upstream downstream scour geometries positioning two tandem piers inline and the third pier eccentrically in the middle of tandem piers with a fixed eccentricity of magnitude 3b. The experiments were physically performed by gradually varying the intermediate longitudinal spacing between tandem piers. After each experimental run, the scour formation around the pier group and the dune formation downstream of the pier group were investigated. The main aim was to experimentally identify and highlight the nature and location of the scour formed around and also to identify the location of the dune formed downstream of this pier group due to combined interference of flow. The mutual interactions of these horseshoe and wake vortices that occurred around each pier played a considerable role in setting up and forming patterns of the larger scouring depths around all piers. For such three pier combinations, the scour so formed near staggered piers was found maximum and around the tandem downstream pier was found minimum. It confirmed the shifting of sediment load away from this pier group and was deposited downstream, drifting more towards the staggered pier that was towards the channel sidewall.

Malik and Setia (2020) analysed that being in a staggered arrangement, the rear piers were placed at an angle of 45° with respect to the front pier. For determination of the maximum scour depth, if the spacing between the bridge piers was zero, then both the piers behaved like a single pier and the scour depth was found to be 41% greater than that of a single pier. But when the clear spacing was greater than 2.5 times for staggered arrangement, the piers behaved independently. In a staggered arrangement, as the distance between the piers was increased, the maximum scour depth at the rear piers was found to be decreased.

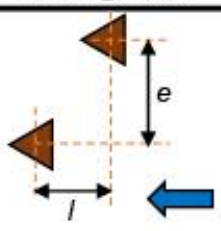
Kuila et al. (2020) conducted an experiment where two piers were placed in line and the other was set eccentrically in the middle of inline square piers. Mutual interferences

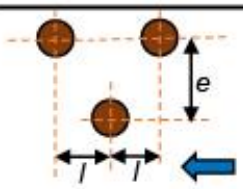
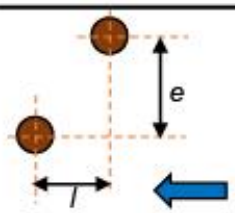
caused by this square pier group lead to enhanced prolonged scour around the eccentric pier. Sand shifting was observed more on the eccentric square pier side (away from the symmetry line) toward the flume wall compared to single or two pier combinations. The strength of vortices near the front-inline pier was found less than that of the eccentric and more than that of the rear-inline pier. Maximum equilibrium scour depth at square front, square eccentric and square rear piers were measured 1.5, 3.1 and 1.4 times larger than the maximum equilibrium scour depth observed for the single pier case. These maximum scour depths at three piers were found more than two-pier experiments with inline eccentric positioning. The plots of velocity vectors depicted that the size of the horseshoe vortex core for the square eccentric-pier was larger than the other two square piers. The wake zone length was found larger for the square front pier, then the square eccentric and then the square rear pier in order. Vortices within the three square piers might be increased scouring hole size of the square eccentrically positioned pier while transporting sediments far off from the line of symmetry.

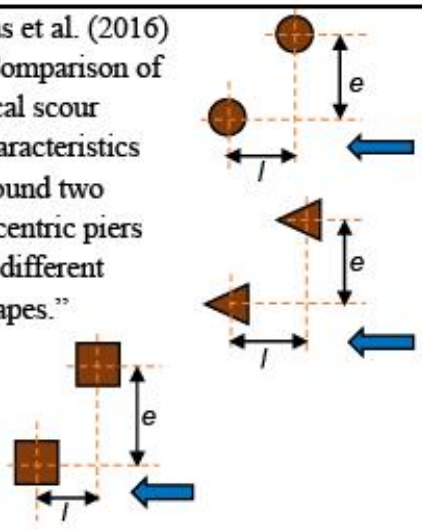
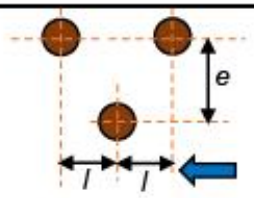
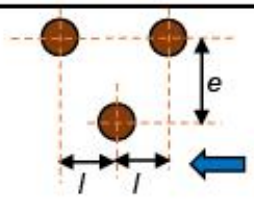
Nandi and Das (2023*a*) performed the validation of experimental results for an isolated circular pier using established literature equations and cross-verified with other published data. Predictive equations were introduced for two to three piers with eccentric in-line arrangements, emphasizing intermediate spacings as crucial variables. Formulation of equations involved dimensional analysis and non-linear regression. The proposed equations offered accurate predictions for temporal scour across selected pier combinations within designated experimental ranges. Equilibrium scour depths for isolated triangular and square piers exceed those of circular piers by 4–7%. In the arrangements of dual and triple piers, d_{se} values at front piers were measured 19–32% and 12–30% higher than isolated circular piers, respectively. Eccentric circular, triangular, and square piers exhibited d_{se} values 35–54% and 44–73% higher than isolated circular piers.

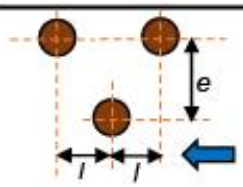
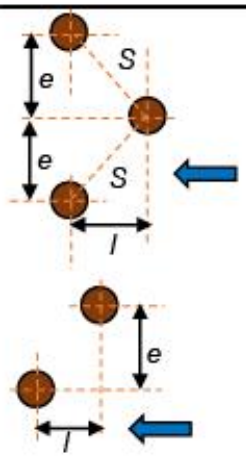
Table 2.1 shows a comparative review of the literatures on eccentric piers. Table 2.2 shows pier arrangement, and experimental conditions in different flume sizes used in previous literatures.

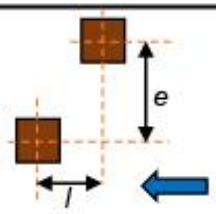
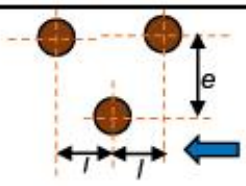
Table 2.1. Comparative review of literatures on eccentric piers.

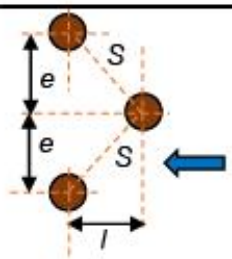
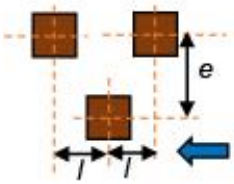
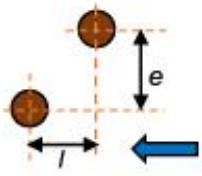
References with title	Schematic of eccentric-pier arrangement	Investigation/findings
Das et al. (2014*a*) "Kinematics of horseshoe vortex in a scour hole around two eccentric triangular piers."		• Fixing eccentricity (e) and longitudinal spacing (l) between two equilateral triangular piers the contours and distributions of the time-averaged velocity components, turbulence intensities and turbulence kinetic energy were elaborated at 0°, ±45° and ±90° azimuthal planes. • The horseshoe vortex is a forced vortex type of flow since the whirl velocity increases in the outward direction from the vortex centre.

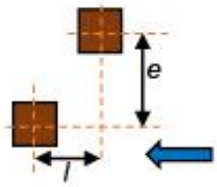
		• The magnitude of circulation of the horseshoe vortex for the eccentric rear pier was found always higher than the magnitude of circulation for the inline front pier. It may be due to the presence of strong mixing of turbulent flow between the piers.
Das et al. (2014*b*) "Clear water local scour around eccentric multiple piers to shift the line of sediment deposition."		• Shift the sediment deposition line by arranging two in-line piers with one eccentric pier. • Determination of the optimal spacing between in-line piers for maximum scour under different Froude numbers and inflow depths. • **Scour volume was found to be higher for 3*b* eccentricity compared to 2*b* eccentricity.** • Sediments removed around the pier group were deposited downstream, resulting in a more pronounced diversion angle of the scour and dune formation on the eccentric pier side. • Maximum scour occurred around the eccentric pier, while the minimum scour was observed around the in-line rear pier.
Das et al. (2014*c*) "Analysis of clear-water equilibrium scour around two eccentric circular piers to increase self-dredging."		• Clear water equilibrium scour around two eccentric piers was studied experimentally for longitudinal spacing 0.25, 0.375, 0.5, 0.625, and 0.75 times the maximum equilibrium length of sediment transportation (L) for a single pier with constant eccentricity ($3b$). • In the pier group, group effects were also an important parameter which affected scouring around a single pier. • The scour depth of the eccentric pier was always higher than that of the front pier. • For closer l, the scour holes overlapped with each other and the sediment removed from the pier group was deposited downstream, more on the side of the eccentric pier. • With $e = 3b$ and $l = 0.625L$, the shifting of sediment towards the flume wall was maximum. The transported sediment load in a river or open channel can be shifted towards the bank by self-dredging with the help of suitable two pier combinations, eccentricity and longitudinal spacing.

Das et al. (2016) "Comparison of local scour characteristics around two eccentric piers of different shapes."		• Maintaining $e = 3b$ with the varying longitudinal spacing 0.25, 0.375, 0.5, 0.625, and 0.75 times the scour-affected lengths for a single-pier experiment, it was found at $l = 0.75L$ the maximum scour depth at the eccentric rear pier is found about 45–60% greater than that in the single-pier case. • At $l = 0.75L$, the maximum depth of the scour hole at the upstream of in-line front pier is about 35% more than at the single-pier case.
Das et al. (2017) "Hydrodynamic behaviour of flow past three typically arranged circular piers on different horizontal planes"		• Study the hydrodynamic behaviour of flow in terms of three-dimensional turbulent flow patterns and characteristics around three identical circular piers at two horizontal planes. • Three pier groups were placed with inline and eccentric arrangements in a staggered manner on a flume. • The scour depth of the eccentric circular pier was observed to be higher than the inline front and inline rear circular piers. • The longitudinal velocity increased between the inline and eccentric pier and the velocity downstream of the piers near the bed. • The transverse velocity changed direction on either side of the contour lines. • High turbulence intensity was observed near the bed compared to those at the upper middle level. • The magnitude of longitudinal turbulence intensity was found to be higher than the transverse and vertical turbulence intensities. The behaviour of turbulence kinetic energy was noticed similar to the turbulent intensities.
Jaman et al. (2017*a*) "Hydrodynamics of flow obstructed by inline and		• Two piers were aligned in line with the flow, and a third pier was eccentrically placed between them, maintaining a transverse distance (= 3*b*).

eccentrically arranged circular piers on a horizontal bed surface."		• Analysed the hydrodynamic effects, including flow patterns and characteristics. • Longitudinal spacing between the front and rear piers was set at 0.5 times the scour depth to achieve maximum scour depth. • Dune formation was observed to be more pronounced on the side of the eccentric pier, away from the line of symmetry. • Sediment diversion angles were higher on the side of the eccentric pier. • The time-mean longitudinal velocity increased between inline and eccentric piers, with the strongest vortices and circulation occurring at the eccentric middle pier.
Jaman et al. (2017*b*) "Hydrodynamic flow patterns around three inline eccentrically arranged circular piers."		• Experiments were conducted to measure flow formations and characteristics in local scour holes around three identical circular piers arranged inline and eccentrically in a staggered manner. • The three-pier combination and their interferences caused an enhancement of greater scour depth near the eccentric middle pier and more shifting of sand towards the side. • Maximum d_{se} of all scour holes gauged for inline-front, eccentric-middle and inline-rear piers are about 40, 61 and 15% larger than the depth for one single-pier experiment. • As the dune formation was identified more on the eccentric-middle pier side, the diversion angle was also more on the eccentric-middle pier side.
Khaple et al. (2017) "Interference of an upstream pier on local scour at downstream piers."		• Experimented arrangements: (i) two piers staggered, and (ii) three piers symmetrically staggered. • Staggered piers: Scour depth at downstream pier equals upstream pier at $S = 8b$ for $e/b = 4$. • Three staggered piers: Increasing lateral spacing reduces downstream scour; scour depths exceed single pier values for streamwise spacing < $8b$ and narrow lateral spacing ($2b$) due to wake vortices.

		• Increased streamwise spacing (S = 10b) and radial distance decrease downstream scour. • Temporal scour depth variations within ±20% error band for downstream piers, allowing a safety factor of 1.2 in design calculations.
Das and Mazumdar (2018) "Evaluation of hydrodynamic consequences for horseshoe vortex system developing around two eccentrically arranged identical piers of diverse shapes."		• Contour profiles of tangential, radial, and vertical velocities, along with kinetic energy and turbulence intensities, were presented at various azimuth angles. • Results compared with previous studies using cylindrical and triangular piers under similar conditions. • Square pier arrangement, wake, and horseshoe vortex interaction led to increased scour depths near the eccentric rear pier. • The presence of bluff bodies reduced the effectiveness of friction drag compared to pressure drag. • Square piers exhibited dominant radial velocity and larger horseshoe vortex cores compared to other shapes. • Downflow upstream of square piers surpassed that of triangular and circular piers.
Das et al. (2019) "Impact of upstream bridge pier on the scouring around adjacent downstream bridge pier."		• The upstream downstream scour geometries when two tandem piers were placed inline and the third pier was placed eccentrically in the middle of tandem piers with fixed eccentricity (e = 3b). • The experiments were physically performed by gradually varying the intermediate longitudinal spacing between tandem piers. • In three pier combinations, the scour so formed near staggered piers was found maximum and around the tandem downstream pier was found minimum. • The shifting of sediment load away from this pier group was deposited downstream, drifting more towards the staggered pier that was towards the channel sidewall.

Malik and Setia (2020) "Interference between pier models and its effects on scour depth"		• Being in a staggered arrangement, the rear piers were placed at an angle of 45° with respect to the front pier. • In determining the maximum scour depth, the spacing between the bridge piers was zero, then both the piers behaved like a single pier and the scour depth was found to be 41% greater than that of a single pier. • When the clear spacing was greater than 2.5 times for staggered arrangement, the piers behaved independently. • In the staggered arrangement, as the distance between the piers increases, the maximum scour depth at the rear piers decreases.
Kuila et al. (2020) "Computing equilibrium flow structures at three interfering square piers causing relative scour."		• Two piers were placed in line and the other was set eccentrically in mid of in-line square piers. • Mutual interferences caused by this square-shaped pier group lead to enhanced prolonged scour around the eccentric pier. • Sand shifting was found more on the eccentric square pier side (away from the symmetry line) toward the flume wall compared to single or two pier combinations. • Maximum equilibrium scour depth at the square front, square eccentric and square rear piers were about 1.5, 3.1 and 1.4 times larger than the maximum equilibrium scour depth for the single pier. Maximum equilibrium scour depths at three piers were observed higher than two pier experiments with inline eccentric positioning. • The size of the horseshoe vortex core for the square eccentric pier was found larger than the other two square piers. • The wake zone length was larger for the square front pier, then the square eccentric and then the square rear pier in order.
Nandi and Das (2023*a*) "Equation for time-dependent local scour at pier-like		• Validation of experimental results for an isolated circular pier was done using established literature equations and cross-verified with other published data. • Predictive equations were introduced for two to three piers with eccentric in-line

structures with eccentric in-line arrangements."		arrangements, emphasizing intermediate spacings as crucial variables. • Formulation of equations involved dimensional analysis and non-linear regression. The proposed equations offered accurate predictions for temporal scour across selected pier combinations within designated experimental ranges. • Equilibrium scour depths for isolated triangular and square piers exceed those of circular piers by 4–7%. • In dual and triple pier arrangements, d_{se} values at front piers were observed 19–32% and 12–30% higher than isolated circular piers, respectively. • Eccentric circular, triangular, and square piers exhibited d_{se} values 35–54% and 44–73% higher than isolated circular piers.

Note: Distances between the piers shown in the table are not in scale.

Table 2.2. Pier arrangement, experimental conditions in different flume sizes used in previous literatures and present study.

Pier arrangement	Literature	Flume size ($M\times B\times H$) (m × m × m)	V/V_c (--)	h/b (--)	b/d_{50} (--)	B/b (--)
Inline eccentric	Das et al. (2014)	11×0.81×0.60	0.90–1.07	1.2-1.6	136.99	11.57
Eccentric	Das et al. (2016)	11×0.81×0.60	0.78	1.79	95.89	11.57
Eccentric /Staggered	Khaple et al. (2017)	15.5×0.91×0.70	0.90	2.67	33.333	11.10-15.17
Inline eccentric	Das et al. (2019)	11×0.81×0.60	0.73	1.79	84.85	11.57
Staggered	Malik and Setia (2019)	15×0.40×0.60	0.96-0.98	3.10-3.57	140	9.5
Eccentric	Nandi and Das (2023*a*)	11×0.81×0.60	0.71	1.79	84.85	11.57
Eccentric	Present study	11×0.81×0.60	0.67-0.97	1.20-1.65	96.69	11.57

Note: V/V_c – flow intensity; h/b – flow shallowness; b/d_{50} – sediment coarseness; B/b – blockage ratio.

2.2 Literature equations for eccentric-pier arrangement

Some previous literatures have given various equations from which we can generate scour depth using values of defined scour parameters. Here, d_{st} = scour depth measured at any instant from initial bed level; d_{sf} = maximum scour depth at upstream pier; d_{sr1} = temporal scour depth at downstream pier; d_{sr2} = temporal scour depth at eccentric in lined pier; d_{se} = equilibrium scour depth at an isolated single pier; V = depth-averaged approaching velocity; V_c = critical velocity; e = lateral spacing between the front and rear pier; b = pier diameter; l = longitudinal spacing between the front and rear pier; t = instantaneous time; t^* = equilibrium time scale, Vt_e/b; s = relative density of sand, ρ_s/ρ_f; d_{50} = median diameter of sand; h = approaching flow depth; K = parameter (varies between 0.95-1.78 for various pier arrangements, Nandi and Das (2023*a*); T = pier position factor (varies between 0-2); d_{xx} = max scour depth where xx indicates three different piers like the front pier, eccentric pier and rear pier. Table 2.3 shows functional parameters used in literatures to develop equations in estimating maximum scour depth around the eccentric pier arrangement.

1. Das et al. (2016)

Eccentric pier: For the sake of practical applications, regression equations for these dimensionless parameters with relatively high correlation coefficients, $r^2(\approx 0.99)$, are given in Eq. (2.1-2.2) as follows:

$$\frac{d_{sf}}{b} = -0.011\left(\frac{l}{b}\right)^2 + 0.145\left(\frac{l}{b}\right) + 0.489 \tag{2.1}$$

$$\frac{d_{sr1}}{b} = -0.007\left(\frac{l}{b}\right)^2 + 0.092\left(\frac{l}{b}\right) + 0.691 \tag{2.2}$$

2. Khaple et al. (2017)

Three piers in staggered: Equations (2.3-2.4) to estimate the temporal variation of scour depths at the two downstream piers in the arrangements of three staggered piers are given by

$$\frac{d_{sr1}}{d_{se}} = \exp\left[-0.0383\left\{\frac{V}{V_c}\log\left(\frac{1}{78.68}\left(\frac{e}{b}\right)^{0.25}\frac{t}{t^*}\left(\frac{l}{b}\right)^{-0.25}\right)\right\}^2\right] \tag{2.3}$$

$$\frac{d_{sr1}}{b} = \left(\frac{d_{se}}{b}\right)\exp\left[-0.0383\left\{\frac{V}{V_c}\log\left(\frac{1}{78.68}\left(\frac{e}{b}\right)^{0.25}\frac{t}{t^*}\left(\frac{l}{b}\right)^{-0.25}\right)\right\}^2\right] \tag{2.4}$$

3. Das et al. (2019)

The equation for the eccentric arrangement to calculate the maximum scour depth of an upstream pier and two downstream piers arranged inline and the third pier was placed eccentrically in the middle of tandem piers are given in Eq. (2.5), and Eq. (2.6) respectively.

$$\frac{d_{xx}}{b} = 0.0703\left(\frac{l}{b}\right) + \left(-0.243T^2 + 0.407T + 0.696\right) \tag{2.5}$$

$$\frac{d_{xx}}{b} = -0.038\left(\frac{l}{b}\right) + \left(-0.243T'^2 + 0.407T' + 1.258\right) \tag{2.6}$$

where the value of pier position factor T and T' for rising and decreasing scour depth are given as follows:

$T = T' = 0$ for frontal pier;

$T = T' = 1$ for the middle pier;

$T = T' = 2$ for the downstream rear pier.

4. Malik and Setia (2020)

The equation for the eccentric arrangement to calculate the maximum scour depth near an upstream pier and two downstream piers arranged symmetrically staggered are given in Eq. (2.7), Eq. (2.8), and Eq. (2.9) respectively with r^2 value of 0.779.

$$\frac{d_{sf}}{b} = 0.0342\left(\frac{S}{b}\right)^2 - 0.27\left(\frac{S}{b}\right) + 1.3581 \tag{2.7}$$

$$\frac{d_{sr1}}{b} = 0.0342\left(\frac{S}{b}\right)^2 - 0.27\left(\frac{S}{b}\right) + 1.3581 \tag{2.8}$$

$$\frac{d_{sr2}}{b} = 0.0479\left(\frac{S}{b}\right)^2 - 0.3774\left(\frac{S}{b}\right) + 1.4632 \tag{2.9}$$

5. Nandi and Das (2023*a*)

Equations 2.10-2.11 are provided for a combined equation for the in-line and eccentric arrangement of the pier group which is valid for the ranges $0.008 \leq d_{50}/b \leq 0.012$, $5.43 \leq l_d/b \leq 5.99$ and $10 \leq l/b \leq 10.37$, $h/b = 1.26\text{-}1.79$ and $t/t^* = 0\text{-}36$.

$$\frac{d_{st}}{d_{se}} = K \times \exp\left[-0.045\left\{\ln\left(3.3\left(\frac{d_{50}}{b}\right)\left(\frac{h}{b}\right)^{-1} \times \left(\frac{l_d}{b}\right)^{-0.25}\left(\frac{l}{b}\right)^{-0.4}\left(\frac{t}{t^*}\right)\right)\right\}^2\right] \tag{2.10}$$

$$\frac{d_{st}}{b}=\frac{d_{se}}{b}K\times\exp\left[-0.045\left\{\ln\left(3.3\left(\frac{d_{50}}{b}\right)\left(\frac{h}{b}\right)^{-1}\times\left(\frac{l_d}{b}\right)^{-0.25}\left(\frac{l}{b}\right)^{-0.4}\left(\frac{t}{t^*}\right)\right)\right\}^2\right] \quad (2.11)$$

where the value of constant parameter K is given as follows:

K=1, l_d/b, l/b are not applicable for an isolated pier;

K=1.25, l_d/b=1, l/b is not applicable for the front pier of two piers;

K=1.16, l_d/b=1, l/b is not applicable for the front pier of three piers;

K=1.60, l/b is not applicable for the eccentric pier in two piers;

K=1.78, l/b is not applicable for the eccentric pier in three piers;

K=0.95 for the rear pier of three piers.

Table 2.3. Functional parameters used in literatures to develop equations to estimate maximum scour depth around the eccentric pier arrangement.

References	Functions used
Khaple et al. (2017)	$d_{sr1}/b = f(d_{se}/b,\ V/V_c,\ t/t^*,\ l/b,\ e/b)$
Das et al. (2016)	$d_{sf}/b = f(l/b),\ d_{sr1}/b = f(l/b)$
Das et al. (2019)	$d_{xx}/b = f(l/b,\ T,\ T')$
Malik and Setia (2020)	$d_{sf}/b = f(S/b),\ d_{sr1}/b = f(S/b),\ d_{sr2}/b = f(S/b)$

2.3 Research gaps identified

Bridge piers obstruct the flow of floodwaters, causing an increase in velocity and the development of vortices. The unique flow field with the higher velocity can seriously damage bridge foundations. Thus, if the depth of the foundation is not deep enough, the likelihood of bridge failure becomes higher. The damage to and failure of bridges caused by scour are problems of great significance all over the world. In spite of significant investment in bridge scour research, bridges still fail due to excessive scour. It is believed that this is partially a consequence of inadequacies in both design criteria adopted for older bridges and also the present state of knowledge about some aspects of bridge hydraulics and scouring. It is also due to the lack of convenient and appropriate availability of the results of the past scour research to practitioners. A summary of the present state of knowledge on bridge scour is needed. Two very important reasons for this failure are the lack of adequate knowledge over the years on the scour that takes place and insufficient regular surveys of the river bed condition around the bridge piers.

Many investigations have been performed since the late 1950s to understand the flow and erosion mechanisms around bridge piers and to estimate the scour depth. However, the complexities of the three-dimensional (3D) separated flow, its interaction with the transport of sediment and the changing mobile boundary, present great difficulties in analysing the problem theoretically. Hence, the early investigations concentrated mostly on scour estimation based on dimensional analysis and data correlation of small-scale laboratory experiments (Breusers et al., 1977; Raudkivi, 1991). Several researches have been carried out

on bridge pier scour. However, even now in modern times, pier undermining due to scouring and riverbed erosion has been widely recognised as being the main cause of bridge damage and failure (Melville and Coleman, 2000).

1. Local scour at a single pier has been extensively studied by many investigators. However, much less work is available on scour around multiple piers placed nearby.
2. Despite many investigations around single pier, a comprehensive understanding of scour geometry around multiple piers with eccentric arrangement (Das et al., 2014*b*; Das et al., 2019) is not enough because most of the pier group investigations were confined to side-by-side and in-line arrangements that focused on the prediction of the scour geometry (Ashtiani and Beheshti, 2006, Wang et al., 2016) and the effect of pier spacing on scour depth (Elliott and Baker, 1985). Therefore, engineering solutions, concerning especially the selection of scour countermeasures and their placement details, would be subject to uncertainty.
3. For each pier from the pier groups, collective effects are reasonably significant in counting those parameters which affect the scouring near the single pier. Several researches on double pier arrangement were also conducted, where the piers were longitudinally positioned in tandem along the flow (Sheppard et al., 1995; Das et al., 2016) and found that both reinforcing and sheltering effects influence the scouring but the same effects in eccentric pier arrangements are very rare. A few researchers also worked on interference effects on scouring around bridge piers. However, work on interference effects has not been fully explored and established.
4. The literature review reveals that significantly minimal research was undertaken on prediction of the the equilibrium scour depth and temporal variation of scour depth around eccentric piers.
5. The local scour development is a reflection of the complexity of the flow characteristics, which provide the driving force for the scouring process. Therefore, it is necessary to investigate the scour and the flow characteristics synchronously during the scouring process instead of focusing traditionally only on the equilibrium state.

2.4 Need of the work

Scour depth measurement is crucial for any bridge pier arrangement, especially when piers are eccentrically placed. Here is how it plays a vital role:

1. **Understanding scour depth:** Scour depth refers to the depth of soil or sediment erosion around bridge piers or abutments due to obstructing the flow of water. This erosion can compromise the stability of the bridge structure.
2. **Eccentric pier arrangement:** When piers are eccentrically placed, i.e., not symmetrically aligned with the flow of water, they can induce complex flow patterns around them. This can lead to uneven scour depths around different parts of the pier base.

3. **Risk assessment:** Measuring scour depth helps engineers assess the risk of bridge pier foundation exposure. Eccentrically placed piers can experience differential scour depths, where one side may erode more than the other, potentially leading to differential settlement or tilting of the pier.
4. **Design considerations:** Scour depth measurements influence the design of bridge foundations. For eccentric piers, designers need accurate data on scour depth to ensure adequate foundation depth and stability against varying scour scenarios.
5. **Monitoring and maintenance:** Regular monitoring of scour depth is essential post-construction. For eccentric pier arrangements, monitoring becomes even more critical due to potential asymmetric scour patterns that may develop over time.

In summary, scour depth measurement is essential for eccentric pier arrangements to ensure the structural integrity and longevity of bridges. It informs design, risk assessment, and maintenance strategies to mitigate the effects of scour on bridge piers.

2.5 Aim of the present study

Due to the complex nature of flow around bridge piers and various uncertainties on different parameters affecting the scour depth, a laboratory-based experimental study is a widely adopted method for achieving accurate and reliable results. Hence the present study aims to carry out an experimental investigation and provide a notable contribution to the body of knowledge through the following innovations:

1. Investigation of the interaction of bridge piers (group effect) on the flow structure and scouring process around the bridge piers using the models of two circular bridge piers arranged eccentrically with different lateral spacings and different flow depths.
2. Experimentally identify and highlight the nature and location of scour forming around the piers, also to identify the location of the dune forming downstream of this pier group due to combined interference of flow.
3. Investigating sediment shifting processes experimentally while using scour maximisation criteria might be very beneficial for navigation and cost-effective for self-dredging.

CHAPTER-3

OBJECTIVES AND METHODOLOGY

3.1 Objectives

The main objective of this study is to carry out an experimental investigation on scour around the models of bridge piers comprising two circular columns arranged eccentrically. The study is confined to uniform cohesionless bed material and clear water flow conditions to find out the quasi-temporal variation of equilibrium scour around such two piers.

The safe and economical design of bridge piers, caisson, groyne etc. requires accurate prediction of the maximum scour depth around them. An underestimation of the scour will result in failure, while its over-estimation will increase the cost of the structures. Hence the knowledge of accurately predicting scour depth under various conditions is essential.

The effects of horizontal spacing between two piers on flow structure and local scour around the bridge pier models are proposed to study in depth. In order to achieve this goal, the following specific objectives are proposed:

1. To carry out experiments with the eccentric arrangement of two pier groups by varying the lateral spacing and delineating the scour geometry.
2. To find out the hydraulic parameters which are involved in causing scour where many non-dimensional parameters can be derived by making dimensional analysis. These parameters will help in understanding the relationship between various factors influencing scour depth, such as flow velocity, sediment properties, pier geometry, and so on. Each influencing parameter may have a different sensitivity of dependent parameters (i.e. maximum scour depth).
3. To observe the physical phenomena during the experiments.
4. To focus mainly on sediment shifting phenomena throughout the experiments by considering the criteria of scour maximization ($l = 5.19b$), as mentioned in Das et al. (2016). It may be symmetric or non-symmetric due to the eccentric arrangement of piers. If it is non-symmetric then to find out on which side of the pier the scour is more.
5. To identify which relative lateral spacing produces the maximum (which may help in self-dredging) and minimum scour depth (which may help in designing a safer bridge pier). The findings of this study may be used to facilitate the positioning of piers when scouring is a design concern.

6. To determine and evaluate the temporal variation of the local scour depth around both the piers based on the experimental data.
7. To determine comparisons of scour depths between a single pier and that around eccentric-pier arrangements.

3.2 Experimental conditions adopted by previous researchers

Before conducting the experiments, care should be taken about all the effects which can be assumed negligible while making experimental conditions. Some of the experimental conditions which are taken from the previous literatures are addressed in Table 3.1.

Table 3.1. Experimental conditions adopted based on literatures review.

Effects	Conditions adopted by different research groups	References	Range of data set for the present study
Negligible side wall effect	$B/b \geq 8$	Shen et al. (1969)	11.57
	$B/b \geq 6.25$	Raudkivi and Ettema (1983)	
	$B/b \geq 10$	Chiew and Melville (1987)	
	$B/b \geq 3$	Ballio et al. (2009)	
	$B/b \geq 6.5$	Ashtiani (2012)	
Negligible sediment size effect	$b/d_{50} > 25$	Melville (1997)	96.69
	$b/d_{50} > 50$	Ettema (1980), Sheppard et al. (2004)	
	$b/d_{50} \sim 25$ to 130	Tafarojnoruz et al. (2012)	
Uniform sediment	$\sigma_g < 1.4$	Dey et al. (1995)	1.93
	$\sigma_g < 2$	Rauddkivi (1998)	
Negligible flow viscosity	Re > 7000	Monti (1994) [as referred in Khaple et al. (2017)]	24696-24824
Threshold for sediment movement	$V/V_c \geq 0.4$	Chiew (1995)	0.67 – 0.97
	$V/V_c \geq 0.5$	Breusers (1977)	
	$V/V_c \geq 0.3$	Jone and Sheppard (2000)	
Negligible effect of flow shallowness	$h/b >$ 1-3	Ettema (1980)	1.2 – 1.65
	$h/b > 0.6$	Rauddkivi (1983)	
	$h/b > 2.6$	Melville and Southerland (1988)	
	$h/b > 3$	Breusers (1977)	
Achieved equilibrium condition	Variation of $d_{se} <$ 0.05b in 24 hrs	Melville and Chiew (1999)	12 hrs

3.3 Pier dimension

In the present study, the two piers are constructed using Perspex sheets. Two circular piers of 7 cm diameter (b) have been used in the present study as some other experiments have already been conducted in the same flume specification with the same pier dimension to neglect the side wall effect (Das et al., 2014). The height of the piers (H) is 45.5 cm (Fig. 3.1). In the present study, it is kept in mind that the width of the experimental flume is more than 11.57 times the pier width in order to minimise contraction scour, which satisfies the whole criterion given by the above researchers.

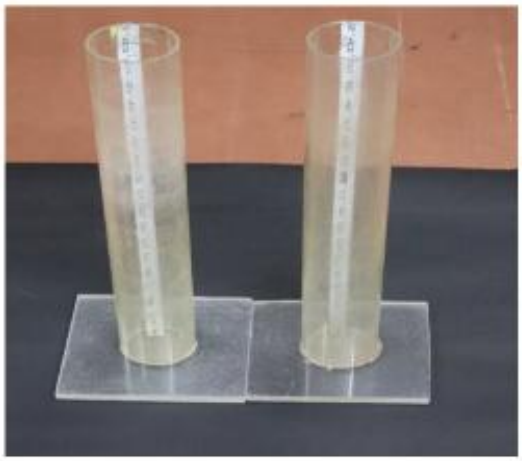


Fig. 3.1. Circular piers of each 7 cm diameter.

3.4 Flow conditions

The flow discharge is selected in such a way that the normalised bed shear stress should not exceed the critical value for the incipient sediment movement at the plane sand bed of mean grain size d_{50} = 0.724 mm. The flume experiments are conducted using fixed flow discharge 20 lps with corresponding water depths of 0.116 m, 0.105 m, 0.095 m, and 0.084 m above the flat sand bed. Here, the flow intensity ratio, $V/V_c < 1$ is provided for this fixed discharge, where V is the depth average approaching flow velocity at the centerline of the flume, and V_c is the critical velocity for the inception of sediment motion. The 24 experiments have been conducted for four different flow depths with six different eccentric-pier arrangements with fixed discharge with Reynolds number (Re) varying from 24696 to 24824 and Froude number (Fr) varying from 0.20 to 0.32 with different flow intensity ratios (V/V_c) ranging from 0.67 to 0.97 (Table 3.2).

Table 3.2. Flow parameters set to carry out experiments.

Q	h	V	V_c	V/V_c	Re = Vh/ν	Re_p = Vb/ν	Fr = $V/(gh)^{0.5}$
(lps)	(m)	(m/s)	(m/s)	(--)	(--)	(--)	(--)
20	0.116	0.213	0.315	0.67	24824	14964	0.20
20	0.105	0.235	0.311	0.75	24675	16461	0.23
20	0.095	0.261	0.306	0.85	24795	18290	0.27
20	0.084	0.293	0.300	0.97	24696	20576	0.32

Note: Q – discharge; h – approaching flow depth; V – depth-averaged approaching velocity; V_c – critical velocity; V/V_c – flow intensity; Re – flow Reynolds number; Re_p – pier Reynolds number; Fr – Froude number of flow; ν – kinematic viscosity; g – gravitational acceleration.

3.5 Setting the gap between the piers

The front pier is located in the middle of the zone to ensure the formation of a fully developed, logarithmic velocity profile at the working section. The two piers are aligned at zero degree angle with respect to the centerline of the flume. The centre-to-centre longitudinal spacing (l) between the front and eccentric piers is fixed by 5.19b for the maximum scour depth of the eccentric-pier arrangement of circular piers from Das et al. (2016) (0.75L=0.75×48.4= 36.3 cm = 5.19b, where L is the maximum length of sediment transportation of a single pier =48.4 cm). Here 24 experiments have been carried out with two identical piers of eccentricity e = 2b - 3.5b because this is the maximum permissible limit for piers that are b = 7 cm wide within which the equilibrium scour formed is expected to remain independent of the wall effects of the laboratory flume having a width of 81 cm. The combination 3b is found to be more efficient in terms of removing more sediment from the channel bed. Moreover, the sediment removed from the channel bed is deposited on one side of the channel. The diversion angle of the scour and also the dune is more on the side of the eccentric pier. This is significant as it proves that the transported sediment load in a channel can be shifted towards the bank with the help of a suitable pier combination (Das et al., 2013*a*; Das et al., 2013*b*; Das et al., 2014*b*; Das et al., 2016). The centre-to-centre transverse distance or eccentricity (e) between the front and eccentric-pier is varied by 3.5b, 3b, 2.75b, 2.5b, 2.25b, and 2b. Figure 3.2 shows a schematic diagram illustrating eccentric-pier arrangement with flow direction. Table 3.3 shows the setting of the gap between piers adopted based on literatures where l_d is the diagonal spacing between two eccentric piers.

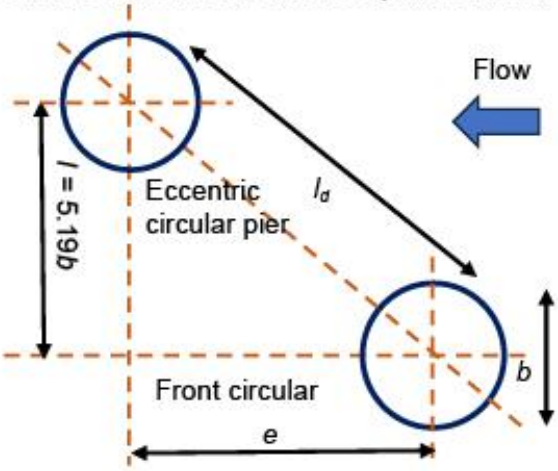


Fig. 3.2. Schematic diagram showing eccentric-pier arrangement with flow direction.

Table 3.3. Setting the gap between piers for the present study adopted based on literatures.

Literature	Arrangement	b (cm)	e/b (--)	l/b (--)	l_d/b (--)
Das et al. (2014)	Inline eccentric circular	5	3	5	5.83
		5	2	5	5.39
		5	3	5.2	6
		5	2	5.2	5.57
Das et al. (2016)	Eccentric circular	7	3	1.73	3.46
		7	3	2.59	3.96
		7	3	3.46	4.58
		7	3	4.32	5.26

		7	3	5.19	5.99
Khaple et al. (2017)	Eccentric circular	6	4	2	4.47
		6	4	4	5.66
		6	4	6	7.21
		6	4	8	8.94
		6	4	10	10.77
Khaple et al. (2017)	Symmetrical staggered circular	6	2	2	2.83
		6	2	4	4.47
		6	2	6	6.32
		6	2	8	8.25
		6	2	11	11.18
		6	3	3	4.24
		6	3	5	5.83
		6	3	7	7.62
		6	3	9	9.49
		6	3	11	11.4
Das et al. (2019)	Inline eccentric circular	7	3	0.86	3.12
		7	3	1.3	3.27
		7	3	1.73	3.46
		7	3	2.16	3.7
		7	3	2.59	3.96
		7	3	3.03	4.26
		7	3	3.46	4.58
		7	3	3.89	4.91
		7	3	4.32	5.26
Malik and Setia (2020)	Symmetrical staggered circular	4.2	0.7	0.7	0.99
		4.2	1	1	1.41
		4.2	1.4	1.4	1.98
		4.2	1.8	1.8	2.55
		4.2	2.1	2.1	2.97
		4.2	2.5	2.5	3.54
		4.2	2.8	2.8	3.96
		4.2	3.2	3.2	4.53
		4.2	3.5	3.5	4.95
Present study	Eccentric circular	7	3.5	5.19	6.26
		7	3	5.19	5.99
		7	2.75	5.19	5.87
		7	2.5	5.19	5.76
		7	2.25	5.19	5.66
		7	2	5.19	5.56

Note: b – pier diameter; l_d – diagonal spacing between two eccentric piers; l – longitudinal spacing between the front and eccentric piers; e – lateral spacing (eccentricity) between the front and eccentric piers.

3.6 Other hydraulic parameters

The increase in the local scour depths under the pressure flow conditions is due to many parameters. In the present study, keeping some parameters constant experiments generally are run with varying some other parameters. All parameters for the present eccentric-pier arrangements are summarised in the following Tables 3.4-3.5.

Table 3.4. Parameters kept constant during the present study.

b (cm)	d_{50} (mm)	Q (lps)	b/d_{50} (--)	B/b (--)	(l) (--)
7	0.724	20	96.69	11.57	5.19b

Note: b – pier diameter; d_{50} – median diameter of sand; Q – discharge; b/d_{50} – sediment coarseness; B/b – blockage ratio; l – longitudinal spacing between the front and eccentric-pier.

Table 3.5. Parameters varied during the present study.

h (m)	V (m/s)	V/V_c (--)	h/b (--)	Fr (--)
0.116	0.213	0.67	1.65	0.20
0.105	0.235	0.75	1.5	0.23
0.095	0.261	0.85	1.35	0.27
0.084	0.293	0.97	1.2	0.32

Note: h – approaching flow depth; V – depth-averaged approaching flow velocity; V_c – critical velocity; V/V_c – flow intensity; h/b – flow shallowness; Fr – Froude number of flow.

3.7 Experimental conditions

All 24 experiments have been performed varying the eccentricity (e) between the front pier and eccentric pier with a major focus on the time required to achieve a quasi-equilibrium scour condition. Additional 4 single pier experiments also have been carried out with the above mentioned experiments. Experiments are conducted under clear-water conditions at a fixed discharge of 20 lps and minimum and maximum depth of scour is measured. Tables 3.6 and 3.7 show a list of parameters set for eccentric pier arrangements and for the single pier experiments.

Table 3.6. List of parameters set for each experiment.

Exp. (--)	b (cm)	B (cm)	d_{50} (mm)	Q (lps)	h (cm)	V (m/s)	V/V_c (--)	h/b (--)	Fr (--)	B/b (--)	b/d_{50} (--)	l (--)	e (--)
1	7	81	0.724	20	11.6	0.213	0.67	1.65	0.20	11.57	96.69	5.19b	3.5b
2	7	81	0.724	20	10.5	0.235	0.75	1.5	0.23	11.57	96.69	5.19b	3.5b
3	7	81	0.724	20	9.5	0.261	0.85	1.35	0.27	11.57	96.69	5.19b	3.5b
4	7	81	0.724	20	8.4	0.293	0.97	1.2	0.32	11.57	96.69	5.19b	3.5b
5	7	81	0.724	20	11.6	0.213	0.67	1.65	0.20	11.57	96.69	5.19b	3b
6	7	81	0.724	20	10.5	0.235	0.75	1.5	0.23	11.57	96.69	5.19b	3b
7	7	81	0.724	20	9.5	0.261	0.85	1.35	0.27	11.57	96.69	5.19b	3b
8	7	81	0.724	20	8.4	0.293	0.97	1.2	0.32	11.57	96.69	5.19b	3b
9	7	81	0.724	20	11.6	0.213	0.67	1.65	0.20	11.57	96.69	5.19b	2.75b
10	7	81	0.724	20	10.5	0.235	0.75	1.5	0.23	11.57	96.69	5.19b	2.75b
11	7	81	0.724	20	9.5	0.261	0.85	1.35	0.27	11.57	96.69	5.19b	2.75b
12	7	81	0.724	20	8.4	0.293	0.97	1.2	0.32	11.57	96.69	5.19b	2.75b
13	7	81	0.724	20	11.6	0.213	0.67	1.65	0.20	11.57	96.69	5.19b	2.5b
14	7	81	0.724	20	10.5	0.235	0.75	1.5	0.23	11.57	96.69	5.19b	2.5b
15	7	81	0.724	20	9.5	0.261	0.85	1.35	0.27	11.57	96.69	5.19b	2.5b
16	7	81	0.724	20	8.4	0.293	0.97	1.2	0.32	11.57	96.69	5.19b	2.5b
17	7	81	0.724	20	11.6	0.213	0.67	1.65	0.20	11.57	96.69	5.19b	2.25b
18	7	81	0.724	20	10.5	0.235	0.75	1.5	0.23	11.57	96.69	5.19b	2.25b
19	7	81	0.724	20	9.5	0.261	0.85	1.35	0.27	11.57	96.69	5.19b	2.25b
20	7	81	0.724	20	8.4	0.293	0.97	1.2	0.32	11.57	96.69	5.19b	2.25b
21	7	81	0.724	20	11.6	0.213	0.67	1.65	0.20	11.57	96.69	5.19b	2b
22	7	81	0.724	20	10.5	0.235	0.75	1.5	0.23	11.57	96.69	5.19b	2b
23	7	81	0.724	20	9.5	0.261	0.85	1.35	0.27	11.57	96.69	5.19b	2b
24	7	81	0.724	20	8.4	0.293	0.97	1.2	0.32	11.57	96.69	5.19b	2b

Note: b – pier diameter; B – flume width; d_{50} – median diameter of sand; Q – discharge; h – approaching flow depth; V – depth-averaged approaching flow velocity; V_c – critical velocity; V/V_c – flow intensity; h/b – flow shallowness; B/b – blockage ratio; b/d_{50} – sediment coarseness; l – longitudinal spacing between the front and eccentric-pier; e – lateral spacing (eccentricity) between the front and eccentric-pier; t – experimental duration.

Table 3.7. List of parameters set for single pier experiments.

Exp. (--)	b (cm)	Q (lps)	h (cm)	V (m/s)	V/V_c (--)	h/b (--)	Fr (--)
1	7	20	11.6	0.213	0.67	1.65	0.20
2	7	20	10.5	0.235	0.75	1.5	0.23
3	7	20	9.5	0.261	0.85	1.35	0.27
4	7	20	8.4	0.293	0.97	1.2	0.32

3.8 Methodology

The critical condition for bed material movement was checked before each experiment using the following steps:

1. The flow depth in the flume is regulated using a tailgate. The approach flow depth (h) during the experimental run is kept fixed at 0.116, 0.105, 0.095, and 0.084 m by operating the tailgate. The bed slope for all the experiments is fixed at 1 V: 2400 H.
2. The depth-averaged approaching flow velocity (V) is set at about 77-99% of the critical velocity (V_c) of the uniform sand bed considering the side-wall effect to satisfy the clear water scour condition. It indicates that the present research considers only clear water approach flow conditions described by a threshold/critical Froude number of $0.77 \leq \mathrm{Fr}_t = V/V_c \leq 0.99$, where V is the approach flow velocity and V_c is the threshold or critical velocity (Oliveto and Hanger, 2002; Dey and Raikar, 2007). The depth-averaged approaching velocity is determined from the measured vertical profile of the approaching flow velocity at 2 m upstream of the pier where the presence of the pier did not affect the approaching flow.
3. A different ratio between the approach flow depth (h) and pier diameter (b) is selected for every four sets of experiments and it varies between $1.2 < h/b < 1.65$.
4. Considering steady uniform flow in a rectangular flume, the bed shear stress (τ_o) can be expressed as $\tau_o = \rho_f \times g \times R \times \sin\varphi_r$, where ρ_f is the mass density of the fluid/water, g is the gravitational acceleration, R is the hydraulic radius (wetted area/wetted perimeter) and φ_r is the angle between the longitudinal sloping bed and the horizontal direction. Here the resistance between water-air interfaces is usually very small when the water surface is smooth and can be conveniently neglected. It was considered that $\sin\varphi_r \approx \tan\varphi_r = S_o$ as the bed slope (S_o) is small. The bed shear stress (τ_o) is calculated.
5. The critical bed shear stress (τ_{oc}) is determined using the expression $\tau_{oc} = \Theta_c \Delta \rho_f g d_{50}$, where $\Delta = s\text{-}1$, Θ_c is the critical Shields parameter and is calculated using the following van Rijn's empirical equations for the Shields curve (van Rijn, 1984).

$$\Theta_c = \begin{cases} 0.24/D_* & D_* \leq 4 \\ 0.14/D_*^{0.64} & 4 < D_* \leq 10 \\ 0.04/D_*^{0.10} & 10 < D_* \leq 20 \\ 0.013 D_*^{0.29} & 20 < D_* \leq 150 \\ 0.55 & 150 < D_* \end{cases}$$

   where D_* is the dimensionless particle parameter, expressed as $D_* = d_{50}(\Delta g/\nu^2)^{1/3}$.
6. The critical velocity (V_c) is calculated from the equation, $V_c = u_{*c}[5.75\log\{h/(2d_{50})\} + 6]$, where u_{*c} is the critical shear velocity, expressed as $u_{*c} = (\tau_o/\rho_f)^{0.5}$. Finally, the critical discharge (Q_c) is determined using the continuity equation. The critical shear flow Reynolds number (Re_{*c}) is expressed as $\mathrm{Re}_{*c} = (u_{*c} d_{50})/\nu$, and is determined at a water temperature of 20°C. Figure 3.3 shows Shields' experimental results which relate critical Shields parameters (Θ_c) and (Re_{*c}) and is known as the Shields diagram

(1936). The threshold of sediment motion occurs when $\Theta > \Theta_c$ or $\tau_o > \tau_{oc}$ or $u_* > u_{*c}$. All the experiments are carried out under clear water scour condition.

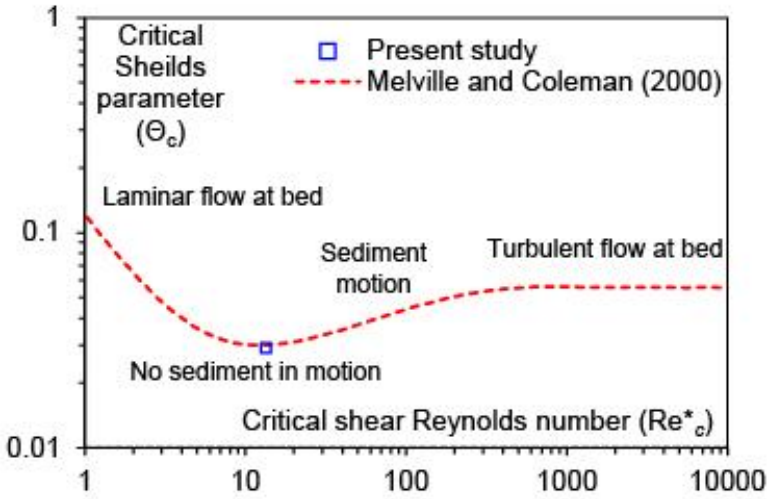


Fig. 3.3. Shields diagram showing no sediment motion for the present study.

7. During the experiment when a negligible (1 mm or less) difference in scour depth is observed at an interval of 1 hour after up to 12 hours of experimental run, it is considered that an equilibrium stage of the scour hole is attained. However, each experiment is carried out for up to 12 hours as it is considered adequate for achieving the equilibrium scour condition. After the run is stopped, the equilibrium scour depths are observed at the upstream base of the in-line front and eccentric rear piers. Then the scour depth at an equilibrium state is carefully measured by an LDS (laser distance sensor). The near equilibrium criteria used is similar to that proposed by Melville and Chiew (1999), i.e., the experiments are stopped when the change in scour depth does not exceed $0.05b$ (5% of the pier diameter) during a 24 h period.
8. The contour lines of the scour holes and sand depositions around the circular piers are plotted using the Surfer software.

Figure 3.4 shows a flowchart illustrating the methodology set for the present study.

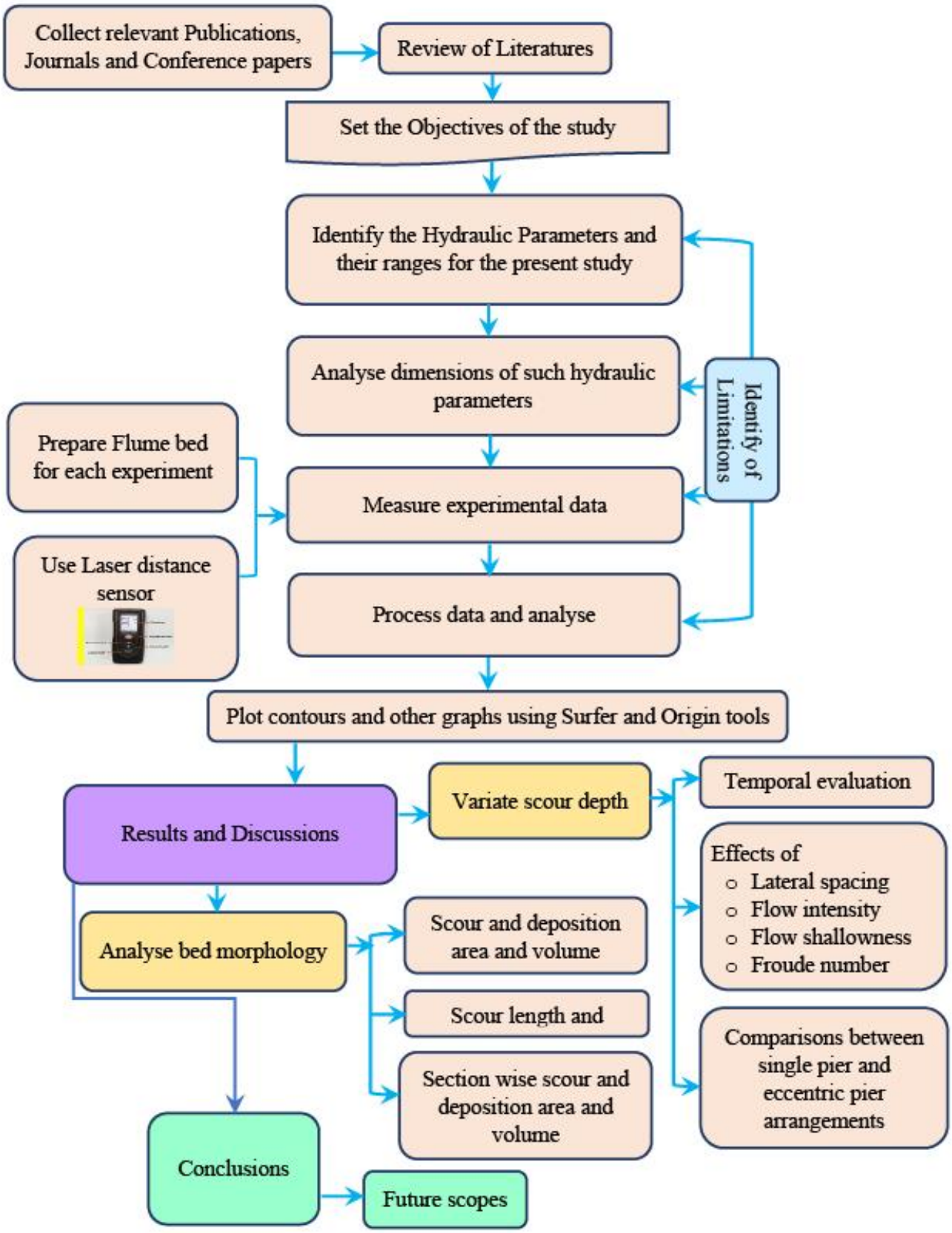


Fig. 3.4. Flowchart showing the methodology set for the present study.

CHAPTER-4

EXPERIMENTAL SETUP

4.1 Experimental setup

The experimental arrangement, data acquisition system and variables measured in the model study are described. Typical investigation of scour depth development around a bridge pier model has been carried out through various experiments. The experimental setup and conditions of the work are described in detail with the help of the schematic diagrams. All experiments are conducted in the Fluvial Hydraulics Laboratory of the School of Water Resources Engineering in Jadavpur University, Kolkata, West Bengal, India.

4.1.1 Experimental flume and equipment

In the present study, all experiments are executed in a large recirculating rectangular flume 11 m long, 0.81 m wide (internal) and 0.60 m deep (Figs. 4.1-4.2). The rectangular flume is divided into three sections: inlet, outlet and working section in the middle. At the inlet, a concrete stilling basin, consisting of a perforated baffle wall and two vertical steel screens is present, covering the entire cross section to dampen the flow disturbance. The working section of the flume is 5 m long and 3 m away from the inlet gate to cause the turbulence to become fully developed and is made up of a steel bottom and Plexiglas side walls along two sides for most of its length to facilitate visual observations. The water level in the flume is observed for a significant duration of time and observing no further change, it is declared to be steady and uniform. The water discharge is measured by a flowmeter connected to the upstream pipe at the inlet of the flume and maintained at 20 lps throughout the experiment by adjusting the outlet valve and bypass valve. The selected flow depth of water for each experiment is adjusted by a tailgate provided at the downstream



Fig. 4.1. Tilting flume to carry out all the laboratory experiments.

end of the flume. The water thereafter is flowing over the downstream obstruction. A movable trolley with a Vernier point gauge attached to it is placed on the flume. A vertical scale is fixed with the point gauge to measure the water level, initial bed level and scour depth.

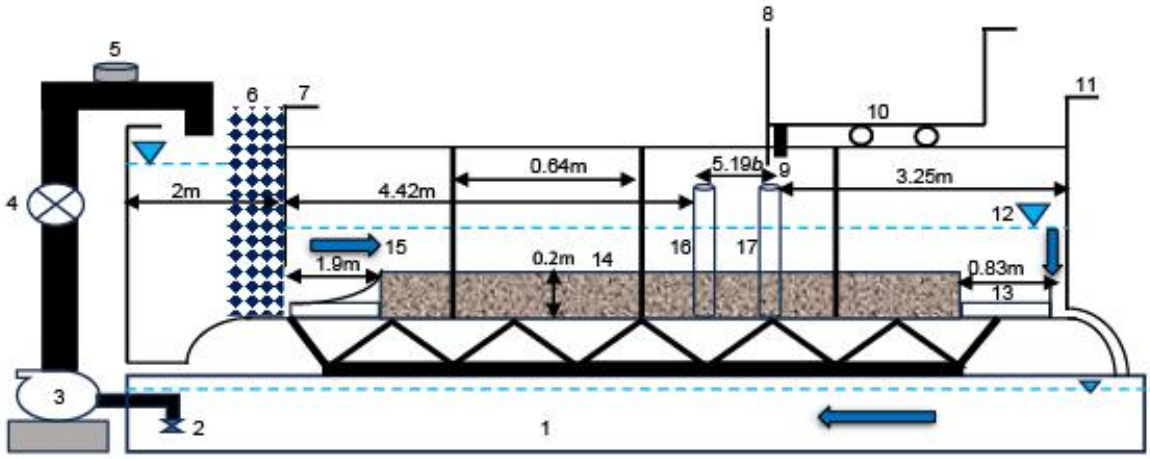


Fig. 4.2. Schematic diagram showing the tilting flume on which two piers are positioned eccentrically (1-reservoir, 2-foot valve, 3-pump, 4-control valve, 5-flow meter, 6-baffle plates and screens, 7-inlet gate, 8-point gauge, 9-laser distance sensor, 10-movable trolley, 11-outlet gate, 12-water level, 13-collector, 14-working section, 15-flow direction, 16-front pier model, and 17-eccentric pier model).

4.1.2 Pump

The hydraulic machines which convert mechanical energy into hydraulic energy are called pumps. The hydraulic energy is in the form of pressure energy. The re-circulating flow system is served by a 10-hp variable speed centrifugal pump (Fig. 4.3) with a maximum discharge of 30 lps. The pump has a rotational speed of 1430 rpm and a power of 7.5 kW. Water enters through a 20 cm diameter pipeline which goes directly to the flume. There are two pumps for alternative use.



Fig. 4.3. Pump used to recirculate the flow.

4.1.3 Laser distance sensor

The Leica DISTO^{TM} D110 Laser Distance Sensor (LDS) (Fig. 4.4) is used to measure the bed topography and the final scour profiles around the pier longitudinally and transversally. It can able to measure 70 m (≈ 230 ft) and measure tolerance ± 1.5 mm. The frequency used in the instrument is (2402 – 2480) MHz. Generally, it can take 500 readings in every battery set.

The weight of the Laser Distance Sensor is approximately 92 gm and it can work in the temperature range of (-25°C to 70°C). There is a Bluetooth with the instrument. One of the disadvantages of that instrument is that if the calibration is not made properly, a measurement error exists. There is one caution which indicates a potentially hazardous situation or unintended use, if not avoided may result in minor injury or appreciable damage in the material. The major advantage of the instrument is that it can give a quick and correct measurement.



Fig. 4.4. Laser distance sensor.

4.1.4 Flowmeter

A flowmeter is a device designed to monitor, measure or record the flow rate, pressure or discharge of liquids or gases. It serves a crucial role in various applications across industries, ensuring precise management and control of fluid dynamics. In our experiments, we have used a DASMESH model flowmeter (Fig. 4.5) for these measurements, ensuring the application of precise and dependable data for our analysis.


Fig. 4.5. Flowmeter.

4.1.5 Sediment bed

The Shields diagram remains the most effective way of determining threshold conditions for uniform sediments. For given fluid density, viscosity and sediment density, the Shields diagram can be used to obtain a plot of critical shear velocity (u_{*c}) against median particle size (d_{50}). The determination of threshold conditions for non-uniform sediment is not clear cut. The effects of particle size distribution may be important and thus u_{*c} would depend upon both d_{50} and geometric standard deviation of the sand (σ_g). With non-uniform sediments, a flow can disturb the grain, removing some but simply rearranging others into a stable pattern that develops into an armoured bed and stabilizes. Such flow is considered here to be above the threshold.

The mobile bed (stilling basin) zone about 5.3 m long is filled with sand of depth 0.2 m (Fig. 4.7). This section is established 2.9 m downstream region from the flume inlet gate to make the fully developed flow. A mechanical sieve analysis experiment is carried out to characterize the sand bed material used for the study. The results of the experiment show that the material of the bed with a median particle size (d_{50}) of 0.724 mm. The geometric standard deviation of the sand ($\sigma_g = (d_{84}/d_{16})^{0.5}$, ($d_{84}$ = 1.42 mm; d_{16} = 0.38 mm) is 1.93(<2), which

implies that the sand is of uniform size distribution (Raudkivi, 1998). Therefore, the scour depths to be measured after the experiments can reach their maximum clear water value. The downward grade of the prepared bed (S_o) is kept as 1:2400 for each experiment. The relative density (s) of the sand is 2.63. The plot of the grain size distribution test is depicted in Fig. 4.6. The pier diameter is also carefully chosen so that there is a negligible effect of sediment size on the depth of the scour. It is known that the bed material grain size does not affect the depth of scour if the pier width to grain size ratio (sediment coarseness) exceeds a value of about 25 according to Melville (1997). For the present study, the ratio is about 96.69 for the pier of 7 cm, which satisfies the criterion of Melville (1997). Table 4.1 shows sieve analysis data obtained from laboratory experimentation.

Table 4.1. Sieve analysis data obtained from laboratory experimentation.

Source of the soil	**Fluvial hydraulics laboratory**				**Pan weight (gm)**	371.13
Description of the soil	**Medium and non-uniform sand**		**Total weight (gm)**	1246	**Sample weight (gm)**	500
IS sieve aperture dimension (mm)	**Mass of each sieve (gm)**	**(Mass of sieve + retained soil) (gm)**	**Mass of soil retained in each sieve (gm)**	**% of mass retained in each sieve**	**Cumulative % retained**	**Cumulative % passing**
15	442.38	442.38	0.00	0.00	0.00	100.00
5.6	441.45	441.45	0.00	0.00	0.00	100.00
4.75	409.80	410.44	0.64	0.13	0.13	99.87
3.35	438.93	439.46	0.53	0.11	0.23	99.77
2.3	390.64	393.26	2.62	0.52	0.76	99.24
1.7	409.82	437.23	27.41	5.49	6.25	93.75
0.85	351.60	501.65	150.05	30.04	36.29	63.71
0.5	324.40	515.12	190.72	38.18	74.47	25.53
0.3	343.59	422.79	79.20	15.86	90.32	9.68
0.12	337.49	383.98	46.49	9.31	99.63	0.37
0.09	370.60	370.71	0.11	0.02	99.65	0.35
0.063	380.74	381.99	1.25	0.25	99.90	0.10
0.053	376.40	376.62	0.22	0.04	99.95	0.05
0.025	353.73	353.99	0.26	0.05	100.00	0.00
Pan	371.13	371.13	0.00	0.00	100.00	0.00
		Total	499.5	100		

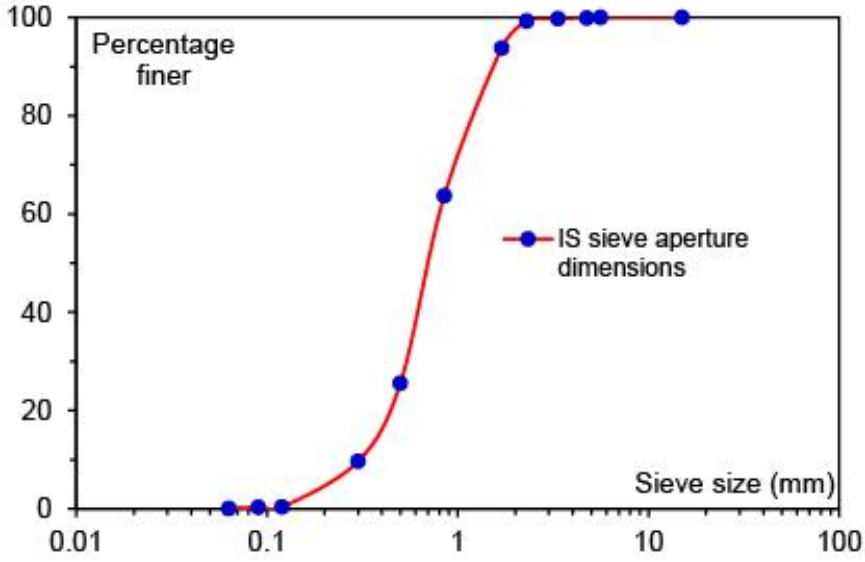


Fig. 4.6. Grain size distribution curve.

Small triangular sand waves with long gradual upstream slope (approximately 6°) and short steep downstream slope (approximately 32°) are called ripples. In the case of fine sediments ($d_{50} < 0.7$ mm), ripples are formed, while coarse sediments usually form dunes. The wave lengths of ripples are usually shorter than 300 mm or approximately equaling $150d_{50}$. It is assumed that ripples are formed if the viscous sub-layer is present when the threshold shear stress is just suppressed, while dunes are formed if the bed is hydraulically rough. The length of the ripples depends on the sediment size and the flow velocity but is essentially independent of the flow depth. Ripples may be superposed upon the upstream side of dunes.

Dunes are the bed-forms larger than ripples, whose profile is out of phase with the free surface profile. The stream-wise profile of a dune is roughly triangular with a mild upstream slope and a downstream slope approximately equal to the angle of repose. Dunes are formed in coarse sediment ($d_{50} > 0.6$ mm).

Above this, a zone of high turbulence exists, where a large production and dissipation of turbulent energy takes place. Near the zone of reattachment, the sediment particles are transported by turbulence, even when the local bed shear stress is below its threshold value. On the upstream side of the dune, the bed shear stress drives sediment particles uphill until they pass over the crest and eventually are buried in the bed for a period. As sediment is transported from the upstream side and deposited on the lee side of a dune, the result is a slow continuous downstream migration of the dunes.

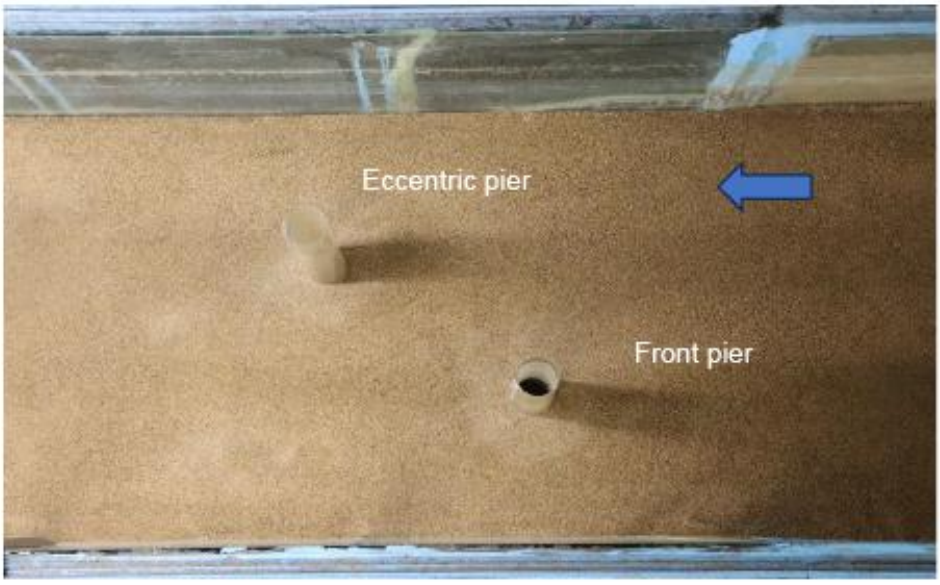


Fig. 4.7. Dry flume bed without water before performing the eccentric pier experiment.

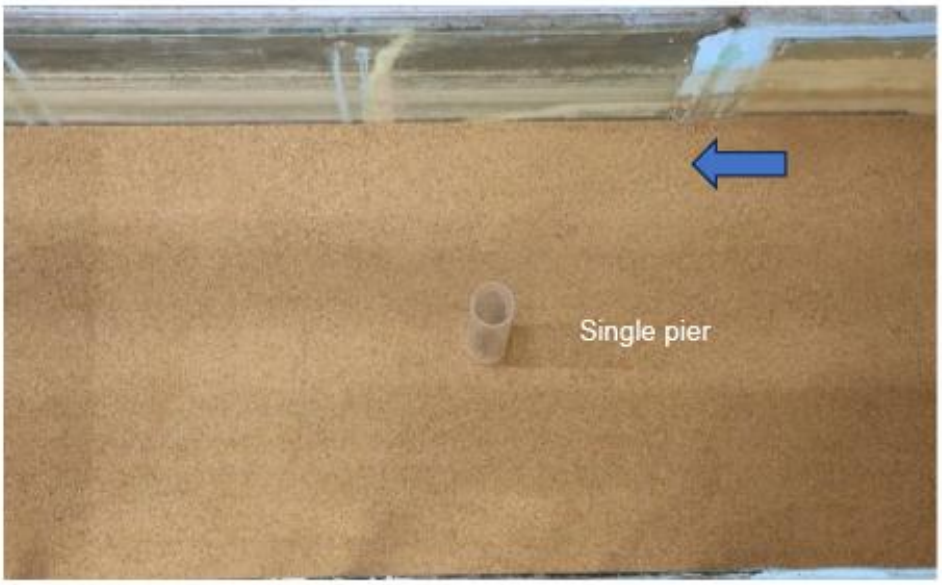


Fig. 4.8. Dry flume bed without water before performing the single pier experiment.

After placing the piers in the proper position with proper alignment properly flat sand bed is prepared. A very good experiment requires a properly prepared flat sand bed which is essential for attaining good experiment results. The flatness of the sand bed is checked with a spirit level. The sand bed preparation is done for every new setup of eccentric-pier arrangement.

4.2 Experimental procedure

In the present study investigation of scour depth around two identical circular shaped eccentric-pier arrangements has been carried out. In order to ensure repeatability and to isolate the effects of various parameters on equilibrium scour depth and rate of scour, a strict procedure is followed throughout these experiments. The following procedure is adopted for all experiments, performed on steady subcritical flow at clear water condition with plain bed, i.e., no formation of ripple or dune through the upstream portion at the working section:

1. Pier models are fixed vertically to their place. The front pier is within the middle of the working section and the longitudinal distance between the front and the eccentric piers is fixed, only the downstream pier is moved to set it at the desired pier lateral spacing in the next experiment (Table 3.6).
2. The sediment bed of the working section is filled with a layer of sand with a thickness of 20 cm.
3. The bed surface is levelled using a trowel. Levels are also checked for uniformity of the bed surface by using the spirit level and the point gauge.
4. To start the experiment, the flume is slowly filled with water to the required depth from downstream. It should be noted that extra care is required when filling the flume with water, especially for experiments of this nature where no sediment movement is allowed. Any deformity in the bed surface may develop ripples or dunes and general movement of the sand if the shear stress on the smooth bed is close to the critical shear stress.
5. The tailgate is closed and the working area is filled with water by hose from the upstream portion of the flume in order to allow any air bubbles to percolate out of the bed to avoid any settlement around the piers and to prevent any abrupt high-velocity which causes the disturbance in sand bed after starting pumping.
6. The water discharge is measured by a flowmeter connected to the upstream pipe at the inlet of the flume and maintained at 20 lps throughout the experiment by adjusting the outlet valve and bypass valve.
7. After the pumping starts, the selected flow depths (0.116 m, 0.105 m, 0.095 m, 0.084 m) of water for each experiment is adjusted by a tailgate provided at the downstream end of the flume. The flow thereafter is flowing over the downstream obstruction. A movable trolley with a LDS attached to it is placed on the flume.
8. Each experiment is conducted up to 12 hours. Time is recorded using a stopwatch during each experiment and at the end of time the flow is stopped then the scour depth is recorded using the Laser Distance Sensor (LDS).
9. The flume is drained slowly to avoid any change of the scour topography, the sand is allowed to dry and then the required measurements of sand bed upstream, downstream, longitudinally and transversely are recorded and photos of the scour topography around the pier are taken.
10. The sand bed is re-levelled and all steps are repeated by changing the lateral spacing between the front and eccentric piers ($3.5b$, $3b$, $2.75b$, $2.5b$, $2.25b$, $2b$).

CHAPTER-5

PARAMETER FRAMEWORK

5.1 Dimensional Analysis

Dimensional analysis is an efficient technique used to translate the phenomenon behaviour into a mathematical model or empirical equation. The physical regime of local scour around bridge piers cannot be understood accurately unless the correct dimensionless parameters describing the phenomenon are chosen in the proper way. The variables, which affect the local scour can be summarized in the following table.

5.1.1 Analysis of scouring parameters

The magnitude which interests the designer in determining the scouring depth of the pier is the temporal scour depths during the scouring process. The quantitative study is on the temporal depth d_{st} near the scour hole around the pier-limited. The d_{st} is measured below the bed level. Limiting the study to the case of the eccentric pier in a river whose flow is assumed to be steady and uniform, there are many parameters (Table 5.1) which may influence the scouring phenomenon.

Table 5.1. The classification of parameters that affect the local scour mechanism in MLT system.

Symbol	Parameter characterizing the flow	Unit	Dimension
ρ_f	Mass density of the fluid	kg/m^3	ML^{-3}
v	Kinematic viscosity of the fluid	m^2/s	L^{2}T^{-1}
g	Gravitational acceleration	m/s^2	LT^{-2}
h	Approach flow depth	m	L
V	Approach flow velocity	m/s	LT^{-1}
V_c	Critical mean approach flow	m/s	LT^{-1}
Re	Reynolds number	-	-
$Fr_{d_{50}}$	Densimetric Froude number	-	-
Symbol	**Parameter characterizing the bed material**	**Unit**	**Dimension**
ρ_s	Density of the sediment	kg/m^3	ML^{-3}
d_{50}	Median sediment size	mm	L

σ_g	Standard deviation of particle size distribution	-	-
Symbol	**Parameter characterizing the flume**	**Unit**	**Dimension**
S_o	Channel bed slope	-	-
B	Channel width	m	L
Symbol	**Parameter characterizing the pier**	**Unit**	**Dimension**
b	Pier diameter or pier width	m	L
K_S	Pier shape factor	-	-
α	Angle of approach flow to the axis	-	-
l	Longitudinal spacing	m	L
e	Transversal spacing (eccentricity)	m	L
β	Correction factor for alignment of the pier	-	-
Symbol	**Time**	**Unit**	**Dimension**
t	Duration of experiment	min	T

5.1.2 Dimensionless analysis

Temporal scour depth d_{st} increases over time t which can be a function of several parameters as represented in Eq. (5.1).

$$f_2\left(d_{st}, \rho_f, \nu, g, h, V, d_{50}, \rho_s, V_c, S_o, b, \alpha, e, \sigma_g, B, t, l, K_S, \beta\right) = 0 \tag{5.1}$$

For dimensionless analysis, here we have considered the Buckingham π theorem method, but not considered Rayleigh method as the number of variables is more than three or four. Here we have also considered the repeating variables such as b, V and ρ_f, where b is the geometric property, V is the flow property and ρ_s is the bed material property. Here total number of parameters (n) is equal to 19 and the number of independent parameters (m) is equal to 3. So we will get a total (n-m = 19-3 =16) i.e. 16 number of π terms (Eqs. 5.2-5.3).

$$f_3\left(\pi_1, \pi_2, \pi_3, \cdots\cdots\cdots, \pi_{n-m}\right) = 0 \tag{5.2}$$

$$f_4\left(\pi_1, \pi_2, \pi_3, \cdots\cdots\cdots, \pi_{16}\right) = 0 \tag{5.3}$$

After considering the repeating variables in the above stated way, all the 16 π-terms are represented as below-

$\pi_1 = b^{a1}\, V^{b1}\, \rho_s^{c1}\, d_{st}$

$\pi_2 = b^{a2}\, V^{b2}\, \rho_s^{c2}\, \nu$

$\pi_3 = b^{a3}\, V^{b3}\, \rho_s^{c3}\, g$

$\pi_4 = b^{a4}\, V^{b4}\, \rho_s^{c4}\, h$

$\pi_5 = b^{a5}\, V^{b5}\, \rho_s^{c5}\, d_{50}$

$\pi_6 = b^{a6}\, V^{b6}\, \rho_s^{c6}\, \rho_f$

$\pi_7 = b^{a7}\, V^{b7}\, \rho_s^{c7}\, V_c$

$\pi_8 = b^{a8}\, V^{b8}\, \rho_s^{c8}\, S_o$

$\pi_9 = H^{a9}\, V^{b9}\, \rho_s^{c9}\, \alpha$

$\pi_{10} = H^{a10}\, V^{b10}\, \rho_s^{c10}\, e$

$\pi_{11} = H^{a11}\, V^{b11}\, \rho_s^{c11}\, \sigma_g$

$\pi_{12} = H^{a12}\, V^{b12}\, \rho_s{}^{c12}\, B$
$\pi_{13} = H^{a13}\, V^{b13}\, \rho_s{}^{c13}\, t$
$\pi_{14} = H^{a14}\, V^{b14}\, \rho_s{}^{c14}\, l$
$\pi_{15} = H^{a15}\, V^{b15}\, \rho_s{}^{c15}\, K_s$
$\pi_{16} = H^{a16}\, V^{b16}\, \rho_s{}^{c16}\, \beta$

1. **Now for the first π term, we can write**

$\pi_1 = b^{a1}\, V^{b1}\, \rho_s{}^{c1}\, d_{st}$
As shown below, the dimensions of the π_1, b, V, ρ_s and d_{st} are put on the above equation to obtain the values of the coefficients a_1, b_1, and c_1.
$[M^0\, L^0\, T^0] = [M^0\, L^1\, T^0]^{a1}\, [M^0\, L^1\, T^{-1}]^{b1}\, [M^1\, L^{-3}\, T^0]^{c1}\, [M^0\, L^1\, T^0]$
Equating the power of M, L and T on either side we get the values, $a_1 = -1$, $b_1 = 0$, $c_1 = 0$ and by putting these values in the above π-term we get the first non-dimensional term as, $\pi_1 = b^{-1}\, V^0\, \rho_s{}^0\, d_{st}$ so, $\pi_1 = d_{st}/b$.

2. **Similarly, we can write the 2nd π term as**

$\pi_2 = b^{a2}\, V^{b2}\, \rho_s{}^{c2}\, v$
As shown below, the dimensions of the π_2, b, V, ρ_s and v are put on the above equation to obtain the values of the coefficients a_2, b_2, and c_2.
$[M^0\, L^0\, T^0] = [M^0\, L^1\, T^0]^{a2}\, [M^0\, L^1\, T^{-1}]^{b2}\, [M^1\, L^{-3}\, T^0]^{c2}\, [M^0\, L^2\, T^{-1}]$
Equating the power of M, L and T on either side we get the values, $a_2 = -1$, $b_2 = -1$, $c_2 = 0$ and by putting these values in the above π-term we get the first non-dimensional term as, $\pi_2 = b^{-1}\, V^{-1}\, \rho_s{}^0 v$ so, $\pi_2 = v/bV$.

3. **Similarly, we can write the 3rd π term as**

$\pi_3 = b^{a3}\, V^{b3}\, \rho_s{}^{c3}\, g$
As shown below, the dimensions of the π_3, b, V, ρ_s and g are put on the above equation to obtain the values of the coefficients a_3, b_3, and c_3.
$[M^0\, L^0\, T^0] = [M^0\, L^1\, T^0]^{a3}\, [M^0\, L^1\, T^{-1}]^{b3}\, [M^1\, L^{-3}\, T^0]^{c3}\, [M^0\, L^1\, T^{-2}]$
Equating the power of M, L and T on either side we get the values, $a_3 = 1$, $b_3 = -2$, $c_3 = 0$ and by putting these values in the above π-term we get the first non-dimensional term as, $\pi_3 = b^1\, V^2\, \rho_s{}^0\, g$ so, $\pi_3 = b\, g\, /V^2$.

4. **Similarly, we can write the 4th π term as**

$\pi_4 = b^{a4}\, V^{b4}\, \rho_s{}^{c4}\, h$
As shown below, the dimensions of the π_4, b, V, ρ_s and h are put on the above equation to obtain the values of the coefficients a_4, b_4, and c_4.
$[M^0\, L^0\, T^0] = [M^0\, L^1\, T^0]^{a4}\, [M^0\, L^1\, T^{-1}]^{b4}\, [M^1\, L^{-3}\, T^0]^{c4}\, [M^0\, L^1\, T^0]$

Equating the power of M, L and T on either side we get the values, $a_4 = -1$, $b_4 = 0$, $c_4 = 0$ and by putting these values in the above π-term we get the first non-dimensional term as, $\pi_4 = b^{-1} V^0 \rho_s^0 h$. Therefore, $\pi_4 = h/b$.

5. **Similarly, we can write the 5th π term as**

$\pi_5 = b^{a5} V^{b5} \rho_s^{c5} d_{50}$

As shown below, the dimensions of the π_5, b, V, ρ_s and d_{50} are put on the above equation to obtain the values of the coefficients a_5, b_5, and c_5.

$[M^0 L^0 T^0] = [M^0 L^1 T^0]^{a5} [M^0 L^1 T^{-1}]^{b5} [M^1 L^{-3} T^0]^{c5} [M^0 L^1 T^0]$

Equating the power of M, L and T on either side we get the values, $a_5 = -1$, $b_5 = 0$, $c_5 = 0$ and by putting these values in the above π-term we get the first non-dimensional term as, $\pi_5 = b^{-1} V^0 \rho_s^0 d_{50}$. So, $\pi_5 = d_{50}/b$.

6. **Similarly, we can write the 6th π term as**

$\pi_6 = b^{a6} V^{b6} \rho_s^{c6} \rho_f$

As shown below, the dimensions of the π_6, b, V, ρ_s and ρ_f are put on the above equation to obtain the values of the coefficients a_6, b_6, and c_6.

$[M^0 L^0 T^0] = [M^0 L^1 T^0]^{a6} [M^0 L^1 T^{-1}]^{b6} [M^1 L^{-3} T^0]^{c6} [M^1 L^{-3} T^0]$

Equating the power of M, L and T on either side we get the values, $a_6 = 0$, $b_6 = 0$, $c_6 = -1$ and by putting these values in the above π-term we get the first non-dimensional term as, $\pi_6 = b^0 V^0 \rho_s^{-1} \rho_f$. Therefore, $\pi_6 = \rho_f/\rho_s$.

7. **Similarly, we can write the 7th π term as**

$\pi_7 = b^{a7} V^{b7} \rho_s^{c7} V_c$

As shown below, the dimensions of the π_7, b, V, ρ_s and V_c are put on the above equation to obtain the values of the coefficients a_7, b_7, and c_7.

$[M^0 L^0 T^0] = [M^0 L^1 T^0]^{a7} [M^0 L^1 T^{-1}]^{b7} [M^1 L^{-3} T^0]^{c7} [M^0 L^1 T^{-1}]$

Equating the power of M, L and T on either side we get the values, $a_7 = 0$, $b_7 = -1$, $c_7 = 0$ and by putting these values in the above π-term we get the first non-dimensional term as, $\pi_7 = b^0 V^{-1} \rho_s^0 V_c$. Therefore, $\pi_7 = V_c/V$.

8. **Similarly, we can write the 8th π term as**

$\pi_8 = b^{a8} V^{b8} \rho_s^{c8} S_o$

As shown below, the dimensions of the π_8, b, V, ρ_s and S_o are put on the above equation to obtain the values of the coefficients a_8, b_8, and c_8.

$[M^0 L^0 T^0] = [M^0 L^1 T^0]^{a8} [M^0 L^1 T^{-1}]^{b8} [M^1 L^{-3} T^0]^{c8} [M^0 L^0 T^0]$

Equating the power of M, L and T on either side we get the values, $a_8 = 0$, $b_8 = 0$, $c_8 = 0$ and by putting these values in the above π-term we get the first non-dimensional term as, $\pi_8 = b^0 V^0 \rho_s^0 S_o$. Therefore, $\pi_8 = S_o$.

9. Similarly, we can write the 9th π term as

$\pi_9 = b^{a9}\, V^{b9}\, \rho_s^{c9}\, \alpha$

As shown below, the dimensions of the π_9, b, V, ρ_s and α are put on the above equation to obtain the values of the coefficients a_9, b_9, and c_9.

$[M^0\, L^0\, T^0] = [M^0\, L^1\, T^0]^{a9}\, [M^0\, L^1\, T^{-1}]^{b9}\, [M^1\, L^{-3}\, T^0]^{c9}\, [M^0\, L^0\, T^0]$

Equating the power of M, L and T on either side we get the values, $a_9 = 0$, $b_9 = 0$, $c_9 = 0$ and by putting these values in the above π-term we get the first non-dimensional term as, $\pi_9 = b^0\, V^0\, \rho_s^0\, \alpha$. Therefore, $\pi_9 = \alpha$.

10. Similarly, we can write the 10th π term as

$\pi_{10} = b^{a10}\, V^{b10}\, \rho_s^{c10}\, e$

As shown below, the dimensions of the π_{10}, b, V, ρ_s and e are put on the above equation to obtain the values of the coefficients a_{10}, b_{10}, and c_{10}.

$[M^0\, L^0\, T^0] = [M^0\, L^1\, T^0]^{a10}\, [M^0\, L^1\, T^{-1}]^{b10}\, [M^1\, L^{-3}\, T^0]^{c10}\, [M^0\, L^1\, T^0]$

Equating the power of M, L and T on either side we get the values, $a_{10} = -1$, $b_{10} = 0$, $c_{10} = 0$ and by putting these values in the above π-term we get the first non-dimensional term as, $\pi_{10} = b^{-1}\, V^0\, \rho_s^0\, e$. Therefore, $\pi_{10} = e/b$.

11. Similarly, we can write the 11th π term as

$\pi_{11} = b^{a11}\, V^{b11}\, \rho_s^{c11}\, \sigma_g$

As shown below, the dimensions of the π_{11}, b, V, ρ_s and σ_g are put on the above equation to obtain the values of the coefficients a_{11}, b_{11}, and c_{11}.

$[M^0\, L^0\, T^0] = [M^0\, L^1\, T^0]^{a11}\, [M^0\, L^1\, T^{-1}]^{b11}\, [M^1\, L^{-3}\, T^0]^{c11}\, [M^0\, L^0\, T^0]$

Equating the powers of M, L and T on either side we get the values, $a_{11} = 0$, $b_{11} = 0$, $c_{11} = 0$ and by putting these values in the above π-term we get the first non-dimensional term as, $\pi_{11} = b^0\, V^0\, \rho_s^0\, \sigma_g$. Therefore, $\pi_{11} = \sigma_g$.

12. Similarly, we can write the 12th π term as

$\pi_{12} = b^{a12}\, V^{b12}\, \rho_s^{c12}\, B$

As shown below, the dimensions of the π_{12}, b, V, ρ_s and B are put on the above equation to obtain the values of the coefficients a_{12}, b_{12}, and c_{12}.

$[M^0\, L^0\, T^0] = [M^0\, L^1\, T^0]^{a12}\, [M^0\, L^1\, T^{-1}]^{b12}\, [M^1\, L^{-3}\, T^0]^{c12}\, [M^0\, L^1\, T^0]$

Equating the powers of M, L and T on either side we get the values, $a_{12} = -1$, $b_{12} = 0$, $c_{12} = 0$ and by putting these values in the above π-term we get the first non-dimensional term as, $\pi_{12} = b^{-1}\, V^0\, \rho_s^0\, B$. Therefore, $\pi_{12} = B/b$.

13. Similarly, we can write the 13th π term as

$\pi_{13} = b^{a13}\ V^{b13}\ \rho_s^{c13}\ t$

As shown below, the dimensions of the π_{13}, b, V, ρ_s and t are put on the above equation to obtain the values of the coefficients a_{13}, b_{13}, and c_{13}.

$[M^0\ L^0\ T^0] = [M^0\ L^1\ T^0]^{a13}\ [M^0\ L^1\ T^{-1}]^{b13}\ [M^1\ L^{-3}\ T^0]^{c13}\ [M^0\ L^0\ T^1]$

Equating the powers of M, L and T on either side we get the values, $a_{13} = -1$, $b_{13} = 1$, $c_{13} = 0$ and by putting these values in the above π-term we get the first non-dimensional term as, $\pi_{13} = b^{-1}\ V^1\ \rho_s^0 t$. Therefore, $\pi_{13} = Vt/b$.

14. Similarly, we can write the 14th π term as

$\pi_{14} = b^{a14}\ V^{b14}\ \rho_s^{c14}\ l$

As shown below, the dimensions of the π_{14}, b, V, ρ_s and l are put on the above equation to obtain the values of the coefficients a_{13}, b_{13}, and c_{13}.

$[M^0\ L^0\ T^0] = [M^0\ L^1\ T^0]^{a14}\ [M^0\ L^1\ T^{-1}]^{b14}\ [M^1\ L^{-3}\ T^0]^{c14}\ [M^0\ L^1\ T^0]$

Equating the powers of M, L and T on either side we get the values, $a_{14} = -1$, $b_{14} = 0$, $c_{14} = 0$ and by putting these values in the above π-term we get the first non-dimensional term as, $\pi_{14} = b^{-1}\ V^0\ \rho_s^0\ l$. Therefore, $\pi_{14} = l/b$.

15. Similarly, we can write the 15th π term as

$\pi_{15} = b^{a15}\ V^{b15}\ \rho_s^{c15}\ K_s$

As shown below, the dimensions of the π_{15}, b, V, ρ_s and K_s are put on the above equation to obtain the values of the coefficients a_{15}, b_{15}, and c_{15}.

$[M^0\ L^0\ T^0] = [M^0\ L^1\ T^0]^{a15}\ [M^0\ L^1\ T^{-1}]^{b15}\ [M^1\ L^{-3}\ T^0]^{c15}\ [M^0\ L^0\ T^0]$

Equating the powers of M, L and T on either side we get the values, $a_{15} = 0$, $b_{15} = 0$, $c_{15} = 0$ and by putting these values in the above π-term we get the first non-dimensional term as, $\pi_{15} = b^0\ V^0\ \rho_s^0 K_s$. Therefore, $\pi_{15} = K_s$.

16. Similarly, we can write the 16th π term as

$\pi_{16} = b^{a16}\ V^{b16}\ \rho_s^{c16}\ \beta$

As shown below, the dimensions of the π_{16}, b, V, ρ_s and β are put on the above equation to obtain the values of the coefficients a_{16}, b_{16}, and c_{16}.

$[M^0\ L^0\ T^0] = [M^0\ L^1\ T^0]^{a16}\ [M^0\ L^1\ T^{-1}]^{b16}\ [M^1\ L^{-3}\ T^0]^{c16}\ [M^0\ L^0\ T^0]$

Equating the powers of M, L and T on either side we get the values, $a_{16} = 0$, $b_{16} = 0$, $c_{16} = 0$ and by putting these values in the above π-term we get the first non-dimensional term as, $\pi_{16} = b^0\ V^0\ \rho_s^0\ \beta$. Therefore, $\pi_{16} = \beta$.

Now the dimensionless groups can be written in the following form (Eqs. 5.3-5.4):

$$f_4(\pi_1, \pi_2, \pi_3, \cdots\cdots, \pi_{16}) = 0 \tag{5.3}$$

$$f_5\left(\frac{d_{st}}{b}, \frac{\nu}{bV}, \frac{bg}{V^2}, \frac{h}{b}, \frac{d_{50}}{b}, \frac{\rho_f}{\rho_s}, \frac{V_c}{V}, S_o, \alpha, \frac{e}{b}, \sigma_g, \frac{B}{b}, \frac{Vt}{b}, \frac{l}{b}, K_s, \beta\right) = 0 \tag{5.4}$$

The following explains the justification for establishing the dimensionless groups: The fixed parameters are b/d_{50} – sediment coarseness; B/b – blockage ratio; channel bed slope, S_o – 1 V: 2400 H; ρ_f/ρ_s –density ratio; pier shape factor (K_s) is 1 for the circular pier (Shukur and Obeid, 2016); β – correction factor for alignment of the pier; longitudinal spacing between piers (l) – 5.19b (Das et al., 2016); Reynolds number (Re) is greater than 7000 (Monti, 1994; as referred in Khaple et al., 2017) which is negligible flow viscosity; angle of approach flow to the axis (α) is also negligible as lateral spacing and longitudinal spacing between the piers has taken in the present study. Since in the present study, only one bed material is used, the term sediment coarseness, σ_g can be ignored. Also, the densimetric Froude number $Fr_{d_{50}}$, a very important parameter, can be ignored as it takes into account both the mean particle size of the sediments and inertia force.

Finally, neglecting the above mentioned parameters, Eq. 5.4 can be written as Eq. 5.5.

$$f_6\left(\frac{d_{st}}{b}, \frac{bg}{V^2}, \frac{h}{b}, \frac{V}{V_c}, \frac{e}{b}, \frac{Vt}{b}\right) = 0 \tag{5.5}$$

CHAPTER-6

RESULTS AND DISCUSSION

6.1 Results and discussion

In this study, 24 numbers of experiments with eccentric circular pier arrangements and four single circular pier experiments have been carried out in the tilting flume. Six different lateral spacings between the eccentric piers are used in the present work. Like Fig. 6.1, the front pier is kept fixed while the eccentric pier position is kept variable for each lateral spacing with respect to the front pier. The longitudinal spacing ($l = 5.19b$) is generally kept fixed as per Das et al. (2016). Four different flow depths (11.6 cm, 10.5 cm, 9.5 cm, and 8.4 cm) have been taken during the experiments to observe the bed morphology around the piers. The scour geometry and scour morphology are studied for the piers with 7 cm width with the change of eccentricity between the piers. It should be mentioned that each experimental run was carried out for up to 10 hours. Figure 6.2 shows the single pier experimental set up. The experimental outcomes are discussed below.

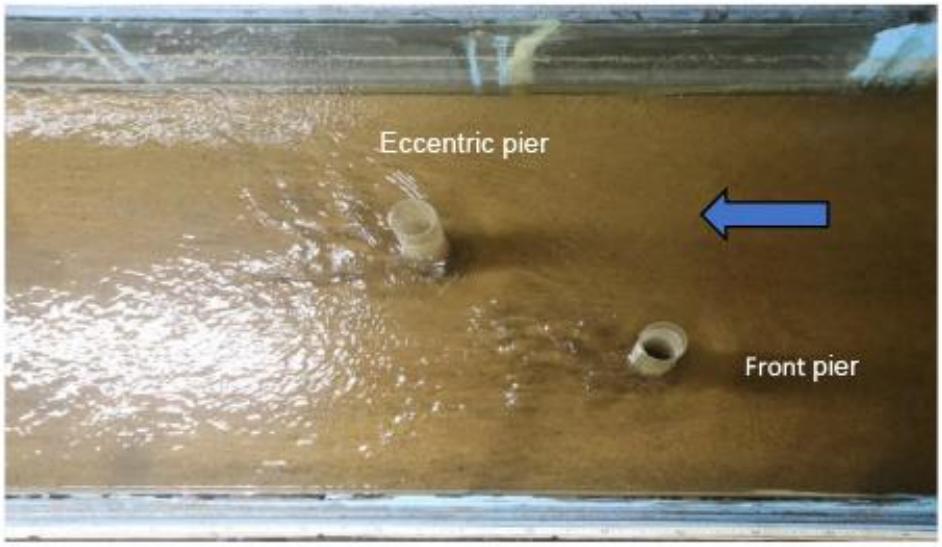


Fig. 6.1. Experimental photograph of eccentric piers captured during Exp. 14.

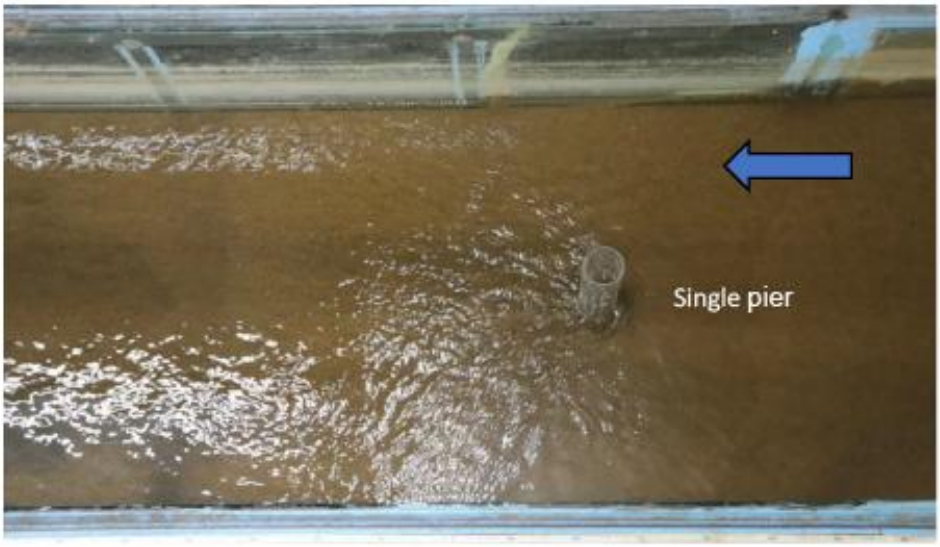


Fig. 6.2. Experimental photograph of a single pier captured during Exp. 4.

6.2 Experimental outcomes based on non-dimensional flow parameters

Table 6.1 presents the experimental results of a single pier and also results with varied eccentricities, including 3.5*b*, 3*b*, 2.75*b*, 2.5*b*, 2.25*b*, and 2*b*, with V/V_c ranging from 0.67 to 0.97 and h/b ranging from 1.65 to 1.2. Additionally, Fr ranging between 0.20 to 0.32 have been examined. Each experiment has a unique run duration (t), which is also displayed in the table. Here, d_{ss}, d_{sr} and d_{sf} represent the maximum scour depths for the single pier, eccentric pier and front pier, respectively. The non-dimensional values of d_{ss}, d_{sr} and d_{sf} are shown in Table 6.1. The included maximum dimensionless time $(Vt/b)_{max}$ is also shown in the table.

Table 6.1. Experimental outcomes based on all the experiments of single pier and eccentric pier arrangements.

Exp.	e/b	V/V_c	h/b	Fr	t (min)	$(Vt/b)_{max}$	d_{ss}/b	d_{sf}/b	d_{sr}/b
1	–	0.678	1.65	0.20	360	98948.67	0.22	–	–
2	3.5	0.678	1.65	0.20	660	120937.30	–	0.36	0.45
3	3	0.678	1.65	0.20	600	109943.00	–	0.41	0.45
4	2.75	0.678	1.65	0.20	660	120937.30	–	0.42	0.46
5	2.5	0.678	1.65	0.20	600	109943.00	–	0.36	0.48
6	2.25	0.678	1.65	0.20	540	98948.67	–	0.45	0.55
7	2	0.678	1.65	0.20	600	109943.00	–	0.36	0.42
8	–	0.757	1.50	0.23	480	133030.99	0.39	–	–
9	3.5	0.757	1.50	0.23	660	133031.00	–	0.40	0.51
10	3	0.757	1.50	0.23	720	145124.70	–	0.49	0.59
11	2.75	0.757	1.50	0.23	660	133031.00	–	0.54	0.66
12	2.5	0.757	1.50	0.23	600	120937.30	–	0.46	0.57
13	2.25	0.757	1.50	0.23	600	120937.30	–	0.59	0.69

14	2	0.757	1.50	0.23	540	108843.50	–	0.52	0.62
15	–	0.854	1.35	0.27	360	120937.26	0.83	–	–
16	3.5	0.854	1.35	0.27	420	94062.32	–	0.91	0.96
17	3	0.854	1.35	0.27	720	161249.70	–	0.87	0.97
18	2.75	0.854	1.35	0.27	420	94062.32	–	0.92	0.95
19	2.5	0.854	1.35	0.27	600	134374.70	–	0.89	0.92
20	2.25	0.854	1.35	0.27	600	134374.70	–	0.89	1.02
21	2	0.854	1.35	0.27	540	120937.30	–	0.87	0.97
22	–	0.979	1.20	0.32	120	52910.05	0.89	–	–
23	3.5	0.979	1.20	0.32	120	30234.32	–	0.95	1.08
24	3	0.979	1.20	0.32	420	105820.10	–	1.02	1.10
25	2.75	0.979	1.20	0.32	80	20156.21	–	0.95	1.08
26	2.5	0.979	1.20	0.32	80	20156.21	–	0.91	0.99
27	2.25	0.979	1.20	0.32	300	75585.79	–	0.95	1.13
28	2	0.979	1.20	0.32	180	45351.47	–	0.96	1.07

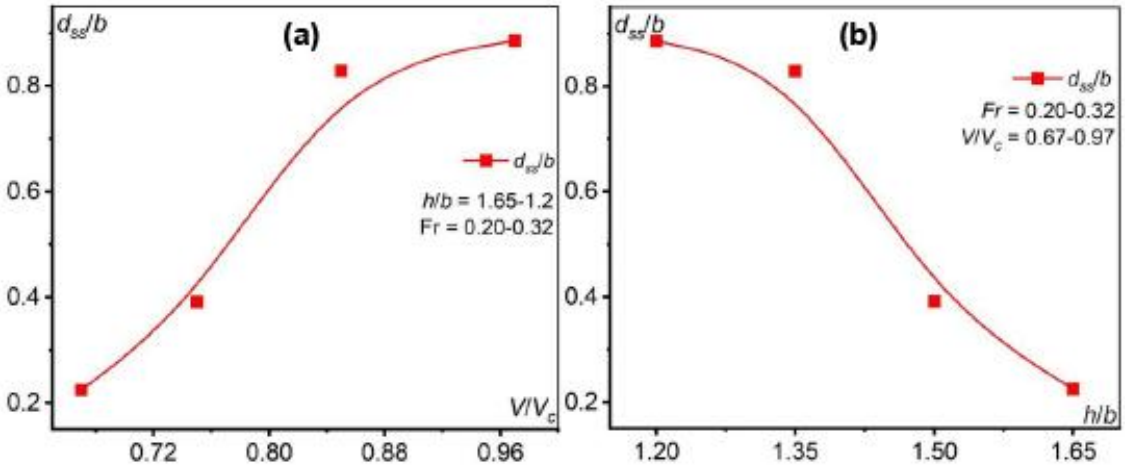
6.2.1 Effect of flow intensity, flow shallowness and Froude number on the scour depth at single pier

In Figure 6.3(a), non-dimensionalised scouring depths (d_{ss}/b) at the single pier are plotted with respect to the flow intensity (V/V_c) which increases with the increase in flow intensity.

In Figure 6.3(b), non-dimensionalised scouring depths (d_{ss}/b) at the single pier are plotted with respect to the flow shallowness (h/b) which decreases with the increase of flow shallowness.

In Figure 6.3(c), non-dimensionalised scouring depths (d_{ss}/b) at the single pier are plotted with respect to the Froude number (Fr) which increases with the increase of the Froude number.

The dimensionless equilibrium scour depths (d_{st}/b) and dimensionless time (Vt/b) for each of the 4 experiments with different flow conditions are displayed in Fig. 6.3(d) where in the flow condition, $V/Vc = 0.97$, $h/b = 1.2$, Fr = 0.32, d_{st}/b gives the maximum value.



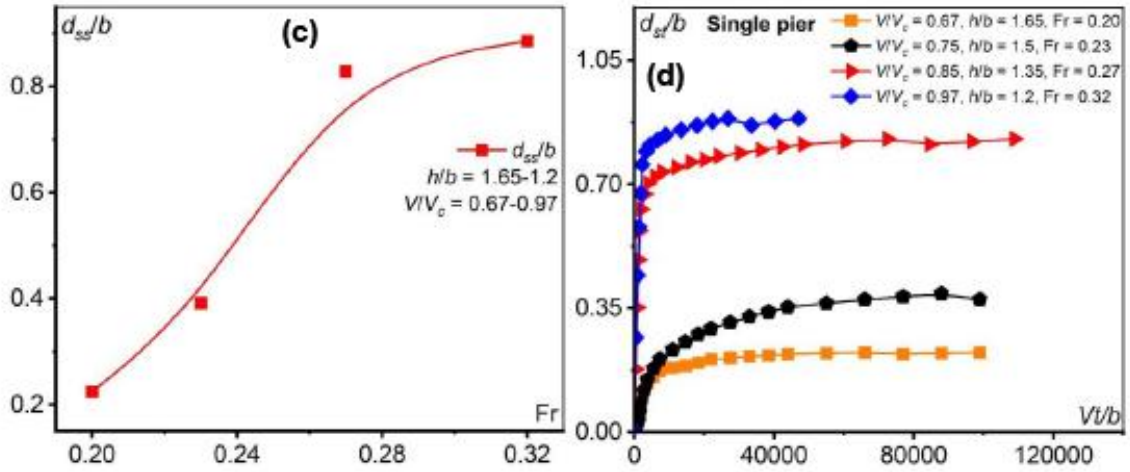


Fig. 6.3. Parameters **(a)** flow intensity, **(b)** flow shallowness, **(c)** Froude number, and **(d)** temporal variation influencing scour depth at a single pier.

6.2.2 Temporal evaluation of scour depth

The dimensionless temporal scour depth (d_{st}/b) and dimensionless time (Vt/b) for each of the 24 experiments with different flow conditions are displayed in Fig. 6.4(a-h).

Given the flow conditions of $V/V_c = 0.67$, $h/b = 1.65$, Fr = 0.20, the highest value of d_{st}/b for the front pier has been determined for $e = 2.25b$, while the lowest value has been found for $e = 3.5b$ and $2b$ as shown in Fig. 6.4(a). The highest value of d_{st}/b for the eccentric pier for the same flow condition has been determined for $e = 2.25b$, while the lowest value has been found for $e = 2b$ as given in Fig. 6.4(b).

From Fig. 6.4 (a-b), it can be seen from experimental data that the value of d_{st}/b for the eccentric pier of above-mentioned flow conditions is always higher than the value of d_{st}/b for the front pier for all eccentric arrangements. It might result from the pier group effects described in section 1.13.

Given the flow conditions of $V/V_c = 0.75$, $h/b = 1.5$, Fr = 0.23, the highest value of d_{st}/b for the front pier has been determined for $e = 2.25b$, while the lowest value has been found for $e = 3.5b$ shown in Fig. 6.4(c). The highest value of d_{st}/b for the eccentric pier for the same flow condition has been determined for $e = 2.25b$, while the lowest value has been identified for $e = 3.5b$ given in Fig. 6.4(d).

From Fig. 6.4(c-d), it can be seen from experimental data that the value of d_{st}/b for the eccentric pier of the above-mentioned flow conditions is always higher than the value of d_{st}/b for the front pier for all eccentric arrangements. It might result from the pier group effects as described in section 1.13.

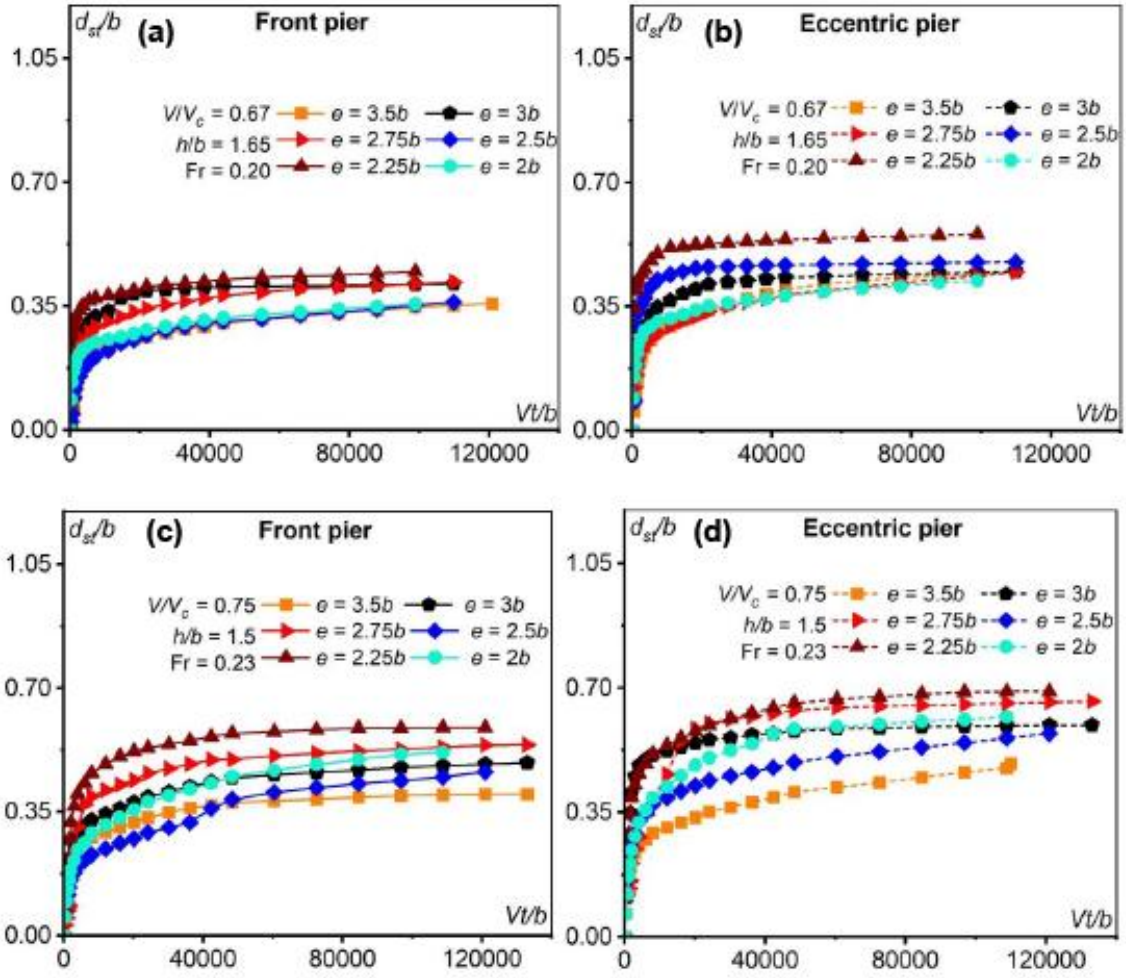
Given the flow conditions of $V/V_c = 0.85$, $h/b = 1.35$, Fr = 0.27, the highest value of d_{st}/b for the front pier has been determined for $e = 2.75b$, while the lowest value has been found for $e = 2b$ and $3b$ shown in Fig. 6.4(e). The highest value of d_{st}/b for the eccentric pier for the same flow condition has been determined for $e = 2.25b$, while the lowest value has been found for $e = 2.5b$ given in Fig. 6.4(f).

From Fig. 6.4(e-f), it can be seen from experimental data that the value of d_{st}/b for the eccentric pier of the above-mentioned flow conditions is always higher than the value of d_{st}/b

for the front pier for all eccentric arrangements. It might result from the pier group effects as detailed in section 1.13.

Given the flow conditions of $V/V_c = 0.97$, $h/b = 1.2$, Fr = 0.32, the highest value of d_{st}/b for the front pier has been determined for $e = 3b$, while the lowest value has been found for $e = 2.5b$ shown in Fig. 6.4(g). The highest value of d_{st}/b at the eccentric pier for the same flow condition has been determined for $e = 2.25b$, while the lowest value has been noticed for $e = 2.5b$ given in Fig. 6.4(h).

From Fig. 6.4(g-h), it can be seen from experimental data that the value of d_{st}/b for the eccentric pier of the above-mentioned flow conditions is always higher than the value of d_{st}/b for the front pier for all eccentric arrangements. It might result from the influence of the pier group as described in section 1.13.



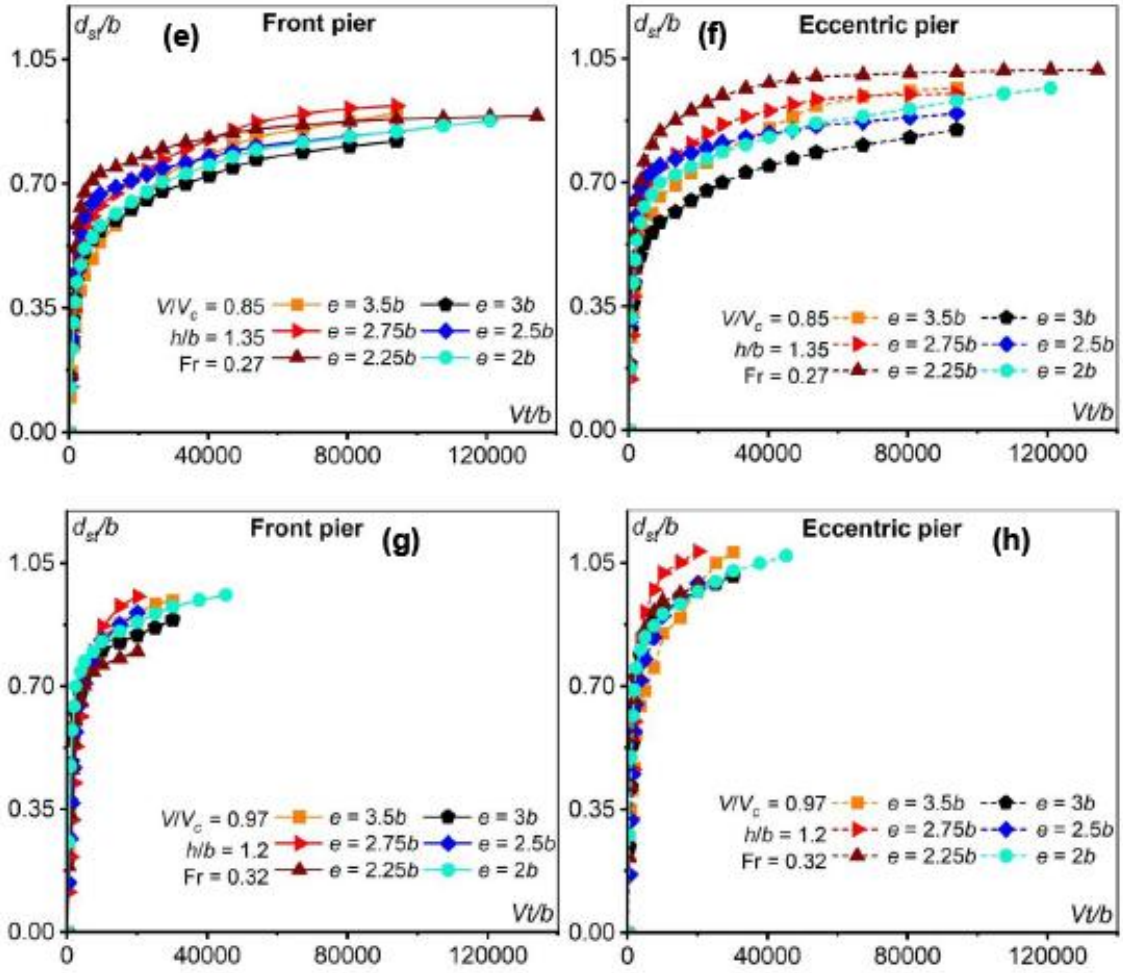


Fig. 6.4. Variation of temporal scour depth in eccentric pier arrangements for various flow conditions **(a-b)** $V/V_c = 0.67$, $h/b = 1.65$, Fr = 0.20, **(c-d)** $V/V_c = 0.75$, $h/b = 1.5$, Fr = 0.23, **(e-f)** $V/V_c = 0.85$, $h/b = 1.35$, Fr = 0.27, and **(g-h)** $V/V_c = 0.97$, $h/b = 1.2$, Fr = 0.32 for front and eccentric piers.

6.2.3 Effect of pier non-dimensional lateral spacing (*e/b*)

In Figure 6.5 (a-d), non-dimensionalised scouring depths (d_{se}/b) at the front and eccentric pier are plotted with respect to the non-dimensionalised lateral spacing (e/b) for different flow conditions.

Given the flow conditions of $V/V_c = 0.67$, h/b =1.65, Fr = 0.20, d_{se}/b for the front pier first increases with subsequent increase in eccentricity until a certain maximum point (e = 2.25b) and then after decreases with increasing eccentricity in Fig. 6.5(a). The d_{se}/b for the eccentric pier is found maximum at $e = 2.25b$, minimum at $e = 2b$ as observed in Fig. 6.5(a) and shows more or less similar phenomena.

Given the flow conditions of $V/V_c = 0.75$, h/b =1.5, Fr = 0.23, and d_{se}/b for the front pier shows increasing and decreasing phenomena in Fig. 6.5(b). The d_{se}/b for the eccentric pier is identified as the maximum at $e = 2.25b$, minimum at $e = 3.5b$ as observed in Fig. 6.5(b) and shows more or less similar phenomena due to the group effect.

Given the flow conditions of $V/V_c = 0.85$, h/b =1.35, Fr = 0.27, and d_{se}/b for the front pier shows increasing and decreasing phenomena in Fig. 6.5(c). The d_{se}/b for the eccentric pier is identified as a maximum at $e = 2.25b$, minimum at $e = 3.5b$ as observed in Fig. 6.5(c) and shows more or less similar phenomena due to the group effect.

Given the flow conditions of $V/V_c = 0.97$, h/b =1.2, Fr = 0.32, d_{se}/b for the front pier always shows a lesser value than the eccentric pier in Fig. 6.5(d). The d_{se}/b for the eccentric pier is identified as a maximum at $e = 2.25b$, minimum at $e = 2.5b$ as observed in Fig. 6.5(d) and it is a result of the group effect.

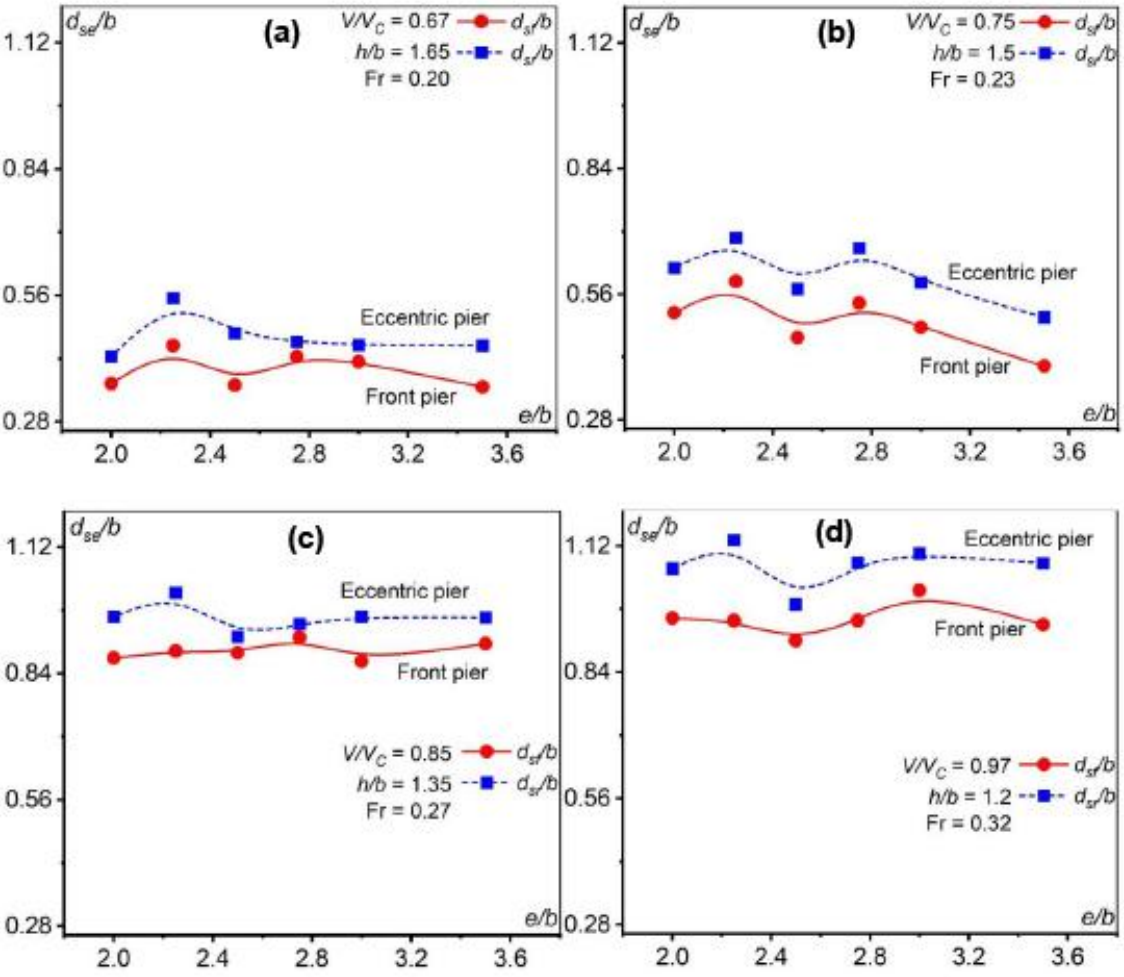


Fig. 6.5. Variation of maximum scour depth with pier lateral spacing for **(a)** $V/V_c = 0.67$, $h/b = 1.65$, Fr = 0.20, **(b)** $V/V_c = 0.75$, $h/b = 1.5$, Fr = 0.23, **(c)** $V/V_c = 0.85$, $h/b = 1.35$, Fr = 0.27, and **(d)** $V/V_c = 0.97$, $h/b = 1.2$, Fr = 0.32.

6.2.4 Effect of flow intensity (V/V_c)

In Figure 6.6(a-f), non-dimensionalised scouring depths (d_{se}/b) at the front and eccentric pier are plotted with respect to the flow intensity (V/V_c) for varying eccentricity (e).

Given the flow conditions of V/V_c=0.67-0.97, h/b =1.65-1.2, $e = 2b$ - $3.5b$, d_{se}/b for both the pier is increasing as V/V_c is increasing. The lowest scour depth for both the front pier is

observed at $V/V_c = 0.67$, while the highest scour depth for both piers is observed in Fig. 6.6(a-f) for $V/V_c = 0.97$.

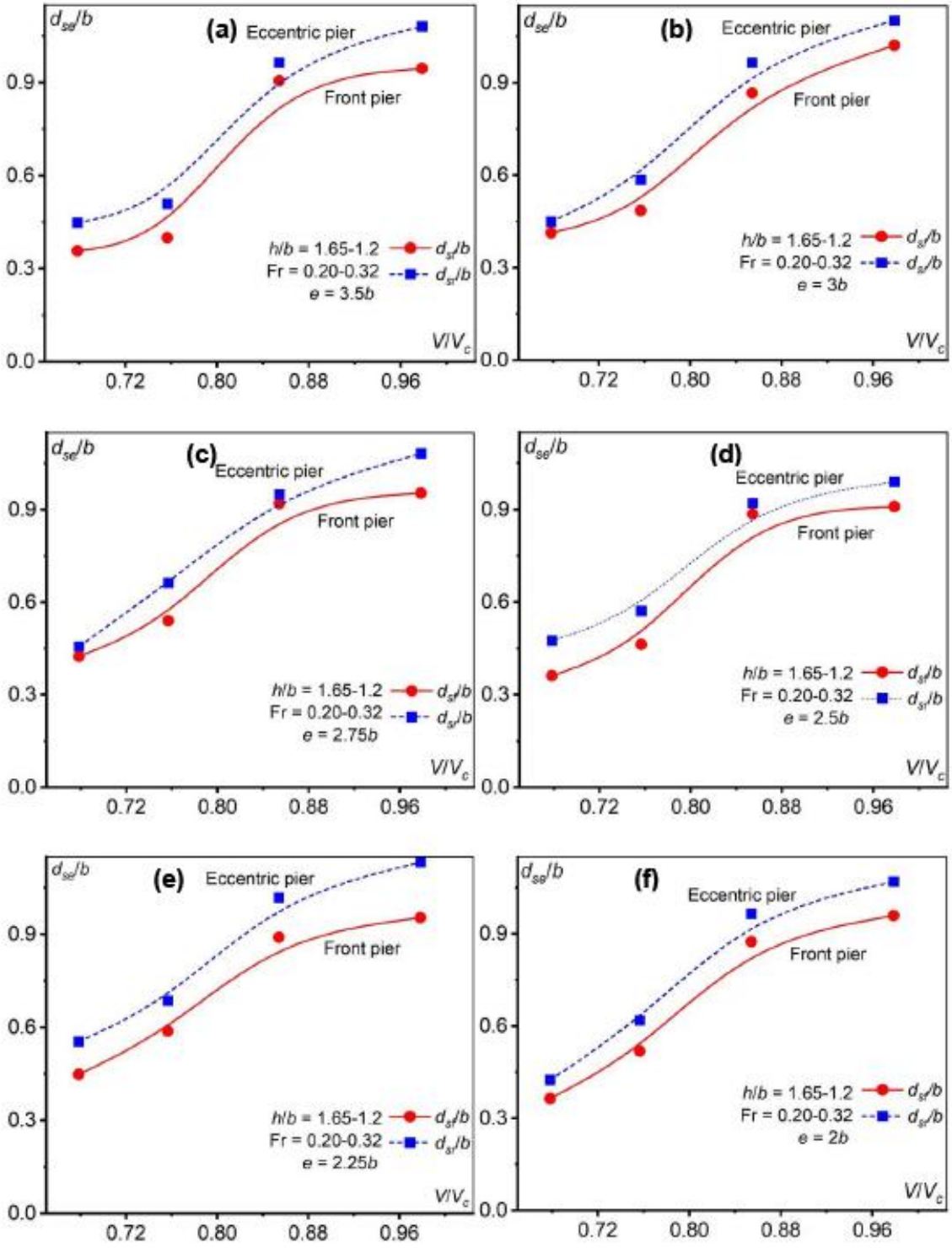
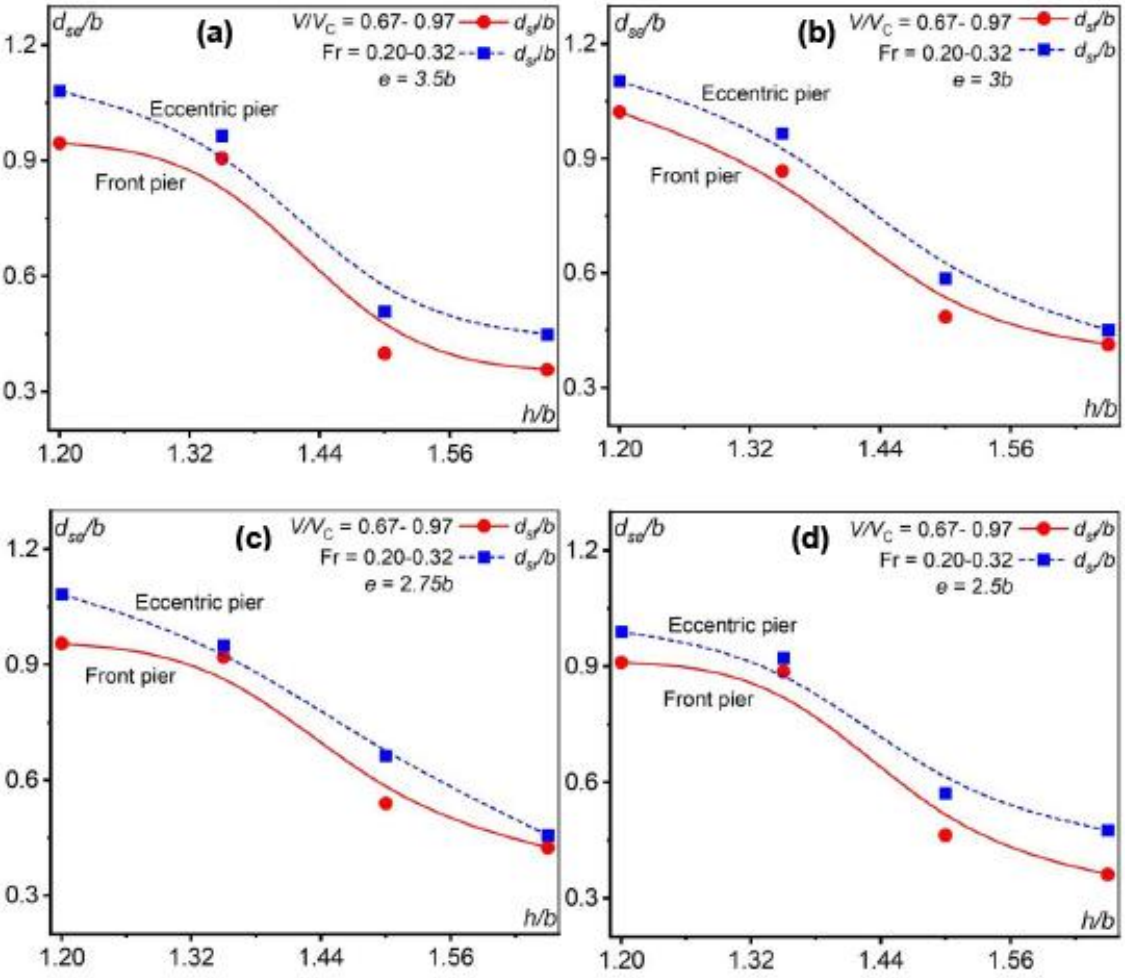


Fig. 6.6. Variation of maximum scour depth with flow intensity for **(a)** $e = 3.5b$, **(b)** $e = 3b$, **(c)** $e = 2.75b$, **(d)** $e = 2.5b$, **(e)** $e = 2.25b$, and **(f)** $e = 2b$.

6.2.5 Effect of flow shallowness (h/b)

In Figure 6.7(a-f), non-dimensionalised scouring depths (d_{se}/b) at the front and eccentric piers are plotted with respect to the flow shallowness (h/b) with varying eccentricity (e).

Given the flow conditions of V/V_c=0.67-0.97, h/b=1.65-1.2, $e = 2b$ - $3.5b$, d_{se}/b for both the d_{se}/b at the piers are found to be decreasing with the increase in h/b. The lowest scour depth for both the front pier is observed at h/b = 1.65, while the highest scour depth for both piers is observed at h/b = 1.20 according to Fig. 6.7(a-f).



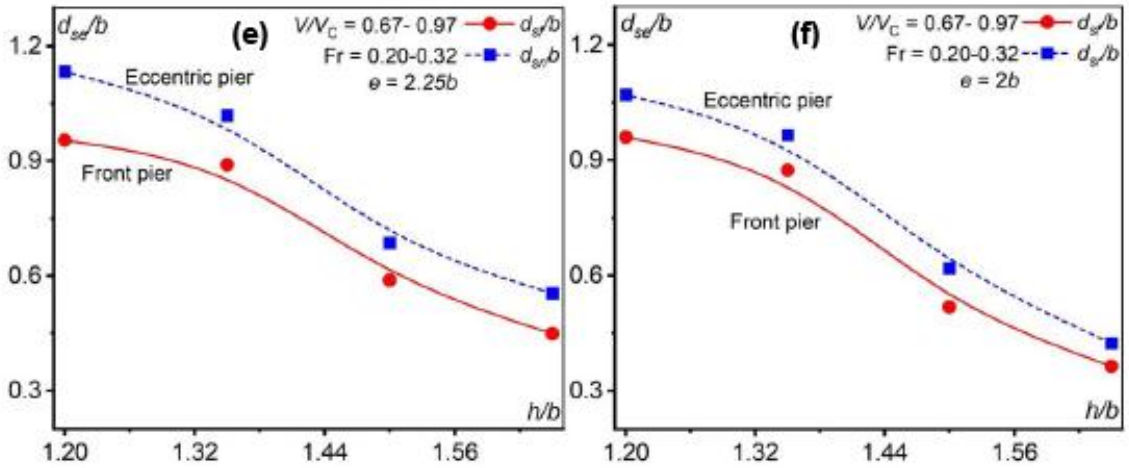
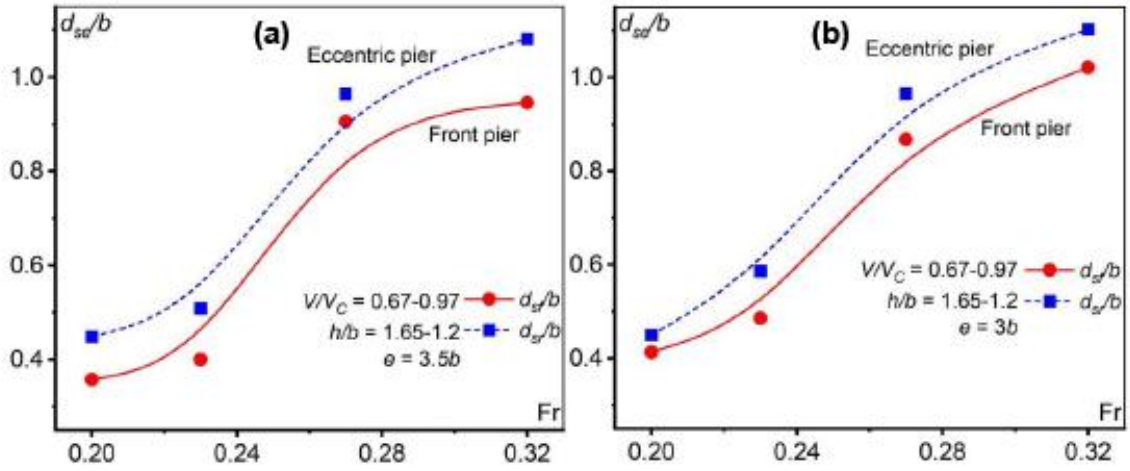


Fig. 6.7. Variation of maximum scour depth with flow shallowness for **(a)** $e = 3.5b$, **(b)** $e = 3b$, **(c)** $e = 2.75b$, **(d)** $e = 2.5b$, **(e)** $e = 2.25b$, and **(f)** $e = 2b$.

6.2.6 Effect of Froude number (Fr)

In Figure 6.8(a-f), non-dimensionalised scouring depths (d_{se}/b) at the front and eccentric piers are plotted with respect to the Froude number (Fr) with varying eccentricity (e).

Given the flow conditions of V/V_c=0.67-0.97, h/b=1.65-1.2, $e = 2b$ - $3.5b$, d_{se}/b for both the piers, the d_{se}/b is found to be increasing when Fr increases. The lowest scour depth for both the front piers is observed at Fr = 0.20, while the highest scour depth for both piers is observed at Fr = 0.32 as per Fig. 6.8(a-f).



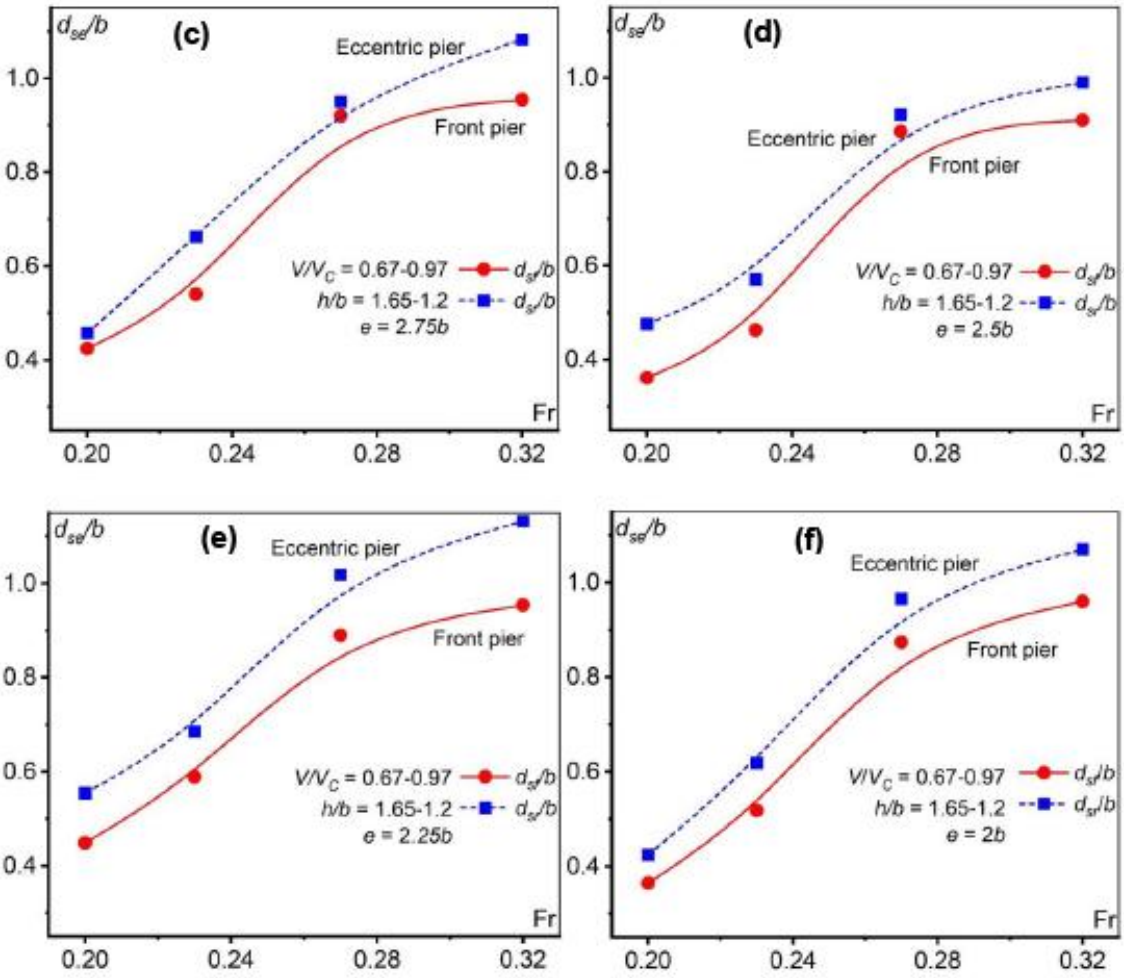


Fig. 6.8. Variation of maximum scour depth with Froude number for **(a)** $e = 3.5b$, **(b)** $e = 3b$, **(c)** $e = 2.75b$, **(d)** $e = 2.5b$, **(e)** $e = 2.25b$, and **(f)** $e = 2b$.

6.2.7 Scour profiles of single pier and different eccentric pier arrangements

Finding out the highest and lowest scour, sediment deposition impacted area and volume using a combination of two eccentric piers is the key goal of the effort. For various lateral spacings and flow depths, the affected area and volume of scour and deposition have been reported. Four single pier experiments have also been conducted to compare the scour depths obtained for eccentric pier experiments. Figures 6.9, 6.11, 6.13, 6.15, 6.17, 6.19 and 6.21 depict the scour and deposition impacted zones from each experimental run around the circular piers with specified eccentricity (e) and variable flow depth (h). Figures 6.10, 6.12, 6.14, 6.16, 6.18, 6.20 and 6.22 illustrate the contour lines of the scour holes at the circular piers, which were plotted using Surfer software, with a specific eccentricity (e) and changing flow depth (h) from each experimental run. A negative sign defines the scour zone area and a positive sign defines the dune zone area.

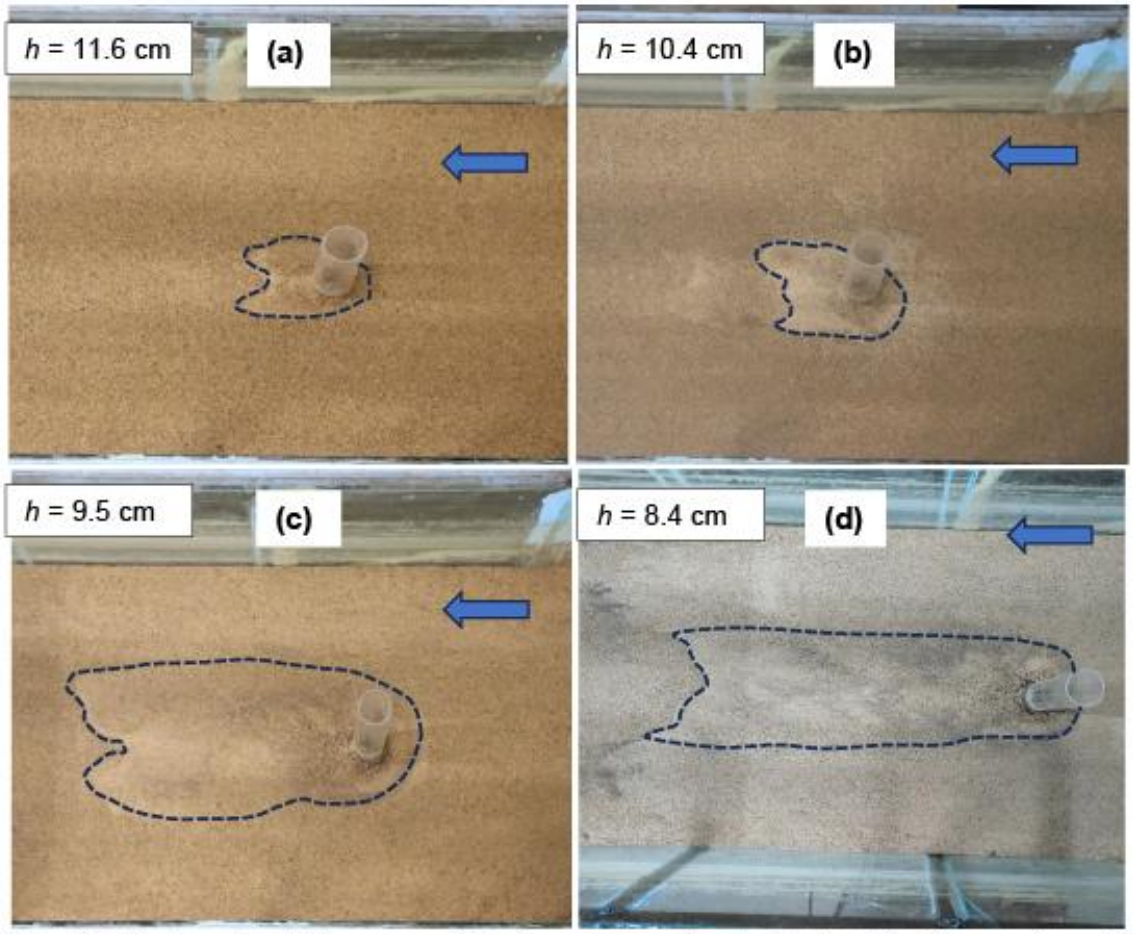
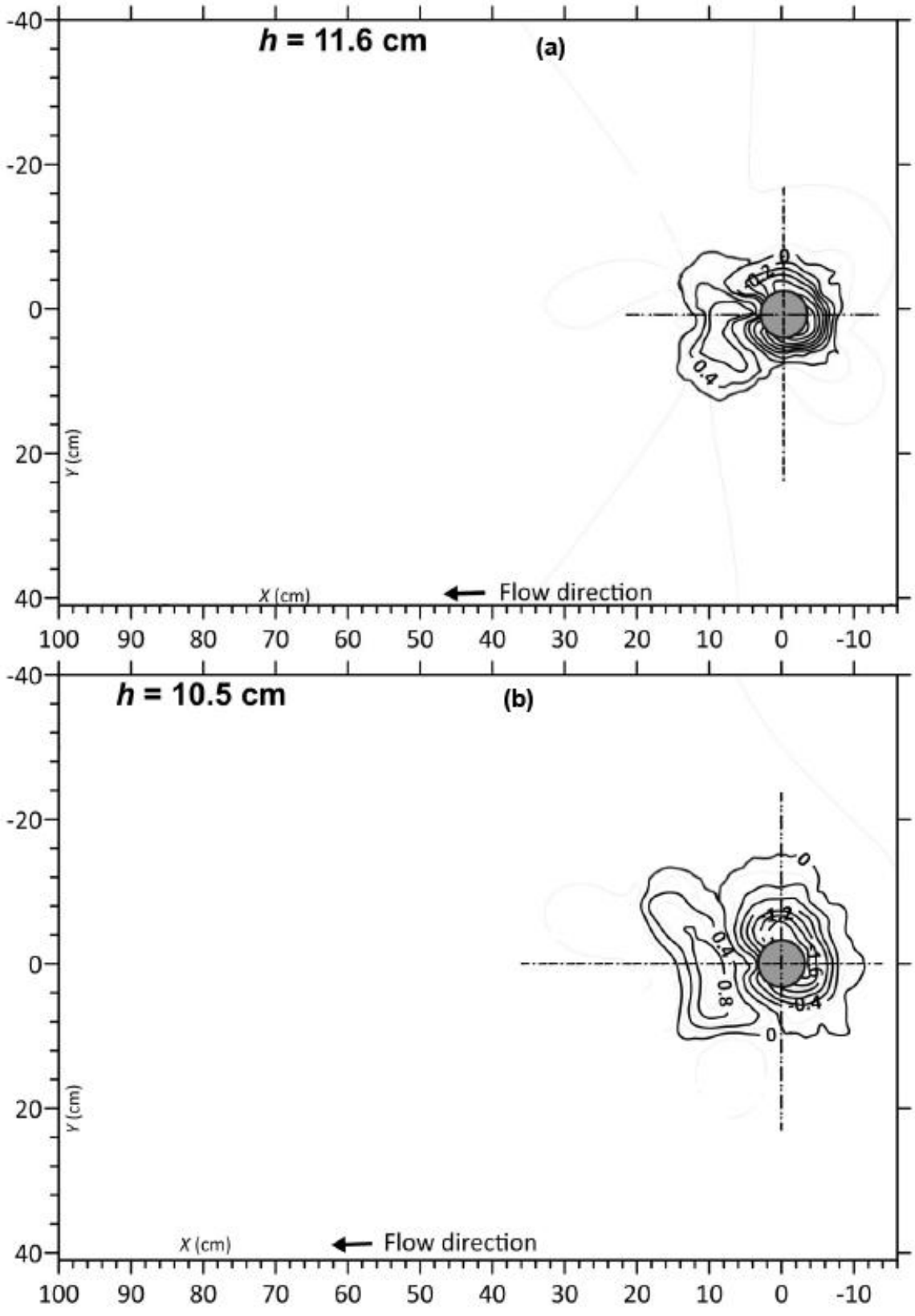


Fig. 6.9. Photographs of the scour-affected zones around a single pier after the experimental run for flow depths **(a)** $h = 11.6$ cm, **(b)** $h = 10.5$ cm, **(c)** $h = 9.5$ cm, and **(d)** $h = 8.4$ cm.


h = 11.6 cm
(a)
-40
-20
0
20
40
Y (cm)
X (cm)
Flow direction
100 90 80 70 60 50 40 30 20 10 0 -10
h = 10.5 cm
(b)
-40
-20
0
20
40
Y (cm)
X (cm)
Flow direction
100 90 80 70 60 50 40 30 20 10 0 -10

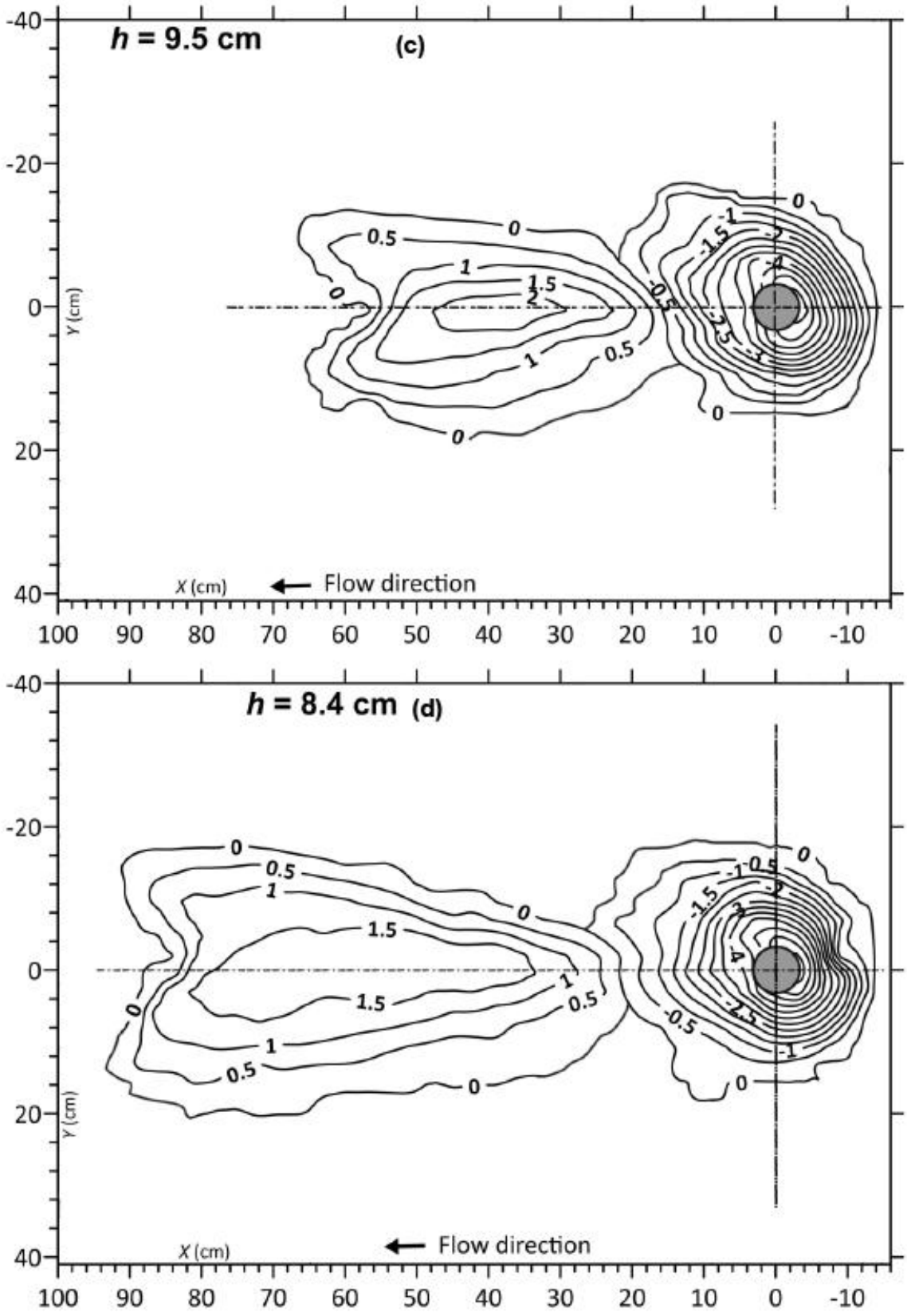


Fig. 6.10. Contours of scour holes and depositions at equilibrium for the single pier with flow depths **(a)** $h = 11.6$ cm, **(b)** $h = 10.5$ cm, **(c)** $h = 9.5$ cm, and **(d)** $h = 8.4$ cm.

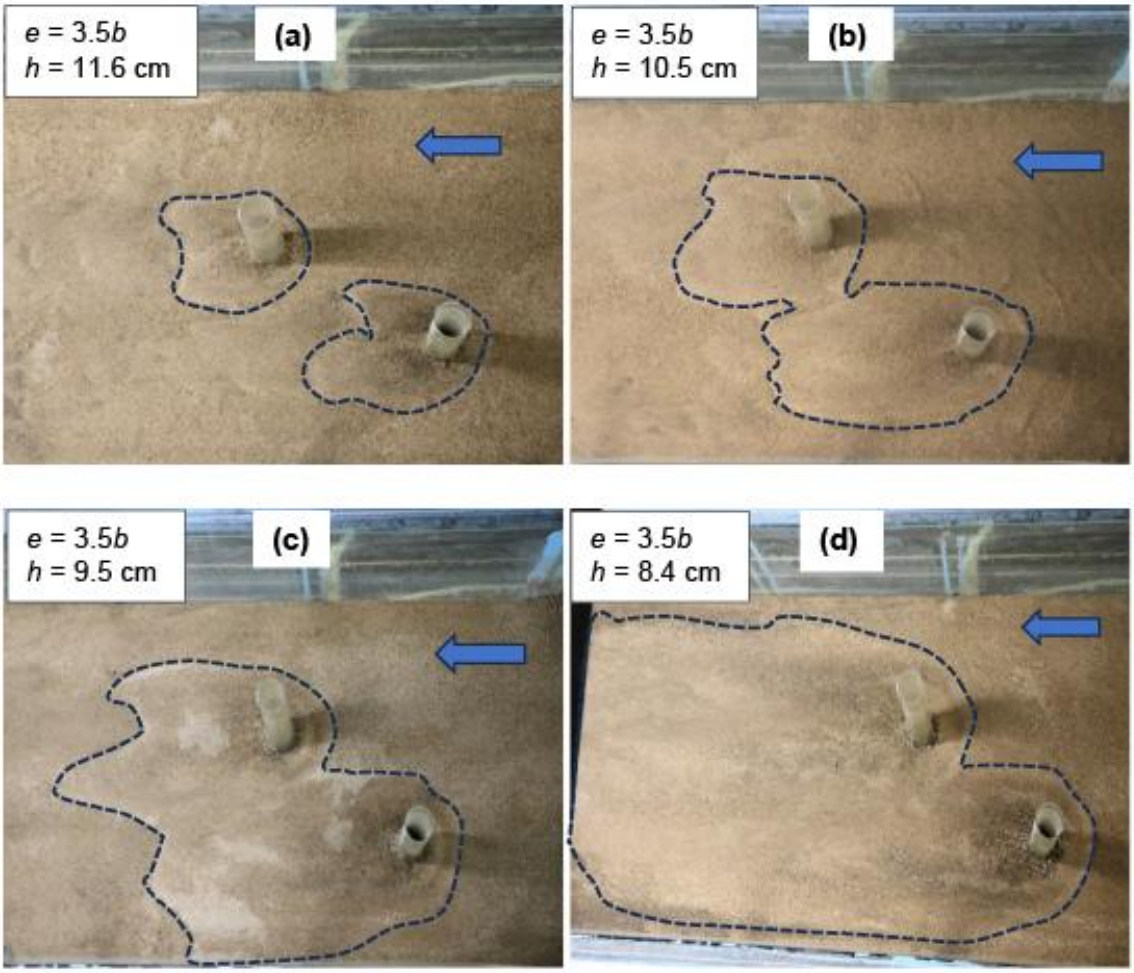
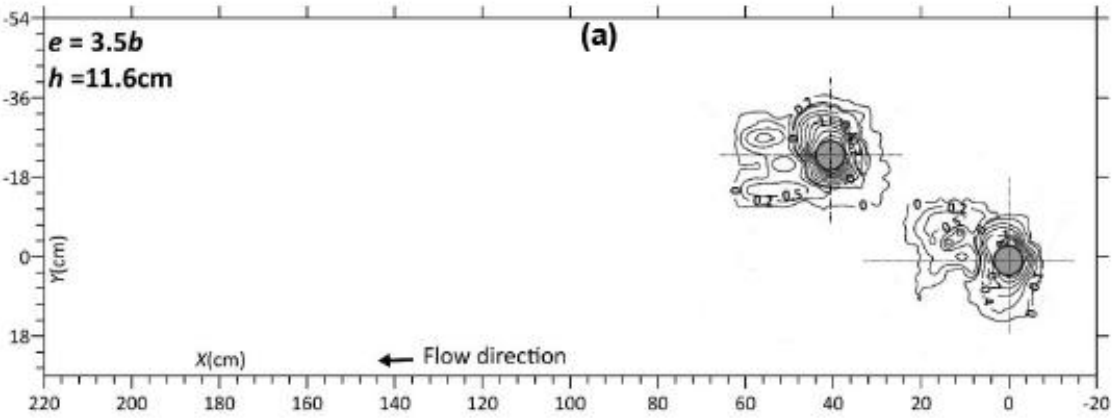


Fig. 6.11. Photographs of the scour-affected and sediment-deposited zones around the eccentric piers after the experimental runs for eccentricity $e = 3.5b$ with flow depths **(a)** $h =$ 11.6 cm, **(b)** $h = 10.5$ cm, **(c)** $h = 9.5$ cm, and **(d)** $h = 8.4$ cm.



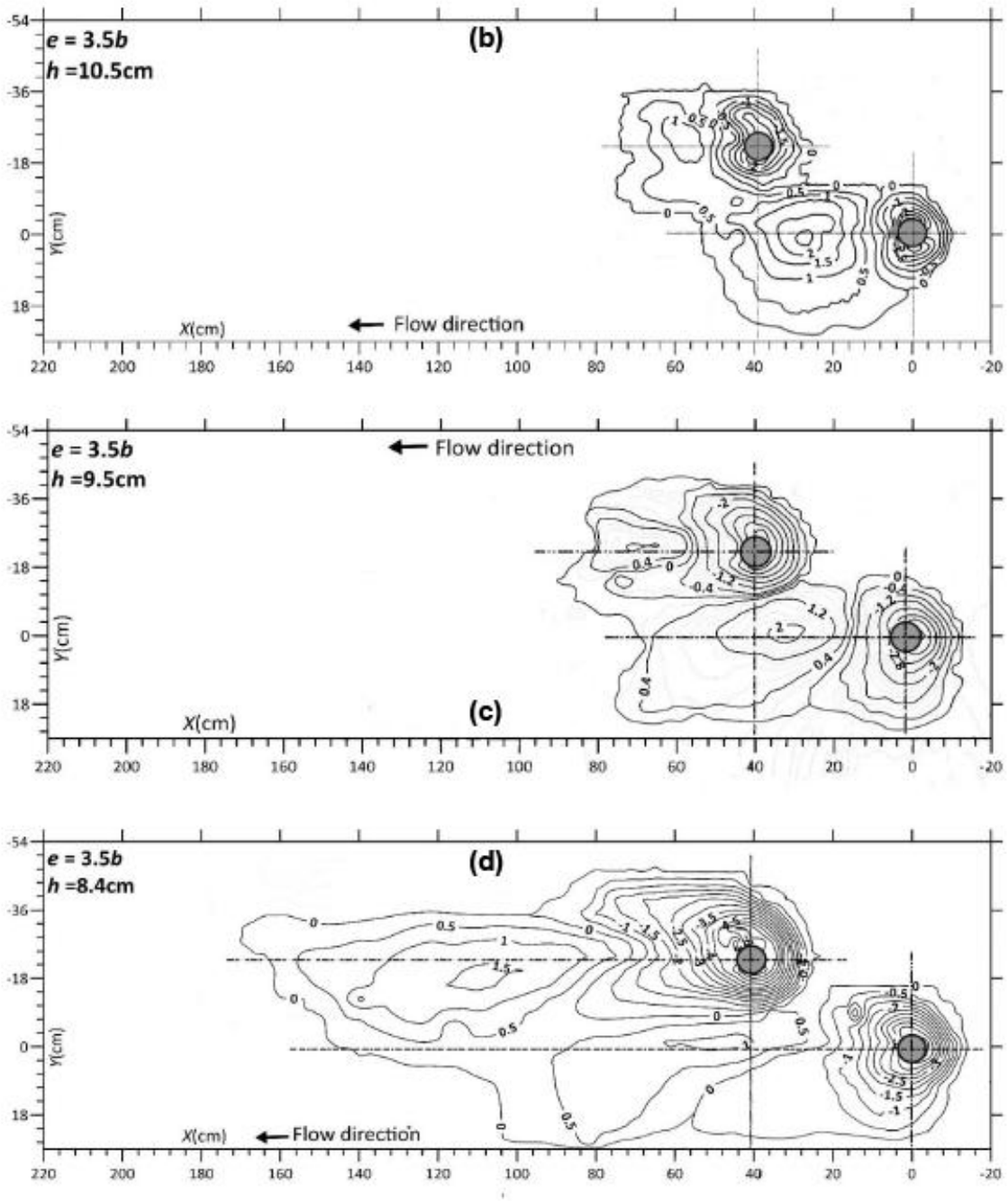


Fig. 6.12. Contours of scour holes at equilibrium for the eccentricity $e = 3.5b$ and flow depths of **(a)** $h = 11.6$ cm, **(b)** $h = 10.5$ cm, **(c)** $h = 9.5$ cm, and **(d)** $h = 8.4$ cm.

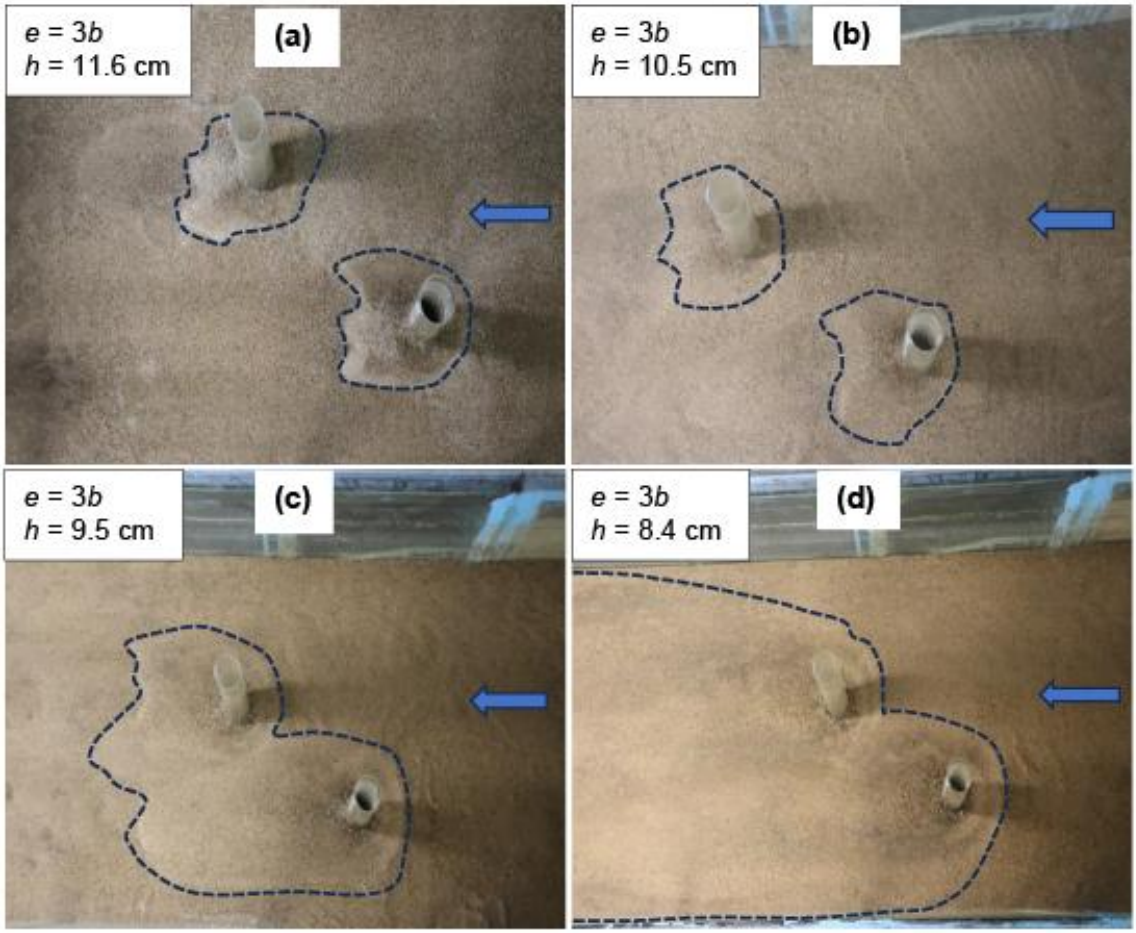
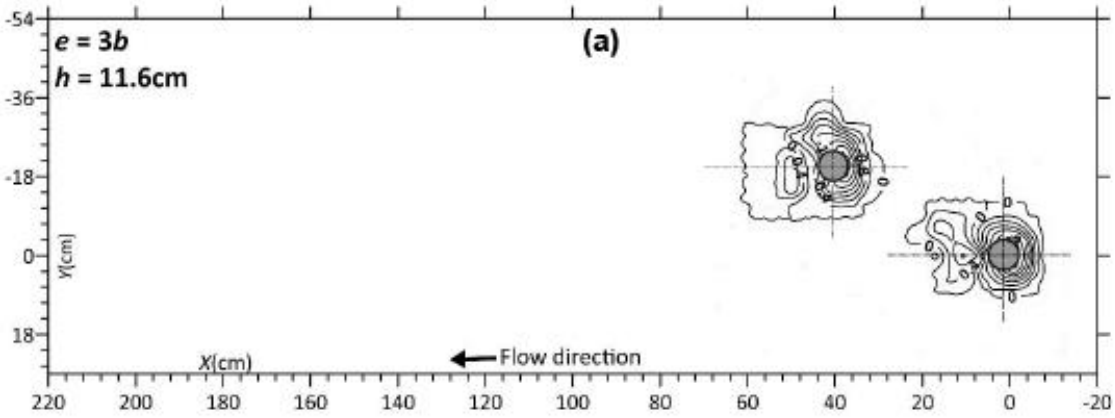


Fig. 6.13. Scour affected zones around piers after the experimental run for eccentricity $e = 3b$ for flow depths **(a)** $h = 11.6$ cm, **(b)** $h = 10.5$ cm, **(c)** $h = 9.5$ cm, and **(d)** $h = 8.4$ cm.



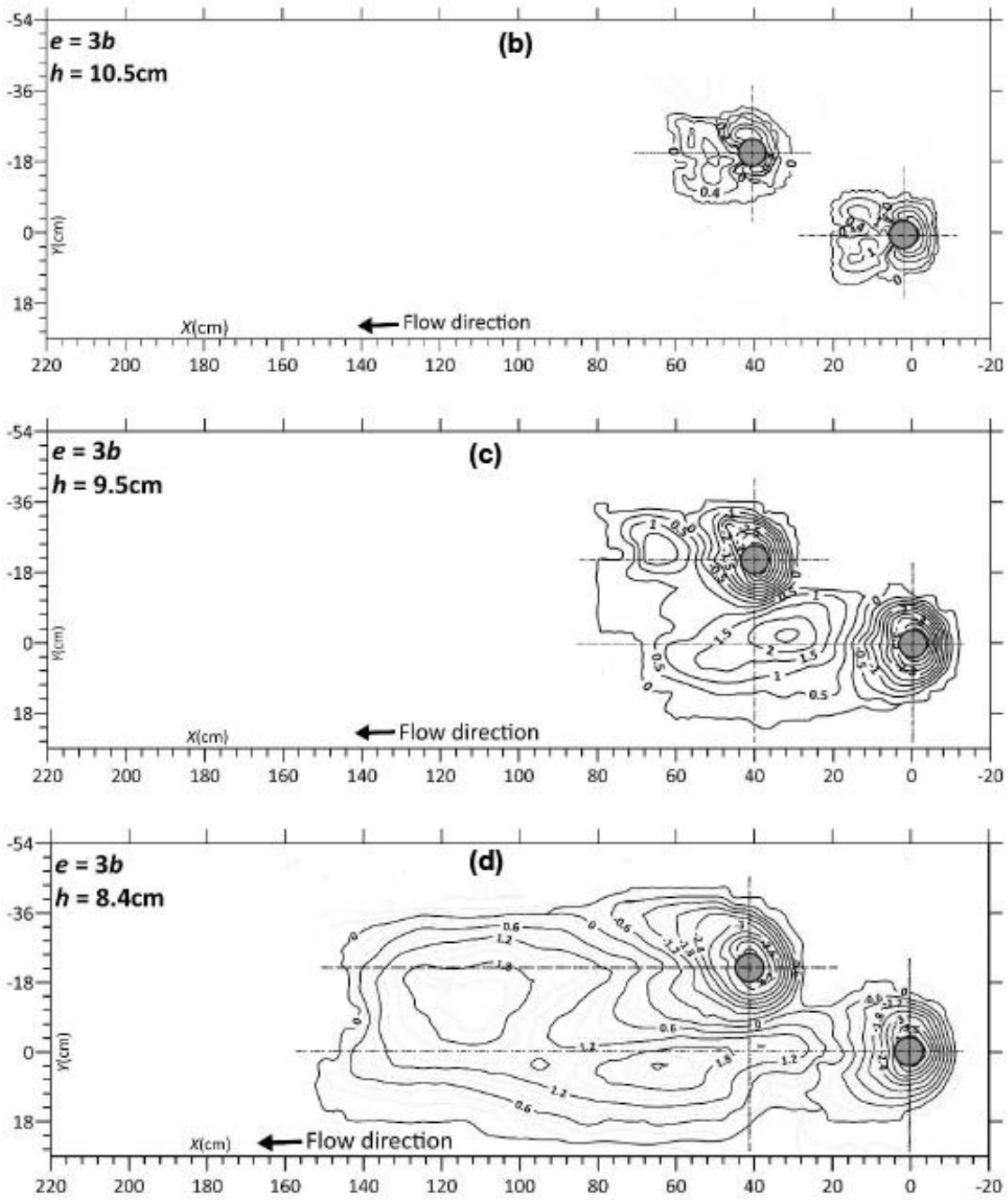


Fig. 6.14. Contours of scour holes at equilibrium for eccentricity $e = 3b$ for flow depths **(a)** $h = 11.6$ cm, **(b)** $h = 10.5$ cm, **(c)** $h = 9.5$ cm, and **(d)** $h = 8.4$ cm.

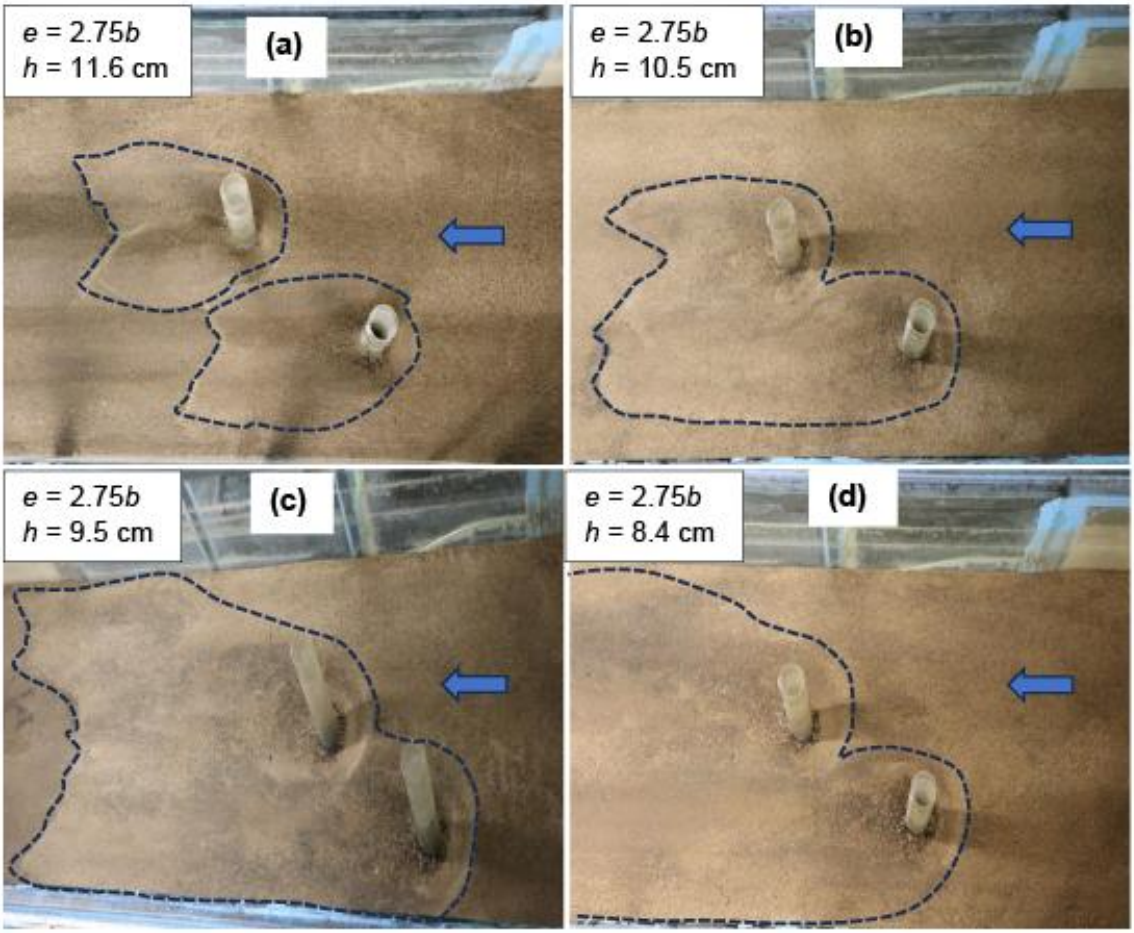
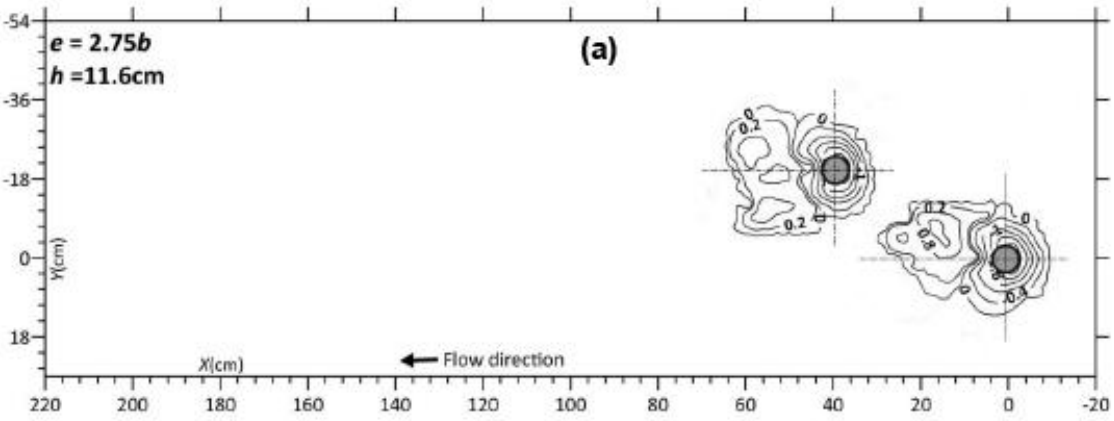


Fig. 6.15. Scour affected zones around piers after the experimental run for eccentricity $e = 2.75b$ with varying inflow depths of **(a)** $h = 11.6$ cm, **(b)** $h = 10.5$ cm, **(c)** $h = 9.5$ cm, and **(d)** $h = 8.4$ cm.



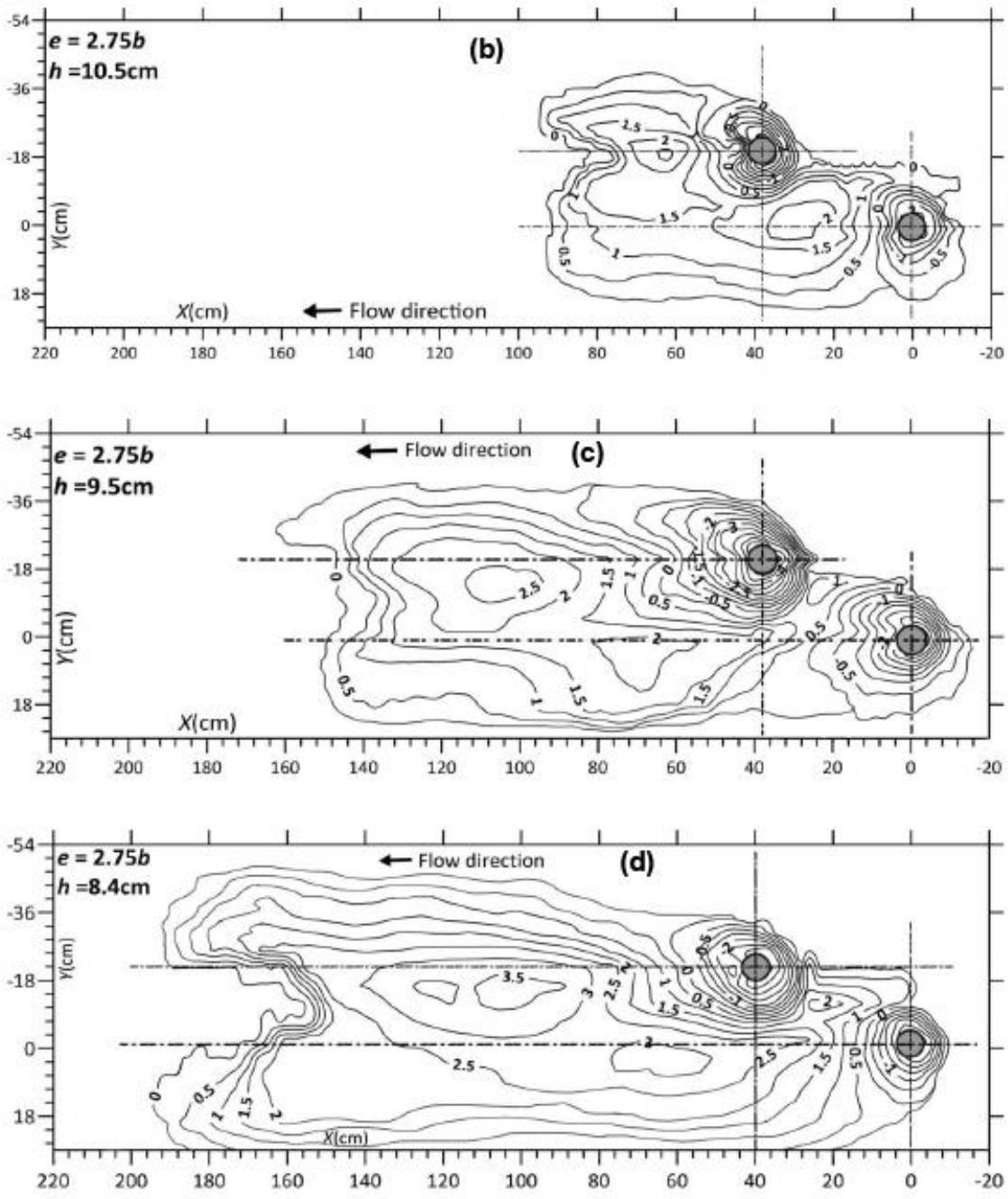


Fig. 6.16. Contours of scour holes at equilibrium for eccentricity $e = 2.75b$ at flow depths of **(a)** $h = 11.6$ cm, **(b)** $h = 10.5$ cm, **(c)** $h = 9.5$ cm, and **(d)** $h = 8.4$ cm.

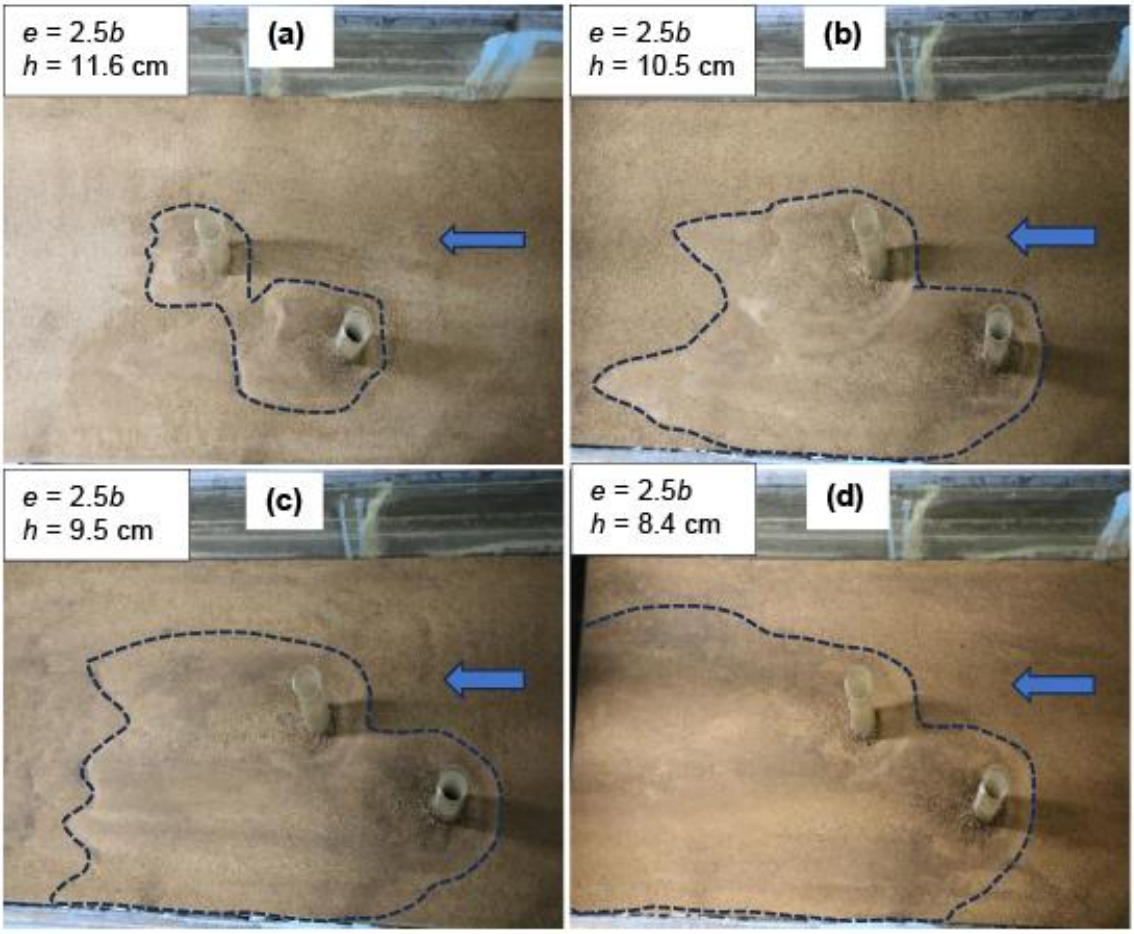
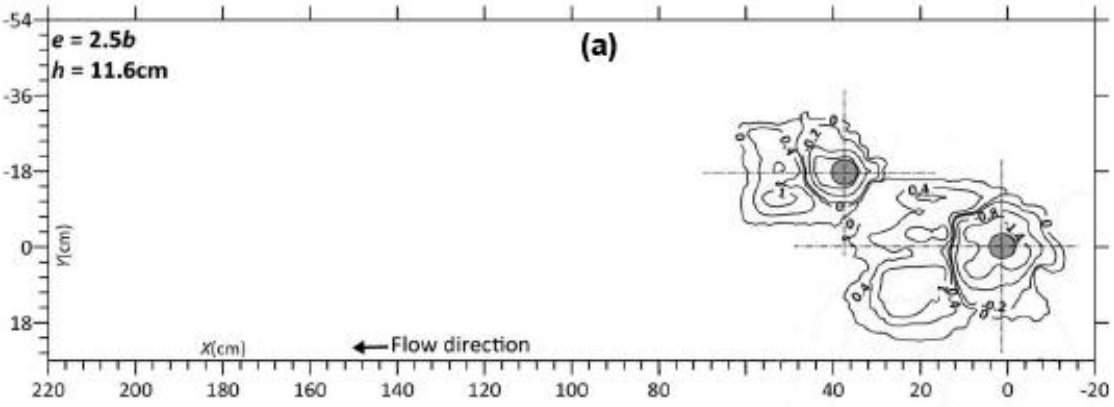


Fig. 6.17. Scour affected zones around piers after the experimental run for eccentricity $e = 2.5b$ with flow depths **(a)** $h = 11.6$ cm; **(b)** $h = 10.5$ cm; **(c)** $h = 9.5$ cm; **(d)** $h = 8.4$ cm.



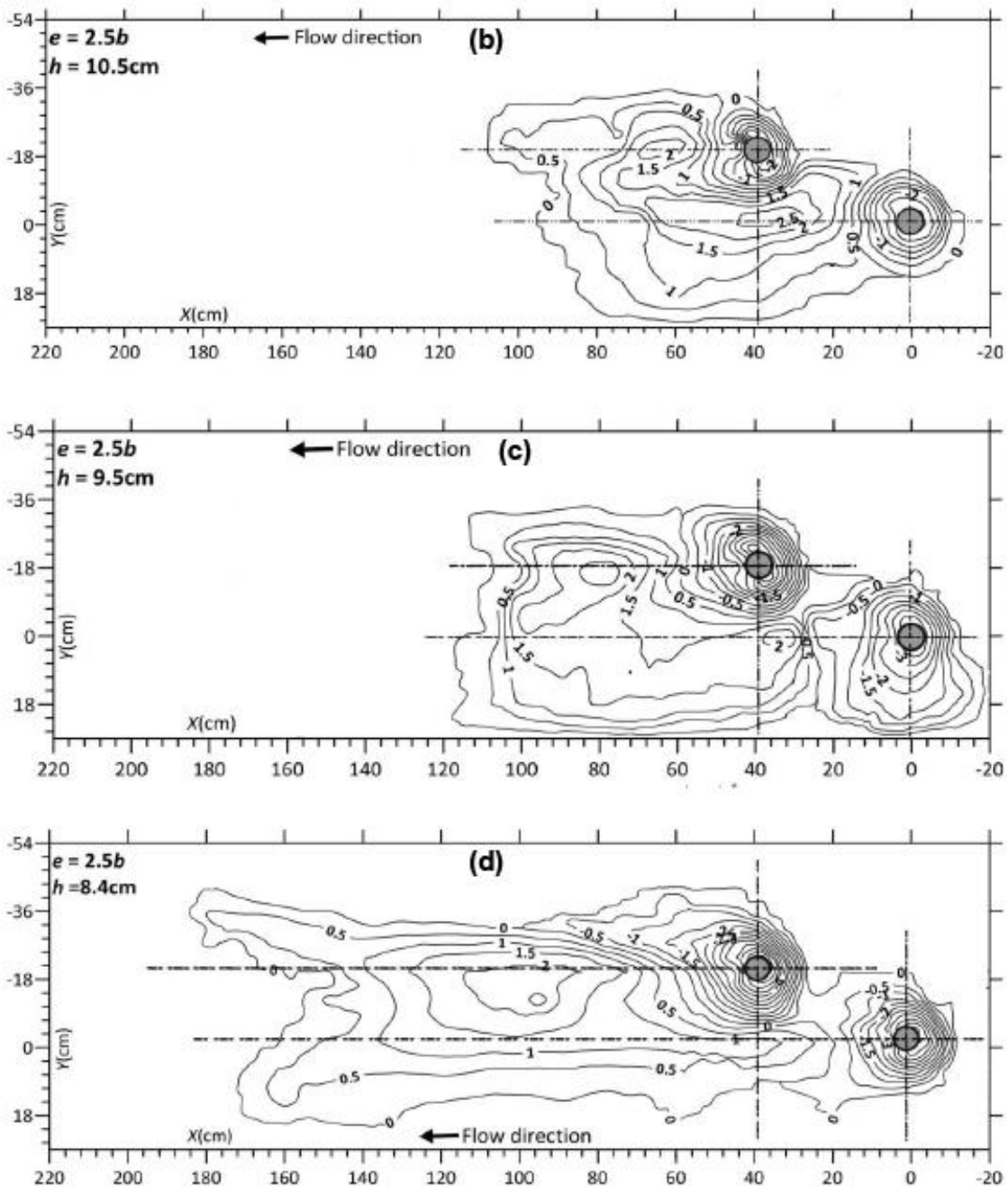


Fig. 6.18. Contours of scour holes for equilibrium at eccentricity $e = 2.5b$ at flow depths **(a)** $h = 11.6$ cm; **(b)** $h = 10.5$ cm; **(c)** $h = 9.5$ cm; **(d)** $h = 8.4$ cm.

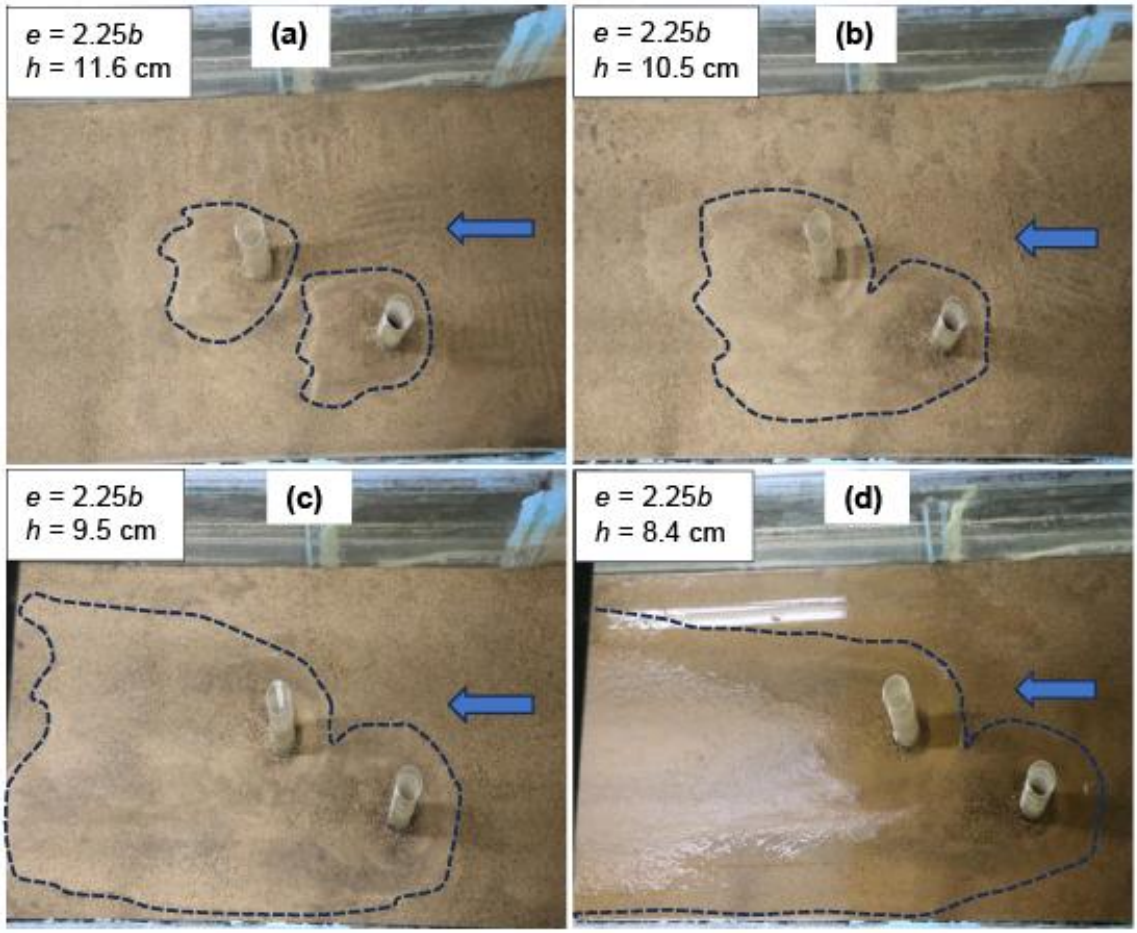
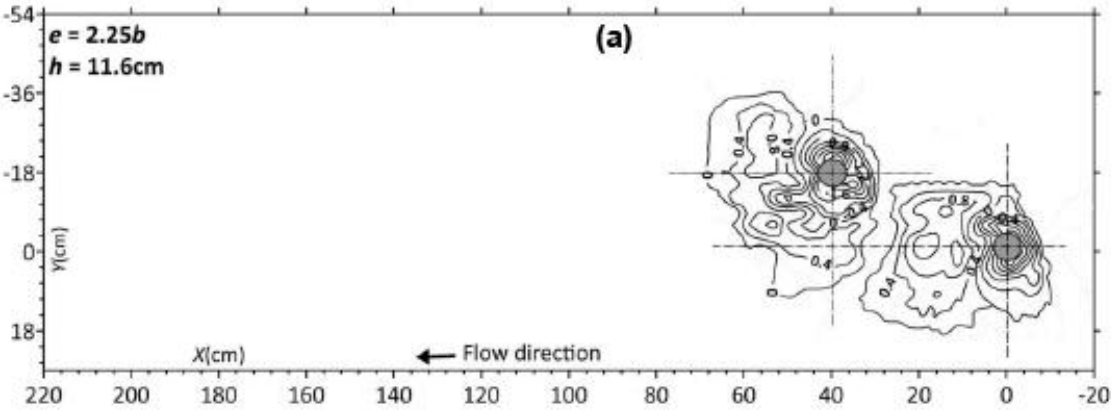


Fig. 6.19. Scour affected zones around piers after experimental run at eccentricity $e = 2.25b$ with flow depths **(a)** $h = 11.6$ cm; **(b)** $h = 10.5$ cm; **(c)** $h = 9.5$ cm; **(d)** $h = 8.4$ cm.



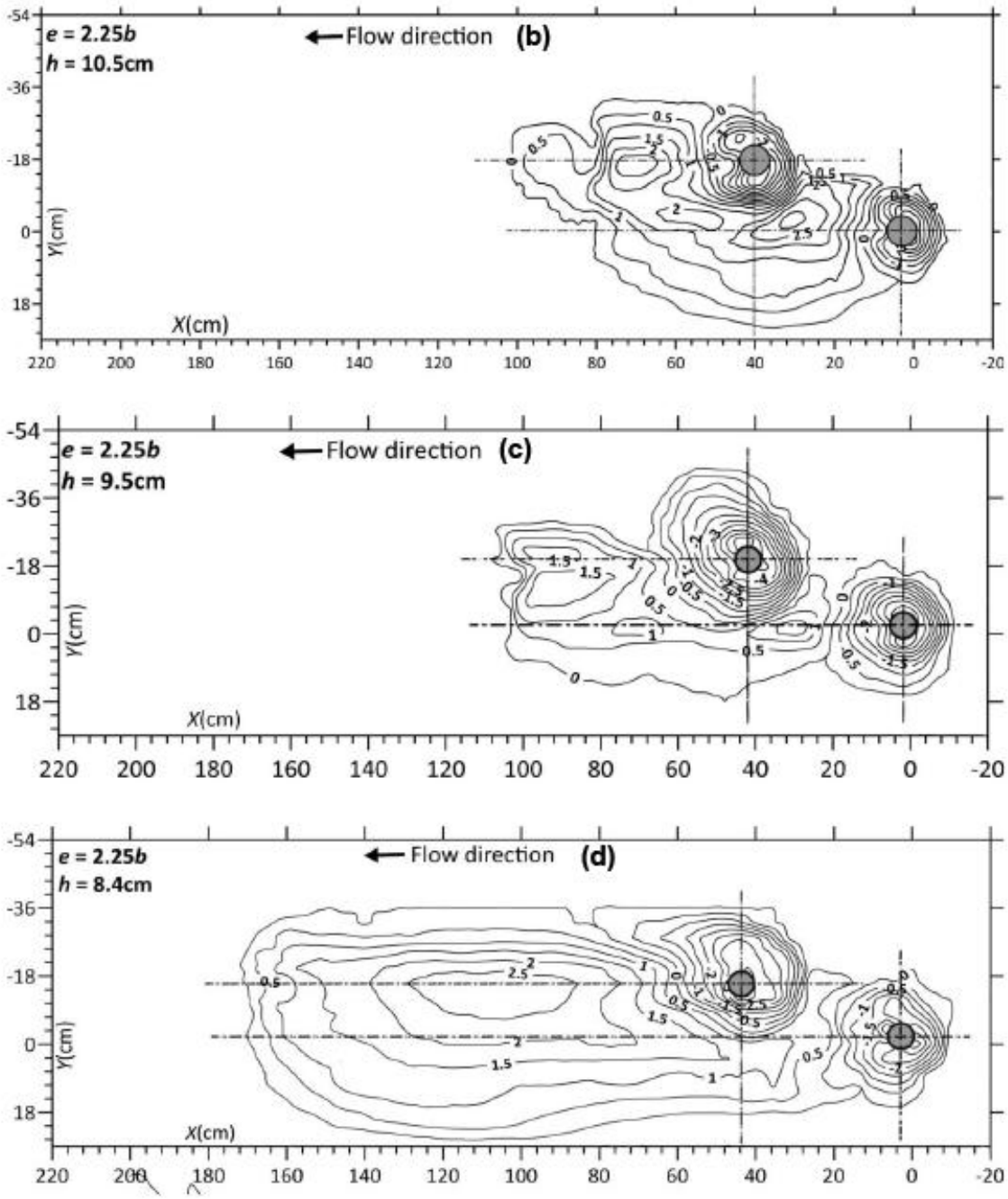


Fig. 6.20. Contours of scour holes for equilibrium at eccentricity $e = 2.25b$ at flow depths **(a)** $h = 11.6$ cm; **(b)** $h = 10.5$ cm; **(c)** $h = 9.5$ cm; **(d)** $h = 8.4$ cm.

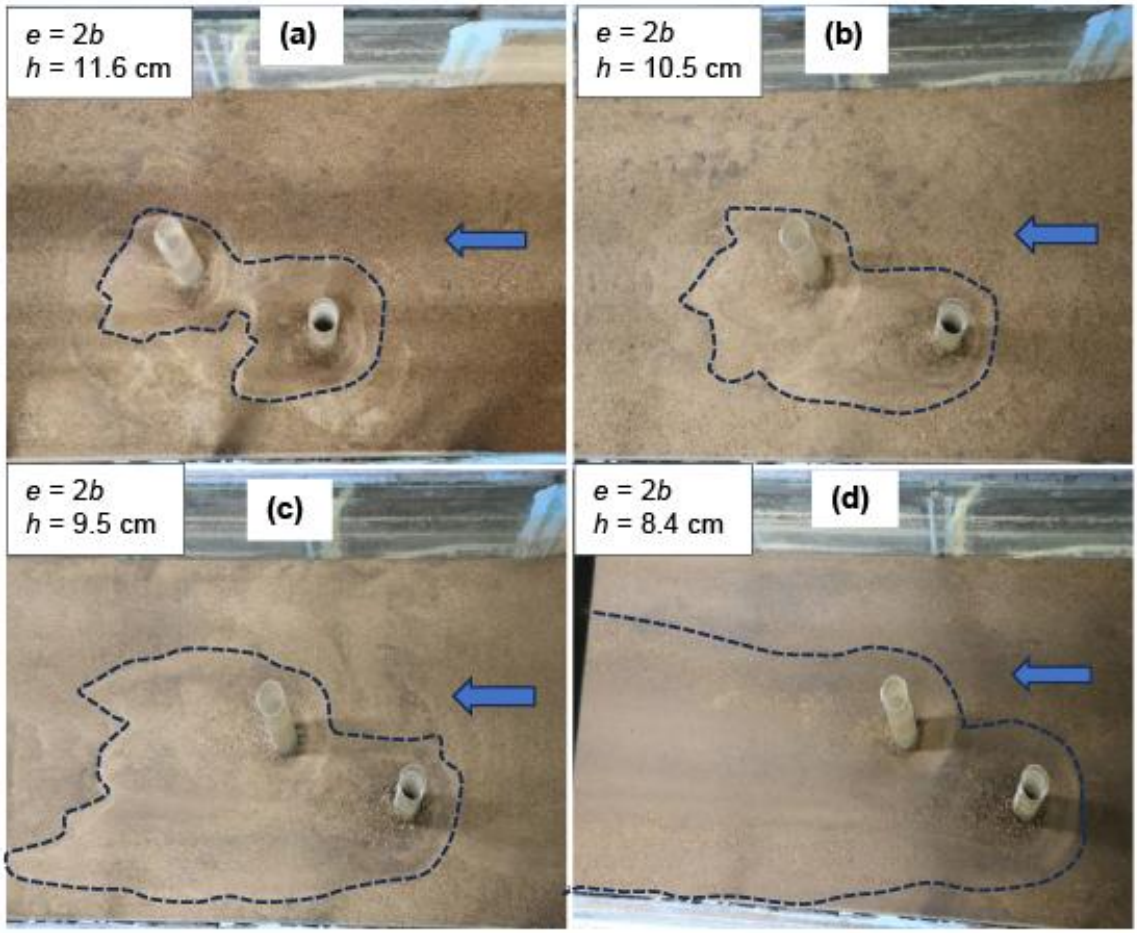
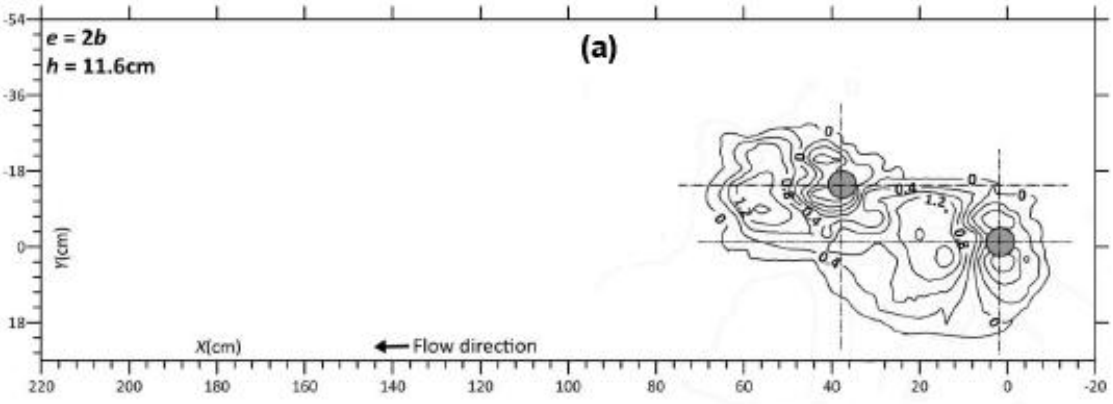


Fig. 6.21. Scour affected zones around piers after the experimental run for eccentricity $e = 2b$ for flow depths **(a)** $h = 11.6$ cm; **(b)** $h = 10.5$ cm; **(c)** $h = 9.5$ cm; **(d)** $h = 8.4$ cm.



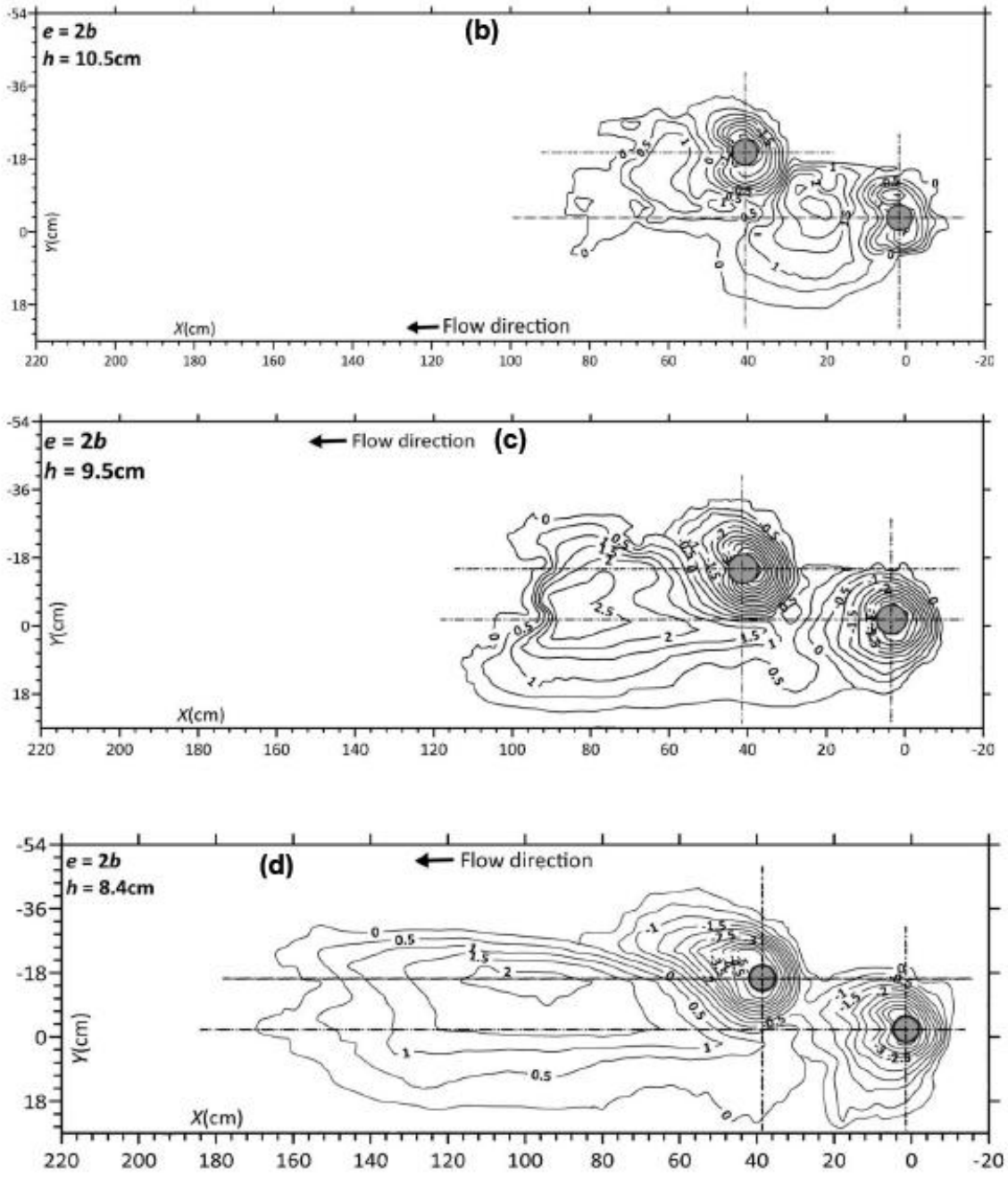


Fig. 6.22. Contours of scour holes for equilibrium at eccentricity $e = 2b$ at flow depths **(a)** $h = 11.6$ cm; **(b)** $h = 10.5$ cm; **(c)** $h = 9.5$ cm; **(d)** $h = 8.4$ cm.

6.3 Analysis of bed morphology

The experiments were carried on for up to 10 hours. The quasi-equilibrium scour condition was accepted to be attained when the increase in the scour depth is below a limiting value. Scour geometry and bed morphology are crucial factors in understanding and managing the potential risks associated with bridge pier scour. Scour geometry refers to the shape and

dimensions of the scour hole formed around a bridge pier due to erosive forces, such as flowing water. It includes parameters like maximum scour depth, scour width (the horizontal extent of the scour hole) and scour length (the longitudinal extent of the scour hole along the flow direction).

Bed morphology, on the other hand, refers to the overall shape and characteristics of the riverbed, including the bed material composition, sediment grain size distribution, bed roughness and bedform features (such as ripples, dunes or antidunes). Understanding bed morphology is important because it influences the erosive process that can lead to scour formation.

Together, scour geometry and bed morphology provide valuable insights into the stability of bridge piers and the potential for scour-induced failures.

With V/V_c ranging from 0.67 to 0.97 and h/b ranging from 1.65 to 1.2, Tables 6.2-6.3 display the experimental results with a range of eccentricities, including 3.5b, 3b, 2.75b, 2.5b, 2.25b, and 2b. Furthermore, Fr values of 0.20-0.32 have been studied. The table also includes varying scour volume ($\forall$), scour surface area (A_s), and planar surface area (A_p) with the aforementioned ranges. Three portions have been identified as the left, right, and mid-sections based on the division of the scour and deposition-affected zones from Fig. 6.23. By comparing the geometry of the three sections, the current work aims to comprehend the scour geometry and bed morphology following each experimental run.

For analysing scour profiles following parameters have been taken into consideration:

- l_R, l_L; w_R, w_L; A_{pR}, A_{pL}; $\forall_R$, $\forall_L$ – maximum length, width, planar area and volume of the overlapping area corresponding above the centre line of the eccentric pier and below the centre line of the front pier;
- A_{pM}, $\forall_M$ – planar area and volume of mid-section.

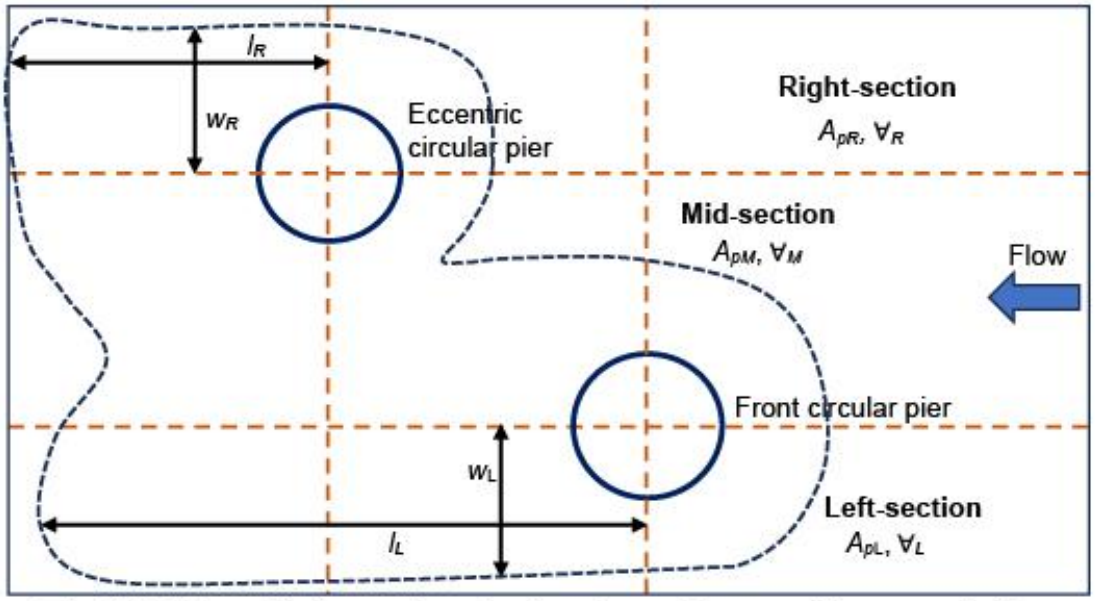


Fig. 6.23. Schematic diagram showing the entire section around the eccentric piers.

Table 6.2. Experimental outcomes based on grid data of scour shown in contour graphs.

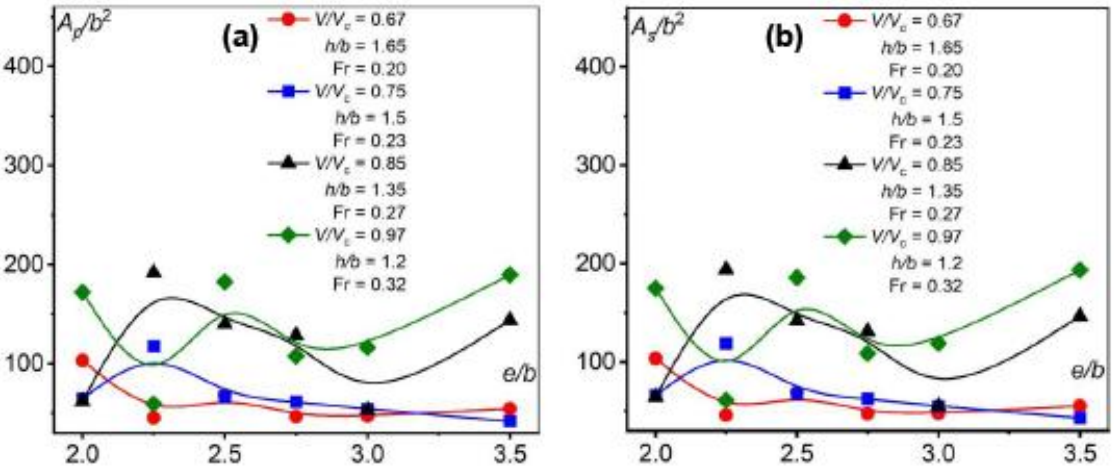
Exp.	e/b	V/V_c	h/b	Fr	A_s/b^2	A_p/b^2	$\forall/b^3$	Left-section				Right-section				Mid-section	
	(--)	(--)	(--)	(--)	(--)	(--)	(--)	w_L/b	l_L/b	A_{pL}/b^2	$\forall_L/b^3$	w_R/b	l_R/b	A_{pR}/b^2	$\forall_R/b^3$	A_{pM}/b^2	$\forall_M/b^3$
1	3.5	0.678	1.65	0.20	55.33	54.59	1.73	0.24	0.36	7.80	0.25	1.00	0.39	35.75	1.01	69.13	2.01
2	3	0.678	1.65	0.20	55.33	54.59	1.73	0.17	0.29	8.96	0.38	1.83	0.36	7.72	0.52	58.02	1.04
3	2.75	0.678	1.65	0.20	48.00	47.12	2.03	0.31	0.41	6.87	0.55	1.00	0.44	35.02	1.90	58.46	1.19
4	2.5	0.678	1.65	0.20	47.53	46.53	2.23	0.30	0.64	5.55	0.52	0.71	0.39	46.74	1.93	44.55	2.56
5	2.25	0.678	1.65	0.20	68.98	68.30	2.72	0.30	0.59	4.46	0.34	0.71	0.50	20.26	0.58	39.49	0.88
6	2	0.678	1.65	0.20	46.19	45.22	2.08	0.40	1.11	7.40	0.10	0.64	0.54	45.66	0.85	31.12	0.58
7	3.5	0.757	1.50	0.23	103.50	103.00	4.33	0.44	0.93	6.93	0.69	0.58	0.61	45.13	1.32	27.43	1.27
8	3	0.757	1.50	0.23	43.28	42.03	3.26	0.23	0.31	37.67	0.32	1.00	0.37	38.08	1.22	20.10	0.36
9	2.75	0.757	1.50	0.23	55.15	54.26	1.34	0.39	1.61	17.94	0.60	0.93	0.97	23.06	1.41	25.46	1.05
10	2.5	0.757	1.50	0.23	62.88	61.54	3.59	0.47	1.66	7.01	0.83	0.55	1.19	24.96	0.83	34.90	1.11
11	2.25	0.757	1.50	0.23	67.69	66.40	3.56	0.44	1.36	11.79	0.33	0.58	1.07	19.55	1.24	36.36	1.67
12	2	0.757	1.50	0.23	118.96	117.53	5.14	0.37	1.31	22.81	1.05	0.65	0.66	50.02	1.59	29.95	0.83
13	3.5	0.854	1.35	0.27	66.18	64.67	4.49	0.41	1.29	11.53	1.78	0.83	0.74	16.18	3.09	38.62	2.90
14	3	0.854	1.35	0.27	146.70	143.80	12.29	0.37	1.20	53.31	2.01	0.77	0.73	55.58	2.55	51.15	1.81
15	2.75	0.854	1.35	0.27	55.50	53.44	5.92	0.40	2.44	19.71	1.64	0.93	2.14	33.74	3.41	36.07	2.76
16	2.5	0.854	1.35	0.27	131.27	128.74	9.69	0.44	2.01	10.47	0.75	0.65	1.27	28.37	2.49	37.55	2.56
17	2.25	0.854	1.35	0.27	142.33	140.31	12.45	0.34	1.74	7.99	1.09	1.17	1.14	35.13	5.23	41.24	3.47
18	2	0.854	1.35	0.27	194.22	191.77	16.42	0.43	1.91	34.82	2.07	0.77	1.04	33.30	2.57	31.37	2.34
19	3.5	0.979	1.20	0.32	64.70	62.30	8.64	0.46	2.49	23.29	2.42	0.88	2.26	63.20	10.84	39.70	4.70
20	3	0.979	1.20	0.32	193.68	189.67	25.92	0.43	2.63	31.25	2.09	0.83	1.80	48.54	6.45	35.08	3.06
21	2.75	0.979	1.20	0.32	119.21	116.35	13.53	0.57	3.34	5.65	0.64	0.75	2.61	16.59	1.54	22.56	1.28
22	2.5	0.979	1.20	0.32	108.81	107.63	3.85	0.40	2.96	19.92	1.50	1.00	2.50	54.61	6.42	27.56	2.86
23	2.25	0.979	1.20	0.32	186.04	182.78	16.29	0.47	2.90	6.16	1.10	0.73	2.21	25.49	2.94	13.14	2.28
24	2	0.979	1.20	0.32	61.14	59.37	7.54	0.44	2.90	13.47	1.81	0.94	2.19	41.35	5.41	17.67	3.21

6.3.1 Effect of lateral spacing on scour area and volume

In Figure 6.24(a), the non-dimensionalised scour planar area (A_p/b^2) of the equilibrium scour hole is plotted with respect to the varying non-dimensional pier lateral spacing (e/b). Figure 6.24(a) illustrates how, for the provided ranges V/V_c = 0.67-0.97, h/b = 1.65-1.2, and Fr = 0.20-0.32, the planar surface area first decreases as the eccentricity increases, but it then increases again after a certain point, and vice versa. It becomes lower for higher h/b but becomes higher for higher V/V_c and Fr.

In Figure 6.24(b), the non-dimensionalised scour surface area (A_s/b^2) of the equilibrium scour hole is plotted with respect to the varying non-dimensional pier lateral spacing (e/b). Figure 6.24(b) illustrates how, for the provided ranges V/V_c = 0.67-0.97, h/b = 1.65-1.2, and Fr = 0.20-0.32, the scour surface area first decreases as eccentricity increases, but it then increases again after a certain point, and vice versa. It becomes lower for higher h/b but higher for higher V/V_c and Fr.

In Figure 6.24(c), the non-dimensionalised scour volume ($\forall/b^3$) of the equilibrium scour hole is plotted with respect to the varying non-dimensional lateral spacing (e/b). Figure 6.24(c) illustrates how, for the provided ranges V/V_c = 0.67-0.97, h/b = 1.65-1.2, and Fr = 0.20-0.32, the scour volume first starts decreasing with the increase in eccentricity, but it then becomes larger again after a certain point, and vice versa. It decreases for higher h/b but increases for higher V/V_c and Fr.



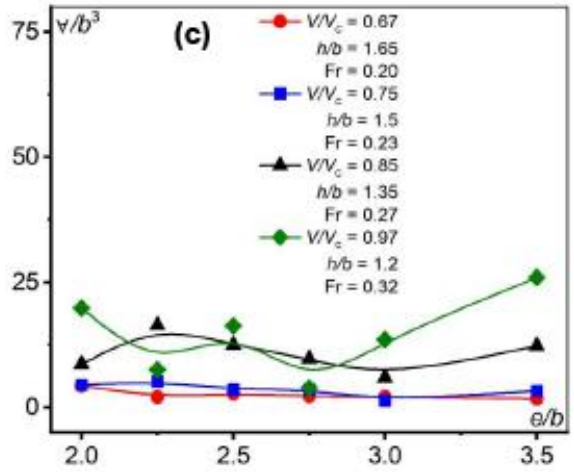


Fig. 6.24. Effect of lateral spacing on scour **(a)** planar area **(b)** surface area and **(c)** volume.

6.3.2 Effect of lateral spacing on maximum scour length

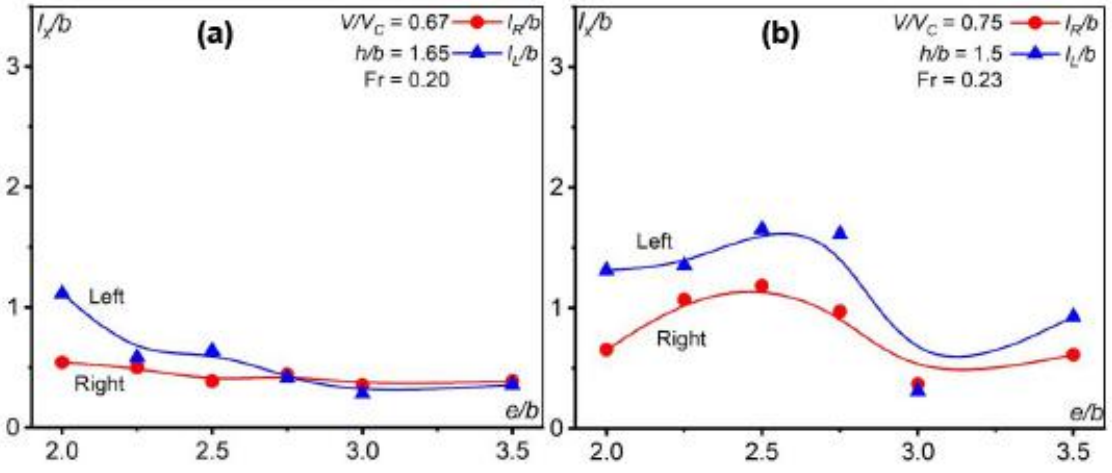
In Figure 6.25(a-d), the non-dimensionalised scour length (l_x/b) of the equilibrium scour hole is plotted with respect to the varying non-dimensional pier lateral spacing (e/b).

Given $V/V_c = 0.67$, $h/b = 1.65$, and Fr = 0.20, the non-dimensionalised maximum scour length (l_x/b) of the equilibrium scour hole of left-section and right-section is found minimum at $e = 3b$ and maximum at $e = 2b$ as highlighted in Fig. 6.25a.

Given $V/V_c = 0.75$, $h/b = 1.5$, and Fr = 0.23, the non-dimensionalised maximum scour length (l_x/b) of the equilibrium scour hole of left-section and right-section is observed minimum at $e = 3b$ and maximum at $e = 2.5b$ as displayed in Fig. 6.25b.

Given $V/V_c = 0.85$, $h/b = 1.35$, and Fr = 0.27, the non-dimensionalised maximum scour length (l_x/b) of the equilibrium scour hole of left-section and right-section is identified minimum at $e = 3b$ and maximum at $e = 2.75b$ as shown in Fig. 6.25c.

Given $V/V_c = 0.97$, $h/b = 1.2$, and Fr = 0.32, the non-dimensionalised maximum scour length (l_x/b) of the equilibrium scour hole of left-section and right-section is detected minimum at $e = 3b$ and maximum at $e = 2.75b$ as illustrated in Fig. 6.25d.



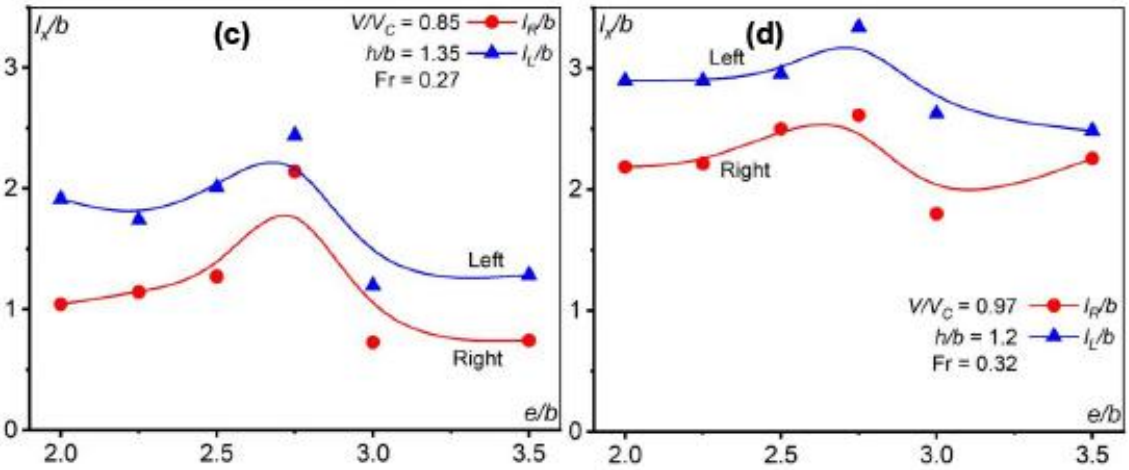


Fig. 6.25. Influence of lateral spacing on maximum scour length for **(a)** $V/V_c = 0.67$, $h/b = 1.65$, Fr = 0.20; **(b)** $V/V_c = 0.75$, $h/b = 1.5$, Fr = 0.23; **(c)** $V/V_c = 0.85$, $h/b = 1.35$, Fr = 0.27; **(d)** $V/V_c = 0.97$, $h/b = 1.2$, Fr = 0.32.

6.3.3 Effect of lateral spacing on maximum scour width

In Figure 6.26(a-d), the non-dimensionalised scour width (w/b) of the equilibrium scour hole is plotted respecting the varying non-dimensional pier lateral spacing (e/b).

The non-dimensionalised maximum scour width (w/b) of the equilibrium scour hole of the left section is minimum at $e = 3b$ and maximum at $e = 2b$. The non-dimensionalised maximum scour width (w/b) of the equilibrium scour hole of the right section is minimum at $e = 2b$ and maximum at $e = 3b$ as indicated in Fig. 6.26a, given $V/V_c = 0.67$, $h/b = 1.65$, and Fr = 0.20.

The non-dimensionalised maximum scour width (w/b) of the equilibrium scour hole of the left section is minimum at $e = 3b$ and maximum at $e = 2.5b$. The non-dimensionalised maximum scour width (w/b) of the equilibrium scour hole of the right section is minimum at $e = 2.5b$ and maximum at $e = 3b$ as indicated in Fig. 6.26b, given $V/V_c = 0.75$, $h/b = 1.5$, and Fr = 0.23.

The non-dimensionalised maximum scour width (w/b) of the equilibrium scour hole of the left section is minimum at $e = 2.25b$ and maximum at $e = 2.5b$. The non-dimensionalised maximum scour width (w/b) of the equilibrium scour hole of the right section is minimum at $e = 2.5b$ and maximum at $e = 2.25b$ as indicated in Fig. 6.26c, given $V/V_c = 0.85$, $h/b = 1.35$, and Fr = 0.27.

The non-dimensionalised maximum scour width (w/b) of the equilibrium scour hole of the left section is minimum at $e = 2.5b$ and maximum at $e = 2.75b$. The non-dimensionalised maximum scour width (w/b) of the equilibrium scour hole of the right section is minimum at $e = 2.25b$ and maximum at $e = 2.5b$ as indicated in Fig. 6.26d, given $V/V_c = 0.97$, $h/b = 1.2$, and Fr = 0.32.

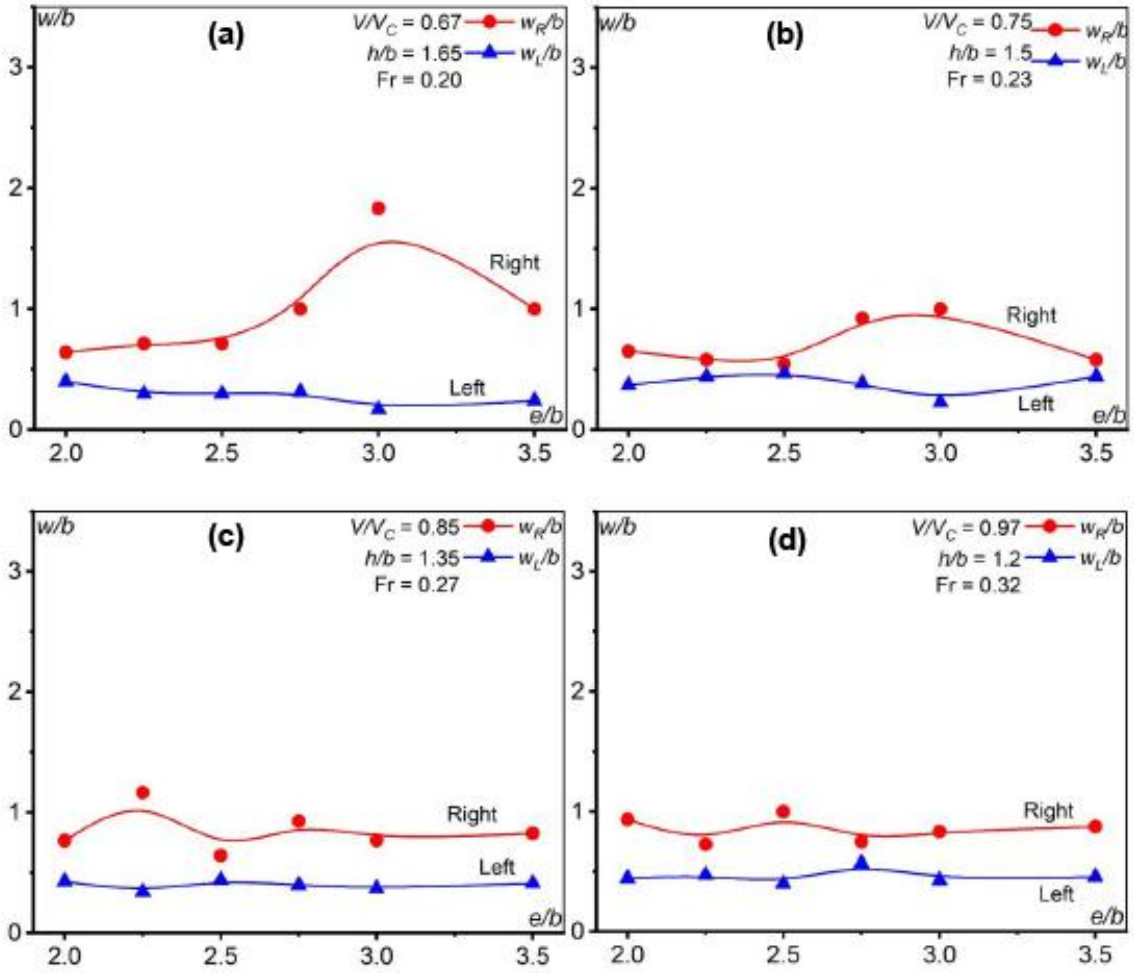


Fig. 6.26. Effect of lateral spacing on maximum scour width for **(a)** $V/V_c = 0.67$, $h/b = 1.65$, Fr = 0.20; **(b)** $V/V_c = 0.75$, $h/b = 1.5$, Fr = 0.23; **(c)** $V/V_c = 0.85$, $h/b = 1.35$, Fr = 0.27; **(d)** $V/V_c = 0.97$, $h/b = 1.2$, Fr = 0.32.

6.3.4 Effect of lateral spacing on scour planar area

Considering the direction of flow, the sediment scour zone was separated into three segments: the right, middle, and left sections (Fig. 6.23).

With the flow conditions of $V/V_c = 0.67$, $h/b = 1.65$, and Fr = 0.20, increasing the eccentricity results in an increase in the scour area in the mid-section. Throughout the different eccentricities, the changes in the scour area in the left section are almost constant. For the right section, the eccentricity of $2.5b$ and $3b$, respectively, shows the maximum and minimum deposition areas (Fig. 6.27a). In comparison to the left section, the scour area was found to be larger throughout the right section for all eccentricities with the exception of e=$3b$.

With the flow conditions of $V/V_c = 0.75$, $h/b = 1.5$, and Fr = 0.23, increasing the eccentricity results in an increase and decrease in the scour area in the mid-section. Throughout the different eccentricities, the changes in the scour area in the left section are almost the same phenomena but lower than right section. For the right section, the eccentricity of $2b$ and $2.25b$, respectively, shows the maximum and minimum scour areas (Fig. 6.27b). In

comparison to the left section, the scour area was found to be larger throughout the right section for all eccentricities.

With the flow conditions of V/V_c = 0.85, h/b = 1.35, and Fr = 0.27, increasing the eccentricity results in an increase and decrease in the scour area in the mid-section. Throughout the different eccentricities, the changes in the scour area in the left section and right section are almost the same phenomena. For the right section, the eccentricity of $2b$ and $2.25b$, respectively, shows the maximum and minimum scour areas (Fig. 6.27c). In comparison to the left section, the deposition area is found to be larger throughout the right section for all eccentricities except for $e = 2b$.

With the flow conditions of V/V_c = 0.97, h/b = 1.2, and Fr = 0.32, increasing the eccentricity results in an increase and decrease in the scour area in the mid-section and lower than the right section. Throughout the different eccentricities, the changes in the scour area in the left section and right section are almost the same phenomena. For the right section, the eccentricity of $3.5b$ and $2.75b$, respectively, shows the maximum and minimum scour areas (Fig. 6.27d). In comparison to the left section, the scour area is found to be larger throughout the right section for all eccentricities.

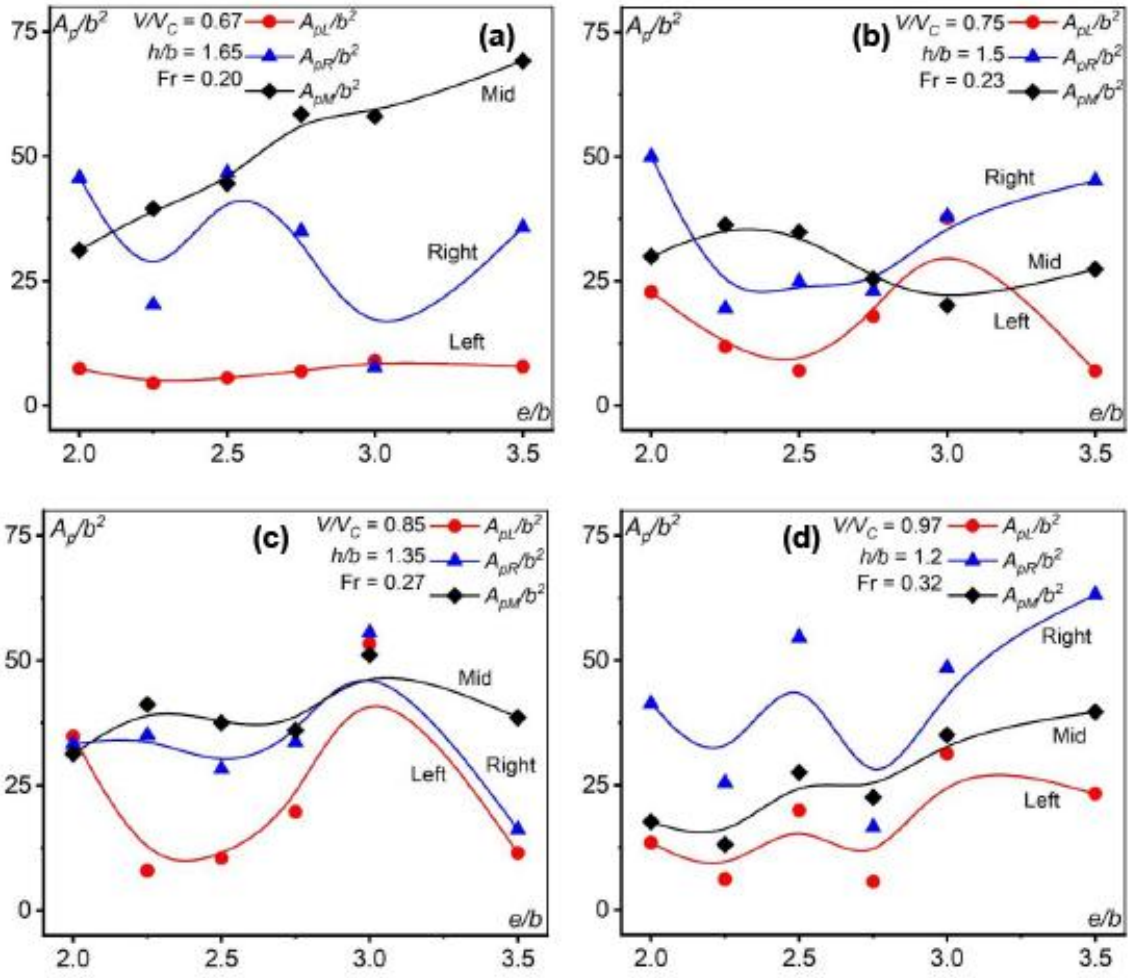


Fig. 6.27. Effect of lateral spacing on scour planar area in the entire section for **(a)** V/V_c = 0.67, h/b = 1.65, Fr = 0.20; **(b)** V/V_c = 0.75, h/b = 1.5, Fr = 0.23; **(c)** V/V_c = 0.85, h/b = 1.35, Fr = 0.27; **(d)** V/V_c = 0.97, h/b = 1.2, Fr = 0.32.

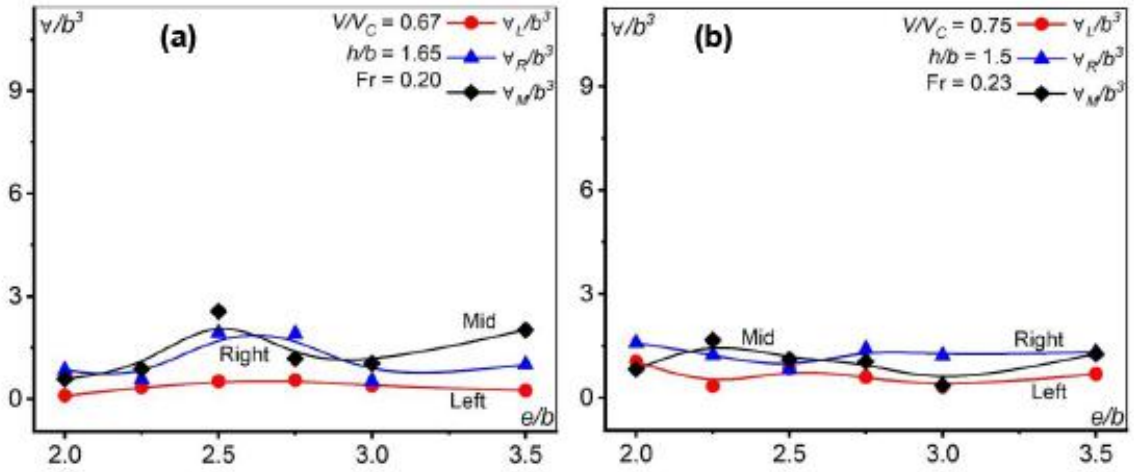
6.3.5 Effect of lateral spacing on scour volume in the entire section

With the flow conditions of V/V_c = 0.67, h/b = 1.65, and Fr = 0.20, increasing the eccentricity resulted in an increase in the scour volume in the left, mid and right sections up to the eccentricity of 2.5b and after that, the declining trend has been found for all three sections. The maximum scour volume found for the mid-section for eccentricity of 2.5b and the minimum volume found for the left section at e = 2b (Fig. 6.28a).

With the flow conditions of V/V_c = 0.75, h/b = 1.5, and Fr = 0.23, increasing the eccentricity resulted in an increase in the scour volume in the mid-section up to the eccentricity of 2.25b and after that, the declining trend has been found. For the left and right sections same but opposite phenomena have been found. The maximum scour volume found for the mid-section for eccentricity of 2.25b and the minimum volume found for the left section at e = 2b and 2.25b (Fig. 6.28b).

With the flow conditions of V/V_c = 0.85, h/b = 1.35, and Fr = 0.27, increasing the eccentricity resulted in an increase in the scour volume in the right and mid-section up to the eccentricity of 2.25b and after that, the declining trend has been found. For the left section, the same but opposite phenomena have been found. The maximum scour volume found for the right section for eccentricity of 2.25b and the minimum volume found for the left section at e =2.5b (Fig. 6.28c).

With the flow conditions of V/V_c = 0.97, h/b = 1.2, and Fr = 0.32, increasing the eccentricity resulted in a decrease in the scour volume in the right, left and mid-section up to the eccentricity of 2.25b and after that, the inclining trend has been found. The maximum scour volume found for the right section for eccentricity of 3.5b and the minimum volume found for the left section at e = 2.75b (Fig. 6.28d).



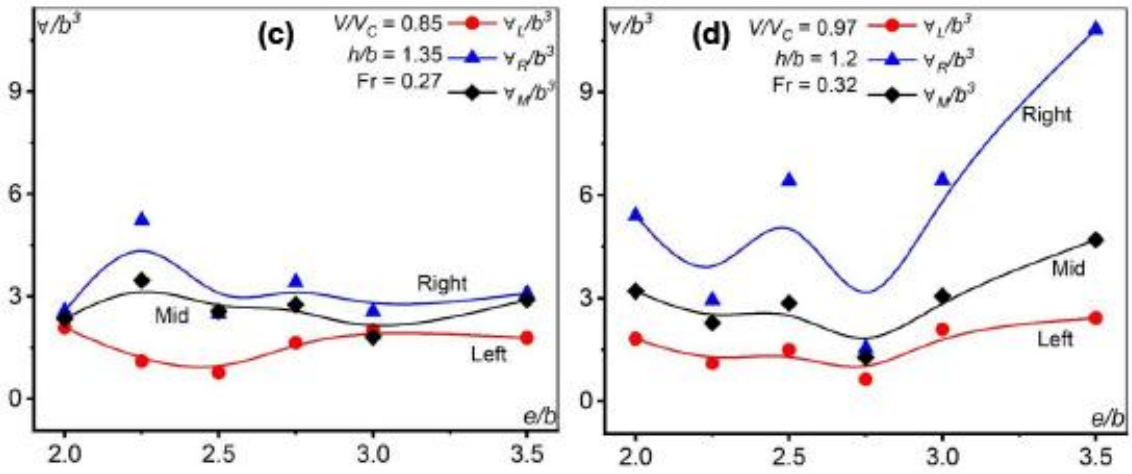


Fig. 6.28. Effect of lateral spacing on scour volume in the entire section for **(a)** $V/V_c = 0.67$, $h/b = 1.65$, Fr = 0.20; **(b)** $V/V_c = 0.75$, $h/b = 1.5$, Fr = 0.23; **(c)** $V/V_c = 0.85$, $h/b = 1.35$, Fr = 0.27; **(d)** $V/V_c = 0.97$, $h/b = 1.2$, Fr = 0.32.

Table 6.3. Experimental outcomes based on grid data of deposition shown in contour graphs.

Exp. no.	e/b	V/V_c	h/b	Fr	A_s/b^2	A_p/b^2	$\forall/b^3$	Left section		Right section		Mid section	
	(--)	(--)	(--)	(--)	(--)	(--)	(--)	A_{pL}/b^2 (--)	$\forall_L/b^3$ (--)	A_{pR}/b^2 (--)	$\forall_R/b^3$ (--)	A_{pM}/b^2 (--)	$\forall_M/b^3$ (--)
1	3.5	0.68	1.65	0.2	53.17	52.97	0.90	21.59	0.13	8.33	0.12	19.04	0.30
2	3	0.68	1.65	0.2	60.67	60.43	1.24	35.12	0.24	36.37	0.46	15.45	0.29
3	2.75	0.68	1.65	0.2	61.47	61.02	2.14	37.22	0.45	9.06	0.22	15.01	0.63
4	2.5	0.68	1.65	0.2	93.79	93.06	4.56	23.83	0.42	12.03	0.20	14.23	0.71
5	2.25	0.68	1.65	0.2	77.74	77.23	3.46	24.93	0.51	38.52	0.45	19.28	0.86
6	2	0.68	1.65	0.2	83.38	82.74	4.12	7.29	0.36	13.11	0.38	12.96	1.25
7	3.5	0.76	1.5	0.23	78.78	78.17	5.64	37.15	1.45	13.65	0.40	22.44	1.74
8	3	0.76	1.5	0.23	53.80	53.30	1.38	11.31	0.39	10.90	0.20	17.10	0.49
9	2.75	0.76	1.5	0.23	168.10	167.03	16.46	11.45	1.93	27.41	1.74	25.01	4.02
10	2.5	0.76	1.5	0.23	195.98	194.82	19.97	37.07	2.99	38.86	1.83	23.88	3.46
11	2.25	0.76	1.5	0.23	166.99	165.57	17.32	32.29	4.59	22.60	3.10	22.42	6.24
12	2	0.76	1.5	0.23	83.33	82.26	6.70	6.57	0.79	23.45	0.76	14.13	1.77
13	3.5	0.85	1.35	0.27	131.95	131.41	5.98	32.55	1.40	34.29	0.66	21.93	1.24
14	3	0.85	1.35	0.27	73.75	73.09	5.99	20.16	2.24	17.89	0.67	22.32	1.91
15	2.75	0.85	1.35	0.27	264.30	263.10	29.69	24.37	4.62	39.73	3.76	37.40	6.80
16	2.5	0.85	1.35	0.27	170.67	169.64	21.48	8.09	1.44	29.51	1.87	21.23	3.21
17	2.25	0.85	1.35	0.27	114.56	113.86	5.99	21.40	0.83	22.01	0.97	17.54	1.98
18	2	0.85	1.35	0.27	167.54	166.27	14.62	23.96	3.84	37.94	1.27	12.72	2.43
19	3.5	0.98	1.2	0.32	178.24	177.68	9.48	20.79	1.15	54.36	1.48	48.46	3.72
20	3	0.98	1.2	0.32	170.40	169.36	17.97	56.91	6.55	69.01	3.04	38.39	5.17
21	2.75	0.98	1.2	0.32	580.65	578.09	108.73	31.16	8.52	56.88	11.09	50.91	14.40
22	2.5	0.98	1.2	0.32	222.38	221.31	16.24	38.86	2.52	62.94	4.17	31.21	4.38

23	2.25	0.98	1.2	0.32	301.23	299.81	43.60	37.93	7.77	62.67	7.25	45.64	10.13
24	2	0.98	1.2	0.32	255.28	254.44	21.37	30.61	3.41	46.82	3.74	26.41	3.94

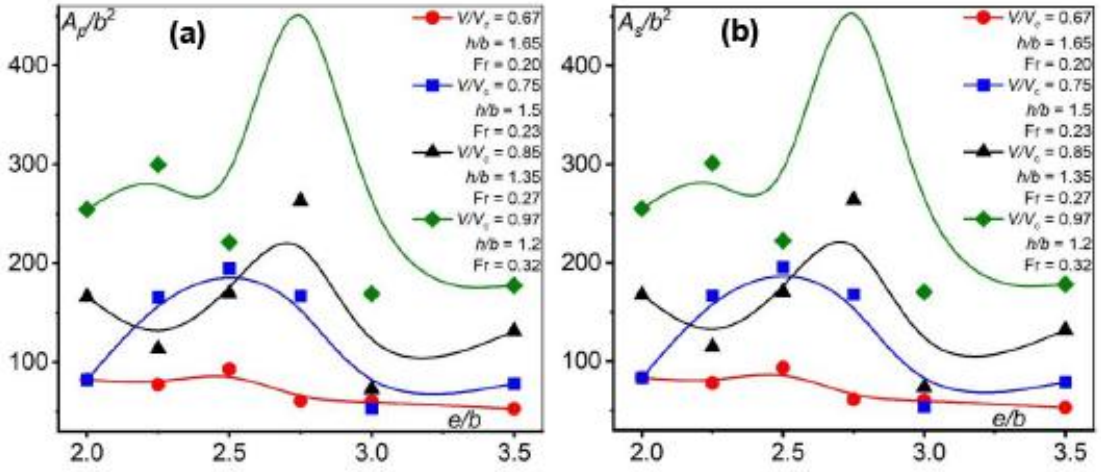
6.3.6 Effect of lateral spacing on deposition area and volume

In Figure 6.29(a), the non-dimensionalised scour planar area (A_p/b^2) of the equilibrium scour hole is plotted with respect to the varying non-dimensional pier lateral spacing (e/b).

Figure 6.29(a) illustrates how, for the provided ranges V/V_c = 0.67-0.97, h/b = 1.65-1.2, and Fr = 0.20-0.32, the planar surface area first decreases as the eccentricity increases, but it then increases again after a certain point, and vice versa. It is observed lower for higher h/b but higher for higher V/V_c and Fr.

In Figure 6.29(b), the non-dimensionalised scour surface area (A_s/b^2) of the equilibrium scour hole is plotted with respect to the varying non-dimensional pier lateral spacing (e/b). Figure 6.29(b) illustrates how, for the provided ranges V/V_c = 0.67-0.97, h/b = 1.65-1.2, and Fr = 0.20-0.32, the deposition surface area first falls as eccentricity increases, but it then increases again after a certain point, and vice versa. It is observed lower for higher h/b but higher for higher V/V_c and Fr.

In Figure 6.29(c), the non-dimensionalised scour volume ($\forall/b^3$) of the equilibrium scour hole is plotted with respect to the varying non-dimensional pier lateral spacing (e/b). Figure 6.29(c) illustrates how, for the ranges of V/V_c = 0.67-0.97, h/b = 1.65-1.2, and Fr = 0.20-0.32, the deposition volume first decreases as eccentricity increases, but it then increases again after a certain point, and vice versa. It decreases when h/b increases but it increases when both V/V_c and Fr increase.



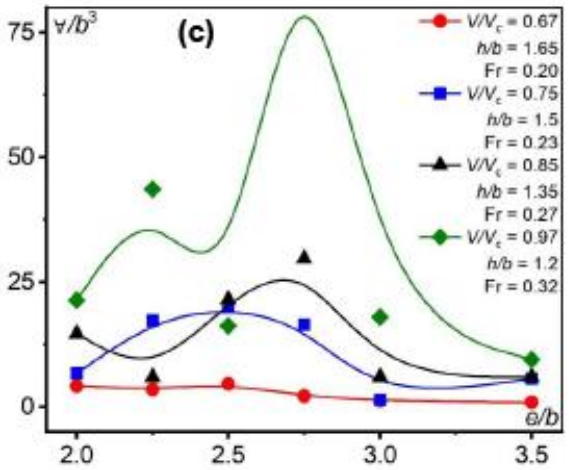


Fig. 6.29. Effect of lateral spacing on deposition **(a)** planar area **(b)** surface area and **(c)** volume.

6.3.7 Effect of lateral spacing on deposition planar area in the entire section

Considering the direction of flow, the sediment deposition zone was separated into three segments: the right, middle, and left sections (Fig. 6.23).

With the flow conditions of V/V_c = 0.67, h/b = 1.65, and Fr = 0.20, increasing the eccentricity results in an increase in the deposition area in the left section. Throughout the different eccentricities, the changes in the deposition area in the mid-section are found almost constant. For the right section, the eccentricities of 2.25b and 3.5b, respectively, the maximum and minimum deposition areas are observed (Fig. 6.30a). In comparison to the left section, the deposition area is found to be larger throughout the right section for all eccentricities except for e = 2.25b.

With the flow conditions of V/V_c = 0.75, h/b = 1.5, and Fr = 0.23, increasing the eccentricity resulted in an increase and decrease in the deposition area in the mid-section. Throughout the different eccentricities, the changes in the deposition area in the left section are almost the same phenomena but lower than right section. For the right section, the eccentricity of 2.5b and 3.5b, respectively, shows the maximum and minimum deposition area (Fig. 6.30b).

With the flow conditions of V/V_c = 0.85, h/b = 1.35, and Fr = 0.27, increasing the eccentricity results in an increase and decrease in the deposition areas in the left and right sections. Throughout the different eccentricities, the changes in the deposition area in the left section and right section are found to be almost the same. In the right section, for the eccentricity of 2.75b and 3b, respectively, the maximum and minimum deposition areas are observed (Fig. 6.30c). In comparison to the left section, the deposition area is found to be larger throughout the right section for all eccentricities.

With the flow conditions of V/V_c = 0.97, h/b = 1.2, and Fr = 0.32, increasing the eccentricity results in an increase and decrease in the deposition area in the mid-section and lower than the right section. Throughout the different eccentricities, the changes in the deposition area in the left section and right section are almost found to be similar. In the right section, maximum and minimum deposition areas are observed for the eccentricity of 3b and

2.75*b*, respectively (Fig. 6.30d). In comparison to the left section, the deposition area is found to be larger throughout the right section for all eccentricities.

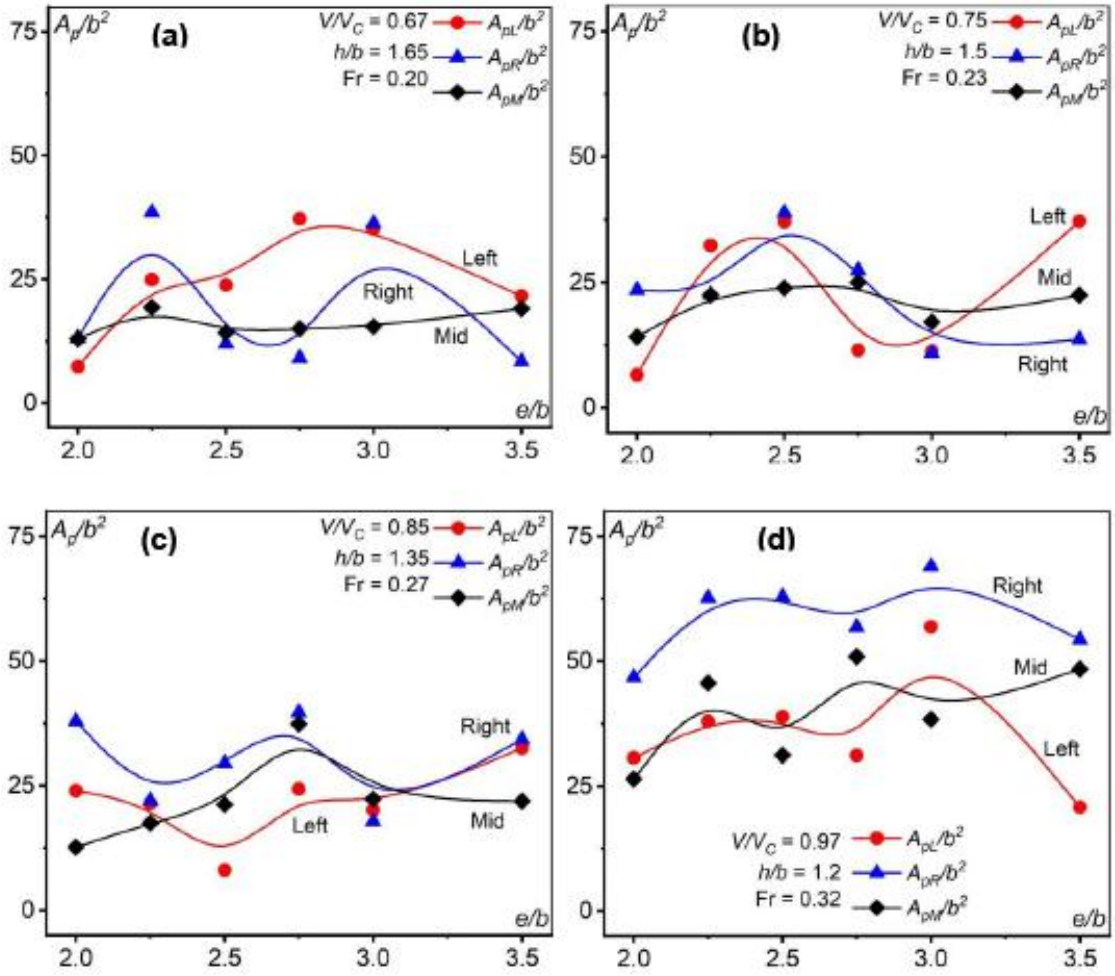


Fig. 6.30. Effect of lateral spacing on scour planar area in the entire section for **(a)** V/V_c = 0.67, h/b = 1.65, Fr = 0.20; **(b)** V/V_c = 0.75, h/b = 1.5, Fr = 0.23; **(c)** V/V_c = 0.85, h/b = 1.35, Fr = 0.27; **(d)** V/V_c = 0.97, h/b = 1.2, Fr = 0.32.

6.3.8 Effect of lateral spacing on deposition volume in the entire section

With the flow conditions of V/V_c = 0.67, h/b = 1.65, and Fr = 0.20, increasing the eccentricity results in an increase in the deposition volume in the left and right sections up to the eccentricity of 2.5*b* and after that, the declining trend has been found for all the sections. The maximum deposition volume is found in the mid-section for eccentricity of 2*b* and the minimum volume is found in the left and right sections for e = 3.5*b* (Fig. 6.31a).

With the flow conditions of V/V_c = 0.75, h/b = 1.5, and Fr = 0.23, increasing the eccentricity results in an increase in the deposition volume in all the sections up to a certain eccentricity and after that a declining trend is observed. The maximum deposition volume is found in the mid-section for the eccentricity of 2.75*b* and the minimum volume is found in the right section for e =3.5*b* (Fig. 6.31b).

With the flow conditions of V/V_c = 0.85, h/b = 1.35, and Fr = 0.27, increasing the eccentricity results in an increase in the deposition volume in the mid-section up to the eccentricity of 2.75b and after that a declining trend has been noticed. In the left section, the same but opposite phenomena have been observed. The maximum deposition volume is found in the mid section for the eccentricity of 2.25b and the minimum volume is found in the right section at $e = 3b$ (Fig. 6.31c).

With the flow conditions of V/V_c = 0.97, h/b = 1.2, and Fr = 0.32, increasing the eccentricity results in an increase in the deposition volume in the right, left and mid sections up to the eccentricity of 2.25b and after that, the declining trend has been found. The maximum deposition volume is found in the mid section for the eccentricity of 2.75b and the minimum volume is identified in the left section at $e = 3.5b$ (Fig. 6.31d).

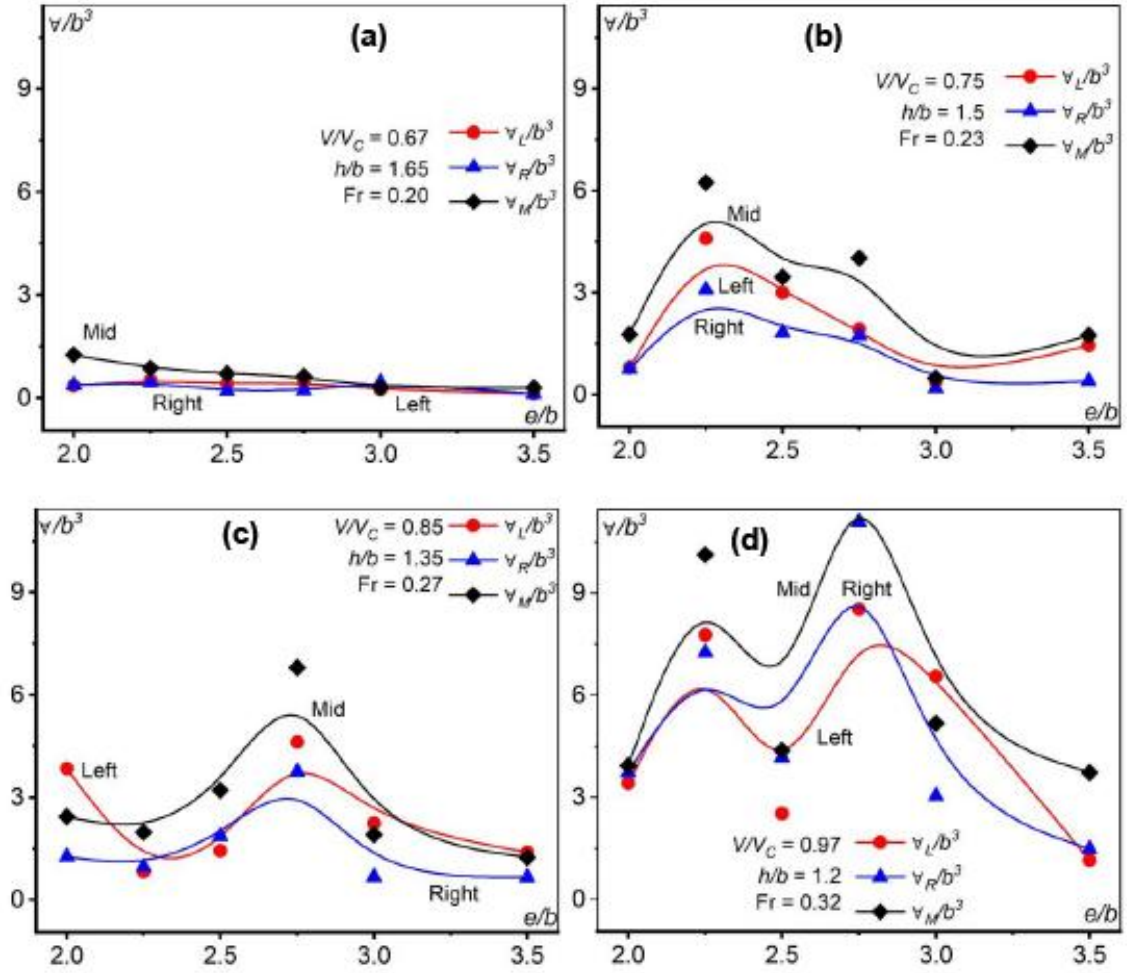


Fig. 6.31. Effect of lateral spacing on deposition volume in the entire section for **(a)** V/V_c = 0.67, h/b = 1.65, Fr = 0.20; **(b)** V/V_c = 0.75, h/b = 1.5, Fr = 0.23; **(c)** V/V_c = 0.85, h/b = 1.35, Fr = 0.27; **(d)** V/V_c = 0.97, h/b = 1.2, Fr = 0.32.

6.4 Comparisons of scour depths between single pier and eccentric pier arrangements

Different hydraulic processes are revealed when scour depths between single pier and eccentric pier setups are compared. Because of the symmetrical flow pattern, scour depths usually show a more uniform distribution around the pier in single pier systems, where the pier is positioned in the centre.

Deeper scour holes frequently occur downstream of eccentric pier configurations, which place the pier at a distance from the centreline of the flow. This is explained by the vortices and flow separation at the downstream side. It exacerbates erosion and results in asymmetric scour.

In single pier systems, the scour depth stability is generally more predictable than in eccentric setups, where scour depths are mostly shaped by variations in flow patterns and sediment transport dynamics. It is essential to comprehend these distinctions in order to properly construct and safeguard bridge foundations against scour erosion. Table 6.4 shows the percentage change of scour depths with respect to the single pier in each experimental setup.

Table 6.4. Percentage change of scour depths with respect to the single pier.

Exp. no.	e/b (--)	V/V_c (--)	h/b (--)	Fr (--)	d_{ss}/b (--)	d_{sf}/b (--)	d_{sr}/b (--)	E_{sf} (%)	E_{sr} (%)
1	3.5	0.67	1.65	0.2	0.22	0.36	0.45	59.24	100.00
2	3	0.67	1.65	0.2	0.22	0.41	0.45	84.08	100.64
3	2.75	0.67	1.65	0.2	0.22	0.42	0.46	89.17	103.82
4	2.5	0.67	1.65	0.2	0.22	0.36	0.48	61.15	112.10
5	2.25	0.67	1.65	0.2	0.22	0.45	0.55	100.00	147.13
6	2	0.67	1.65	0.2	0.22	0.36	0.42	62.42	89.17
7	3.5	0.75	1.5	0.23	0.39	0.40	0.51	2.19	29.93
8	3	0.75	1.5	0.23	0.39	0.49	0.59	24.09	49.64
9	2.75	0.75	1.5	0.23	0.39	0.54	0.66	37.96	69.34
10	2.5	0.75	1.5	0.23	0.39	0.46	0.57	18.25	45.99
11	2.25	0.75	1.5	0.23	0.39	0.59	0.69	50.36	75.18
12	2	0.75	1.5	0.23	0.39	0.52	0.62	32.48	58.03
13	3.5	0.85	1.35	0.27	0.83	0.91	0.96	9.31	16.38
14	3	0.85	1.35	0.27	0.83	0.87	0.97	4.66	16.55
15	2.75	0.85	1.35	0.27	0.83	0.92	0.95	11.03	14.66
16	2.5	0.85	1.35	0.27	0.83	0.89	0.92	6.90	11.21
17	2.25	0.85	1.35	0.27	0.83	0.89	1.02	7.41	22.93
18	2	0.85	1.35	0.27	0.83	0.87	0.97	5.52	16.55
19	3.5	0.97	1.2	0.32	0.89	0.95	1.08	6.77	22.10
20	3	0.97	1.2	0.32	0.89	1.02	1.10	15.32	24.52
21	2.75	0.97	1.2	0.32	0.89	0.95	1.08	7.74	22.26
22	2.5	0.97	1.2	0.32	0.89	0.91	0.99	2.74	11.77
23	2.25	0.97	1.2	0.32	0.89	0.95	1.13	7.74	27.90
24	2	0.97	1.2	0.32	0.89	0.96	1.07	8.39	20.81

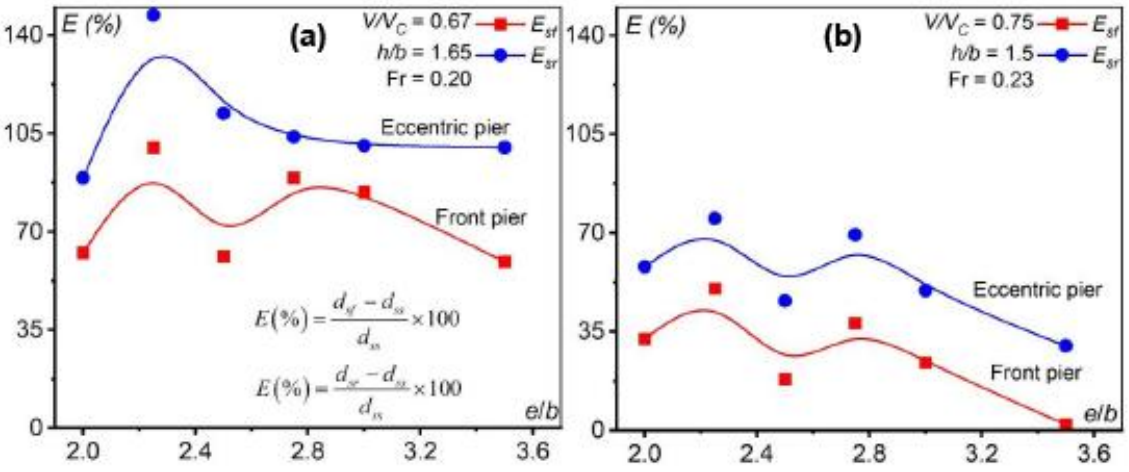
In Figure 6.32(a-d), the percentage change of scour depths at the front and eccentric piers with respect to the single pier are plotted with the non-dimensionalised lateral spacing (e/b) at different flow conditions.

Given the flow conditions of $V/V_c = 0.67$, $h/b = 1.65$, Fr = 0.20, E_{sf} for the front pier and E_{sr} for the eccentric pier show increasing and decreasing phenomena in Fig. 6.32(a). The maximum and minimum E_{sf} are 100.00 ($e = 2.25b$) and 59.24 ($e = 3.5b$) and the maximum and minimum E_{sr} are 147.13 ($e = 2.25b$) and 100.00 ($e = 3.5b$) in Fig. 6.32(a) and shows more or less similar phenomena due to group effect.

Given the flow conditions of $V/V_c = 0.75$, $h/b = 1.5$, Fr = 0.23, E_{sf} for the front pier and E_{sr} for the eccentric pier show increasing and decreasing phenomena in Fig. 6.32(b). The maximum and minimum E_{sf} are 50.36 ($e = 2.25b$) and 2.19 ($e = 3.5b$) and the maximum and minimum E_{sr} are 75.18 ($e = 2.25b$) and 29.93 ($e = 3.5b$) in Fig. 6.32(b) and shows more or less similar phenomena due to group effect.

Given the flow conditions of $V/V_c = 0.85$, $h/b = 1.35$, Fr = 0.27, E_{sf} for the front pier and E_{sr} for the eccentric pier show increasing and decreasing phenomena in Fig. 6.32(c). The maximum and minimum E_{sf} are 11.03 ($e = 2.75b$) and 4.66 ($e = 3b$) and the maximum and minimum E_{sr} are 22.93 ($e = 2.25b$) and 11.21 ($e = 2.5b$) in Fig. 6.32(c) and shows more or less similar phenomena due to group effect.

Given the flow conditions of $V/V_c = 0.97$, $h/b = 1.2$, Fr = 0.32, E_{sf} for the front pier and E_{sr} for the eccentric pier show increasing and decreasing phenomena in Fig. 6.32(d). The maximum and minimum E_{sf} are 15.32 ($e = 3b$) and 2.74 ($e = 2.5b$) and the maximum and minimum E_{sr} are 27.90 ($e = 2.25b$) and 11.77 ($e = 2.5b$) in Fig. 6.32(d) and shows more or less similar phenomena due to group effect.



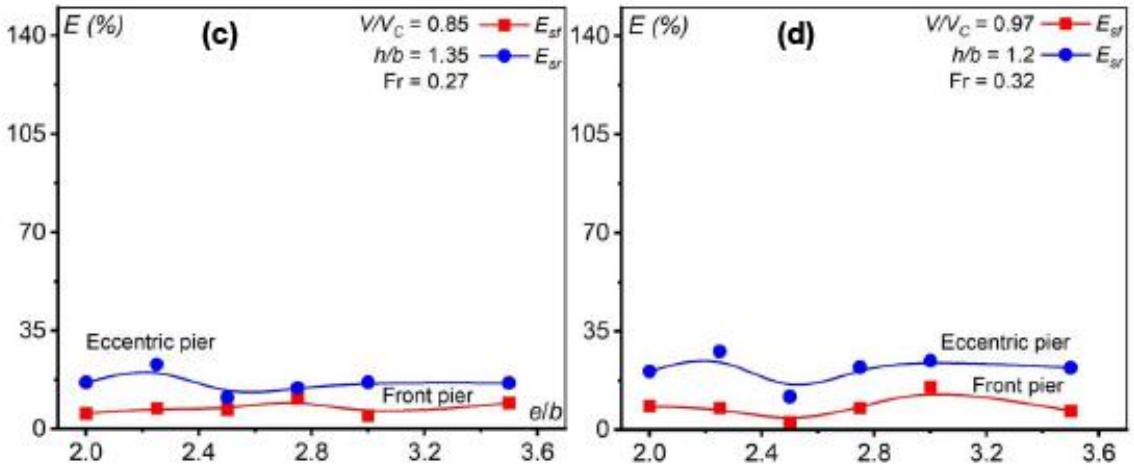


Fig. 6.32. Comparisons of scour depths between single pier and eccentric pier arrangements for **(a)** $V/V_c = 0.67$, $h/b = 1.65$, Fr = 0.20; **(b)** $V/V_c = 0.75$, $h/b = 1.5$, Fr = 0.23; **(c)** $V/V_c = 0.85$, $h/b = 1.35$, Fr = 0.27; **(d)** $V/V_c = 0.97$, $h/b = 1.2$, Fr = 0.32.

Table 6.5. Scour geometry after overall experimental analysis.

Scour parameters		*e/b*	V/V_c	*h/b*	Fr	Observed data
Scour depth at the front pier (d_{sf}/b)	Max.	3	0.97	1.2	0.32	1.02
	Min.	3.5	0.67	1.65	0.23	0.36
Scour depth at the eccentric pier (d_{sr}/b)	Max.	2.25	0.97	1.2	0.32	1.13
	Min.	2	0.67	1.65	0.2	0.42
Scour length at the left section (l_L/b)	Max.	2.75	0.979	1.2	0.32	3.34
	Min.	3	0.678	1.65	0.2	0.29
Scour length at the right section (l_R/b)	Max.	2.75	0.979	1.2	0.32	2.61
	Min.	3	0.678	1.65	0.2	0.36
Scour width at the left section (w_L/b)	Max.	2.75	0.979	1.2	0.32	0.57
	Min.	3	0.678	1.65	0.2	0.17
Scour width at the right section (w_R/b)	Max.	3	0.678	1.65	0.2	1.83
	Min.	2.5	0.757	1.5	0.23	0.55
Scour volume ($\forall/b^3$)	Max.	3	0.979	1.2	0.32	25.92
	Min.	2.75	0.757	1.5	0.23	1.34
Planar scour area (A_p/b^2)	Max.	2	0.854	1.35	0.27	191.77
	Min.	3	0.757	1.5	0.23	42.03
Scour surface area (A_s/b^2)	Max.	2	0.854	1.35	0.27	194.22
	Min.	3	0.757	1.5	0.23	43.28
Scour volume in the left section ($\forall_L/b^3$)	Max.	3.5	0.979	1.2	0.32	2.42
	Min.	2	0.678	1.65	0.2	0.1
Scour volume on the right section ($\forall_R/b^3$)	Max.	3.5	0.979	1.2	0.32	10.84
	Min.	3	0.678	1.65	0.2	0.52
Planar scour area in the left section (A_{pL}/b^2)	Max.	3	0.854	1.35	0.27	53.31

Planar scour area on the right section (A_{pR}/b^2)	Min.	2.25	0.678	1.65	0.2	4.46
	Max.	3.5	0.979	1.2	0.32	63.2
	Min.	3	0.678	1.65	0.2	7.72

6.5 Experimental limitations

Due to the complex nature of flow around bridge piers and various uncertainties on different parameters affecting the scour depth, a laboratory-based experimental study is a widely preferred method for achieving accurate and reliable results. Hence the present study was aimed to carry out an experimental investigation. However, there are some limitations to the experimental setup and the parameters given as under:

1. It was a small-scale laboratory setting, which may not entirely reflect real-world conditions. There may be scale issues.
2. Only a circular pier model with a circular cross-section was used.
3. It was considered that there is the occurrence of local scour around eccentric circular piers under clear water scour conditions.
4. It is worth mentioning that each experiment was carried out for a maximum of 10 hours. Two factors account for the variation in time: first, the equilibrium scour depth has already been attained and second, the wall effect of the flume wall causes the sediment washout phenomenon to occur uncontrollably (Table 6.1).
5. In our current study, the maximum equilibrium scour depth was measured after the end of the experiment, but it is a quasi-equilibrium scour depth due to the short duration of the experiment.
6. Cohesionless and uniformly graded sand as bed material was used for all the experiments.
7. The eccentric piers comprising a maximum number of two circular columns were adopted throughout the research work.
8. The columns of a bridge pier model were installed in an eccentric arrangement i.e. eccentric angle of 21.07°-33.99°.

CHAPTER-7

CONCLUSIONS

7.1 Conclusions

The safety and structural integrity of bridge piers are assessed under a variety of loading scenarios, such as typical traffic volumes, severe weather, and seismic activity, with the aid of bridge pier model studies. Through the use of controlled environments to simulate these conditions, engineers are able to pinpoint possible failure modes and create risk mitigation plans. It enables engineers to meet safety and performance standards while designing bridge piers with maximum efficiency and economy. In general, bridge pier model studies are essential to the planning, assessment, and administration of bridge infrastructure; they also promote sustainability, innovation, and safety in the field of fluvial hydraulics and bridge engineering.

To assure repeatability and isolate the impacts of parameters on scour depth, this study conducted 24 experiments with accurate procedures to explore the scour depth around two identical, eccentrically oriented circular piers and 4 single pier experiments. The findings demonstrate that higher scour depths at the eccentric pier are largely caused by the interaction between the horseshoe vortex at the eccentric pier and the wake vortex from the front pier or the horseshoe vortex of both piers for close spacing. These findings emphasise the complexity of local scour around eccentric piers in alluvial channels and the importance of physical modelling to understand the contributing factors.

The erosion of sediment surrounding bridge piers caused by water flow over time is known as temporal scour development around the eccentric piers, and it is important for a number of reasons. Because scouring weakens the base of bridge piers, it can jeopardise their stability. Piers that are eccentric and are not oriented in the direction of the flow are found more vulnerable because they can create intricate flow patterns that generate more concentrated scour. The normal flow patterns of rivers and streams can be changed by scouring, which can have an impact on downstream erosion processes, sediment movement, and aquatic habitats. Additionally, it may contribute to sedimentation in water bodies, which could be detrimental to ecosystems and water quality. In general, preserving the integrity, safety, and functionality of eccentric piers requires an understanding of and mitigation of the impacts of temporal scour development.

Based on the experimental work carried out and subsequent analysis following conclusions are drawn:

1. Dimensionless analysis reveals flow shallowness (h/b), flow intensity (V/V_c), Froude number (Fr), dimensionless time (Vt/b), and dimensionless lateral spacing (e/b) as the key parameters influencing the scour depths around both front piers and eccentric piers as per the present experimental observations.
2. Maximum and minimum scour depths for eccentric pier arrangements have been adopted for sediment shifting (one side of the river bank) phenomena by considering scour maximisation criteria for varying longitudinal spacing. Maximum scour measurements are crucial for understanding how to control sediment movement toward riverbanks in real-world scenarios which are useful for self-dredging and navigation purposes. Minimum scour measurements are essential for constructing bridge piers in a safe and cost-effective manner because repairing or annual maintenance costs will be low. For maximum and minimum un-symmetric sediment movement which is towards both sides of the flume wall, the relative lateral spacing is $e = 2.75b$ and $e = 3.5b$.
3. The maximum and minimum scour depth for front and eccentric piers are found to correspond to the maximum value of flow intensity, Froude number, dimensionless time and minimum value of flow shallowness and vice versa. For the majority of the time, the relative lateral spacing for the maximum scour depth is at $e = 2.25b$, and the minimum scour depth is at greater eccentricity, based on all the flow conditions used in the present study.
4. Only considering the diagonal distance between the piers (l_d), in place of the other two spacings (l, longitudinal spacing, and e, eccentricity) will not suffice the solution for minimisation of the number of parameters. Instead, it is kept close to the same range of l_d in accordance with the literature review (Table 3.3). This is because if l_d is kept fixed then the other two spacings (e and l) between the piers may not represent their significant characteristics shown in Fig. 7.1.

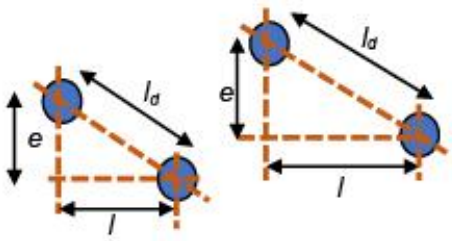


Fig. 7.1. Schematic diagram of significance of scour parameters.

5. The left section has the maximum and minimum scour lengths, whereas the right and left sections have the maximum and minimum scour widths, as can be seen by an analysis of all the eccentric pier arrangements. It is also shown that the scour volume and planar surface area are greatest in the right section and lowest in the left. The deposition volume and planar surface area are greatest in the left section and lowest in the right. Overall, it can be said that sediment deposition spreads in the right section of the flow direction when eccentricity increases, and the same things happen in the left section when eccentricity decreases.
6. In a nutshell, single pier configurations are straightforward and have a smaller environmental impact. But they may not be able to support all span lengths and are susceptible to scour. On the other hand, eccentric pier arrangements which consist of several piers improve load distribution and stability, making them appropriate for complex or longer bridges. However, they also increase construction complexity and

may cause environmental disturbance. The selection of these configurations strikes a balance between simplicity of construction and structural and environmental performance, considering variables such as span requirements, site limitations, and environmental concerns. The maximum scour depth around a single pier in several flow conditions was examined in the present study. The maximum scour depth is found consistently lower than that of the two piers utilised in eccentric pier arrangements. Compared to the single pier, the maximum increase in scour depth, for the front pier and eccentric pier in an eccentric arrangement is around 60-100% and 90-150%, respectively for V/V_c = 0.67. Similarly, compared to the single pier, the minimum increase in scour depth, for the front pier and eccentric pier is around 3-16% and 12-30%, respectively for V/V_c = 0.97.

7.2 Future scopes

Although the geometry of the scour around eccentric-pier arrangements has been studied, still there remain some more aspects which need to be studied thoroughly to make more robust conclusive remarks. These are stated below:

1. Similar experiments may be carried out using different bed materials and variations of results may be observed.
2. The variation of non-dimensional scour depth with h/b ratio may be examined in more detail with the help of more experiment data.
3. The same experiments may be carried out using different shapes and sizes to observe the variation of results.
4. Many other different arrangements of piers may be applied for experimentation.
5. Update bridge design codes and guidelines to incorporate specific provisions for eccentric piers, considering the unique scour mechanisms and risk factors associated with these structures. This may help in ensuring the safety and longevity of bridges built over rivers and waterways.
6. In this study, all the experiments on scouring were conducted under clear water condition. In reality, bridge sites experience different types of flow conditions, especially during floods or rainy seasons, scouring often happens under live bed conditions. Hence, a well-designed physical model is recommended to investigate the scour characteristics under live bed conditions.
7. The angle of attack is another important parameter that needs to be considered during the experiments. In the present study, only zero angle of attack was employed. However, the variation of the angle of attack is strongly recommended to be taken into account for future research to investigate its interference effects on the horseshoe vortex system.
8. Lower flow intensity may be taken into account to investigate the effect of flow intensity on the scour depth evolution using more advanced measuring equipment.

REFERENCES

Al-Shukur, A. H. K., and Obeid, Z. H. (2016). Experimental study of bridge pier shape to minimize local scour. *International Journal of Civil Engineering and Technology*, Vol. 7, Issue 1, pp. 162-171.

Ataie-Ashtiani, B., and Aslani-Kordkandi, A. (2012). Flow field around side-by-side piers with and without a scour hole. *European Journal of Mechanics-B/Fluids*, Vol. 36, pp. 152-166. https://doi.org/10.1016/j.euromechflu.2012.03.007.

Ataie-Ashtiani, B., and Beheshti, A. A. (2006). Experimental investigation of clear-water local scour at pile groups. *Journal of Hydraulic Engineering*, Vol. 132, Issue 10, pp. 1100-1104. https://doi.org/10.1061/(ASCE)0733-9429(2006)132:10(1100).

Ballio, F., Teruzzi, A., and Radice, A. (2009). Constriction effects in clear-water scour at abutments. *Journal of Hydraulic Engineering*, Vol. 135, Issue 2, pp. 140-145. https://doi.org/10.1061/(ASCE)0733-9429(2009)135:2(140).

Brandimarte, L., Paron, P., & Di Baldassarre, G. (2012). Bridge pier scour: A review of processes, measurements and estimates. *Environmental Engineering and Management Journal*, Vol. 11, Issue 5, pp. 975-989.

Breusers, H. N. C., and Raudkivi, A. J. (1991). *Scouring*. Rotterdam: Balkema.

Breusers, H. N. C., Nicollet, G., and Shen, H. W. (1977). "Local scour around bridge piers." J. Hydraul. Res., Vol. 15, Issue 3, pp. 211–252. https://doi.org/10.1080/00221687709499645.

Chabert, J., and Engeldinger, P. (1956). Etude des affouillements autourdes piles des ponts. Laboratoire d'Hydraulique, Chatou, France (inFrench)

Chien, N., and Wan, Z. (1999). Mechanics of sediment transport.

Chiew, Y. M. (1984). *Local scour at bridge piers* (Doctoral dissertation, ResearchSpace@ Auckland). http://hdl.handle.net/2292/2520.

Chiew, Y. M. (1995). Mechanics of riprap failure at bridge piers. *Journal of Hydraulic Engineering*, Vol. 121, Issue 9, pp. 635-643. https://doi.org/10.1061/(ASCE)0733-9429(1995)121:9(635).

Chiew, Y. M., and Melville, B. W. (1987). Local scour around bridge piers. *Journal of Hydraulic Research*, Vol. 25, Issue 1, pp. 15-26. https://doi.org/10.1080/00221688709499285.

Coleman, S. E., Lauchlan, C. S., and Melville, B. W. (2003). Clear-water scour development at bridge abutments. *Journal of Hydraulic Research*, Vol. 41, Issue 5, pp. 521-531. https://doi.org/10.1080/00221680309499997.

Das, R., Khwairakpam, P., Das S, Mazumdar A (2014) Clear-water local scour around eccentric multiple piers to shift the line of sediment deposition. *Asian Journal of Water Environment and Pollution,* Vol. 11, Issue 3, pp. 47–54.

Das S, Das R, Mazumdar A (2016) Comparison of local scour characteristics around two eccentric piers of different shapes. *Arabian Journal of Science and Engineering,* Vol. 41, Issue 4, pp. 1199-1213. https://doi.org/10.1007/s13369-015-1817-4.

Das, R., Das, S., Jaman, H., and Mazumdar, A. (2019). Impact of upstream bridge pier on the scouring around adjacent downstream bridge pier. *Arabian Journal for Science and Engineering*, Vol. 44, pp. 4359-4372. https://doi.org/10.1007/s13369-018-3418-5.

Das, S., and Mazumdar, A. (2018). Evaluation of hydrodynamic consequences for horseshoe vortex system developing around two eccentrically arranged identical piers of diverse shapes. *KSCE Journal of Civil Engineering*, Vol. 22, pp. 2300-2314. https://doi.org/10.1007/s12205-017-1842-9.

Das, S., Das, R., and Mazumdar, A. (2013). Circulation characteristics of horseshoe vortex in scour region around circular piers. *Water Science and Engineering*, Vol. 6, Issue 1, pp. 59-77. https://doi.org/10.3882/j.issn.1674-2370.2013.01.005.

Das, S., Das, R., Kuila, A., and Mazumdar, A. (2014). Analysis of clear-water equilibrium scour around two eccentric circular piers to increase self-dredging. In *Seminar on Dredging: Equipment and Applications, (EADA), Kolkata, India*.

Das, S., Ghosh, R., Das, R., and Mazumdar, A. (2014). Clear water scour geometry around circular piers. *Ecology, Environment and Conservation*, Vol. 20, Issue 2, pp. 479-492.

Das, S., Ghosh, S., and Mazumdar, A. (2014). Kinematics of Horseshoe Vortex in a Scour Hole around Two Eccentric Triangular Piers. *International Journal of Fluid Mechanics Research*, Vol. 41, Issue 4, pp. 296-317. https://doi.org/10.1615/InterJFluidMechRes.v41.i4.20.

Das, S., Jaman, H., Chatterjee, A., Das, R., and Mazumdar, A. (2017). Hydrodynamic behaviour of Flow past three typically arranged circular piers on different horizontal planes. *International Journal of Fluid Mechanics Research*, Vol. 44, Issue 5. https://doi.org/10.1615/InterJFluidMechRes.2017019421.

Das, S., Midya, R., Das, R., and Mazumdar, A. (2013). A study of wake vortex in the scour region around a circular pier. *International Journal of Fluid Mechanics Research*, Vol. 40, Issue 1, pp. 42-59. https://doi.org/10.1615/InterJFluidMechRes.v40.i1.40.

Dey, S., Bose, S. K., and Sastry, G. L. (1995). Clear water scour at circular piers: a model. *Journal of Hydraulic Engineering*, Vol. 121, Issue 12, pp. 869-876. https://doi.org/10.1061/(ASCE)0733-9429(1995)121:12(869).

Elliott, K. R., and Baker, C. J. (1985). Effect of pier spacing on scour around bridge piers. *Journal of Hydraulic Engineering*, Vol. 111, Issue 7, pp. 1105-1109. https://doi.org/10.1061/(ASCE)0733-9429(1985)111:7(1105).

Ettema, R. (1980). Scour at Bridge Piers. Ph.D. Thesis. Department of Civil Engineering, University of Auckland, New Zealand. https://researchspace.auckland.ac.nz/docs/uoa-docs/rights.htm.

Ettema, R., Kirkil, G., and Muste, M. (2006). Similitude of large-scale turbulence in experiments on local scour at cylinders. *Journal of Hydraulic Engineering*, Vol. 132, Issue 1, pp. 33-40. https://doi.org/10.1061/(ASCE)0733-9429(2006)132:1(33).

Ettema, R., Melville, B. W., and Constantinescu, G. (2011). *Evaluation of bridge scour research: Pier scour processes and predictions*. Washington, DC, USA: Transportation Research Board of the National Academies.

Franzetti, S., Radice, A., Rebai, D., and Ballio, F. (2022). Clear water scour at circular piers: A new formula fitting laboratory data with less than 25% deviation. *Journal of*

Hydraulic Engineering, Vol. 148, Issue 10, Art. No. 04022021. https://doi.org/10.1061/(ASCE)HY.1943-7900.0002009.

Jaman, H., Das, S., Das, R., and Mazumdar, A. (2017). Hydrodynamics of flow obstructed by inline and eccentrically-arranged circular piers on a horizontal bed surface. *Journal of The Institution of Engineers (India): Series A*, Vol. 98, pp. 77-83. https://doi.org/10.1007/s40030-017-0187-1.

Jaman, H., Das, S., Kuila, A., and Mazumdar, A. (2017). Hydrodynamic flow patterns around three inline eccentrically arranged circular piers. *Arabian Journal for Science and Engineering*, Vol. 42, pp. 3973-3990. https://doi.org/10.1007/s13369-017-2536-9.

Jones, J. S., and Sheppard, D. M. (2000). Local scour at complex pier geometries. In *Building Partnerships,* pp. 1-9. https://doi.org/10.1061/40517(2000)409.

Khaple, S., Hanmaiahgari, P. R., Gaudio, R., and Dey, S. (2017). Interference of an upstream pier on local scour at downstream piers. *Acta Geophysica*, Vol. 65, pp. 29-46. https://doi.org/10.1007/s11600-017-0004-2.

Khwairakpam, P., and Mazumdar, A. (2009). Local scour around hydraulic structures. *International Journal of Recent Trends in Engineering*, Vol. 1, Issue 6, Art. No. 59.

Kothyari, U. C., Hager, W. H., and Oliveto, G. (2007). Generalized approach for clear-water scour at bridge foundation elements. *Journal of Hydraulic Engineering*, Vol. 133, Issue 11, pp. 1229-1240. https://doi.org/10.1061/(ASCE)0733-9429(2007)133:11(1229).

Kuila, A., Jaman, H., Das, S., and Mazumdar, A. (2020). Computing equilibrium flow structures at three interfering square piers causing relative scour. *Topics in intelligent computing and industry design (ICID)*, Vol. 1, pp. 20-24. http://doi.org/10.26480/cic.01.2020.20.24.

Laursen, E. M., and Toch, A. (1953). *A generalized model study of scour around bridge piers and abutments* (No. HR-24). State University of Iowa.

Malik, R., and Setia, B. (2020). Interference between pier models and its effects on scour depth. *SN Applied Sciences*, Vol. 2, pp. 1-12. https://doi.org/10.1007/s42452-019-1868-3.

Melville, B. (2008). The physics of local scour at bridge piers. In Fourth International conference on scour and erosion, pp. 28-38.

Melville, B. W. (1997). Pier and abutment scour: integrated approach. *Journal of Hydraulic Engineering*, Vol. 123, Issue 2, pp. 125-136. https://doi.org/10.1061/(ASCE)0733-9429(1997)123:2(125).

Melville, B. W., and Chiew, Y. M. (1999). Time scale for local scour at bridge piers. *Journal of Hydraulic Engineering*, Vol. 125, Issue 1, pp. 59-65. https://doi.org/10.1061/(ASCE)0733-9429(1999)125:1(59).

Melville, B. W., and Coleman, S. E. (2000). *Bridge scour*. Water Resources Publication.

Melville, B. W., and Southerland, A. J. (1988). "Design method for local scour at bridge piers." *Journal of Hydraulic Engineering*, Vol. 114, Issue 10, pp. 1210–1226. https://doi.org/10.1061/(ASCE)0733-9429(1988)114:10(1210).

Monti, R. (1994). Indagine sperimentale delle caratteristiche fluidodinamiche del campo di moto intorno a una pila circolare, Polytechnic of Milan, Milan, Italy (in Italian).

Nandi, B. (2019): Analysis of Time Variation of Scour around Three Cylindrical Tandem Piers. M.E. Thesis, School of Water Resources Engineering, Jadavpur University, Kolkata, India.

Nandi, B., and Das, S. (2023*a*). Equation for time-dependent local scour at pier-like structures with eccentric in-line arrangements. In *Proceedings of the Institution of Civil Engineers-Water Management*, pp. 1-14. https://doi.org/10.1680/jwama.23.00006.

Nandi, B., Das, S., (2023*b*). Identify most promising temporal scour depth formula for circular piers proposed over last six decades. *Ocean Engineering*. Vol. 286, Part 2, Art. No. 115639. https://doi.org/10.1016/j.oceaneng.2023.115639.

Nandi, B., Patel, G., and Das, S. (2024*b*). Prediction of maximum scour depth at clear water conditions: Multivariate and robust comparative analysis between empirical equations and machine learning approaches using extensive reference metadata. *Journal of Environmental Management*, Vol. 354, Art. No. 120349. https://doi.org/10.1016/j.jenvman.2024.120349.

Nandi, B., Sasmal, K., and Das, S. (2024*a*). Evolution of Four Formulae Derived Over Five Decades to Predict Temporal Scour at Circular Pier. In International Conference on Science, Technology and Engineering, pp. 131-139. Singapore: Springer Nature Singapore. https://doi.org/10.1007/978-981-99-4665-5_14.

Oliveto, G., and Hager, W. H. (2002). Temporal evolution of clear-water pier and abutment scour. *Journal of Hydraulic Engineering*, Vol. 128, Issue 9, pp. 811-820. https://doi.org/10.1061/(ASCE)0733-9429(2002)128:9(811).

Raikar, R. V., and Dey, S. (2005). Clear-water scour at bridge piers in fine and medium gravel beds. *Canadian Journal of Civil Engineering*, Vol. 32, Issue 4, pp. 775-781. https://doi.org/10.1139/l05-022.

Rajendran, R. (2018). Bridge failures case studies in India (2016-2019).

Raudkivi, A. J. (1986). Functional trends of scour at bridge piers. *Journal of Hydraulic Engineering*, Vol. 112, Issue 1, pp. 1-13. https://doi.org/10.1061/(ASCE)0733-9429(1986)112:1(1).

Raudkivi, A. J. (2020). Scour at bridge piers. In *Scouring*, pp. 61-98. CRC Press.

Raudkivi, A. J., and Ettema, R. (1983). Clear-water scour at cylindrical piers. *Journal of Hydraulic Engineering*, Vol. 109, Issue 3, pp. 338-350. https://doi.org/10.1061/(ASCE)0733-9429(1983)109:3(338).

Raudkivi, A.J. 1998. Loose Boundary Hydraulics. A.A. Balkema Publishers, Netherlands. https://doi.org/10.1201/9781003077800.

Shen, H. W., Schneider, V. R., and Karaki, S. (1969). Local scour around bridge piers. *Journal of the Hydraulics Division*, Vol. 95, Issue 6, pp. 1919-1940. https://doi.org/10.1061/JYCEAJ.0002197.

Sheppard, D. M., Odeh, M., and Glasser, T. (2004). Large scale clear-water local pier scour experiments. *Journal of Hydraulic Engineering*, Vol. 130, Issue 10, pp. 957-963. https://doi.org/10.1061/(ASCE)0733-9429(2004)130:10(957).

Sheppard, D. M., Zhao, G., and Copps, T. H. (1995). Local scour near multiple pile piers in steady currents. In *Water Resources Engineering*, pp. 1804-1808. ASCE.

Tafarojnoruz, A., Gaudio, R., and Calomino, F. (2012). Evaluation of flow-altering countermeasures against bridge pier scour. *Journal of Hydraulic Engineering*, Vol. 138, Issue 3, pp. 297-305. https://doi.org/10.1061/(ASCE)HY.1943-7900.0000512.

Wang, C., Yu, X., and Liang, F. (2017). A review of bridge scour: mechanism, estimation, monitoring and countermeasures. *Natural Hazards*, Vol. 87, pp. 1881-1906. https://doi.org/10.1007/s11069-017-2842-2.